TECHNISCHE UNIVERSITÄT MÜNCHEN

Lehrstuhl T31 Univ.-Prof. Dr. A. J. Buras
Physik Department

Two Complementary Approaches to Right-Handed Currents

Katrin M. Gemmler

"Learning is like rowing upstream: not to advance is to drop back."

Laozi

Abstract

Flavour observables impose strong constraints on models of new physics. In this thesis we study whether right-handed currents can provide a realistic extension to the Standard Model. We analyse two complementary models, addressing right-handed currents by a bottom-up and a top-down approach with a global and local $SU(2)_L \times SU(2)_R \times U(1)_{B-L}$ electroweak symmetry respectively. This setup leads to new flavour violating interactions in the right-handed sector, which are governed by a right-handed mixing matrix. We first consider an effective theory approach assuming a left-right symmetric flavour group broken only by the Yukawa couplings, termed Right-Handed Minimal Flavour Violation. We classify relevant interactions and study $\Delta F = 2$ processes as well as various rare decays, such as $B_{s,d} \to \mu^+ \mu^-$, $B \to \{X_s, K, K^*\}\nu\bar{\nu}$ and $K \to \pi\nu\bar{\nu}$. Emphasis is put on investigating correlations among observables, the structure of the right-handed mixing matrix and resolving flavour anomalies of the Standard Model. In particular, the $|V_{ub}|$ problem can be solved in this framework, but a tension between ε_K and $S_{\psi K_S}$ remains under the assumption of a large $S_{\psi\phi}$. Secondly we study the Left-Right Model. In this model heavy new particles, such as the gauge bosons W_R and heavy Higgs particles can provide new contributions to observables related to flavour changing neutral currents. While the effects of the neutral and charged heavy Higgs field are often neglected in the literature, we find that they have a significant impact on $\Delta F = 2$ processes and the decay $B \to X_s\gamma$ respectively. Subsequently, we perform a comprehensive numerical analysis, including all known experimental constraints from tree-level decays, electroweak precision observables, $\Delta F = 2$ observables related to particle-antiparticle mixings and the decay $B \to X_s\gamma$ simultaneously. We observe that there exist regions in parameter space in accordance with the all data and with a mass of W_R in reach of the Large Hadron Collider. An enhancement of $\mathrm{Br}(B \to X_s\gamma)$ relative to the Standard Model brings the value in better agreement with experiment. In this model all flavour anomalies can be resolved except the $|V_{ub}|$ problem, precluded mainly by an increased direct lower bound on the mass of W_R boson in conjunction with constraints from flavour and electroweak precision observables. Furthermore, we have analysed the general structure of the right-handed mixing matrix in detail. We also present a new simplified parametrisation of the right-handed mixing matrix motivated by resolving tensions present in flavour observables within the Standard Model. Finally, a comparison to other new physics models is presented which helps to distinguish them from our setups.

Zusammenfassung

Flavourobservablen liefern starke Einschränkungen für Modelle der neuen Physik. In dieser Dissertation untersuchen wir, ob rechtshändige Ströme eine realistische Erweiterung des Standardmodells darstellen können. Wir analysieren zwei komplementäre Modelle, die rechtshändige Ströme einerseits durch einen „bottom-up" Zugang, andererseits durch einen „top-down" Zugang mit einer globalen beziehungsweise lokalen $SU(2)_L \times$

$SU(2)_R \times U(1)_{B-L}$ elektroschwachen Symmetrie behandeln. Dieser Ansatz führt zu neuen flavourverletzenden Wechselwirkungen im rechtshändigen Sektor, welcher durch eine rechtshändige Mischungsmatrix bestimmt wird. Wir betrachten zunächst eine effektive Theorie, genannt rechtshändige minimale Flavourverletzung, unter der Annahme, dass eine links-rechts symmetrische Flavourgruppe nur durch die Yukawakopplungen gebrochen wird. Wir klassifizieren relevante Wechselwirkungen und untersuchen $\Delta F = 2$ Prozesse sowie verschiedene seltene Zerfälle, wie zum Beispiel $B_{s,d} \to \mu^+ \mu^-$, $B \to \{X_s, K, K^*\}\nu\bar{\nu}$ und $K \to \pi\nu\bar{\nu}$. Wir legen besonderen Wert auf Korrelationen zwischen Observablen, die Struktur der rechtshändigen Mischungsmatrix und die Aufhebung von Flavouranomalien des Standardmodells. Insbesondere kann in diesem Rahmen das $|V_{ub}|$ gelöst werden, jedoch bleibt unter der Annahme eines großen $S_{\psi\phi}$ ein Konflikt zwischen ε_K und $S_{\psi K_S}$ bestehen. Als zweites untersuchen wir das Links-Rechts Modell. In diesem Modell gibt es durch neue schwere Teilchen, wie das Eichboson W_R und schwere Higgsteilchen, neue Beiträge zu Observablen, die im Zusammenhang mit flavourverletzenden neutralen Strömen stehen. Während in der bisherigen Literatur die Effekte von neutralen beziehungsweise geladenen schweren Higgsfeldern oft vernachlässigt wurden, finden wir, dass diese erhebliche Auswirkungen auf $\Delta F = 2$ Prozesse beziehungsweise den Zerfall $B \to X_s\gamma$ haben. Anschließend machen wir eine umfassende numerische Analyse, die alle bekannten experimentellen Einschränkungen von „tree-level" Zerfällen, elektroschwachen Präzisionsobservablen, $\Delta F = 2$ Observablen, die im Zusammenhang mit Teilchen-Antiteilchenmischungen und dem Zerfall $B \to X_s\gamma$ stehen, gleichzeitig berücksichtigt. Wir beobachten, dass im Parameterraum Regionen existieren, die mit allen Daten und einer Masse von W_R in Reichweite des LHC übereinstimmen. Eine Erhöhung von $\mathrm{Br}(B \to X_s\gamma)$ führt zu einer besseren Übereinstimmung von theoretischem und experimentellem Wert im Vergleich zum Standardmodell. In diesem Modell können alle Flavouranomalien gelöst werden, außer dem $|V_{ub}|$ Problem. Jene Lösung wird hauptsächlich durch eine erhöhte direkte untere Schranke für die Masse von W_R in Verbindung mit den Einschränkungen durch Flavour- und elektroschwachen Präzisionobservablen verhindert. Außerdem haben wir die allgemeine Struktur der rechtshändigen Mischungsmatrix im Detail analysiert. Wir präsentieren eine neue vereinfachte Parametrisierung der rechtshändigen Mischungsmatrix, die sich dadurch auszeichnet, dass Konflikte zwischen den Flavourobservablen des Standardmodells gelöst werden. Ein abschließender Vergleich zu anderen Modellen der neuen Physik grenzt unsere Ansätze von diesen ab.

Contents

1. Introduction

Over the last decades fundamental physics has focused on pushing our understanding at the largest and smallest scales ever approached. At the smallest distances probed so far, the Standard Model (SM) of elementary particles provides an astoundingly accurate description of observed data. However, there are reasons to believe that the SM is just an effective theory at low energy scales of a more fundamental framework. The nature of physics beyond the Standard Model is an intriguing mystery, driving much of current research in particle physics.

Already within the SM, various open questions centre around the Higgs boson, which has not been observed yet. The Higgs mechanism is linked to the origin of masses and the mechanism of electroweak symmetry breaking (EWSB), which are consequently not yet fully understood. The Large Hadron Collider (LHC) is expected to shed light on the existence of the SM Higgs by the end of this year. And indeed initial hints of the Higgs might already be appearing.

On the other hand, motivations for an extension of the SM are manifold. On the theoretical side, the Higgs boson again plays a central role. Within the SM its mass obtains quantum corrections of the order of the Planck scale, unnaturally large compared to the scale of EWSB. This is usually referred to as the hierarchy problem and provides strong hints that new physics (NP) must appear at the TeV scale. In addition the SM lacks an explanation for the hierarchical pattern of masses and mixings. However, this issue is not as fundamental as the gauge hierarchy problem since these patterns are stable under quantum corrections. On the experimental side, we have evidence for the existence of dark matter and neutrino masses, also not explained within the SM.

While these are well known problems, we want to concentrate in the following on the hints for NP indicated by the flavour sector. The origin of flavour and flavour mixing is still not understood. Additionally, the meticulous study of flavour data has revealed the existence of a few anomalies and tensions within the SM picture of flavour. These give strong hints that new sources of CP violation apart from those in the SM are needed. Note that the consideration of the current baryon asymmetry of the universe leads to the same conclusion. Moreover, the examination of models with generic flavour structure has shown that large new sources of flavour symmetry breaking beyond the SM are already excluded at the TeV scale [1]. Hence, the flavour structure of NP models cannot be arbitrary, but must follow a specific pattern. Attempts to classify such patterns have been made in terms of considering flavour symmetries. For example, in the Minimal Flavour Violation (MFV) principle [2–6] all flavour violation in the NP model

is governed by the SM Yukawa couplings. In a much older idea, the Froggatt-Nielsen mechanism [7], flavour mixing is characterised by a spontaneously broken flavour symmetry. This not only constrains the flavour structure, but also explains the hierarchies in the SM Yukawa couplings. Generally, for any NP model, constraints from flavour observables have to be considered seriously in order to ensure consistency with experiment.

Let us take a closer look at the SM picture of flavour. Parity is maximally broken at low energy scales and flavour violation at the tree-level takes place entirely through left-handed (LH) charged currents. This picture is compactly described by the CKM matrix [8, 9]. Its unitarity is an important ingredient for the GIM mechanism [10], which turns out to be a powerful protection mechanism with immediate consequences on the pattern of flavour changing neutral current (FCNC) processes. We can extract two lessons from the flavour structure of the SM. Firstly, the loop suppression of FCNCs within the SM makes them an excellent tool to examine whether NP enters in such processes. This can be analysed by the study of low-energy observables, providing an alternative to high energy searches for new particles. Secondly, one could ask whether parity is restored as a symmetry at high energy scales. This would imply the inclusion of the $SU(2)_R$ symmetry.

In the past years, it has turned out that an additional $SU(2)_R$ symmetry is an attractive ingredient for a model beyond the SM. This is mainly because the $SU(2)_L \times SU(2)_R$ symmetry provides a custodial symmetry for the NP framework, constraining parameters like the mass ratio of the W- and the Z-boson masses and helping to keep electroweak precision (EWP) observables consistent with the experiment [11, 12]. One example of such a model is the Randall Sundrum model with custodial protection (RSc) [13–19]. In this model, a warped extra dimension solves the hierarchy problem and can also naturally generate the hierarchies of fermion masses and mixings [20, 21]. A similar class of models are the so called Higgsless models [22–27], where the EWSB is also induced by boundary conditions.

There also exist left-right (LR) symmetric models, which implement RH currents only by extending the SM by the $SU(2)_R$ gauge symmetry. First studied more than 35 years ago [28–32], their two simplest forms of appearance are the so called "manifest" scenario [32] and the "pseudo-manifest" scenario [33–35]. Each of them is characterised by special assumptions about new CP violating phases and is either ruled out or constrained to have large mass scales for the new heavy particles. Recent studies allow for a more general structure with respect to CP violation [36, 37] while requiring a full restoration of parity at high scale. Most of these previous studies concentrate on finding lower bounds on the masses of new heavy gauge bosons, appearing within this framework due to the additional $SU(2)_R$ symmetry. Constraints from flavour observables are usually considered separately. Furthermore, there is a lack of studies taking into account the most recent collider bounds. A few papers make attempts to analyse details of the underlying flavour structure in the RH sector [38, 39], which is characterised in this class of models by an additional RH mixing matrix in contrast to the

LH counterpart, the CKM matrix. However, these proposals are ad hoc or already experimentally disfavoured. In order to investigate if this class of LR models still provides an attractive NP framework in the decade of the LHC, we need an improved and comprehensive analysis. Such a study is particularly attractive since high energy experiments at the LHC, ATLAS and CMS, have the potential to discover the heavy gauge bosons. First studies for the early LHC data can be found in [40, 41]. Finally, it is worth mentioning that in the LR symmetric setup one can naturally implement the see-saw mechanism to generate neutrino masses [42, 43].

A very different approach was taken by the authors of [44–46], who analyse RH currents from a flavour point of view. It was shown that in the presence of RH currents it is possible to resolve the $|V_{ub}|$ problem describing the tension between inclusive and exclusive determinations of the $|V_{ub}|$ element of the CKM matrix. This conclusion is already apparent when considering a basic effective field theory (EFT) approach [45, 46]. However, in order to describe a realistic model, constraints from all flavour observables have to be taken into account. An effective protection mechanism for FCNCs induced by higher dimensional operators is mandatory in this case. Solely a consideration of the elements $|V_{ub}|$ and $|V_{cb}|$ as done by the authors of [45, 46] is insufficient.

Previous attempts to analyse the possibility of RH currents clearly require an improved and updated analysis to check whether RH currents provide a sensible extension of the SM in accordance with all data. In this thesis, we will take a two-sided approach to this issue with emphasis on the well-measured FCNC observables, such as from particle-antiparticle mixing and rare decays. New experimental input from flavour precision experiments are expected soon from the LHCb experiment, and also from future B-factories such as SuperB. In particular, we consider the following two models:

The first approach we follow is a bottom-up approach, which we call Right-Handed Minimal Flavour Violation. Right-handed currents are incorporated through an effective theory approach under consideration of an extended MFV principle, which helps to protect the model against FCNCs automatically. Additionally, our studies go beyond the discussion of the $|V_{ub}|$ problem by considering various known tensions in SM flavour observables. To this end we analyse flavour observables, their constraints and correlations, and are able to make predictions for some of them. In particular we deduce the full RH mixing matrix, discuss its impact on $\Delta F = 2$ observables and various rare decays. This part of the thesis is based on [47, 48].

Subsequently, we discuss a top-down approach, the Left-Right Model. This model emerges from the concept of left-right symmetric models including all input parameters without simplifying assumptions. We allow for a breaking of parity in order to adopt a more general framework. Instead of focusing our analysis on lower bounds on the masses of heavy gauge bosons, we perform a full and simultaneous analysis of flavour observables, in particular $\Delta F = 2$ observables and the decay $B \to X_s \gamma$, under incorporation of all existing experimental constraints. We ask if these constraints can

be satisfied while keeping new heavy particles within the reach of the LHC. We also focus on a very general study of the RH mixing matrix and corresponding flavour effects. The question of flavour anomalies is also addressed in this context. These studies were published by us in [49].

The goals of this thesis can be summarised in the following questions:

- Do RH currents provide a realistic extension of the SM?

- Do they solve the existing tensions between flavour observables in the SM while satisfying all the existing bounds? In particular, can the new CP-violating phases cure the existing SM anomalies in CP-violating observables? And, can the $|V_{ub}|$ problem be solved?

- Can the new RH effects reach present experimental bounds?

- How far do the two approaches we follow overlap? Does the same RH mixing structure appear in both models?

- What is the structure of the RH mixing matrix?

We address these questions throughout the thesis, and summarise the answers at the end.

Outline

The present thesis is organised as follows. Chapter 2 is dedicated to the effective theory approach, called Right-Handed Minimal Flavour Violation. After a short introduction to recent anomalies, providing a main motivation of this setup and necessary basics, we give an extensive description of the model. To this end we consider in detail the particle content and the flavour symmetry. Subsequently we classify all relevant dimension-six operators and study the RH mixing matrix in detail. In this context we also show how the $|V_{ub}|$ problem can be solved. In chapter 3, we introduce the second model for RH currents considered in this thesis, termed the Left-Right Model. We briefly discuss the basic setup and explain in detail all relevant constraints from tree-level decays and electroweak precision observables necessary for a flavour analysis of the model. In chapter 4, we give a brief general overview of flavour observables for both $\Delta F = 2$ processes and rare decays. In particular, we introduce the general operator basis for the effective Hamiltonians and show a collection of general formulae, which allow for an efficient derivation of $\Delta F = 2$ observables. Furthermore, we review the present experimental status and compare the experimental values to those predicted in the SM. In chapter 5, we study the flavour phenomenology of Right-Handed Minimal Flavour Violation. First we focus on $\Delta F = 2$ observables. We derive Wilson coefficients and renormalisation group effects and study the impact on meson anti-meson mixing. In particular we investigate the question whether anomalies occurring within the SM can be resolved. In the case of $\Delta F = 1$ observables, we restrict our considerations to the decays $B_{s,d} \to \mu^+ \mu^-$, $B \to \{X_s, K, K^*\} \nu \bar{\nu}$, and $K \to \pi \nu \bar{\nu}$. In chapter 6, we take a closer look at the flavour phenomenology of the Left-Right Model. Following the general procedure we determine Wilson coefficients and renormalisation group effects in order to obtain the NP contributions to $\Delta F = 2$ observables. Moreover, we consider the decay $B \to X_s \gamma$ for the model in question. We also study in detail the impact of the heavy Higgs fields for both $\Delta F = 2$ processes and $B \to X_s \gamma$. We continue by describing the numerical strategy, specifying the parameter scan and the constraints imposed. Then we present an extensive discussion of our numerical results considering the RH mixing matrix, correlations among various observables and the $|V_{ub}|$ problem. We end the chapter with a new proposal for a simplified parametrisation of the RH mixing matrix, which would be able to resolve the anomalies of flavour observables existing in the SM. Chapter 7 is devoted to a comparison between the two models considered in this thesis. We also include additional comparisons to a two Higgs doublet model and the Randall Sundrum model with custodial protection. Such studies will help to distinguish between different NP models, once improved flavour data become available. Finally, in chapter 8 we conclude by summarising our results. Some additional information about the Left-Right Model, such as details about the Higgs sector, the gauge sector, a parameter counting and a comprehensive set of Feynman rules, are relegated to the appendices.

2. Right-handed currents: An effective field theory approach

This chapter is dedicated to the bottom-up approach to RH currents. This study is motivated by various recent flavour anomalies, in particular the $|V_{ub}|$ problem, which might be addressed by RH currents. In an effective field theory framework we first examine the structure of relevant dimension-six operators respecting a left-right flavour symmetry broken only by the Yukawa couplings. A new mixing matrix appears in the RH sector. One of the main goals of this chapter is a detailed determination of this matrix. We begin this chapter with a very brief overview of recent anomalies in the flavour data. Furthermore, we introduce necessary basic principles such as the concepts of effective field theory and Minimal Flavour Violation.

2.1. Preliminaries

2.1.1. Recent SM anomalies in the flavour sector

The study of flavour observables reveals anomalies and tensions in the SM. Many of these anomalies lie in the (2–3) σ region, so that for a clear confirmation of physics beyond the SM higher statistics will be necessary. Yet, they can provide information about where possible discrepancies with respect to the SM can appear. In this section we give a short summary of the recent phenomenological anomalies following the discussions of [50–55], where further information can be found. We restrict our considerations to issues relevant for our analysis.

The enhanced value of $S_{\psi\phi}$ - First we mention the possibility of a large enhancement over the SM value in CP violating observables in $B_s^0 - \bar{B}_s^0$ mixing, in particular in the time-dependent mixing-induced CP asymmetry $S_{\psi\phi}$ of the decay $B_s \to \psi\phi$. While the corresponding SM value is expected to be very small, roughly $S_{\psi\phi}^{\text{SM}} \simeq 0.038$ dependent on the choice of input parameters, this topic has attracted a lot of attention in the last years mainly induced by the direct measurement by CDF [56] and D0 [57] providing $S_{\psi\phi} = 0.81^{+0.12}_{-0.32}$ [58]. This hope was softened when higher statistics became available [53, 59, 60]. Still a value of $S_{\psi\phi}$ above 0.5 was not yet excluded [52]. Again new data from the Tevatron published in spring 2011, combined with the results from the measurement of the same sign dimuon asymmetry of the D0 experiment, allowed a

larger value of $S_{\psi\phi} \approx 0.8$ [61–63]. Consequently, at present the situation is quite confusing. Recent measurements by CDF and D0 [64,65] and the first even more accurate results of LHCb [66] imply significantly lower values, in particular [67]

$$-0.1 \le S_{\psi\phi} \le 0.4 \,, \tag{2.1}$$

being in accordance with the SM expectation. There is still room for NP, which can enter in $S_{\psi\phi}$ through new CP violating phases. We hope that in the future further precision data will help to clarify the situation.

Since during the considerations of the first model proposed in this thesis, a large $S_{\psi\phi}$ was still favoured we explored mainly this possibility, while in the second model considered here the analysis is much more general. In particular in the second approach we do not make use of $S_{\psi\phi}$ as an input, rather we obtain a prediction which can be compared to the data.

The $\varepsilon_K - S_{\psi K_S}$ anomaly - Next, we discuss the so called ε_K anomaly [68,69]. It describes the fact that the value of $|\varepsilon_K|$ given by the data deviates from the SM prediction, determined from the measured values of its components, e.g. from $\sin(2\beta)$, the ratio $\Delta M_d / \Delta M_s$ and the value of $|V_{cb}|$. After an update of input parameters from nonperturbative factors of unquenched lattice calculations [70], a suppression factor including the latest long-distance effects and departure of the phase ϕ_ε from $\pi/4$ [71] and finally NNLO-QCD effects [72], the updated SM value reads $|\varepsilon_K|_{\mathrm{SM}} = (1.81 \pm 0.28) \times 10^{-3}$ [73]. On the contrary, the experimental result is given by $|\varepsilon_K|^{\mathrm{exp}} = (2.229 \pm 0.010) \times 10^{-3}$ [74].

The above stated ε_K problem is closely linked with the $\varepsilon_K - S_{\psi K_S}$ tension of the SM [68,75,76]. As in the SM the CP asymmetry in the decay $B_d \to \psi K_S$ $S_{\psi K_S}$ is equal to $\sin(2\beta)$, one finds that in the SM $|\varepsilon_K|$ and $S_{\psi K_S}$ cannot simultaneously agree with the experimental data. The $\sin(2\beta)$ tension of the CKM fit is also confirmed by both the UTfit group [77] and the CKMfitter group [78]. They find a 2σ tension, where the unitarity triangle fit of $\sin(2\beta)$ is generally larger than the one extracted from experiment $S_{\psi K_S}^{\mathrm{exp}} = 0.672 \pm 0.023$ [79].

Possible impact of new CP violating phases - New physics can enter through new CP violating phases and modify both the relations for $S_{\psi K_S}$ and $S_{\psi\phi}$, in particular

$$S_{\psi K_S}(B_d) = \sin(2\beta + 2\varphi_{B_d}) \,, \qquad S_{\psi\phi}(B_s) = \sin(2|\beta_s| - 2\varphi_{B_s}) \,, \tag{2.2}$$

where φ_{B_d} and φ_{B_s} represent the NP phases and β and β_s can be extracted from elements of the CKM matrix (see section 4.2.2 for a detailed definition), and hence are governed by the CKM phase γ responsible for CP violation within the SM. Undoubtedly, new sources of CP violation play a crucial role when we want to explain deviations from the SM expectation in these observables. Furthermore, requiring that SM tensions become softened implies that we can obtain information about the possible structure

of NP. Considering as an example the $\varepsilon_K - S_{\psi K_S}$ anomaly, a negative phase φ_{B_d} turns out to be favourable, so that the true $\sin(2\beta)$ is larger implying a higher value for $|\varepsilon_K|$ [68,75]. It should be stressed that in this example in principle NP could also enter in $|\varepsilon_K|$. This situation will become more clear once more precise data on the CKM matrix, in particular the values of γ, $|V_{ub}|$ and $|V_{cb}|$ [68,69], will be available. These will be improved by LHCb and also Belle II and SuperB. As we will see later, for RH currents this $|V_{ub}|$ dependence is of particular interest.

The $|V_{ub}|$ problem - For completeness we want to mention briefly that within the SM framework different measurements of $|V_{ub}|$, in particular from inclusive decays and exclusive decays cannot be explained. Right-handed currents can potentially cure this problem [44–46], representing one of the main motivations of our analyses in this thesis. The $|V_{ub}|$ problem will be discussed in detail below.

2.1.2. Effective field theory

Our first model makes use of an effective theory approach, where the NP can be described by an effective Lagrangian with the SM as the low-energy EFT. The goal of this section is rather to clarify the notation for our further considerations than giving an introduction to EFT methods.

In general an effective field theory is characterised by an effective cut-off scale Λ below which the theory provides a good description. For low energy physics it turns out to be sufficient to consider only light degrees of freedom below the cut-off scale. The effects of the heavier degrees of freedom can be efficiently described by means of an effective Lagrangian

$$\mathcal{L}_{\text{eff}} = \mathcal{L}_{\text{SM}} + \sum \frac{c_i}{\Lambda^{n-4}} O_i^{(n)} \, , \qquad (2.3)$$

where $\mathcal{O}_i^{(n)}$ are dimension-n effective operators and c_i are dimensionless coefficients. The details of the underlying interactions at higher scales are then hidden in the coupling coefficients c_i. It turns out that only dimension-six operators are relevant for the discussion of FCNCs, and we will restrict to these in the following.

2.1.3. Minimal Flavour Violation

As stated above, a generic flavour structure is excluded at the TeV scale [1]. One possibility to keep the pattern of FCNCs under control is to make use of Minimal Flavour Violation (MFV) principle. As we will consider a modified mechanism of MFV in the first part of this thesis, let us briefly summarise the main points of the original MFV idea, following [2]. Since we are interested in quark flavour-changing dynamics, we will concentrate only on the quark flavour symmetry.

The SM gauge group commutes with the following global quark flavour symmetry

$$SU(3)_q^3 = SU(3)_{Q_L} \otimes SU(3)_{U_R} \otimes SU(3)_{D_R} \, , \qquad (2.4)$$

This global symmetry is already explicitly broken in the full SM Lagrangian by the Yukawa interactions. The full flavour invariance can in principle be formally recovered by the introduction of the two spurions

$$Y_u \sim (3, \bar{3}, 1)_{\mathrm{SU}(3)_q^3} \ , \qquad Y_d \sim (3, 1, \bar{3})_{\mathrm{SU}(3)_q^3} \ , \qquad (2.5)$$

where the transformation properties are given with respect to equation (2.4). These spurions encode then the full information about the SM flavour symmetry breaking. Using an EFT approach in order to describe a NP model, the higher dimensional operators can be written in terms of flavour invariant combinations of these spurions and SM fields. The implementation of no further sources of flavour symmetry breaking allows to naturally suppress the dangerous appearance of FCNCs effectively and is independent of the specific structure of the NP model. In MFV the CKM matrix is the only source of flavour violation. In the original setup no additional flavour blind phases were included, hence CP violation was also entirely described by the CKM phase.

Recent studies often include such new flavour-blind CP-violating phases [80–82], which are not contradictory to the original MFV principle. This is especially due to the fact that without new sources of CP violation one can immediately conclude that $S_{\psi\phi}$ is expected to be SM like and consequently if large $S_{\psi\phi}$ was confirmed by higher statistics then MFV models would be automatically excluded.

Note that the MFV approach is not to be confused with the constrained MFV version [5,6], where in contrast to the MFV approach the contributing operators are restricted to the ones already present in the SM.

2.2. Right-Handed Minimal Flavour Violation setup

2.2.1. Symmetry and particle content

In this section we describe the details of the model which is the focus of this chapter. In Right-Handed Minimal Flavour Violation (RHMFV) introduced by us in [47], we consider an effective theory approach in the spirit of [2]. However we generalise MFV by including right-handed currents. The SM with its different treatment of left- and right-handed currents appears after symmetry breaking as a low-energy limit of a more fundamental theory which is assumed to be left-right symmetric. The main assumption is then made by choosing a left-right symmetric flavour symmetry $SU(3)_L \times SU(3)_R$ which is broken just by the Yukawas, similar to the MFV case. In this approach the fundamental theory is not specified, and we only make assumptions about the global symmetry and the pattern of its breaking. In order to obtain the minimal model, the SM gauge group is embedded into a global $SU(2)_L \times SU(2)_R \times U(1)_{B-L}$ group, which we call the electroweak symmetry. Only the $SU(2)_L$ and $U(1)_Y$ subgroups are effectively gauged below the TeV scale. Let us stress that the global electroweak symmetry might stem from a local gauge group, but for our EFT approach there is no need to

make additional specifications.

In figure 2.1 we compare our model with respect to MFV. RHMFV is clearly beyond MFV if considered in comparison to the $SU(3)_q^3$ quark flavour symmetry of MFV as given in (2.4). This is because the extended flavour group of RHMFV allows for a bigger set of operators. These contribute to flavour violating processes as discussed in detail below. However since the LR symmetric flavour group is only broken by the Yukawas RHMFV is in analogy with the MFV framework.
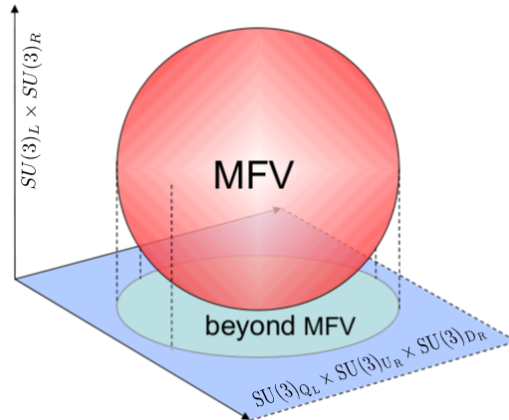
Figure 2.1.: A schematic depiction of RHMFV.

Let us now take a closer look at the field content of the RHMFV model.

Quark fields The quark fields,

$$Q_L^i = \begin{pmatrix} u_L^i \\ d_L^i \end{pmatrix} \sim (2,1)_{1/3} \; , \qquad Q_R^i = \begin{pmatrix} u_R^i \\ d_R^i \end{pmatrix} \sim (1,2)_{1/3} \; , \qquad i = 1\ldots3 \; , \quad (2.6)$$

given here with their transformation properties under the electroweak symmetry, form three LH and RH doublets with generation index i. The SM hypercharge is then given by $Y = T_{3R} + (B-L)/2$. In principle, leptons, including RH neutrinos, can be introduced in an analogous way (with assigning the $B-L$ charge to be $B-L = -1$). However, we restrict our analysis to the quark case, since the mass of the RH neutrinos is large enough to not contribute to the processes analysed below.

The Higgs field The electroweak symmetry breaking is achieved by the vacuum expectation value of a SM-like Higgs field, in particular,

$$H \sim (2,\bar{2})_0 \; , \qquad \langle H \rangle = \begin{pmatrix} v & 0 \\ 0 & v \end{pmatrix} \; , \qquad (2.7)$$

which breaks $SU(2)_L \times SU(2)_R$ spontaneously down to the custodial symmetry $SU(2)_{L+R}$ at the electroweak scale. Such a simple scalar structure is chosen as we want to stay within a minimal model. Note that main parts of the following analysis can also be applied to models with a more complicated Higgs sector or even Higgless models, when the electroweak symmetry has the $SU(2)_L \times SU(2)_R \to SU(2)_{L+R}$ breaking pattern. For example, such an extended Higgs sector is required in explicit left-right models. In the Higgless case, following the arguments in [83], the Higgs field H can be re-written as a product of the real part including the VEV v and a unitary matrix U encoding the Goldstone bosons.

Gauge bosons Our effective model contains only the SM electroweak gauge bosons W and Z. We introduce the kinetic term

$$\mathcal{L}_{\text{Higgs}}^{\text{kin}} = \frac{1}{4} \text{Tr}[(D_\mu H)^\dagger D^\mu H] \ , \tag{2.8}$$

where the covariant derivative reads $D_\mu H = \partial_\mu H - ig W_\mu^a T_a H + ig' H T_3 B_\mu$. The standard tree-level expressions for the W and Z masses are recovered for $v \approx 246$ GeV.

Note that we have adopted the convention for the normalisation of the Higgs field which is usually used in composite Higgs models. The Higgs field appears then in the following form

$$H = \sqrt{2} \begin{pmatrix} \phi^{0\star} & \phi^+ \\ -\phi^- & \phi^0 \end{pmatrix} . \tag{2.9}$$

Although we will not use this explicit form when considering RHMFV, it should help to clarify the notation when considering an explicit left-right model.[1]

In summary, we only have SM fields with a single effective light Higgs. Heavy fields do not appear explicitly but affect higher dimensional operators.

2.2.2. Yukawa couplings and flavour invariance

In addition to the above started particles, two spurions

$$P_{u(d)} \sim (1,3)_0 \tag{2.10}$$

are required in order to generate different masses for up- and down-type quarks and break the custodial $SU(2)_{L+R}$ symmetry. Their background values are given by

$$P_u = \begin{pmatrix} 1 & 0 \\ 0 & 0 \end{pmatrix} , \qquad P_d = \begin{pmatrix} 0 & 0 \\ 0 & 1 \end{pmatrix} . \tag{2.11}$$

---

[1] This convention differs from the one chosen in the explicit left-right model in the second part of this thesis.

Under the electroweak symmetry we obtain the following invariant quark Yukawa coupling

$$\mathcal{L}_{\mathrm{Y}} = \frac{1}{\sqrt{2}} \left(\bar{Q}_L Y_u H P_u Q_R + \bar{Q}_L Y_d H P_d Q_R \right) + \mathrm{h.c.} \; . \tag{2.12}$$

$\mathcal{L}_{\mathrm{Y}}$ is equivalent to the SM Yukawa coupling taking into account the structure of P_u and P_d. Finally, we assume an additional $U(1)$ symmetry, under which Y_u and Y_d have different charges, and P_u and P_d have the corresponding opposite charges.

So far we have not discussed the quark flavour symmetry. Under the left-right symmetric flavour symmetry $SU(3)_L \times SU(3)_R$ the quarks form triplets according to the following transformation properties

$$\begin{aligned} Q_L &\rightarrow f_L Q_L & \text{with} && f_L &\in SU(3)_L \,, \\ Q_R &\rightarrow f_R Q_R & \text{with} && f_R &\in SU(3)_R \,. \end{aligned} \tag{2.13}$$

$SU(3)_L \times SU(3)_R$ becomes an exact global symmetry of the full Lagrangian in the limit of $Y_{u(d)} \rightarrow 0$. The flavour invariance can be formally recovered by introducing spurions for $Y_{u(d)}$, both transforming as $(3, \bar{3})$ under $SU(3)_L \times SU(3)_R$:

$$Y_{u(d)} \rightarrow f_L \; Y_{u(d)} \; f_R^\dagger \; . \tag{2.14}$$

As Q_L and Q_R can be rotated in flavour space, it is always possible to choose a basis where one of the Yukawa couplings is diagonal. Furthermore this diagonal matrix can be made real by rotation of the relative phases of the quark fields. We obtain for a diagonal Y_d

$$Y_d \big|_{d-\mathrm{base}} = \lambda_d \,, \qquad \lambda_d = \frac{\sqrt{2}}{v} \mathrm{diag}(m_d, m_s, m_b) \equiv \mathrm{diag}(y_d, y_s, y_b) \,,$$

$$Y_u \big|_{d-\mathrm{base}} = V^\dagger \lambda_u \widetilde{V}, \qquad \lambda_u = \frac{\sqrt{2}}{v} \mathrm{diag}(m_u, m_c, m_t) \equiv \mathrm{diag}(y_u, y_c, y_t) \,, \tag{2.15}$$

where V and $\widetilde{V}$ are both unitary and complex 3×3 mixing matrices. While V denotes the CKM matrix as usual, an additional matrix $\widetilde{V}$ appears controlling the flavour mixing in the RH sector. A detailed analysis of $\widetilde{V}$ will be deferred to section 2.4. After setting the Higgs to its VEV the mass terms are generated

$$\mathcal{L}_{\mathrm{Y}}^{\mathrm{mass}} = \frac{v}{\sqrt{2}} \bar{u}_L V^\dagger \lambda_u \widetilde{V} u_R + \frac{v}{\sqrt{2}} \bar{d}_L \lambda_d d_R + \mathrm{h.c.} \tag{2.16}$$

In this basis in the down sector the mass term is already diagonal, and hence

$$d_L \rightarrow d'_L = d_L \,, \qquad d_R \rightarrow d'_R = d_R \,, \tag{2.17}$$

in the up sector the following diagonalisation is necessary:

$$u_L \rightarrow u'_L = V u_L \,, \qquad u_R \rightarrow u'_R = \widetilde{V} u_R \; . \tag{2.18}$$

The quark mass eigenstates are denoted by the primed fields. The quark mass matrices are given by $M_u = v \lambda_u$ and $M_d = v \lambda_d$.

2.3. The impact of dimension-six operators

2.3.1. Yukawa insertions

We proceed by building the effective Lagrangian as described in section 2.1.2. For this purpose all dimension-six operators formally invariant under the LR symmetric flavour group have to be constructed. In this manner, the so called Yukawa insertions emerge. The Yukawa insertions encode the flavour dynamics of the high scale. Due to this specific parametrisation, the flavour symmetry breaking can only take place through sources already inherent in the Yukawas. For example under the $SU(3)_L \times SU(3)_R$ flavour group the up-insertions transform according to $Y_u Y_u^\dagger \sim (8,1)$ and $Y_u^\dagger Y_u \sim (1,8)$. These insertions can be evaluated in our basis where the down Yukawa is already diagonal. We obtain

$$(Y_u Y_u^\dagger)_{i\neq j} \big|_{d-\text{base}} = (V^\dagger \lambda_u^2 V)_{ij} \approx y_t^2 V_{3i}^* V_{3j} , \tag{2.19}$$

$$(Y_u^\dagger Y_u)_{i\neq j} \big|_{d-\text{base}} = (\widetilde{V}^\dagger \lambda_u^2 \widetilde{V})_{ij} \approx y_t^2 \widetilde{V}_{3i}^* \widetilde{V}_{3j} . \tag{2.20}$$

In the last step it has been used that only the top quark has a large Yukawa coupling, hence $\lambda_u \approx \text{diag}(0,0,y_t)$. For the same reason down-insertions give rise to a very small effect and will be neglected in the following.

2.3.2. Collection of bilinears

In order to study the relevance of possible dimension-six operators, we first collect all quark bilinear currents compatible with the LR symmetric flavour symmetry. It is sufficient to consider terms with at most two spurions. Denoting the Dirac structure by Γ, the bilinears are given by

$$\mathcal{O}(Y^0): \qquad \bar{Q}_L \Gamma Q_L , \qquad\qquad \bar{Q}_R \Gamma Q_R , \tag{2.21}$$

$$\mathcal{O}(Y^1): \qquad \bar{Q}_L \Gamma Y_u P_u Q_R , \qquad \bar{Q}_L \Gamma Y_d P_d Q_R , \tag{2.22}$$

$$\mathcal{O}(Y^2): \qquad \bar{Q}_L \Gamma Y_u Y_u^\dagger Q_L , \qquad \bar{Q}_R \Gamma Y_u^\dagger Y_u Q_R . \tag{2.23}$$

Note that we already neglected the down-insertions $Y_d Y_d^\dagger$ and $Y_d^\dagger Y_d$ as stated before. Most of these bilinear structures are already known from the MFV framework [2]. For example the $\bar{Q}_R \Gamma Y_u Y_u^\dagger Q_R$ bilinear will appear in LH mediated FCNCs. The new effects arise mainly from two bilinears:

1. $\bar{Q}_R \Gamma Q_R$ with its charged-current component

2. $\bar{Q}_R \Gamma Y_u^\dagger Y_u Q_R$ with its neutral-current component

In the second case the Yukawa insertion $Y_u^\dagger Y_u$ characterises the strength of RH mediated FCNCs and contains elements of a new RH mixing matrix $\widetilde{V}$. We will focus within this thesis on the effects of these bilinears.

2.3.3. Charged current operators

We first investigate the list of operators which affect charged currents and will help us to probe the rotation in the RH sector. We restrict our discussion to operators involving two quark fields as only these will be relevant for our phenomenology of right-handed charged currents. They are given by

$$O_{R\ell1}^{(6)} = \bar{Q}_R \gamma^\mu \tau_i Q_R \; \bar{L}_L \gamma_\mu \tau^i L_L \; ,$$

$$O_{Rh1}^{(6)} = i \bar{Q}_R \gamma^\mu H^\dagger D_\mu H Q_R \; , \qquad O_{Rh2}^{(6)} = i \bar{Q}_R \gamma^\mu \tau_i Q_R \; \mathrm{Tr}\left(H^\dagger D_\mu H \tau^i\right) \; , \quad (2.24)$$

where τ_i are the Pauli matrices. Specifically it turns out that for our analysis lepton-quark charged currents play the leading role. In this case all three operators of equation (2.24) are equally important. We do not consider RH neutrinos under the assumption that they are heavy.

In principle, one also has to take into account analogous operators formed from the bilinears of equations (2.22)–(2.23). These however can safely be neglected due to the smallness of the Yukawa couplings as long as only up-type quarks of the first two generations contribute to the decay processes analysed below.

2.3.4. $\Delta F = 2$ operators

We now turn to dimension-six operators which contribute to $\Delta F = 2$ processes such as particle-antiparticle mixing. Here we just list the relevant operators, a detailed discussion of the phenomenology can be found in chapter 5. Using the bilinears of equations (2.22)–(2.23) various combinations can be found which contribute. However as we only want to extract the pattern of the flavour phenomenology of the model, a detailed analysis of all possible operators is beyond the scope of this work. Instead, in order to keep both the notation and structure minimal, we restrict ourselves to the operators giving the main contributions. The list of operators then reads

$$O_{LL}^{(6)} = [\bar{Q}_L^i (Y_u Y_u^\dagger)_{ij} \gamma_\mu Q_L^j]^2 \; , \tag{2.25}$$

$$O_{RR}^{(6)} = [\bar{Q}_R^i (Y_u^\dagger Y_u)_{ij} \gamma_\mu Q_R^j]^2 \; , \tag{2.26}$$

$$O_{LR}^{(6)} = [\bar{Q}_L^i (Y_u Y_u^\dagger)_{ij} \gamma^\mu Q_L^j][\bar{Q}_R^i (Y_u^\dagger Y_u)_{ij} \gamma_\mu Q_R^j] \; . \tag{2.27}$$

The first operator and its effects are well known from both MFV [2] and its constrained version [5]. From equation (2.19) one can immediately see that the CKM pre-factor is analogous to the $\Delta F = 2$ contribution in the SM. Moreover, the helicity structure is also in accordance with the SM. Consequently, $O_{LL}^{(6)}$ will not lead to modifications in CP violating observables with respect to the SM. On the contrary, interesting effects are expected from $O_{RR}^{(6)}$ and $O_{LR}^{(6)}$, not only though the input of the RH mixing matrix but also due to the LR structure which is known to renormalise strongly under renormalisation group effects.

Guided by these expectations, we will concentrate on the latter two operators in our further analysis of $\Delta F = 2$ processes.

2.3.5. $\Delta F = 1$ operators

As before, among $\Delta F = 1$ operators, we focus on the leading contributions to $\Delta F = 1$ operators. These are given by the following operators

$$
\begin{aligned}
O_{RZ1}^{(6)} &= i\bar{Q}_R^i (Y_u^\dagger Y_u)_{ij} \gamma^\mu H^\dagger D_\mu H Q_R^j \,, \\
O_{RZ2}^{(6)} &= i\bar{Q}_R^i (Y_u^\dagger Y_u)_{ij} \gamma^\mu \tau_i Q_R^j \, \text{Tr} \left(H^\dagger D_\mu H \tau^i \right) \,.
\end{aligned}
\tag{2.28}
$$

In addition the corresponding LH operators can also be present, obtained through the replacements $Q_R \to Q_L$ and $Y_u \leftrightarrow Y_u^\dagger$ from equation (2.28). These have been studied widely within the MFV framework. The new operators give rise to effective right-handed flavour non-universal couplings of the Z boson to down-type quarks. These affect $Z \to b\bar{b}$ and rare K and B decays. We postpone a detailed analysis to chapter 5.

So far we have concentrated on operators with two quarks and two Higgs fields. In principle, operators with two quarks and two lepton fields also have to be included. However, they will not lead to new effects compared to equation (2.28) after the Z boson has been integrated out. We will demonstrate this with an example of the effective quark-lepton charged current below. There is also a third class of dipole-type operators with two quarks and one SM gauge field which we do not consider further in this thesis.

In summary, we will restrict ourselves to the analysis of the operators collected in equation (2.28).

2.4. The right-handed mixing matrix

2.4.1. The parametrisation

As stated in section 2.2.2 the matrix $\widetilde{V}$ appears due to misalignment between the Yukawas in the up- and down-type sector and controls the RH flavour mixing. Let us now review in detail how this matrix can be determined. We start with its parametrisation, which can be chosen as

$$
\widetilde{V} = D_U \widetilde{V}_0 D_D^\dagger \,,
\tag{2.29}
$$

where $\widetilde{V}_0$ is a CKM like matrix and $D_{U,D}$ are two diagonal matrices, in particular

$$
D_U = \text{diag}(1, e^{i\phi_2^u}, e^{i\phi_3^u}) \,, \qquad D_D = \text{diag}(e^{i\phi_1^d}, e^{i\phi_2^d}, e^{i\phi_3^d}) \,.
\tag{2.30}
$$

These phases are physical since we have used the freedom to rotate phases of quark fields in order to get rid of unphysical phases in the CKM matrix. In $\widetilde{V}_0$ we shift the phase from 1–3 mixing to 2–3 mixing as we will assume small phases except the phase for $\widetilde{V}_{ub}$. This will become more clear when we analyse the bounds from $b \to u$ transitions in the next section. Then $\widetilde{V}_0$ reads

$$
\widetilde{V}_0 = \begin{pmatrix}
\tilde{c}_{12}\tilde{c}_{13} & \tilde{s}_{12}\tilde{c}_{13} & \tilde{s}_{13} \\
-\tilde{s}_{12}\tilde{c}_{23} - \tilde{c}_{12}\tilde{s}_{23}\tilde{s}_{13}e^{-i\phi} & \tilde{c}_{12}\tilde{c}_{23} - \tilde{s}_{12}\tilde{s}_{23}\tilde{s}_{13}e^{-i\phi} & \tilde{s}_{23}\tilde{c}_{13}e^{-i\phi} \\
-\tilde{c}_{12}\tilde{c}_{23}\tilde{s}_{13} + \tilde{s}_{12}\tilde{s}_{23}e^{i\phi} & -\tilde{s}_{12}\tilde{c}_{23}\tilde{s}_{13} - \tilde{s}_{23}\tilde{c}_{12}e^{i\phi} & \tilde{c}_{23}\tilde{c}_{13}
\end{pmatrix} \,.
\tag{2.31}
$$

In total, the RH mixing matrix $\widetilde{V}$ altogether contains three new real mixing angles and six new complex phases. It is restricted by various bounds, in particular from charged current data, unitarity and FCNC phenomenology, which we discuss in detail.

2.4.2. Bounds from charged currents

Using data on tree-level charged current transitions, we can set bounds on elements of the RH mixing matrix $\widetilde{V}_0$. In this section we investigate various tree-level decays based on quark-lepton charged currents, which allow us to extract these bounds in the cleanest way. The related impact on the CKM matrix V will also be discussed.

The effective quark-lepton charged current

With the operators defined in equation (2.24) we can derive the effective coupling of the RH current. After the breaking of the electroweak symmetry the operators $O^{(6)}_{R_{hi}}$ contribute via tree-level diagrams with internal W boson exchange. Evaluating $O^{(6)}_{R_{\ell 1}}$ is straightforward. Integrating out the W boson and summing over all contributions leads to an effective RH coupling: $c_R = -2(c_{R_{h1}} + 2c_{R_{h2}} - c_{R_{\ell 1}})$. The resulting effective quark-lepton charged current interaction can be written as

$$\mathcal{L}^{c.c.}_{\text{eff}} = \left(-\frac{g^2}{2M_W^2} + \frac{c_L}{\Lambda^2} \right) \bar{u}_L \gamma^\mu d_L \, \bar{\ell}_L \gamma_\mu \nu_L + \frac{c_R}{\Lambda^2} \, \bar{u}_R \gamma^\mu d_R \, \bar{\ell}_L \gamma_\mu \nu_L \; + \; \text{h.c.} . \qquad (2.32)$$

The coefficient c_L parametrises the modification of the LH interaction obtained from equation (2.24) with the replacement $Q_R \to Q_L$. The SM result is then recovered in the limit $c_L = c_R = 0$.

We proceed by performing the rotation to mass eigenstates of the quark fields by using equations (2.17) and (2.18) and additionally omit the prime indices in order to keep a simple notation. The result reads

$$\mathcal{L}^{c.c.}_{\text{eff}} = -\frac{4G_F}{\sqrt{2}} \, \bar{u}\gamma^\mu \left[(1 + \epsilon_L) V P_L + \epsilon_R \widetilde{V} P_R \right] d \, (\bar{\ell}_L \gamma_\mu \nu_L) \; + \; \text{h.c.} \qquad (2.33)$$

where

$$P_L = \frac{1 - \gamma_5}{2} \, , \qquad P_R = \frac{1 + \gamma_5}{2} \, , \qquad (2.34)$$

are the left and right projection operators and

$$\epsilon_R = -\frac{c_R v^2}{2\Lambda^2} = \frac{v^2}{\Lambda^2}(c_{R_{h1}} + 2c_{R_{h2}} - c_{R_{\ell 1}}) \, , \qquad \epsilon_L = -\frac{c_L v^2}{2\Lambda^2} \qquad (2.35)$$

are the effective couplings, which will be important for the analysis of this section. At this stage we should stress that elements of $\widetilde{V}$ and ϵ_R appear always in combination. As a result it is impossible to disentangle the sign and phase of ϵ_R and $\widetilde{V}_{ub}$, hence we

define ϵ_R to be real and positive.

Strategy for determination of the effective CKM elements

From the effective charged current Lagrangian (2.33) the branching ratios for the decays in question can be derived. The left and right operators in $\mathcal{L}_{\text{eff}}^{\text{c.c.}}$ do not mix through renormalisation group effects as QED and QCD both respect chiral symmetry. Hence they can be multiplicatively renormalised in the same way and radiative corrections can be implemented straightforwardly using SM results.

We do not compare directly the branching ratios with the experimental value to extract the bounds on the elements of $\widetilde{V}_0$ and V. Instead we make use of the CKM element extracted from the comparison of the SM result and the experimental value defined as $|V_{ij}|_{\text{SM}}^{\text{exp}}$. We compare this CKM element to our effective combination including the RH current contribution. This allows us to find the "true" values of the elements of $\widetilde{V}_0$ and V in an elegant way.

Bounds from $u \to d$ and $u \to s$ transitions

We start by describing the bounds on $|V_{ud}|$ making use of the constraints from super-allowed ($0^+ \to 0^+$) nuclear beta decays and by the pion decay $\pi \to e\nu$ [74]:

$$|V_{ud}(0^+ \to 0^+)|_{\text{SM}}^{\text{exp}} = 0.97425(022) , \qquad (2.36)$$

$$|V_{ud}(\pi \to e\nu)|_{\text{SM}}^{\text{exp}} = 0.97410(260) . \qquad (2.37)$$

While super-allowed nuclear beta decays are only sensitive to the $u \to d$ vector current, the pion decay is solely dependent on the $u \to d$ axial current. This implies that we can immediately impose the following conditions

$$\left| (1 + \epsilon_L) V_{ud} + \epsilon_R \widetilde{V}_{ud} \right| = |V_{ud}(0^+ \to 0^+)|_{\text{SM}}^{\text{exp}} , \qquad (2.38)$$

$$\left| (1 + \epsilon_L) V_{ud} - \epsilon_R \widetilde{V}_{ud} \right| = |V_{ud}(\pi \to e\nu)|_{\text{SM}}^{\text{exp}} . \qquad (2.39)$$

These two equations can be solved for combinations of $(1 + \epsilon_L) V_{ud}$ and $\epsilon_R \widetilde{V}_{ud}$. As $\epsilon_{L,R}$ are expected to be small, we can use them as expansion parameters with $\epsilon_{L,R} \ll 1$, assuming they are real. Without making additional assumptions on the phases of $\widetilde{V}_{ud}$, at first order in $\epsilon_{L,R}$ we get

$$|(1 + \epsilon_L) V_{ud}| = 0.9742 \pm 0.0013 , \qquad \epsilon_R \, \text{Re} \left(\frac{\widetilde{V}_{ud}}{V_{ud}} \right) = (0.1 \pm 1.3) \times 10^{-3} . \quad (2.40)$$

A completely analogous argument holds for the extraction of the bounds from $s \to u$ transitions. Here, $K \to \pi\ell\nu$ and $K \to \mu\nu$ decays are only sensitive to the vector and

the axial current, respectively. The SM results are given by [84],

$$|V_{us}(K \to \pi\ell\nu)|^{\text{exp}}_{\text{SM}} = 0.2243(12) , \tag{2.41}$$

$$|V_{us}(K \to \mu\nu)|^{\text{exp}}_{\text{SM}} = 0.2252(13) , \tag{2.42}$$

Pursuing the strategy presented above the two conditions can be written as

$$\left|(1 + \epsilon_L)V_{us} + \epsilon_R \widetilde{V}_{us}\right| = |V_{us}(K \to \pi\ell\nu)|^{\text{exp}}_{\text{SM}} , \tag{2.43}$$

$$\left|(1 + \epsilon_L)V_{us} - \epsilon_R \widetilde{V}_{us}\right| = |V_{us}(K \to \mu\nu)|^{\text{exp}}_{\text{SM}} , \tag{2.44}$$

with the following solutions

$$|(1 + \epsilon_L)V_{us}| = 0.2248 \pm 0.0009 , \qquad \epsilon_R \, \text{Re}\left(\frac{\widetilde{V}_{us}}{V_{us}}\right) = -(2.0 \pm 3.9) \times 10^{-3} . \tag{2.45}$$

Determination of ϵ_L

In the next step we make use of the CKM unitarity relation

$$|V_{ud}|^2 + |V_{us}|^2 + |V_{ub}|^2 = 1 \tag{2.46}$$

in order to determine the parameter ϵ_L. It can be easily deduced that

$$\epsilon_L = \left[(1 + \epsilon_L)^2(|V_{ud}|^2 + |V_{us}|^2 + |V_{ub}|^2)\right]^{1/2} - 1 . \tag{2.47}$$

Since $|V_{ub}| = \mathcal{O}(10^{-3})$ appears quadratically, its contribution to CKM unitarity is negligible and we can simplify $|V_{ud}|^2 + |V_{us}|^2 = 1 + \mathcal{O}(10^{-4})$. Hence adding the constraints for $|(1 + \epsilon_L)V_{ud(s)}|$ given in equations (2.40) and (2.45) yields

$$\epsilon_L = (0.2 \pm 1.2) \times 10^{-3} . \tag{2.48}$$

This allows us to eliminate ϵ_L from equations (2.40) and (2.45) and we obtain the following results

$$|V_{ud}| = 0.9742 \pm 0.0013 , \qquad \epsilon_R \, \text{Re}(\widetilde{V}_{ud}) = (0.1 \pm 1.3) \times 10^{-3} , \tag{2.49}$$

$$|V_{us}| = 0.2248 \pm 0.0009 , \qquad \epsilon_R \, \text{Re}(\widetilde{V}_{us}) = -(0.5 \pm 0.9) \times 10^{-3} . \tag{2.50}$$

As stated by [85] in their analysis of RH currents in semileptonic K decays, for $\epsilon_R = \mathcal{O}(10^{-3})$ these results do not imply small mixing angles among the first two generations in the RH sector.

Due to the smallness of ϵ_L, we neglect it in our further analysis. This is perfectly justified as the best experimental measurements of $b \to c$ and $b \to u$ transitions have

errors of at least $\mathcal{O}(1\%)$.

Bounds from $b \to c$ transitions

We now briefly review the formulas necessary for $b \to c$ transitions. First we take a look at inclusive decay $B \to X_c \ell \nu_\ell$. Recall that in case of inclusive decays the matrix element consists of a sum of a LH and a RH contribution. This has to be squared in order to obtain the decay rate, so that a non-trivial mixing between left and right-handed contribution is generated. It is possible to apply the procedure of comparing this combination to the SM result as stated above. The result reads

$$\left(|V_{cb}|_{\text{SM-exp}}^{\text{incl}}\right)^2 = |V_{cb}|^2 \left[1 + |\epsilon_R|^2 \left|\frac{\widetilde{V}_{cb}}{V_{cb}}\right|^2 - r_{\text{int}} \, \text{Re}\left(\epsilon_R \frac{\widetilde{V}_{cb}}{V_{cb}}\right)\right] , \qquad (2.51)$$

where [86]

$$|V_{cb}|_{\text{SM-exp}}^{\text{incl}} = (41.54 \pm 0.73) \times 10^{-3} . \qquad (2.52)$$

The strength of interference is given by

$$r_{\text{int}} = 16 \frac{m_c}{m_b} \frac{h(\frac{m_c}{m_b})}{f(\frac{m_b}{m_c})} , \qquad (2.53)$$

with $f(x) = 1 - 8x^2 + 8x^6 - x^8 - 24x^4 \log x$ and $h(x) = 1 - 3x^2 + 3x^4 + x^6 + 6(x^2 + x^4) \log x$. The numerical value $r_{\text{int}} = 0.97 \times 10^{-3}$, shows that RH currents have little impact on inclusive decays. This is in agreement with [46].

The exclusive decays $B \to D^* \ell \nu_\ell$ and $B \to D \ell \nu_\ell$ can be used to elaborate two further conditions for the determination of V_{cb} and $\epsilon_R \widetilde{V}_{cb}$, respectively. It turns out that the differential decay rate is a more useful quantity as it has been studied by various experiments [87]. Furthermore, a simple description is provided by considering the heavy-quark limit. Instead of two and four form factors respectively, one form factor, the Isgur-Wise function, is sufficient to describe the long distance contributions from the hadronic matrix elements. For completeness we show the SM differential decay rates [88]:

$$\frac{d\Gamma(\bar{B} \to D^* \ell \bar{\nu}_\ell)}{dw} = \frac{G_F^2}{48\pi^3} |V_{cb}^{\text{SM}}|^2 m_{D^*}^3 (w^2 - 1)^{1/2} P(w) |\mathcal{F}(w)|^2 , \qquad (2.54)$$

$$\frac{d\Gamma(\bar{B} \to D \ell \bar{\nu}_\ell)}{dw} = \frac{G_F^2}{48\pi^3} |V_{cb}^{\text{SM}}|^2 (m_B + m_D)^2 m_D^3 (w^2 - 1)^{3/2} |\mathcal{G}(w)|^2 , \quad (2.55)$$

where the variable $w = E_{D^{(*)}}/m_{D^{(*)}}$ in the rest frame of the B meson. $\mathcal{F}(w)$ and $\mathcal{G}(w)$ are the hadronic form factors and $P(w)$ denotes the phase space factor. At the zero-recoil point $(w = 1)$, where the momentum transfer to the leptons is at its maximum, we have $P(1) = 12(m_B - m_{D^*})^2$. The products $\mathcal{F}(1)|V_{cb}|$ and $\mathcal{G}(1)|V_{cb}|$ can be determined

with high accuracy from a fit to the measured recoil spectrum after expanding the hadronic form factors around $w = 1$, in particular [86],

$$\mathcal{F}(1)|V_{cb}|_{\text{SM-exp}}^{B \to D^*} = (35.41 \pm 0.52) \times 10^{-3} \,, \tag{2.56}$$

$$\mathcal{G}(1)|V_{cb}|_{\text{SM-exp}}^{B \to D} = (42.4 \pm 1.6) \times 10^{-3} \,. \tag{2.57}$$

In the heavy-quark limit only axial and vectorial contributions are involved in the rates of $B \to D^* \ell \nu_\ell$ and $B \to D \ell \nu_\ell$, respectively. Hence our conditions read

$$|V_{cb}|_{\text{SM-exp}}^{B \to D^*} = |V_{cb} - \epsilon_R \widetilde{V}_{cb}| \,, \tag{2.58}$$

$$|V_{cb}|_{\text{SM-exp}}^{B \to D} = |V_{cb} + \epsilon_R \widetilde{V}_{cb}| \,. \tag{2.59}$$

In order to proceed we have to specify the values of the form factors at $w = 1$. In general $\mathcal{F}(1)$ and $\mathcal{G}(1)$ can be determined in two ways [87]:

- Heavy quark symmetry yields the normalisation $\mathcal{F}(1) = 1$, but short distance radiative corrections and symmetry breaking effects must be taken into account. This can be analysed in a controlled way within heavy quark expansion and heavy quark effective theory.

- However, a second method using lattice calculations allows us to also consider effects from finite quark masses.

Using the lattice method leads to $\mathcal{G}(1) = 1.074 \pm 0.018 \pm 0.0016$ [89], $\mathcal{F}(1) = 0.921 \pm 0.013 \pm 0.0020$ [90], and hence one can deduce

$$|V_{cb}|_{\text{SM-exp}}^{B \to D} = (39.4 \pm 1.7) \times 10^{-3} \,, \qquad |V_{cb}|_{\text{SM-exp}}^{B \to D^*} = (38.3 \pm 1.2) \times 10^{-3} \,. \tag{2.60}$$

A global fit to V_{cb} and $\epsilon_R \widetilde{V}_{cb}$ using the three constraints in equations (2.52), (2.58), and (2.59) is subsequently performed, we then obtain the following results

$$|V_{cb}| = (40.7 \pm 0.6) \times 10^{-3}, \qquad \epsilon_R \, \text{Re}\left(\frac{\widetilde{V}_{cb}}{V_{cb}}\right) = (2.5 \pm 2.5) \times 10^{-2} \tag{2.61}$$

and the final result

$$\epsilon_R \, \text{Re}(\widetilde{V}_{cb}) = (1.0 \pm 1.0) \times 10^{-3} \,. \tag{2.62}$$

The best fit solution with $\chi^2/N_{\text{dof}} = 4.3$ shows that RH currents cannot provide an explanation for the different values of V_{cb} within the different determinations. This was expected as both exclusive values in equation (2.60) are below the inclusive one. It was already pointed out by [91] that the inconsistency of data between the different determinations of V_{cb} could emerge from an overestimate of $\mathcal{G}(1)$ on the lattice. [91] suggests a lowered value of $\mathcal{G}(1) = 0.86$. Repeating the fit with the same error gives a much better fit, $\chi^2/N_{\text{dof}} = 0.9$, with the result for $\epsilon_R \, \text{Re}(\widetilde{V}_{cb})$ lying perfectly in the range of equation (2.62). For this reason we keep the value obtained in equation (2.62)

for the following analysis.

Bounds from $b \to u$ transitions

In analogy to the decays analysed above, the conditions for $b \to u$ transitions can be obtained straightforwardly. For the inclusive term the interference is completely negligible and we have

$$\left(|V_{ub}|_{\text{SM-exp}}^{\text{incl}}\right)^2 = |V_{ub}|^2 + |\epsilon_R|^2|\widetilde{V}_{ub}|^2 \,, \tag{2.63}$$

with [86]

$$|V_{ub}|_{\text{SM-exp}}^{\text{incl}} = (4.11 \pm 0.28) \times 10^{-3} \,. \tag{2.64}$$

Let us now collect the conditions for the exclusive decays. Only the axial part enters in $B \to \pi \ell \nu$, hence

$$|V_{ub}|_{\text{SM-exp}}^{B \to \pi} = |V_{ub} + \epsilon_R \widetilde{V}_{ub}| = (3.38 \pm 0.36) \times 10^{-3} \,, \tag{2.65}$$

where the experimental value is taken from [86]. Finally, we have the pure leptonic decay $B \to \tau\nu$ decay, within the SM described by [92]

$$\text{Br}(B \to \tau\nu)_{\text{SM}} = \frac{G_F^2 m_B m_\tau^2}{8\pi}\left(1 - \frac{m_\tau^2}{m_B^2}\right)^2 f_B^2|V_{ub}^{\text{SM}}|^2\tau_B \,. \tag{2.66}$$

Using the experimental value for the branching ratio $\text{Br}(B \to \tau\nu)^{\text{exp}} = (1.73 \pm 0.34) \times 10^{-4}$ [93], and $f_B = (192.8 \pm 9.9)$ MeV [94], encoding the non-perturbative effects of the transition matrix element leads to the condition

$$|V_{ub}|_{\text{SM-exp}}^{B \to \tau} = |V_{ub} - \epsilon_R \widetilde{V}_{ub}| = (5.14 \pm 0.57) \times 10^{-3} \,. \tag{2.67}$$

Eventually we perform a global fit using the three conditions which leads to the following solution:

$$|V_{ub}| = (4.1 \pm 0.2) \times 10^{-3}, \qquad \epsilon_R \, \text{Re}\left(\frac{\widetilde{V}_{ub}}{V_{ub}}\right) = -0.19 \pm 0.07 \,. \tag{2.68}$$

In contrast with the $b \to c$ transition, in this case the fit is excellent with $\chi^2/N_{\text{dof}} = 0.3$. While in the SM the different determinations of V_{ub} do not match, commonly formulated as the $|V_{ub}|$ problem, here the situation is significantly improved. The fact that RH currents can provide a solution for the $|V_{ub}|$ problem was first stated by [44–46]. We show our global fit solution in figure 2.2. Obviously, the discrepancy between inclusive and exclusive determinations is resolved in the presence of RH currents. Here the true value of $|V_{ub}|$ turns out to be $(4.1 \pm 0.2) \times 10^{-3}$, shown as a black dot, selecting the inclusive determination as the true value. The SM case then corresponds to the top of the vertical axis, where the three determinations of $|V_{ub}|$ are clearly different.
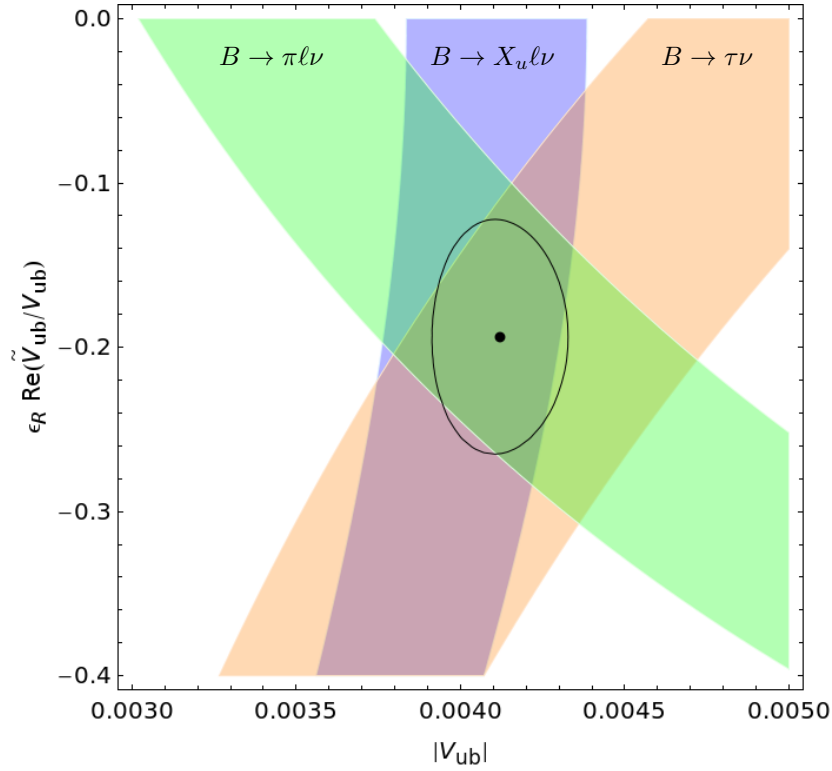
Figure 2.2.: The constraints on the CKM element $|V_{ub}|$ and the RH mixing matrix element $\epsilon_R \, \mathrm{Re} \left(\frac{\widetilde{V}_{ub}}{V_{ub}} \right)$ from the three analysed decays $B \to \pi \ell \nu$ (green), $B \to X_u \ell \nu$ (blue), and $B \to \tau \nu$ (orange). The bands for the various decays represent the $\pm 1\sigma$ deviation and the best fit solution is shown as a black dot with the ellipse giving the 1σ region around it.

The combination $\epsilon_R \, \mathrm{Re} \left(\frac{\widetilde{V}_{ub}}{V_{ub}} \right)$ was chosen to avoid assumptions on the phases of the RH matrix. It is also possible to keep $\mathrm{Im}(\widetilde{V}_{ub}/V_{ub})$ as an additional free parameter, however without imposing further assumptions the solution is not unique. For example, when assuming $|\widetilde{V}_{ub}| < |V_{ub}|$, equation (2.68) is the best-fit solution for a large interval of $\mathrm{Im}(\widetilde{V}_{ub}/V_{ub})$ around zero. Indeed, allowing for a phase of $\widetilde{V}_{ub}/V_{ub}$ within a conservative range finally yields

$$|\epsilon_R \widetilde{V}_{ub}| = (1.0 \pm 0.4) \times 10^{-3} \,, \qquad \text{for} \qquad -\frac{\pi}{4} < \arg \left(\frac{\widetilde{V}_{ub}}{V_{ub}} \right) < \frac{\pi}{4} \,. \qquad (2.69)$$

Summary

Constraints from the data on tree-level charged current transitions, in particular $u \to d$,

$u \to s$, $b \to u$ and $b \to c$, can be summarised as

$$|\widetilde{V}| \sim \begin{pmatrix} < 1.4 & < 1.4 & 1.0 \pm 0.4 \\ - & - & < 2.0 \\ - & - & - \end{pmatrix} \times \left(\frac{10^{-3}}{\epsilon_R} \right) . \tag{2.70}$$

We have assumed small phases except for $\widetilde{V}_{ub}$, hence for the other elements we have not performed a phase variation. The bounds presented here lie in the $\pm 1\sigma$ range of the previously determined bounds.

2.4.3. Bounds from unitarity and from phenomenology

Having derived the bounds on the full first row of the RH mixing matrix, we can make use of unitarity and get a bound on ϵ_R

$$|\epsilon_R| = \left(|\epsilon_R \widetilde{V}_{ud}|^2 + |\epsilon_R \widetilde{V}_{us}|^2 + |\epsilon_R \widetilde{V}_{ub}|^2 \right)^{1/2} = (1.0 \pm 0.5) \times 10^{-3} . \tag{2.71}$$

It turns out that ϵ_L, given in (2.48), and ϵ_R lie in the same range. Furthermore the result of (2.71) is in agreement with the naive estimate using $c_R = \mathcal{O}(1)$ and an effective NP scale of $\Lambda = 4\pi v \approx 3$ TeV. Recalling (2.35) we obtain

$$\epsilon_R \sim \frac{c_R v^2}{2\Lambda^2} \sim \mathcal{O}(10^{-3}) . \tag{2.72}$$

From the unitarity of the third column one can deduce that the large $|\widetilde{V}_{ub}|$ constrains the maximal value of $|\widetilde{V}_{tb}|$. A large value of $|\widetilde{V}_{tb}|$ is preferable since it minimises, again due to unitarity, the contribution to the elements $|\widetilde{V}_{ts}|$ and $|\widetilde{V}_{td}|$. These are known to contribute to $B_{d,s}^0 - \bar{B}_{d,s}^0$ mixing which are highly constrained. Furthermore a large $|\widetilde{V}_{tb}|$ could help to improve the agreement of the $Z \to b\bar{b}$ coupling in the RH sector with experiment.

2.4.4. The global fit

As indicated above we perform our global fit by maximizing $|\widetilde{V}_{tb}|$. We adopt the bounds on $\epsilon_R |\widetilde{V}_{ud}|$, $\epsilon_R |\widetilde{V}_{us}|$, $\epsilon_R |\widetilde{V}_{ub}|$, and $\epsilon_R |\widetilde{V}_{cb}|$ from the previous section and use the parametrisation from equation (2.31). The best-fit solution, with $\chi^2 \approx 1.1$, yields the following RH mixing matrix

$$\widetilde{V} \sim \begin{pmatrix} 0 & -0.76 & -0.65 \\ 0.88 & -0.31 & 0.36 \\ 0.48 & 0.57 & -0.67 \end{pmatrix} \tag{2.73}$$

and $\epsilon_R \approx 1.27 \times 10^{-3}$. From this fit we conclude that the RH mixing matrix is well described by the following ansatz, which keeps $|\widetilde{V}_{tb}|$ maximal.

$$\widetilde{V}_0^{(\mathrm{I})} = \begin{pmatrix} \tilde{c}_{12}\tilde{c}_{13} & \tilde{s}_{12}\tilde{c}_{13} & \tilde{s}_{13} \\ -\tilde{s}_{12} & \tilde{c}_{12} & 0 \\ -\tilde{c}_{12}\tilde{s}_{13} & -\tilde{s}_{12}\tilde{s}_{13} & \tilde{c}_{13} \end{pmatrix} . \tag{2.74}$$

This ansatz can be simply obtained from equation (2.31) with taking $\tilde{c}_{23} \to 1$. Again we can perform a global fit, the result reads

$$\widetilde{V}_0^{(\mathrm{I})} \sim \begin{pmatrix} 0.39 & -0.61 & -0.69 \\ 0.84 & 0.54 & 0 \\ 0.37 & -0.58 & 0.73 \end{pmatrix} . \tag{2.75}$$

At 90% C.L. we find $|\widetilde{V}_{tb}| < 0.73$, which is smaller than the corresponding value in the CKM matrix with $|V_{tb}| \sim 1$. By unitarity, $|\widetilde{V}_{ts}|$ and $|\widetilde{V}_{td}|$ are enhanced relative to their CKM counterparts and hence contribute to FCNCs.

The ansatz in equation (2.74) can be simplified further. We can deduce from equation (2.75) that the maximal $|\widetilde{V}_{tb}|$ scenario is described to a good approximation by

$$|\tilde{c}_{13}| \approx -\tilde{s}_{13} \approx 0.7 , \qquad \epsilon_R \approx 1 \times 10^{-3} , \tag{2.76}$$

where we select the sign convention $\mathrm{sgn}(\tilde{c}_{13}\tilde{s}_{12}) = -1$. This implies that

$$\widetilde{V}_0^{(\mathrm{II})} = \begin{pmatrix} \pm\tilde{c}_{12}\frac{\sqrt{2}}{2} & \pm\tilde{s}_{12}\frac{\sqrt{2}}{2} & -\frac{\sqrt{2}}{2} \\ -\tilde{s}_{12} & \tilde{c}_{12} & 0 \\ \tilde{c}_{12}\frac{\sqrt{2}}{2} & \tilde{s}_{12}\frac{\sqrt{2}}{2} & \pm\frac{\sqrt{2}}{2} \end{pmatrix} , \tag{2.77}$$

where the angle of $\tilde{s}_{12}$ and $\tilde{c}_{12}$, is the only free parameter and yields a simple description. We will use $\widetilde{V}_0^{(\mathrm{II})}$ for our phenomenological analysis, which will be performed in chapter 5. As we will show below, this structure of the matrix is crucial for various observables of meson-antimeson mixing. Note that for the full RH mixing matrix we still have to take into account the extra phases (2.30), which contribute to CP-violating effects.

It should mention that the only reasonable alternative to our ansatz in (2.77), consistent with FCNCs, is to expand $\widetilde{V}_0^{(\mathrm{I})}$ in equation (2.74) with the assumption $\tilde{c}_{13} \ll 1$. Thus we can write

$$\widetilde{V}_0^{(\mathrm{III})} = \begin{pmatrix} \tilde{c}_{13}\tilde{c}_{12} & \tilde{c}_{13}\tilde{s}_{12} & -1 \\ -\tilde{s}_{12} & \tilde{c}_{12} & 0 \\ \tilde{c}_{12} & \tilde{s}_{12} & \tilde{c}_{13} \end{pmatrix} . \tag{2.78}$$

This ansatz evades all constraints from charged currents except $b \to u$ transitions. Furthermore, it has small effects in B physics but large effects K physics, which are tightly constrained by the data. This and the smallness of $|\widetilde{V}_{tb}|$ make it less attractive than $\widetilde{V}_0^{(\mathrm{II})}$. This will become fully clear when we examine the flavour structure of the RH mixing matrix appearing in meson anti-meson mixing in section 5.1.3.

3. Right-handed currents: An explicit model

This chapter is devoted to the description of the second model that we discuss in this thesis: the Left-Right Model (LRM). In contrast to the previous model we follow a top-down approach in this case. This model has been widely studied within certain approximations, in particular with exact left-right symmetry. However, to keep the model as general as possible, we allow for a small asymmetry of the left- and right-handed sector. We begin this chapter with a very brief summary of early developments in this class of models. Subsequently, we discuss the setup of the LRM and provide information, including constraints from tree-level decays and electroweak precision observables, necessary to study $\Delta F = 2$ processes, which will follow in a separate chapter.

3.1. Preliminaries

The original idea of left-right symmetric models aiming to establish parity at high scale traces back more than 35 years [29–32, 95]. The enlargement of gauge symmetry by an additional $SU(2)_R$ symmetry with respect to the SM yields, apart from new heavy gauge bosons, mainly two characteristic quantities: a new RH mixing matrix and an additional right-handed gauge coupling. Early studies mainly concentrate on the analysis of two simplified scenarios, which are commonly called "manifest" scenario [32] and "pseudo-manifest" scenario [33–35] characterised by explicit and spontaneous CP violation, respectively. These assumptions determine the form of the RH mixing matrix which appears then either identical to or the complex-conjugate of the CKM matrix up to certain phases. A detailed description of the classification can be found in [39]. Furthermore these early works prefer an exact left-right symmetry implying the left and right gauge couplings to be equal.

The phenomenological implications of these simple setups have been extensively studied [96–99]. The "pseudo-manifest" scenario has already been ruled out by the correlation of ε_K and $\sin(2\beta)$ [100] as well as the prediction of light Higgs triplets [101]. Further in both scenarios the heavy charged gauge boson mass $M_{W_R} \gtrsim 4\,\mathrm{TeV}$ is strongly constrained [36, 96, 102]. This is mainly driven by the $K_L - K_S$ mass difference and CP violation in $K^0 - \bar{K}^0$ mixing. Therefore we conclude that the right-handed mixing matrix must have a different structure than proposed by these simple setups in order for the new gauge bosons to be accesible at the LHC. Subsequently, there have been more general studies on CP violation beyond these two approximations [38, 39, 103].

Recent studies of many flavour observables within this class of models can be found in [36, 37, 104, 105].

Our analysis makes even more general considerations. Apart from allowing for a splitting in left- and right-handed gauge couplings, the right-handed mixing matrix will be incorporated in its most general form. This will subsequently allow us to deduce its structure only based on phenomenology.

3.2. The Left-Right Model

Now we briefly summarise the theoretical setup for the LRM. Since this model has been studied extensively in the literature, here we only present the key features for our analysis. In particular, we orient our notation close to the one given in [36–38].

3.2.1. Symmetry and scales

The basic ingredient of the general left-right model is its left-right symmetric gauge group

$$SU(3)_C \times SU(2)_L \times SU(2)_R \times U(1)_{B-L} \,. \tag{3.1}$$

In this model parity is conserved at high scales but broken at lower scales. This breakdown is not necessarily linked to the mechanism of the SM symmetry breaking or the TeV scale but can originate from a much higher scale [106]. The gauge couplings g_L and g_R, belonging to the left and right $SU(2)$ gauge group respectively, are then expected to exhibit a small splitting [107]. Hence, we adopt a more general scenario than what has been considered in most studies [36–38].

In order to recover the SM as the low energy theory and to give masses to gauge bosons and fermions, we break the symmetry spontaneously in two step. There are two characteristic scales, one for each step of symmetry breaking, which will be incorporated as VEVs of the corresponding Higgs fields. We fix the first breaking at a high scale $\kappa_R \sim \mathcal{O}(\text{TeV})$,

$$SU(2)_R \times U(1)_{B-L} \to U(1)_Y \,, \tag{3.2}$$

where $U(1)_Y$ is the SM hypercharge gauge group. The standard electroweak symmetry breaking

$$SU(2)_L \times U(1)_Y \to U(1)_Q \tag{3.3}$$

takes place at scale v. The value of v will be described in the next section, but generally the scale is such that $v \ll \kappa_R$.[1] The size of κ_R controls the magnitude of the masses of heavy new fields unlike the masses of the SM fields, which are set by v. The hierarchy

---

[1] In order to avoid confusion we want to stress the different conventions used for the parameter v in the LRM and RHMFV. In the LRM, we use $v = 174$ GeV.

of scales can be expressed by the small parameter

$$\epsilon = \frac{v}{\kappa_R} \, , \tag{3.4}$$

in which all NP effects can be expanded. We restrict our phenomenological analysis to the leading corrections which means in practice up to $\mathcal{O}(\epsilon^2)$ effects. Furthermore it should be stressed that ϵ and hence κ_R is restricted by electroweak precision constraints.

3.2.2. Particle content

Next we want to describe the fermion fields, Higgs fields and gauge boson fields in the model.

Fermion fields Chiral fermion fields are grouped in doublets with respect to the corresponding symmetry group, hence the left-handed fermions are embedded as $SU(2)_L$ doublets while right-handed fermions form $SU(2)_R$ doublets. For the opposite symmetry group they act as singlets. In contrast to the SM the setup is now left-right symmetric. We treat the leptons similarly. The transformation properties with respect to the symmetry given in equation (3.1) can be summarised as

$$Q_L = \begin{pmatrix} u_L \\ d_L \end{pmatrix} \sim \left(3, 2, 1, \frac{1}{3}\right) \, , \quad Q_R = \begin{pmatrix} u_R \\ d_R \end{pmatrix} \sim \left(3, 1, 2, \frac{1}{3}\right) \, , \tag{3.5}$$

$$L_L = \begin{pmatrix} \nu_L \\ l_L \end{pmatrix} \sim (1, 2, 1, -1) \, , \quad L_R = \begin{pmatrix} \nu_R \\ l_R \end{pmatrix} \sim (1, 1, 2, -1) \, . \tag{3.6}$$

For these particles the electric charges can be obtained from

$$Q = T_{3L} + T_{3R} + \frac{B - L}{2} \, . \tag{3.7}$$

Note that in this framework the hypercharge numbers do not appear arbitrary as is it the case in the SM [107].

Higgs fields As stated above the pattern of symmetry breaking requires at least two independent Higgs fields, due the LR symmetry at high scales three Higgs fields need to be introduced. For the step one breaking in equation (3.2) a triplet representation is chosen for convenience

$$\Delta_R = \begin{pmatrix} \delta_R^+/\sqrt{2} & \delta_R^{++} \\ \delta_R^0 & -\delta_R^+/\sqrt{2} \end{pmatrix} \sim (1, 1, 3, 2) \tag{3.8}$$

which gets the VEV

$$\langle \Delta_R \rangle = \begin{pmatrix} 0 & 0 \\ \kappa_R & 0 \end{pmatrix} \, . \tag{3.9}$$

Starting from scratch one has to take all VEVs as complex entries, hence a phase should appear in every VEV entry. Here we have used the form from [36], where redundant

phases have already been removed by making appropriate phase transformations. It should be stressed that the triplet representation has the advantage that in the neutrino sector a TeV scale seesaw mechanism is automatically incorporated. Thus Majorana masses are generated for RH neutrinos at TeV scale while light neutrino masses appear suppressed [42, 43, 108]. Doublet or even more complicated representations are possible in principle, however we will not consider them here. This is motivated by the attractive features of the triplet structure in the neutrino sector. Quark flavour phenomenology, on which we concentrate in this thesis, does not depend sensitively on the detailed structure of the Higgs sector. We will elaborate on this statement below.

In order to be able to establish parity at a high scale, the introduction of the Higgs triplet field Δ_R implies the existence of an $SU(2)_L$ triplet. This triplet can then be written as

$$\Delta_L = \begin{pmatrix} \delta_L^+/\sqrt{2} & \delta_L^{++} \\ \delta_L^0 & -\delta_L^+/\sqrt{2} \end{pmatrix} \sim (1, 3, 1, 2). \tag{3.10}$$

Its VEV reads

$$\langle \Delta_L \rangle = \begin{pmatrix} 0 & 0 \\ \kappa_L e^{i\theta} & 0 \end{pmatrix}. \tag{3.11}$$

As we do not want to generate large Majorana masses for the left-handed neutrinos, consequently we have $\kappa_L \lesssim \mathcal{O}(\text{eV})$. This assumption will allow us to simplify our calculations as we can approximately assume $\langle \Delta_L \rangle = 0$.

Finally we have a bidoublet,

$$\phi = \begin{pmatrix} \phi_1^0 & \phi_2^+ \\ \phi_1^- & \phi_2^0 \end{pmatrix} \sim (1, 2, 2, 0), \tag{3.12}$$

which is responsible for the second step symmetry breaking in equation (3.3). This bidoublet will also provide the light SM Higgs. When taking the VEV, we can write

$$\langle \phi \rangle = \begin{pmatrix} \kappa & 0 \\ 0 & \kappa' e^{i\alpha} \end{pmatrix}, \tag{3.13}$$

where we set

$$v = \sqrt{\kappa^2 + \kappa'^2} = 174 \, \text{GeV}. \tag{3.14}$$

Since we know that the masses of up and down type quarks are not equal, we require $\kappa' \neq \kappa$.[2] For our analysis it is convenient to introduce the following parametrisation

$$s = \frac{\kappa'}{v} \qquad \text{and} \qquad c = \frac{\kappa}{v}. \tag{3.15}$$

As v is fixed due to the relation (3.14) the parameters s and c can be associated with sine and cosine. Due to the hierarchy $m_b \ll m_t$, the sine is generally expected to be

---

[2]The limit $\kappa = \kappa'$ is not allowed in our further analysis; this can also be seen from the divergent behaviour of several observables in this limit.

much smaller than the cosine so that $\kappa' \ll \kappa$. We analyse this hierarchy more carefully in our numerical analysis below, using $1 < \kappa/\kappa' < 10$ typically.

We have summarised further details of the Higgs sector of the LRM in appendix A.

Gauge bosons Next we study the gauge boson sector of the model. Associated with the gauge symmetry $SU(2)_L$ and $SU(2)_R$ we obtain the corresponding gauge fields denoted $W^a_{L,\mu}$ and $W^b_{R,\mu}$, respectively. The $U(1)_X$ gauge field is denoted by B_μ. We present relevant formulae for mass eigenstates and masses in appendix C. As expected, after electroweak symmetry breaking gluons and the photon remain massless. In addition to the SM $W^\pm$ and the Z bosons the fields $W'^\pm$ and Z' are also present with heavy masses of $\mathcal{O}(\text{TeV})$. Their parametric dependence can be found in appendix C. Furthermore, the gauge bosons of the same charge mix after transforming to mass eigenstates, for example $W^\pm$ ($W'^\pm$) is dominated by W_L (W_R) with small RH (LH) admixture of $\mathcal{O}(\epsilon^2)$ [109]. A similar argument holds for the neutral gauge bosons.

We note that in the course of our flavour analysis we make use of a simplifying notation. In order to keep the expressions more transparent, instead of W and W' we will use W_L and W_R, respectively, even though they differ by $\mathcal{O}(\epsilon^2)$ corrections. It should be stressed that this is only a matter of notation and all formulae will correctly include these corrections.

3.2.3. Yukawa interaction and quark mixing matrices

In the course of our analysis we need more detailed information about quark flavour mixing. To this end we have to specify the Yukawa sector, most generally given by

$$\mathcal{L}_{\text{Yuk}} = -y_{ij}\overline{Q}_{Li}\phi Q_{Rj} - \tilde{y}_{ij}\overline{Q}_{Li}\tilde{\phi}Q_{Rj} + h.c. \,, \tag{3.16}$$

where $\tilde{\phi} = \sigma_2\phi^*\sigma_2$ and $i,j = 1,2,3$ are flavour indices. It is worth noting that in the quark sector only a coupling to the bidoublet is involved. Fermion mass matrices can be straightforwardly obtained

$$(M_u)_{ij} = v(Y_u)_{ij} \,, \qquad (M_d)_{ij} = v(Y_d)_{ij} \,, \tag{3.17}$$

where

$$(Y_u)_{ij} = y_{ij}c + \tilde{y}_{ij}se^{-i\alpha} \,, \qquad (Y_d)_{ij} = y_{ij}se^{i\alpha} + \tilde{y}_{ij}c \,. \tag{3.18}$$

These matrices can be diagonalised as usual by the bi-unitary transformations

$$M_u^{\text{diag}} = U_L^\dagger M_u U_R \,, \tag{3.19}$$

$$M_d^{\text{diag}} = D_L^\dagger M_d D_R \,, \tag{3.20}$$

where the matrices $U_{L,R}$ and $D_{L,R}$ transform the quarks from flavour into mass eigenstates.

It appears that the charged current interaction of quarks involves now LH and RH mixing matrices for LH and RH currents, respectively. All Feynman rules necessary for our analysis up to $\mathcal{O}(\epsilon^2)$ can be found in appendix F. Here we just define the two mixing matrices in the LH and RH sectors, in particular

$$V^L = U_L^\dagger D_L\,, \quad V^R = U_R^\dagger D_R\,. \tag{3.21}$$

where V^L is the CKM matrix and V^R the new RH mixing matrix.

We adopt the general parametrisation used in RHMFV as given in equation (2.29) for the RH mixing matrix. Note that we distinguish the matrices from RHMFV and the LRM via their notation, $\widetilde{V}$ and V^R respectively. It should be stressed that we follow different procedures in order to develop their structure from phenomenology, even though the general parametrisation is the same.

Finally we want to mention that a full counting of relevant parameters in the quark sector is given in appendix D.

3.2.4. A brief note on the lepton sector

In this thesis, we mainly concentrate on quark flavour physics. Still various leptonic and semi-leptonic decays enter the tree-level constraints on the RH matrix. These allow to extract the constraints on the mixing matrices in a clean way. Hence some knowledge about the structure of the lepton sector is required. In analogy to the quark case one can write down the gauge-invariant Yukawa coupling. A detailed study was performed by the authors of [42, 43]. We just summarise their findings.

In the lepton case we have additional couplings of the Higgs triplets $\Delta_{L,R}$ to the leptons, leading to Majorana mass terms. The bidoublet provides mixing terms. After transformation to mass eigenstates the light neutrinos are dominated by the LH contribution with a small RH admixture. The heavy Majorana neutrinos consist in turn of the RH neutrinos also modified by a small left-handed contribution. The corresponding mixing angle can be estimated from the masses of the heavy and light neutrinos. A conservative estimate for heavy neutrino masses of around 100 GeV yields a mixing of $\mathcal{O}(10^{-6})$ [110]. We conclude that Yukawa couplings have to be very small. In agreement with [111] we find these mixing effects to be safely negligible, remembering that they have to compete with $\mathcal{O}(\epsilon^2)$ effects, which we estimate to be of $\mathcal{O}(10^{-3})$.

3.3. Tree-level constraints

3.3.1. Elaborating relevant effects

From our analysis of RHMFV we know that the RH mixing matrix is constrained by various tree-level decays. In this section we briefly want to repeat this analysis for the

LRM.

In the LRM new contributions can potentially arise from the new RH couplings of the W gauge boson, from the exchange of the heavy W_R gauge boson, and from the heavy charged Higgs boson. We now describe which effects are indeed relevant. The following criteria can be identified:

- As stated above mixing effects in the lepton sector are negligible.

- Only light neutrinos can appear in the final states of the decays.

- Diagrams including the heavy W_R boson are of $\mathcal{O}(\epsilon^4)$, doubly suppressed by the coupling to light neutrinos and the W_R propagator, each of $\mathcal{O}(\epsilon^2)$. At $\mathcal{O}(\epsilon^2)$ then, only the SM couplings are relevant.

- Charged Higgs boson effects are considered only for leading order couplings. Furthermore all processes not involving the top quark are Yukawa suppressed and hence negligible.

The last point raises the question whether charged Higgs effects might be negligible. In order to examine this statement we consider the example of the decay $B^+ \to \tau^+ \nu_\tau$, where a potential contribution is still likely due to the chiral suppression of the diagram involving the gauge boson propagator. Subsequent calculation shows that such diagrams are suppressed by the factor $m_B^2/M_{H^+}^2$. Thus they do not contribute for a heavy charged Higgs. Indeed, we will use a heavy Higgs in our numerical analysis later.

Potentially, the model can also have corrections a modified Fermi coupling G_F. But the analysis of the μ-decay width shows that these arise at $\mathcal{O}(\epsilon^4)$ and consequently have no impact on the tree-level decays.

We conclude this section by completing our list of criteria:

- Charged Higgs effects are negligible.

- G_F obtains no corrections.

3.3.2. Comparison to RHMFV

The constraints on the mixing matrices from RHMFV (see section 2.4.2) can be adapted to the LRM with the following identifications

$$\varepsilon_L = \mathcal{O}(\epsilon^4)\,, \qquad \varepsilon_R = cs\epsilon^2\,, \qquad \tilde{V} = e^{i\alpha}V^R\,. \tag{3.22}$$

This is mainly due to the fact that charged Higgs effects are negligible in the tree-level decays. Note that we can set $\alpha = 0$ since both mixing matrices are simply unitary matrices (see for a more detailed discussion in appendix D).

3.3.3. Summary of inputs and constraints

In the following we use the constraints from section 2.4.2 with updated experimental values (see table 3.1) and also include constraints from elements with higher uncertainty.

$Br(\pi \to \mu\nu) = 0.9998770(4)$	[112]	$f_\pi = 129.5(17)\,\mathrm{MeV}$	
$f_+(0)|V_{us}|^{K \to \pi\ell\nu} = 0.2163(5)$		$f_+(0) = 0.9584(44)$	
$f_K/f_\pi|V_{us}/V_{ud}|^{K \to \mu\mu} = 0.2758(5)$	[84]	$f_K/f_\pi = 1.1931(53)$	
$Br(D_s \to \tau\nu) = 0.0529(28)$		$f_{D_s} = 248.9(39)\,\mathrm{MeV}$	
$Br(B \to \tau\nu) = 1.64(34) \times 10^{-4}$		$f_B = 205(12)\,\mathrm{MeV}$	[94]
$F(1)|V_{cb}|^{B \to D^*\ell\nu} = 0.03604(52)$		$F(1) = 0.908(17)$	[113]
$G(1)|V_{cb}|^{B \to D\ell\nu} = 0.0423(15)$	[114]	$G(1) = 1.074(24)$	[115]

Table 3.1.: Updated values of the most important experimental and theoretical quantities used as input parameters for the constraints from tree-level decays.

We can efficiently summarise the constraints by introducing a short notation for the constraints from vectorial and axial currents. One can write

$$|V_{ij}|_V = \left|V_{ij}^L + cse^{i\alpha}\epsilon^2 V_{ij}^R\right| , \qquad |V_{ij}|_A = \left|V_{ij}^L - cse^{i\alpha}\epsilon^2 V_{ij}^R\right| . \tag{3.23}$$

In some cases we can constrain $|V_{ij}^L|$ directly from the inclusive semileptonic decays, as in the determination of $|V_{ub}^L|$ from $B \to X_u\ell\nu$. We have collected all our results compactly in table 3.2.

Here a few comments are in order:

- In the determination of $|V_{cd}^L|$ and $|V_{tb}^L|$ interference terms between left- and right-handed quarks are suppressed by m_d and m_q/m_t ($q = d, s, b$), respectively. Hence we can drop them.

- The constraints from $c \to d$, $c \to s$ and $t \to b$ transitions suffer from large uncertainties, so they will have little impact.

- The $t \to d$ and $t \to s$ transitions cannot be measured from tree-level decays. Therefore in this case we obtain no constraints.

3.4. Electroweak precision constraints

3.4.1. Introduction

Electroweak precision tests are known to set important constraints on the masses of heavy gauge bosons and electroweak parameters. Due to the high accuracy of the measurements of Z pole observables and W boson properties, these constraints have

transition	considered decay	references	constraint	values
$u \to d$	superallowed $0^+ \to 0^+$	[112]	V	0.97425(22)
	$\pi^+ \to \mu^+\nu$	[116]	A	0.981(13)
$u \to s$	$K \to \pi\ell\nu$	[84]	V	0.2257(12)
	$K \to \mu\nu$	[112]	A	0.2268(32)
$c \to d$	$D \to K\ell\nu, D \to \pi\ell\nu$	[112]	V	0.229(25)
	νN charm production	[112]	A	0.230(11)
$c \to s$	semileptonic D decays	[112]	V	0.98(10)
	$D_s \to \tau^+\nu$	[94]	A	0.978(31)
$b \to u$	$B \to X_u\ell\nu$	[112]	L	$4.27(38) \times 10^{-3}$
	$B \to \pi\ell\nu$	[112]	V	$3.38(36) \times 10^{-3}$
	$B \to \tau\nu$	[94]	A	$4.70(56) \times 10^{-3}$
$b \to c$	$B \to X_c\ell\nu_\ell$	[86]	L	$41.54(73) \times 10^{-3}$
	$B \to D\ell\nu$	[114, 115]	V	$39.4(17) \times 10^{-3}$
	$B \to D^*\ell\nu$	[113, 114]	A	$39.70(92) \times 10^{-3}$
$t \to b$	$\frac{\mathrm{Br}(t \to bW)}{\mathrm{Br}(t \to qW)}$	[117]	L	0.95(2)

Table 3.2.: Summary of all tree-level constraints on the elements of the left -and right-handed mixing matrices. The letters A, V and L stand for constraints on $|V_{ij}|_A$, $|V_{ij}|_V$ and $|V_{ij}^L|$, respectively.

to be seriously considered in order to perform a realistic analysis. Interestingly, EWP constraints are somewhat complementary to the constraints from flavour physics which mainly concern the flavour structure such as quark mixing matrices of a special NP model. That does not imply that effects can be considered completely decoupled from the analysis of the flavour sector, however it is possible to consider them in a two step procedure. We find first allowed ranges for parameters by EWP tests and then further proceed by restricting these ranges though flavour constraints. In this section we will perform the first step in the analysis of the electroweak sector.

It should be stressed that a consideration of the gauge self-energy parameters S, T and U [118] in this context is far from being satisfactory as oblique corrections are not able to capture all NP effects. Rather, non-standard electroweak corrections have to be treated in a systematic approach such as the one followed in a model-independent analysis by Burgess *et al.* [119]. They calculate EWP observables from an effective Lagrangian point of view. The most general effective Lagrangian, being in accordance with the symmetries of the model, is used to work out the relations between measured observables and parameters of SM part of the Lagrangian by rescaling in order to get canonically normalised gauge kinetic terms. These parameters are clearly not identical to the parameters of a pure SM theory as they are modified by the NP contributions, which enter through the coefficients being calculated from the underlying theory. In the last step a fit of theoretical predictions to experimental data is performed in order

to find the allowed regions in the parameter space.

In such a fit about 40 low-and high energy observables are usually considered [112, 120, 121], including the measurements around the Z resonance from LEP I and the high energy data from LEP II. Since this kind of analysis is clearly beyond the scope of this work, we will take the results of [105], which are based on above described ideas from [119]. The authors of [105] present a global fit analysis of EWP observables for various models with $SU(2)_1 \times SU(2)_2 \times U(1)_X$ gauge symmetry, among them the LRM, there denoted by LR-T.

We will now briefly outline the strategy of [105] including a dictionary which translates their notation to ours.

3.4.2. Structure of the analysis

The electroweak sector of the LRM is characterised by six parameters, given in equations (D.25) and (D.26) of appendix D. For the global fit, [105] distinguishes between the so called reference parameters and fit parameters. The reference parameters are commonly chosen to be the three most precisely measured quantities, in particular

$$G_F, \qquad M_Z, \qquad \alpha_e \equiv \alpha(M_Z^2), \tag{3.24}$$

where the electromagnetic fine structure constant at the Z-pole is given in the $\overline{MS}$ scheme by

$$1/\alpha(M_Z^2) = 127.916 \pm 0.015. \tag{3.25}$$

The next step is to express the reference parameters in terms of model parameters. Fixing the reference parameters by input data allows to reduce the number of free parameters. The remaining parameters, describing the NP effects, usually referred to as fit parameters, are used to perform the global fit. When adapting the notation of [105], these fit parameters read

$$\tilde{x} = \frac{1}{\epsilon^2}, \quad c_{\tilde{\phi}} = c_R, \quad \sin 2\tilde{\beta} = 2sc, \tag{3.26}$$

and we have argued in appendix D that we can set $\alpha = 0$. Essentially we perform a change of variables from model parameters to reference and fit parameters The fit observables have to be expressed in terms of the parameters in (3.24) and (3.26). As up to now all our formulae are written in terms of model parameters, we want to illustrate the change with a few important examples.

- We verify that G_F and M_Z are free of $\mathcal{O}(\epsilon^2)$ corrections. Cancellation of such corrections is achieved when using the definitions v and s_W according to [3]

$$v^2 = \frac{1}{2\sqrt{2}G_F}, \qquad s_W^2 c_W^2 = \frac{\pi\alpha(M_Z^2)}{\sqrt{2}M_Z^2 G_F}. \tag{3.27}$$

---

[3]In [105] a different convention for the Higgs bi-doublet is used. In our convention v is chosen by a factor of $\sqrt{2}$ smaller.

- The mass M_W is modified by

$$M_W = M_Z c_W \left[1 + \frac{\epsilon^2}{2} \frac{c_W^2}{c_W^2 - s_W^2} \left(\frac{c_R^4}{4} - 2s^2 c^2 \right) \right] , \tag{3.28}$$

  where now s_W and c_W are defined through (3.27) and we have suppressed the SM one-loop corrections.

- For the heavy masses M_{W_R} and $M_{Z'}$ we choose to drop the $\mathcal{O}(\epsilon^2)$ corrections, hence

$$(M_{W_R})^2 = \frac{e^2 \kappa_R^2}{c_W^2 s_R^2}, \quad (M_{Z'})^2 = \frac{2e^2 \kappa_R^2}{c_R^2 c_W^2 s_R^2} , \tag{3.29}$$

  s_W and c_W are given as before by (3.27). For our estimates the leading term is sufficient, but in case of discovery precisely measured values could help to constrain the parameter space and add them to the list of reference parameters.

While in EWP observables both tree-level and loop corrections are included for the SM, the NP corrections are only incorporated at the tree-level. A global fit is then performed over the fit parameters in (3.26) considering 37 EWP observables with respect to the corresponding data. The fit yields regions in the parameter space which are consistent with EWP data. These findings are summarised in Tables IX and X of [105]. There they show the formulae for corrections to the most constraining observables, which in the LRM are given by σ_{had} and $A_{\text{FB}}(b)$.

3.4.3. Collection of constraints

In this section we collect all relevant constraints from EWP observables. Summarizing the findings from [105] in our notation, using equations (3.26), we find the following constraints:

- Related to the Z pole observables, in particular the total decay width, one can deduce σ_{had}, the partial branching fraction of $Z \to q\bar{q}$,

$$\delta\sigma_{\text{had}}/\sigma_{\text{had,SM}} = \left[-1.13 \frac{c_R^2}{4} - 0.142 \frac{c_R^4}{4} + 0.0432(2s^2 c^2) \right] \epsilon^2 . \tag{3.30}$$

- One can find the forward-backward asymmetry $A_{\text{FB}}(b)$ given by

$$\delta A_{\text{FB}}(b)/A_{\text{FB,SM}}(b) = \left[-30.0 \frac{c_R^2}{4} + 67.6 \frac{c_R^4}{4} - 20.6(2s^2 c^2) \right] \epsilon^2 . \tag{3.31}$$

- From parity violation experiments the weak charges of atoms can be determined, in particular for the caesium-133 nucleus one obtains

$$\delta Q_W(\text{Cs})/Q_{W,\text{SM}}(\text{Cs}) = \left[-0.855 \frac{c_R^4}{4} - 0.145(2s^2 c^2) \right] \epsilon^2 . \tag{3.32}$$

- Deep inelastic ν-N scattering measurements allow us to measure the left-handed coupling and the corresponding constraint reads

$$\delta(g_L^{N\nu})^2/(g_{L,\text{SM}}^{N\nu})^2 = \left[0.0219 + 0.478c_R^2 + 0.210c_R^4 - 1.42(4s^2c^2)\right]\epsilon^2. \quad (3.33)$$

A more detailed description of the several observables can be found in [105, 122]. We find that the best treatment of conditions (3.30) to (3.33) including their analysis of errors is given by

$$|\text{EXP} - \text{SM}(1 + \text{CON})| \leq \sqrt{(\Delta\text{EXP})^2 + (\Delta\text{SM}(1 + \text{CON}))^2}, \quad (3.34)$$

where EXP and SM denote, experimental and the SM value, respectively. CON has to be replaced by the corresponding condition of equation (3.30) to (3.33). We summarise all necessary inputs in table 3.3.

Observable	experimental value	SM value
σ_{had} [nb]	41.541(37)	41.484(8)
$A_{\text{FB}}(b)$	0.0992(16)	0.1034(7)
$Q_W(\text{Cs})$	$-73.20(35)$	$-73.15(2)$
$(g_L^{N\nu})^2$	0.3027(18)	0.30399(17)

Table 3.3.: Inputs for the electroweak analyses from [112].

Furthermore we have to take into account the constraint from the W mass. This constraint can be directly derived from (3.28) after inclusion of the SM loop corrections. Actually the analysis can be simplified by considering only the shift from NP, defined by the difference between experimental and SM value, we obtain

$$(\Delta M_W)^{\text{NP}} = \epsilon^2 \frac{M_Z}{2} \frac{c_W^3}{c_W^2 - s_W^2}\left(\frac{c_R^4}{4} - 2s^2c^2\right) = (0.040^{+0.025}_{-0.029}) \text{ GeV}, \quad (3.35)$$

where the SM and measured value are taken from [120, 123].

We also have to incorporate the direct experimental constraints.

- Collider experiments provide a direct bound for a heavy W_R. The bound depends on the ratio of the gauge couplings g_L and g_R. Usually for unequal couplings this bound is weakened. The most recent experimental bound is roughly $M_{W_R} \geq 2\,\text{TeV}$ [124–127].

- The TWIST Collaboration [128] provides a direct experimental bound on both the ratio of g_R/g_L combined with the mixing angle and the ratio g_L/g_R linked to the W_R mass. Using the relation $s_W/(c_W s_R) = g_R/g_L$ the first constraint can be simplified and at 90% C.L. we obtain

$$sc\epsilon^2 < 0.020 \qquad \text{and} \qquad \frac{c_W s_R}{s_W}M_{W_R} > 578\,\text{GeV}. \quad (3.36)$$

Finally, for completeness we would like to mention that in order to keep the gauge couplings in the perturbative range we impose additionally $g_R^2 < 4\pi$ and $g'^2 < 4\pi$, while g_L is fixed by the input data and the reference parameters.

3.4.4. Numerical pre-analysis of the electroweak parameter space

In this section we provide a numerical analysis of experimentally allowed ranges for electroweak parameters implied by EWP observables. We remark that these parameters cannot be independently constrained from the flavour sector. However, since the analysis of EWP observables does not involve the flavour parameters of the matrix V^R it is possible to pre-constrain them.

We have argued above that the effective number of parameters to be considered can be reduced to three as given in equation (3.26). In order to find the corresponding allowed ranges, we generate random values in their full range and check whether all constraints as collected in section 3.4.3 are fulfilled. In practice we scan over $0 < s < 1/\sqrt{2}$, $0 < s_R < 1$ and $0 < \epsilon < 0.1$. Note that in principle $0 < s < 1$ is possible, but following our arguments of section 3.2.2 the relation of equation (3.14) can be used for this further restriction. The choice for the scan of the parameter ϵ is driven by the fact that we want to examine heavy particles with masses around the TeV scale. Furthermore for every set of valid parameter points the χ^2 function is evaluated. The results are illustrated in figures 3.1 to 3.3 showing the correlations between the three electroweak parameters ϵ, s_R and s.

In figure 3.1 we show the parameter s as a function of ϵ. The colour spectrum identifies preferred regions in parameter space by encoding $\ln(\chi^2/n_{\mathrm{d.o.f.}})$. As indicated by corresponding colours, generally smaller values for ϵ are favoured. The best fit region lies around $\epsilon \sim 0.03$ and $s > 0.1$ as indicated by the color black, where the constraint from $A_{\mathrm{FB}}(b)$ is in accordance within 2σ with the data from LEP. Note that we are not able to fulfill all constraints simultaneously better than 2σ. Consequently, in principle EWP observables hence imply a 2σ tension within the LRM. However the LEP measurement has to be considered with a healthy criticism since the competing SLD experiments did not measure a departure from the value expected in the SM. Furthermore, we can deduce from figure 3.1 the bound $s > 0.1$. It implies that top-inspired LR models [39], which assume $c/s = \kappa/\kappa' = m_t/m_b$, are disfavoured by EWP observables, in particular $A_{\mathrm{FB}}(b)$.

Figure 3.2 illustrates the correlation of s_R with respect to ϵ. As in the previous plot, the colour black confines the preferred region in parameter space pointing towards small values for ϵ implying $s_R > 0.7$. In order to be more general the bound $s_R > 0.1$ is imposed from the perturbativity constraint.
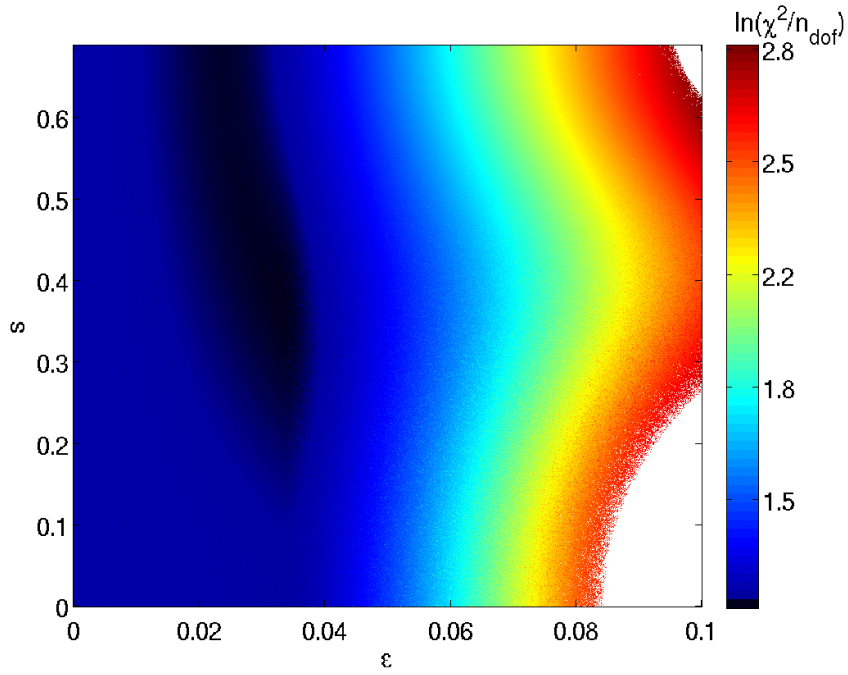
Figure 3.1.: Correlation of parameter s and ϵ. The colour spectrum indicates $\ln(\chi^2/n_{\text{d.o.f.}})$.
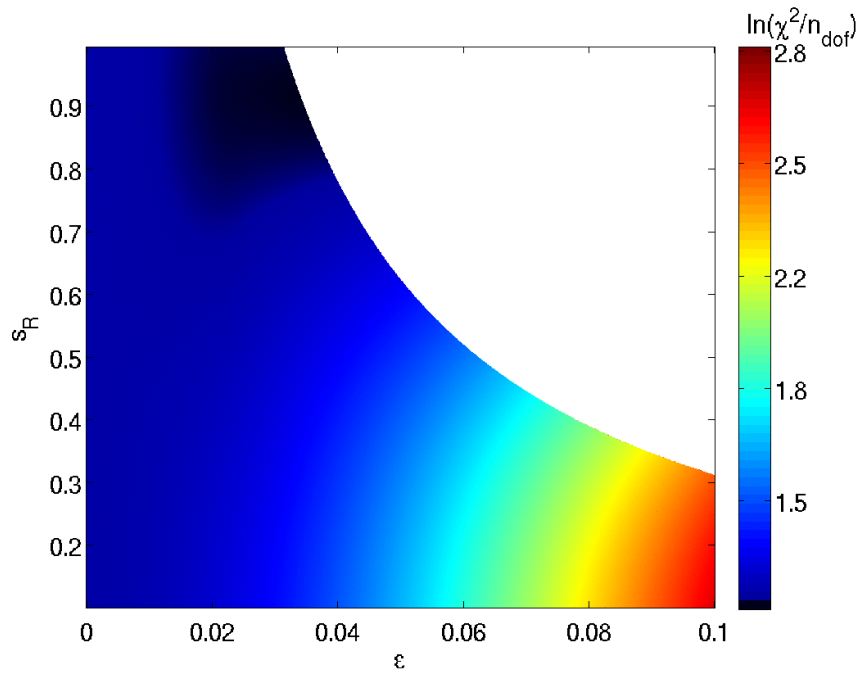
Figure 3.2.: Correlation of parameter s_R and ϵ. The colour spectrum indicates $\ln(\chi^2/n_{\text{d.o.f.}})$.
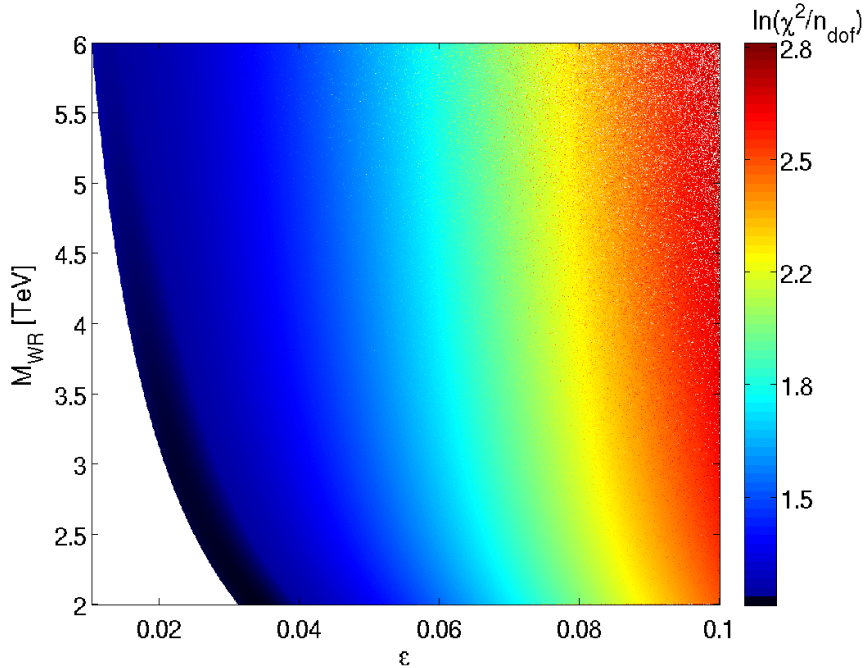
Figure 3.3.: Correlation of mass M_{W_R} and parameter ϵ. The colour spectrum indicates $\ln(\chi^2/n_{\mathrm{d.o.f.}})$.

Finally, we show in figure 3.3 the dependence of the heavy gauge boson mass M_{W_R} with respect to ϵ. A specific choice of electroweak parameters will also fix the masses of heavy gauge bosons and as we will see later also have profound impact on the masses of heavy Higgs fields. As can be seen from parametric dependence of the heavy gauge boson masses, the mass of the W_R boson increases when ϵ is lowered. The reason that we do not obtain a strict correlation is due to additional parameters. It should be stated that the black region, linked with a better agreement with the $A_{\mathrm{FB}}(b)$ constraint as stated above, provides an upper bound of roughly $M_{W_R} < 7$ TeV.

In summary, one of the main results of this section is our best fit region, in particular

$$\epsilon \sim 0.03\,, \qquad 0.1 < s < 1/\sqrt{2}\,, \qquad \text{and} \qquad 0.7 < s_R < 1\,. \tag{3.37}$$

We will incorporate these results as outlined below in section 6.3 into our comprehensive analysis of flavour observables in an appropriate manner.

4. *Intermezzo:* General remarks about flavour observables

Flavour observables play an important role in searching for NP and are complementary to direct collider searches. In this chapter we give a compendium of formulae necessary for the flavour analysis of both models considered. Most of these formulae are valid independent of the particular model and apply to both models considered in this thesis. We do not want to replicate various reviews (see for example [52, 129]) and we just summarise the main points therein useful for our analysis. In particular, we consider particle anti-particle mixing and rare decays. We list their operator basis and provide suitable formulae for the study of NP contributions to flavour observables. Finally, we review the status of current experimental data and compare it to the SM predictions.

4.1. Preliminaries

The starting point of every flavour analysis beyond the SM is the effective Hamiltonian. This effective Hamiltonian encodes both SM and NP effects at the quark level. It can be constructed by incorporating all Feynman diagrams contributing to the process under consideration. It allows us to derive the decay amplitude of meson decays from a meson M to a final state F according to

$$A(M \to F) = \langle F | \mathcal{H}_{\text{eff}} | M \rangle \sim \sum_i C_i(\mu) \langle F | Q_i(\mu) | M \rangle, \qquad (4.1)$$

where $\langle F | Q_i(\mu) | M \rangle$ are the hadronic matrix elements of local operators and $C_i(\mu)$ are the Wilson coefficients. The proportionality represents the fact that as depending upon the model it is useful to extract specific pre-factors, which in principle can also be absorbed in the Wilson coefficients.

Both matrix elements and Wilson coefficients are dependent on an arbitrary scale μ such that the full amplitude is independent of it. Note that when considering quantum corrections there exists also a renormalisation scheme dependence with similar behaviour. The hadronic matrix elements contain physics below μ and have to be evaluated by non-perturbative methods such as lattice calculations, hadronic sum rules, chiral perturbation theory, heavy quark effective theory, just to mention a few. The Wilson coefficients describing the physics above the scale μ can be calculated perturbatively and they also include the new heavy particles through tree-level, box and penguin

diagrams depending on the model and additionally QCD corrections. This perturbativity is guaranteed as long as the scale μ is not chosen too small, usually taken of order of the mass of the decaying hadron. In the case of K decays, however, this scale is taken to be slightly higher, around 2 GeV.

This so called separation of long-distance and short-distance contributions by a scale μ is then compactly described by the operator product expansion (OPE) [130, 131]. Furthermore the OPE allow a systematic classification of contributing operators. We will elaborate on this in the following section.

Apart from the OPE there is another useful tool for handling effects of very different scales like from the scale of the bound states (mesons) up to the scale of heavy NP particles: Large logarithms can be avoided by making use of the so called renormalisation group improved perturbation theory when calculating the Wilson coefficients $C(\mu)$. A detailed description of the these methods can be found in e.g. [129, 132].

For NP effects it turns out that it is sometimes useful to evaluate both Wilson coefficients and hadronic matrix elements at a high scale. We will show this in detail when considering particular models.

4.2. Meson anti-meson mixing

4.2.1. General $\Delta F = 2$ operator basis

In this section we give a complete list of relevant operators for $\Delta F = 2$ transitions [52, 133, 134]. It is common to classify the operators by their chirality: we have five classes of operators, in particular VLL, VRR, LR, SLL and SRR operators, where we use the designations left-handed (L), right-handed (R), vector (V) and scalar (S).

Let us first consider $K^0 - \bar{K}^0$ mixing. Depending on the model only a subset of these operators describes the full basis, so we find it useful to divide these dimension-six operators into two groups. The first group is given by

$$
\begin{aligned}
\mathcal{Q}_1^{VLL}(K) &= \left(\bar{s}^\alpha \gamma_\mu P_L d^\alpha\right)\left(\bar{s}^\beta \gamma^\mu P_L d^\beta\right), \\
\mathcal{Q}_1^{VRR}(K) &= \left(\bar{s}^\alpha \gamma_\mu P_R d^\alpha\right)\left(\bar{s}^\beta \gamma^\mu P_R d^\beta\right), \\
\mathcal{Q}_1^{LR}(K) &= \left(\bar{s}^\alpha \gamma_\mu P_L d^\alpha\right)\left(\bar{s}^\beta \gamma^\mu P_R d^\beta\right), \\
\mathcal{Q}_2^{LR}(K) &= \left(\bar{s}^\alpha P_L d^\alpha\right)\left(\bar{s}^\beta P_R d^\beta\right),
\end{aligned}
\tag{4.2}
$$

and the second group is given by

$$
\begin{aligned}
\mathcal{Q}_1^{SLL}(K) &= \left(\bar{s}^\alpha P_L d^\alpha\right)\left(\bar{s}^\beta P_L d^\beta\right), \\
\mathcal{Q}_1^{SRR}(K) &= \left(\bar{s}^\alpha P_R d^\alpha\right)\left(\bar{s}^\beta P_R d^\beta\right),
\end{aligned}
$$

$$\begin{aligned}
\mathcal{Q}_2^{SLL}(K) &= \left(\bar{s}^\alpha \sigma_{\mu\nu} P_L d^\alpha\right)\left(\bar{s}^\beta \sigma^{\mu\nu} P_L d^\beta\right), \\
\mathcal{Q}_2^{SRR}(K) &= \left(\bar{s}^\alpha \sigma_{\mu\nu} P_R d^\alpha\right)\left(\bar{s}^\beta \sigma^{\mu\nu} P_R d^\beta\right)
\end{aligned} \tag{4.3}$$

where $P_{L,R} = \frac{1}{2}(1 \mp \gamma_5)$ is as usual the chirality projection operator and $\sigma_{\mu\nu} = \frac{1}{2}[\gamma_\mu, \gamma_\nu]$. Summation over the colour indices α and β is understood. In the SM just one operator, namely $\mathcal{Q}_1^{VLL}$, appears. Extending the SM by RH currents according to the operator approach of RHMFV, the basis of dimension-six operators can be described by the first group in equation (4.2). Since in the LRM we extend the SM both by RH currents and additional scalars in the Higgs sector, we also have to take into account operators of the second group as given in equation (4.3). Note that we postpone the explicit comparison of the operator structure of both models to section 7.1, after having discussed $\Delta F = 2$ processes explicitly. Similarly, when considering $B_q^0 - \bar{B}_q^0$ mixing, where $q = d, s$, the operators for $\Delta B = 2$ can be straightforwardly obtained from equations (4.2) and (4.3) by switching the appropriate flavour indices, in particular by replacing $s \to b$ and $d \to q$.

In this notation the decay amplitude (4.1) for particle-antiparticle mixing for $M - \overline{M}$ mixing ($M = K, B_d, B_s$) is modified to

$$A(M \to \overline{M}) = \langle \overline{M} | \mathcal{H}_{\text{eff}}^{\Delta F=2} | M \rangle \sim \sum_{i,a} C_i(\mu_H) \langle \overline{M} | Q_i^a(\mu_H) | M \rangle, \tag{4.4}$$

where in RHMFV the sum runs over all the operators in the first group with $i = 1, 2$ and $a = VLL, VRR, LR$ and in the LRM over the first and the second group $i = 1, 2$ and $a = VLL, VRR, LR, SLL, SRR$. We will come back to the these effective Hamiltonians for each model in a separate section, where we will also define the pre-factors. The Wilson coefficients depend on the particular model and will be derived subsequently.

4.2.2. Collection of formulae for $\Delta F = 2$ observables

We now summarise all $\Delta F = 2$ observables relevant for the flavour phenomenology of RHMFV and the LRM. It should be stressed that a consistent result with the formulae given below will only be obtained when using the standard phase convention for the CKM matrix [135]. These formulae do not depend on the detailed structure of the NP model and have already been successfully applied to various models, in particular the Littlest Higgs model with T-parity [136], a Randall Sundrum model with custodial protection [137] and the SM extended by a fourth generation [138].

Starting with $K^0 - \bar{K}^0$ mixing amplitude, the NP contributions modify the off-diagonal elements of the neutral K-meson mass matrix according to

$$2 m_K \left(M_{12}^K\right)^* = \langle \bar{K}^0 | \mathcal{H}_{\text{eff}}^{\Delta S=2} | K^0 \rangle, \tag{4.5}$$

where the full mixing M_{12}^K consists of a SM and NP contribution as given in the following

$$M_{12}^K = \left(M_{12}^K\right)_{\text{SM}} + \left(M_{12}^K\right)_{\text{NP}}. \tag{4.6}$$

Hence, the NP part of the off-diagonal element is straightforwardly given by

$$2m_K \left(M_{12}^K\right)_{\text{NP}}^* = \langle \bar{K}^0| \left[\mathcal{H}_{\text{eff}}^{\Delta S=2}\right]_{\text{NP}} |K^0\rangle \, . \tag{4.7}$$

We will briefly describe the well known SM contribution $\left(M_{12}^K\right)_{\text{SM}}$ in the following section.

Now we have everything at hand in order to describe two well-measured observables of the $K^0 - \bar{K}^0$ system, in particular the splitting between the two mass eigenstates, the K_L and K_S mass difference

$$\Delta M_K = 2 \operatorname{Re} M_{12}^K + (\Delta M_K)_{\text{LD}} \, , \tag{4.8}$$

where $(\Delta M_K)_{\text{LD}}$ is the unknown part from long-distance contributions. Further we have the CP-violating parameter

$$\varepsilon_K = \frac{\kappa_\varepsilon e^{i\varphi_\varepsilon}}{\sqrt{2}(\Delta M_K)_{\text{exp}}} \operatorname{Im} M_{12}^K \, , \tag{4.9}$$

where $\varphi_\varepsilon = (43.51 \pm 0.05)°$ and $\kappa_\varepsilon = 0.94 \pm 0.02$ [47,68] includes effects from $\varphi_\varepsilon \neq \pi/4$ and also takes into account the additional effects from long-distance contributions.

Considering now the $B_{d,s}^0 - \bar{B}_{d,s}^0$ systems, the off-diagonal element of the mass matrix is similarly given by

$$M_{12}^q = (M_{12}^q)_{\text{SM}} + (M_{12}^q)_{\text{NP}} \tag{4.10}$$

where $q = d, s$. Further details about the SM contribution $\left(M_{12}^d\right)_{\text{SM}}$ are deferred to the next section. It is convenient to rewrite the off-diagonal element M_{12}^q as [139]

$$M_{12}^q = (M_{12}^q)_{\text{SM}} C_{B_q} e^{2i\varphi_{B_q}} \, , \tag{4.11}$$

where

$$\left(M_{12}^d\right)_{\text{SM}} = \left|\left(M_{12}^d\right)_{\text{SM}}\right| e^{2i\beta} \, , \tag{4.12}$$

$$\left(M_{12}^s\right)_{\text{SM}} = \left|\left(M_{12}^s\right)_{\text{SM}}\right| e^{2i\beta_s} \, , \tag{4.13}$$

and the phases β and β_s are defined through the CKM elements in the following way

$$V_{td} = |V_{td}|e^{-i\beta} \quad \text{and} \quad V_{ts} = -|V_{ts}|e^{-i\beta_s} \, . \tag{4.14}$$

The mass differences in the $B_q^0 - \bar{B}_q^0$ system is given by

$$\Delta M_q = 2\,|M_{12}^q| = (\Delta M_q)_{\text{SM}} C_{B_q} \, . \tag{4.15}$$

Next we consider the time-dependent CP asymmetries of the decays $B_d^0 \to \psi K_S$ and $B_s^0 \to \psi\phi$. They are special due to two reasons [140, 141]: first the final state is a CP

eigenstate and second, a single decay mechanism dominates so that hadronic matrix elements with their uncertainties drop out and direct CP violation vanishes. Thus

$$\frac{\Gamma(B_q^0(t) \to f) - \Gamma(\overline{B_q^0}(t) \to f)}{\Gamma(B_q^0(t) \to f) + \Gamma(\overline{B_q^0}(t) \to f)} = -\sin\phi \, \sin(\Delta M_q t) \,, \tag{4.16}$$

where f on the left-hand side gives the final state depending on the decay, and $\phi = 2\phi_D - 2\phi_M^q$ on the right-hand side describes the weak phase difference. Taking the coefficients of $\sin(\Delta M_d t)$ and $\sin(\Delta M_s t)$ in the time dependent asymmetries in $B_d^0 \to \psi K_S$ and $B_s^0 \to \psi\phi$ respectively, yields

$$S_{\psi K_S} = \sin(2\beta + 2\varphi_{B_d}) \,, \tag{4.17}$$

$$S_{\psi\phi} = \sin(2|\beta_s| - 2\varphi_{B_s}) \,. \tag{4.18}$$

These mixing induced CP asymmetries measure $(\beta + \varphi_{B_d})$ and $(|\beta_s| - \varphi_{B_s})$ in presence of the new CP-violating phases φ_{B_d} and φ_{B_s} respectively, as opposed to the SM where they measure β and β_s. Thus they allow us to draw conclusions about the new the CP violating phases entering in M_{12}^q. Note that the SM automatically yields $\phi_D \approx 0$ for these decays. This cannot be assumed in the LRM due to the presence of tree-level corrections. However it turns out that these effects are negligible.

Finally, following the discussions of [136], we consider the width difference $\Delta\Gamma_q$ and the semileptonic CP asymmetry A_{SL}^q, which are defined respectively as

$$\Delta\Gamma_q = \Gamma_L^q - \Gamma_H^q \,, \tag{4.19}$$

$$A_{\mathrm{SL}}^q = \frac{\Gamma(\bar{B}_q^0 \to \ell^+ X) - \Gamma(B_q^0 \to \ell^- X)}{\Gamma(\bar{B}_q^0 \to \ell^+ X) + \Gamma(B_q^0 \to \ell^- X)} \,. \tag{4.20}$$

The calculation of the theoretical predictions of both $\Delta\Gamma_q$ and A_{SL}^q requires a diagonalisation of 2×2 Hamiltonian $H = M - i\Gamma/2$ of the $B_q^0 - \bar{B}_q^0$ system in order to determine the off-diagonal matrix elements M_{12}^q and Γ_{12}^q [141]. Further simplifications can be made when neglecting $\mathcal{O}(m_b^4/m_t^4)$ terms, so that we can write

$$\Delta\Gamma_q = -\Delta M_q \, \mathrm{Re}\left(\frac{\Gamma_{12}^q}{M_{12}^q}\right) \,, \tag{4.21}$$

$$A_{\mathrm{SL}}^q = \mathrm{Im}\left(\frac{\Gamma_{12}^q}{M_{12}^q}\right) \,. \tag{4.22}$$

It should be mentioned that both observables are connected by a model-independent correlation [142, 143]. This correlation can be derived analytically within certain approximations which are accurate for large $S_{\psi\phi}$. However, since we investigate this correlation numerically without further assumptions, we do not show the explicit formula here. Furthermore, it is useful to extract the dependence of these observables on

NP. Using equation (4.11), we obtain the following expressions for the width differences $\Delta\Gamma_q$ and the semileptonic CP-asymmetries A_{SL}^q

$$\frac{\Delta\Gamma_q}{\Gamma_q} = -\left(\frac{\Delta M_q}{\Gamma_q}\right)^{\exp}\left[\mathrm{Re}\left(\frac{\Gamma_{12}^q}{M_{12}^q}\right)^{\mathrm{SM}}\frac{\cos 2\varphi_{B_q}}{C_{B_q}} + \mathrm{Im}\left(\frac{\Gamma_{12}^q}{M_{12}^q}\right)^{\mathrm{SM}}\frac{\sin 2\varphi_{B_q}}{C_{B_q}}\right] \quad (4.23)$$

$$A_{\mathrm{SL}}^q = \mathrm{Im}\left(\frac{\Gamma_{12}^q}{M_{12}^q}\right)^{\mathrm{SM}}\frac{\cos 2\varphi_{B_q}}{C_{B_q}} - \mathrm{Re}\left(\frac{\Gamma_{12}^q}{M_{12}^q}\right)^{\mathrm{SM}}\frac{\sin 2\varphi_{B_q}}{C_{B_q}}\,. \quad (4.24)$$

It should be mentioned that the calculation of both $\Delta\Gamma_q$ and A_{SL}^q requires the knowledge of non-perturbative effects of the off-diagonal matrix element Γ_{12}^q. For this reason we use the results of [61, 144], which give the following values:

$$\mathrm{Re}\left(\frac{\Gamma_{12}^d}{M_{12}^d}\right)^{\mathrm{SM}} = -(5.3 \pm 1.0)\times 10^{-3}\,, \qquad \mathrm{Re}\left(\frac{\Gamma_{12}^s}{M_{12}^s}\right)^{\mathrm{SM}} = -(5.0 \pm 1.0)\times 10^{-3}\,,$$
$$(4.25)$$

$$\mathrm{Im}\left(\frac{\Gamma_{12}^d}{M_{12}^d}\right)^{\mathrm{SM}} = -(4.1 \pm 0.6)\times 10^{-4}\,, \qquad \mathrm{Im}\left(\frac{\Gamma_{12}^s}{M_{12}^s}\right)^{\mathrm{SM}} = (1.9 \pm 0.3)\times 10^{-5}\,. \quad (4.26)$$

Also interesting from an experimental point of view is the like-sign dimuon charge asymmetry of semi-leptonic decays of b-hadrons, which appears as a linear combination of A_{SL}^d and A_{SL}^s. The explicit coefficients and a more detailed description can be found in [145].

4.2.3. SM contribution to $\Delta F = 2$ processes

As the SM is the low-energy limit of any NP model, the main contribution for $\Delta F = 2$ processes comes from the SM, while the NP contributions are small. Therefore, we will briefly summarise the results for $\Delta F = 2$ processes in the SM from [133]. These explicit formulas will mainly become interesting when studying a full theory as it is the case in the LRM, while in the effective approach of RHMFV we are mainly interested in estimating the magnitudes of deviations from the SM contribution.

In the SM, particle anti-particle mixing is described by box diagram contributions with internal W-boson and up-type quark exchanges. The effective Hamiltonian of $\Delta S = 2$ is to a good approximation described by

$$\left[\mathcal{H}_{\mathrm{eff}}^{\Delta S=2}\right]_{\mathrm{SM}} = \frac{G_F^2}{4\pi^2}M_W^2\left[\lambda_c^2\eta_1 S_0(x_c) + \lambda_t^2\eta_2 S_0(x_t) + 2\lambda_c\lambda_t\eta_3 S_0(x_c, x_t)\right]\times \mathcal{Q}_1^{VLL}(K)\,,$$
$$(4.27)$$

where $\lambda_i = V_{is}^* V_{id}$ is given by the relevant CKM elements and the explicit form of the one-loop box functions $S_0(x_i)$ and $S_0(x_i, x_j)$ with $x_i = m_i^2/M_W^2$ can be found in [129]. We have also collected them in appendix E. Short-distance QCD effects are governed by the factors η_i up to NLO level and can be found in [146–150]. Note that here we have made the strong coupling dependent terms implicit as this dependence is absorbed

in the renormalisation group invariant parameter $\hat{B}_K$. It should be stressed again that in the SM effective Hamiltonian only a single operator appears.

Evaluating the matrix elements using equation (4.5), we finally obtain the off-diagonal element of the mass matrix

$$\left(M_{12}^K\right)_{\mathrm{SM}} = \frac{G_F^2}{12\pi^2} F_K^2 \hat{B}_K m_K M_W^2 \left[\lambda_c^{*2}\eta_1 S_0(x_c) + \lambda_t^{*2}\eta_2 S_0(x_t) + 2\lambda_c^*\lambda_t^*\eta_3 S_0(x_c, x_t)\right] .$$
(4.28)

with the K meson decay constant F_K and the K meson mass m_K. We have collected all relevant numerical input parameters in table 6.2.

In an analogous procedure one can derive the off-diagonal element of the mass matrix in $B_q - \bar{B}_q$ mixing, we find

$$\left(M_{12}^q\right)_{\mathrm{SM}} = \frac{G_F^2}{12\pi^2} F_{B_q}^2 \hat{B}_{B_q} m_{B_q} M_W^2 \left[\left(\lambda_t^{(q)*}\right)^2 \eta_B S_0(x_t)\right],$$
(4.29)

where $\lambda_t^{(q)} = V_{tb}^* V_{tq}$. In contrast to the K system now both charm and mixed top-charm contributions are found to be negligible. Again, the relevant input parameters can be found in table 6.2.

4.2.4. Comparison of SM and experimental values

In this section we want to compare the experimental situation to the SM prediction for $\Delta F = 2$ observables. We have already discussed the observables $S_{\psi\phi}$, $|\varepsilon_K|$ and $S_{\psi K_S}$ in section 2.1.1 and refer to that section for more details. Here we additionally give the most recent experimental values for ϕ_s related to $S_{\psi\phi}$.

We have already shown that the SM picture exhibits various tensions within certain $\Delta F = 2$ observables. However, these tensions can be moved to other observables depending upon which inputs are chosen. In particular, performing a global fit of all observables leads to a distinct picture distributing the tensions over various observables.

Now we briefly summarise the situation for the remaining observables discussed in this thesis. Generally, experimental and SM values of the mass differences in $\Delta F = 2$ transitions are in quite good agreement with each other. While there is still room for NP in $B_{d,s}^0 - \bar{B}_{d,s}^0$ mixing, in $K^0 - \bar{K}^0$ mixing we only have information about the short-distance contribution. Hence less accurate predictions can be made due to the large uncertainties from the unknown long-distance part.

Finally, we take a look at the width difference $\Delta\Gamma_q$ and the semileptonic CP asymmetry A_{SL}^q, where detailed numbers are shown in table 4.1. Both observables suffer from large uncertainties. The observable A_{SL}^b is particularly interesting, as it can be measured with more precision than its components A_{SL}^q, as can be seen from table 4.1.

Nevertheless, once experimental precision will improve, this class of observables might help to constrain NP scenarios in the future.

observable	experimental value	SM prediction
$\phi_s = -2(\beta_s + \varphi_{B_s})$	$\in [-1.04, -0.04]$ (CDF [64])	-0.0363(17) [78]
	$-0.55^{+0.38}_{-0.36}$ (D0 [65])	
	$+0.13(18)(7)$ (LHCb [66])	
$\frac{\Delta\Gamma_d}{\Gamma_d}$	$0.011(37)$ [114]	$0.0042(8)$ [61]
$\Delta\Gamma_s$	$0.075(35)(1)\,\mathrm{ps}^{-1}$ (CDF [64])	$0.087(21)\,\mathrm{ps}^{-1}$ [61]
	$0.163^{+0.065}_{-0.064}\,\mathrm{ps}^{-1}$ (D0 [65])	
	$0.123(29)(8)\,\mathrm{ps}^{-1}$ (LHCb [66])	
A^d_{SL}	$-0.12(52)\%$ [145]	$-0.041(6)\%$ [144]
A^s_{SL}	$-1.8(11)\%$ [145]	$0.0019(3)\%$ [144]
A^b_{SL}	$-0.79(20)\%$ [145]	$-0.020(3)\%$ [144]

Table 4.1.: Comparison of experimental bounds and SM expectation of several $\Delta F = 2$ observables related to $B_{s,d} - \bar{B}_{s,d}$ mixing. The numbers in parentheses indicate the uncertainty in the last digits.

4.3. Rare K and B decays

4.3.1. $\Delta F = 1$ operator basis for selected decays with RH currents

We now briefly summarise necessary ingredients for the rare decay studies within this thesis. Let us start again with collecting all contributing operators. The operator structure of $\Delta F = 1$ processes is much richer for rare decays. A full list can be found in [134]. Here we restrict ourselves to operators relevant for decays analysed in this thesis. In RHMFV we consider only decays containing a lepton pair in the final state. This is mainly due to the fact that the effective approach is only powerful in making predictions for decays, which are relatively simple and restricted in their operator structure. In the LRM we concentrate on the analysis of $B \to X_s\gamma$.

First, we give the operator basis of the decay $B_q \to \mu^+\mu^-$ $(q = s, d)$ in the presence of

RH currents, which reads

$$
\begin{aligned}
\mathcal{Q}_{\mu\bar\mu}^{LL} &= (\bar b_L \gamma^\mu q_L)(\bar\mu_L \gamma_\mu \mu_L)\,, \\
\mathcal{Q}_{\mu\bar\mu}^{LR} &= (\bar b_L \gamma^\mu q_L)(\bar\mu_R \gamma_\mu \mu_R)\,, \\
\mathcal{Q}_{\mu\bar\mu}^{RL} &= (\bar b_R \gamma^\mu q_R)(\bar\mu_L \gamma_\mu \mu_L)\,, \\
\mathcal{Q}_{\mu\bar\mu}^{RR} &= (\bar b_R \gamma^\mu q_R)(\bar\mu_R \gamma_\mu \mu_R)\,.
\end{aligned}
\tag{4.30}
$$

We want to stress that this basis does not include scalar currents. This is justified since this decay is only considered in RHMFV, where no scalar currents arise. When building the effective Hamiltonian and subsequently evaluating the matrix elements for the decay amplitude for $B_q \to \mu^+\mu^-$, the following simplifications can be made. The quark and lepton parts can be separated and only the axial part contributes according to

$$
\langle 0|\bar b \gamma_\mu P_{R,L} q|B^0\rangle = \pm\frac{1}{2}\langle 0|\bar b \gamma_\mu \gamma_5 q|B^0\rangle\,, \qquad \langle \bar\mu\mu|\bar\mu \gamma_\mu P_{R,L}\mu|0\rangle = \pm\frac{1}{2}\langle \bar\mu\mu|\bar\mu \gamma_\mu \gamma_5 \mu|0\rangle\,.
\tag{4.31}
$$

We will come back to a detailed consideration in section 5.2.3.

For semileptonic decays with a neutrino pair in the final state, this basis simplifies further

$$
\begin{aligned}
\mathcal{Q}_{\nu\bar\nu}^{LL} &= (\bar b_L \gamma^\mu s_L)(\bar\nu_L \gamma_\nu \nu_L)\,, \\
\mathcal{Q}_{\nu\bar\nu}^{RL} &= (\bar b_R \gamma^\mu s_R)(\bar\nu_L \gamma_\nu \nu_L)\,,
\end{aligned}
\tag{4.32}
$$

where we have chosen the flavour basis for $B \to \{X_s, K, K^*\}\nu\bar\nu$ decays. Recall that in SM only the first operator exists. For $K \to \pi\nu\bar\nu$ decays one only has to switch to appropriate flavours, in particular making the replacements $b \to s$ and $s \to d$ in equation (4.32).

A more complicated operator structure is obtained for the inclusive decay $B \to X_s\gamma$. The dipole operators characteristic for the decay $B \to X_s\gamma$ are given by

$$
\begin{aligned}
\mathcal{Q}_{7\gamma} &= \frac{e}{16\pi^2} m_b \bar s_\alpha \sigma^{\mu\nu} P_R b_\alpha F_{\mu\nu}\,, \\
\mathcal{Q}'_{7\gamma} &= \frac{e}{16\pi^2} m_b \bar s_\alpha \sigma^{\mu\nu} P_L b_\alpha F_{\mu\nu}\,, \\
\mathcal{Q}_{8G} &= \frac{g_s}{16\pi^2} m_b \bar s_\alpha \sigma^{\mu\nu} P_R T^a_{\alpha\beta} b_\beta G^a_{\mu\nu}\,, \\
\mathcal{Q}'_{8G} &= \frac{g_s}{16\pi^2} m_b \bar s_\alpha \sigma^{\mu\nu} P_L T^a_{\alpha\beta} b_\beta G^a_{\mu\nu}\,,
\end{aligned}
\tag{4.33}
$$

where the unprimed operators are already present in the SM. The operators $\mathcal{Q}_{7\gamma}$ and $\mathcal{Q}'_{7\gamma}$ originate from magnetic photon penguins. These are generated when keeping both external b-quark masses and external momenta up to second order in the expansion in the connected photon penguin vertex. Similarly, $\mathcal{Q}_{8G}$ and $\mathcal{Q}'_{8G}$ stem from magnetic

gluon penguins.

We would like to emphasise that the renormalisation group analysis also involves current-current and QCD-penguin operators which we have not shown here. Their explicit form for the SM operators can be found in [129] where they are denoted as $Q_1...Q_6$. In the SM the two sets of operators $(Q_{7\gamma}, Q_{8G})$ and $(Q_1...Q_6)$ do not mix at one-loop level under renormalisation group evolution. Hence in order to calculate the leading mixing contribution one has to perform two-loop calculations. Consequently for next-to-leading order precision a three-loop calculation is necessary. This mixing is very important as it has significant impact on the resulting decay rate. In the LRM the procedure of calculating the strong interaction corrections is even more involved [151]: apart from the above mentioned operators two additional four-quark operators with different chirality structure contribute. Furthermore all chirality flipped four-quark operators have to be included, which increases the total number of operators to 20. The full operator basis is presented in [151]. However in the final analysis only a subset plays an important role. We will study further details below.

4.3.2. Comparison of SM and experimental values

In contrast to the mainly well measured $\Delta F = 2$ observables, the experimental situation for rare decays is quite different. In most cases only upper bounds exist. The predictions for various branching ratios in a NP model are important because these may be confirmed or excluded by experiment. We have collected both experimental and SM value in table 4.2.

observable	experimental value	SM prediction
$\mathrm{Br}(B_s \to \mu^+\mu^-)$	$\leq 3.3\ (5.3) \times 10^{-8}$ [152, 153]	$(3.2 \pm 0.2) \times 10^{-9}$ [138]
$\mathrm{Br}(B_d \to \mu^+\mu^-)$	$\leq 1 \times 10^{-8}$ [152]	$(1.0 \pm 0.1) \times 10^{-10}$ [154]
$\mathrm{Br}(B \to K\nu\bar\nu)$	$< 1.4 \times 10^{-5}$ [155]	$(3.64 \pm 0.47) \times 10^{-6}$ [156–158]
$\mathrm{Br}(B \to K^*\nu\bar\nu)$	$< 8.0 \times 10^{-5}$ [159]	$(7.2 \pm 1.1) \times 10^{-6}$ [156–158]
$\mathrm{Br}(B \to X_s\nu\bar\nu)$	$< 6.4 \times 10^{-4}$ [160]	$(2.7 \pm 0.2) \times 10^{-5}$ [156–158]
$\mathrm{Br}(K_L \to \pi^0\nu\bar\nu)$	$\leq 6.7 \times 10^{-8}$ [161]	$(2.8 \pm 0.6) \times 10^{-11}$ [162]
$\mathrm{Br}(K^+ \to \pi^+\nu\bar\nu)$	$17.3^{+11.5}_{-10.5} \times 10^{-11}$ [163]	$(8.5 \pm 0.7) \times 10^{-11}$ [162]
$\mathrm{Br}(B \to X_s\gamma)$	$(3.55 \pm 0.26) \times 10^{-4}$ [164]	$(3.15 \pm 0.23) \times 10^{-4}$ [165]

Table 4.2.: Comparison of experimental bounds and SM expectation of branching ratios of rare K and B decays

For the decays $\mathrm{Br}(B_q \to \mu^+\mu^-)$, the bound of $\mathrm{Br}(B_s \to \mu^+\mu^-)$ is already relatively close to the SM predictions. In table 4.2 we have collected the 95% C.L. upper limits from

CDF [152] and D0 [153] (the measurements from the D0 experiment is given in parentheses). Improved measurements are expected in the future by LHCb. The $B_s \to \mu^+\mu^-$ decay is the most promising as the sensitivity has to be increased only by one order of magnitude. In table 4.2 we also show the SM predictions, extracted by using the relation of $\mathrm{Br}(B_q \to \mu^+\mu^-)$ to ΔM_q as described in [154] and with updated values [138].

Also promising are the rare K and B decays of the class with a neutrino pair in the final state, as they are theoretically very clean. This is mainly because non-perturbative contributions of both low energy QCD dynamics and photon exchanges are either eliminated in inclusive decays or encoded in an efficient way in the hadronic matrix elements in case of exclusive decays [158]. Even though the measurement of the branching ratios is a big challenge, there is hope for future data from Super-B factories [166, 167]. We have collected experimental values and SM predictions for the decays considered in this thesis in table 4.2. Here a comment is in order: the SM predictions for the decays $B \to \{X_s, K, K^*\}\nu\bar{\nu}$ contain only the short-distance contributions to these decays. As described in [157] these can be derived by a special method where the reducible long-distance effects are subtracted from the corresponding total rates.

We now mention the rare kaon decays $K^+ \to \pi^+\nu\bar{\nu}$ and $K_L \to \pi^0\nu\bar{\nu}$. In the SM they are governed by Z penguins and box diagrams. These decays are theoretically very clean due to the fact that the corresponding hadronic matrix elements can be extracted from $K^+ \to \pi^0 e^+\nu$ including isospin corrections [168]. The SM result is known up to next-to-next-to-leading order (NNLO) level in QCD corrections [169]. Furthermore it should be mentioned that in contrast to the CP conserving decay $K^+ \to \pi^+\nu\bar{\nu}$, $K_L \to \pi^0\nu\bar{\nu}$ is affected by mixing-induced CP violation. Hence its measurement can help to draw conclusions about NP contributions to CP violation [168, 170]. While an experimental value already exists for the branching ratio of $K^+ \to \pi^+\nu\bar{\nu}$, only an upper bound for $K_L \to \pi^0\nu\bar{\nu}$ is available. This upper bound is still two orders of magnitude above the SM value.

Among the rare decays the radiative decay $B \to X_s\gamma$ plays a very special role. As stated already above, the SM calculation of the branching ratio for $B \to X_s\gamma$ is challenging due to vanishing operator mixing under renormalisation at one-loop level. Since 2006 the authors of [165] provided a calculation including three-loop on-shell and four-loop tadpole Feynman diagrams, the SM result is now known up to NNLO QCD correction. Hence together with the measurements from Belle and BaBar at $E_\gamma > 1.6$ GeV, this radiative decay provides now strong constraints on NP scenarios. Note that errors in both the SM branching ratio and experimental value are already below 10%. Having the SM value below the experimental one, models with NP providing a positive contribution to the SM branching ratio are consequently favoured [170].

5. Flavour phenomenology of RHMFV

We now want to examine whether the new flavour mixing in RHMFV is consistent with low energy observables from particle anti-particle mixing and rare decays of B and K mesons. The specific model features of RHMFV were discussed in chapter 2, where we fixed the RH mixing matrix for this framework. We will use the basic tools for analysing flavour observables described in chapter 4. We will further constrain the structure of the RH mixing matrix, study correlations of observables and examine the impact on the anomalies collected in section 2.1.1.

5.1. $\Delta F = 2$ observables in RHMFV

5.1.1. The effective $\Delta F = 2$ Lagrangian of RHMFV

In this chapter we investigate the impact of RH currents on meson anti-meson mixing. As indicated in section 2.3.4 in RHMFV, the NP effects enter through dimension-six operators, contributing by means of an effective Lagrangian

$$\mathcal{L}^{\Delta F=2} = \frac{c_{RR}}{\Lambda^2} O_{RR}^{(6)} + \frac{c_{LR}}{\Lambda^2} O_{LR}^{(6)} \,, \tag{5.1}$$

where the operators were already described in equations (2.26) and (2.27) and c_{RR} and c_{LR} are flavour-blind dimensionless coefficients. The determination of the size of these coefficients is one of the questions which we address below.

As indicated in section 4.2.1, we switch to the operator basis given in equation (4.2). In RHMFV four operators can be relevant, in particular $\mathcal{Q}_1^{VLL}$, $\mathcal{Q}_1^{VRR}$, $\mathcal{Q}_1^{LR}$ and $\mathcal{Q}_2^{LR}$. Assuming a scale μ_R, at which the NP is integrated out, the effective Hamiltonian for the NP part is given by

$$\begin{aligned}
\left[\mathcal{H}_{\text{eff}}^{\Delta F=2}(\mu_R)\right]_{\text{NP}} &= \frac{1}{\Lambda^2}\big[C_1{}^{VLL}(\mu_R, M)\,\mathcal{Q}_1^{VLL} + C_1^{VRR}(\mu_R, M)\,\mathcal{Q}_1^{VRR} \\
&\quad + C_1^{LR}(\mu_R, M)\,\mathcal{Q}_1^{LR} + C_2^{LR}(\mu_R, M)\,\mathcal{Q}_2^{LR}\big] \,,
\end{aligned} \tag{5.2}$$

where $\mu_R = \mathcal{O}(\Lambda) = \mathcal{O}(1\text{ TeV})$. We have neglected QCD corrections at that scale. Furthermore, M stands for the meson system, in particular K and $B_{s,d}$, on which the Wilson coefficients C_i^a with $i = 1, 2$ and $a = VLL, VRR, LR$ depend. At the scale μ_R the Wilson coefficient C_1^{VLL} receives only NP contributions. Integrating out the W

boson and the top quark leads to some additional effects from SM. As in RHMFV we restrict ourselves to the dominant effects from the RH sector, represented by $O_{RR}^{(6)}$ and $O_{LR}^{(6)}$ in (5.1). This coefficient will be set to be zero at this high scale. Similarly, we impose a vanishing C_2^{LR}.

5.1.2. Renormalisation group effects

In the next step we want to evolve (5.2) down to the low scale μ_L. To this end we study renormalisation group (RG) effects following [133]. The scale μ_L depends on the meson system in question and is usually chosen to be of the order of the meson mass. To be specific, we have $\mu_L = 2$ GeV for K system and $\mu_L = \mu_b = 4.6$ GeV for the B_d and B_s. Each of the operators $\mathcal{Q}_1^{VLL}$, $\mathcal{Q}_1^{VRR}$, $\mathcal{Q}_1^{LR}$ and $\mathcal{Q}_2^{LR}$ behaves differently under this evolution: The first two operators are easy to handle. $\mathcal{Q}_1^{VLL}$ renormalises under QCD independently of other operators, as does $\mathcal{Q}_1^{VRR}$. In fact the RG running gives the same contribution to both their Wilson coefficients as QCD is not sensitive to the sign of γ_5. Furthermore, the RG evolution of the SM and the NP part contributing to $\mathcal{Q}_1^{VLL}$ can be considered separately. The other two operators $\mathcal{Q}_1^{LR}$ and $\mathcal{Q}_2^{LR}$ form a two by two system and mix under renormalisation. Note that the coefficient of $\mathcal{Q}_2^{LR}$ vanishes at high scale at the leading order (LO) renormalisation analysis but exists at next-to-leading order (NLO) level and is generally $\mathcal{O}(\alpha_s(\mu_R))$.

The prescribed procedure is a well known technique. However, here we benefit from an additional simplification: We evaluate the hadronic matrix elements of equation (4.7) using the Wilson coefficients $C_i^a(\mu_R, M)$ of the meson system $M = K, B_d, B_s$ at the high scale μ_R according to

$$\langle \bar{K}^0 | Q_i^a(\mu_R, K) | K^0 \rangle = \frac{2}{3} m_K^2 F_K^2 P_i^a(K), \tag{5.3}$$

$$\langle \bar{B}_q^0 | Q_i^a(\mu_R, B_q) | B_q^0 \rangle = \frac{2}{3} m_{B_q}^2 F_{B_q}^2 P_i^a(B_q) \tag{5.4}$$

The coefficients $P_i^a(M)$ compactly encode all RG flow effects from scales below μ_R and capture the long distance effects of hadronic matrix elements. It transparently displays short distance NP effects as opposed to the complicated QCD effects. Analytic formulae for $P_i^a(M)$ factors have been presented in [133]. These expressions explicitly display the dependence on RG QCD factors and non-perturbative parameters $B_i^a(\mu_L)$, where μ_L is the above described low energy scale. More details about the explicit calculation of the $B_i^a(\mu_L)$ parameters are presented in [49].

Here two comments are in order: The LR operators are known to have a sizable impact on NP effects due to their enhancement under RG evolution. In the case of K^0–$\bar{K}^0$ mixing one also has to take the chiral enhancement of the hadronic matrix elements into account.

5.1.3. Wilson coefficients and first statements about right-handed contributions to flavour mixing

From the statements made above we now know that it is necessary to find the Wilson coefficients C_i^a at high scale. They can be easily deduced from matching our effective RHMFV Lagrangian (5.1) to the effective Hamiltonian in the general basis given in (5.2). We collect here our results for K, B_d and B_s system.

First the Wilson coefficients for the K system read

$$
\begin{aligned}
\mathcal{C}_1^{VLL}(\mu_R, K) &= 0\,, \\
\mathcal{C}_1^{VRR}(\mu_R, K) &= -c_{RR} y_t^4 e^{2i(\phi_2^d - \phi_1^d)} \left[(\widetilde{V}_0)_{ts}^* (\widetilde{V}_0)_{td} \right]^2 \approx -\frac{c_{RR}}{4} y_t^4 e^{2i(\phi_2^d - \phi_1^d)} (\tilde{c}_{12} \tilde{s}_{12})^2\,, \\
\mathcal{C}_1^{LR}(\mu_R, K) &= -c_{LR} y_t^4 e^{i(\phi_2^d - \phi_1^d)} V_{ts}^* V_{td} (\widetilde{V}_0)_{ts}^* (\widetilde{V}_0)_{td} \approx -\frac{c_{LR}}{2} y_t^4 e^{i(\phi_2^d - \phi_1^d)} (V_{ts}^* V_{td})(\tilde{c}_{12} \tilde{s}_{12})\,, \\
\mathcal{C}_2^{LR}(\mu_R, K) &= 0\,.
\end{aligned}
\tag{5.5}
$$

It should be mentioned that when evaluating the Yukawas according to equation (2.20) the phase dependence appears through

$$
\widetilde{V}_{3i}^* \widetilde{V}_{3j} = e^{i(\phi_i^d - \phi_j^d)} (\widetilde{V}_0)_{3i}^* (\widetilde{V}_0)_{3j}\,.
\tag{5.6}
$$

while for $\widetilde{V}_0$ we have made use of equation (2.77) as described in chapter 2.4.

Similarly we obtain the non-vanishing Wilson coefficients of the $B_{s,d}$ systems

$$
\begin{aligned}
\mathcal{C}_1^{VRR}(\mu_R, B_q) &= -c_{RR} y_t^4 e^{2i(\phi_3^d - \phi_q^d)} \left[(\widetilde{V}_0)_{tb}^* (\widetilde{V}_0)_{tq} \right]^2\,, \\
\mathcal{C}_1^{LR}(\mu_R, B_q) &= -c_{LR} y_t^4 e^{i(\phi_3^d - \phi_q^d)} V_{tb}^* V_{tq} (\widetilde{V}_0)_{tb}^* (\widetilde{V}_0)_{tq}\,.
\end{aligned}
\tag{5.7}
$$

Inserting the particular structure of the RH mixing matrix yields

$$
\begin{aligned}
\mathcal{C}_1^{VRR}(\mu_R, B_d) &\approx -\frac{c_{RR}}{4} y_t^4 e^{2i(\phi_3^d - \phi_1^d)} \tilde{c}_{12}^2\,, \\
\mathcal{C}_1^{LR}(\mu_R, B_d) &\approx \mp \frac{c_{LR}}{2} y_t^4 e^{i(\phi_3^d - \phi_1^d)} V_{tb}^* V_{td} \tilde{c}_{12}\,,
\end{aligned}
\tag{5.8}
$$

and

$$
\begin{aligned}
\mathcal{C}_1^{VRR}(\mu_R, B_s) &\approx -\frac{c_{RR}}{4} y_t^4 e^{2i(\phi_3^d - \phi_2^d)} \tilde{s}_{12}^2\,, \\
\mathcal{C}_1^{LR}(\mu_R, B_s) &\approx \mp \frac{c_{LR}}{2} y_t^4 e^{i(\phi_3^d - \phi_2^d)} V_{tb}^* V_{ts} \tilde{s}_{12}\,,
\end{aligned}
\tag{5.9}
$$

where the sign $\mp$ appears due to (2.77).

We are now able to draw first conclusions about the flavour structure of our model. It should be noted that c_{RR} and c_{LR} are flavour-blind and hence enter universally in the K,

| Mixing term | K-mixing | B_d-mixing | B_s-mixing |
	$s \to d$	$b \to d$	$b \to s$
$\widetilde{V}_{ti}^* \widetilde{V}_{tj}$	$\frac{1}{2}\tilde{c}_{12}\tilde{s}_{12}e^{i(\phi_2^d-\phi_1^d)}$	$\pm\frac{1}{2}\tilde{c}_{12}e^{i(\phi_3^d-\phi_1^d)}$	$\pm\frac{1}{2}\tilde{s}_{12}e^{i(\phi_3^d-\phi_2^d)}$

Table 5.1.: Structures of flavour mixing in the RH sector contributing to particle anti-particle mixing for the parametrisation $\widetilde{V}_0^{(\text{II})}$ as given in equation (2.77).

B_d and B_s system. Therefore, the full flavour dependence is encoded in the RH mixing matrix. To this end it is sufficient to consider how this matrix manifests itself in the various processes as summarised in table 5.1. We recognise a non-universal structure with the observables in K-mixing, B_d mixing and B_s-mixing which are dominated by $\tilde{c}_{12}\tilde{s}_{12}$, $\tilde{c}_{12}$ and $\tilde{s}_{12}$, respectively. The strong constraints on the K system, mainly by ε_K, point towards either a small $\tilde{c}_{12}$ or $\tilde{s}_{12}$ unless c_{RR} and c_{LR} are very small. Due to the enhanced value of $S_{\psi\phi}$ measured by CDF [56] and D0 [57] collaborations[1], we assume large CP-violating effects in B_s-mixing. Hence we choose $\tilde{s}_{12}$ to be large, which then in combination with ε_K automatically implies negligible effects in B_d mixing. Roughly, the RH mixing matrix appears with the following structure

$$\left|\widetilde{V}_0\right| \sim \begin{pmatrix} 0 & \frac{\sqrt{2}}{2} & \frac{\sqrt{2}}{2} \\ 1 & 0 & 0 \\ 0 & \frac{\sqrt{2}}{2} & \frac{\sqrt{2}}{2} \end{pmatrix} , \tag{5.10}$$

where the zero entries should not be understood as exact zeros. Note that there are additional phases from the diagonal matrices shown in equation (2.29).

We do not want to make such a rough approximation, but the above arguments make clear that assuming $\tilde{c}_{12} \ll 1$ and hence $\tilde{s}_{12} \approx 1$ is natural. In this limit the non-vanishing Wilson coefficients relevant for K^0–$\bar{K}^0$ mixing simplify to

$$\begin{aligned} \mathcal{C}_1^{VRR}(\mu_R, K) &\approx -\frac{c_{RR}}{4}y_t^4 e^{2i\phi_{21}^d}\tilde{c}_{12}^2 , \\ \mathcal{C}_1^{LR}(\mu_R, K) &\approx -\frac{c_{LR}}{2}y_t^4 e^{i\phi_{21}^d}V_{ts}^*V_{td}\tilde{c}_{12} , \end{aligned} \tag{5.11}$$

where we have introduced the notation $\phi_{21}^d = (\phi_2^d - \phi_1^d)$. No further simplifications occur in the B_d sector. For the B_s system we can trivially write

$$\begin{aligned} \mathcal{C}_1^{VRR}(\mu_R, B_s) &\approx -\frac{c_{RR}}{4}y_t^4 e^{2i\phi_{32}^d} , \\ \mathcal{C}_1^{LR}(\mu_R, B_s) &\approx \mp\frac{c_{LR}}{2}y_t^4 e^{i\phi_{32}^d}V_{tb}^*V_{ts} , \end{aligned} \tag{5.12}$$

where we have also defined the compact notation $\phi_{3i}^d = (\phi_3^d - \phi_i^d)$ for the B system.

---

[1]These earlier measurements served as a motivation for this analysis, recent measurements from LHCb seem to favour lower values of $S_{\psi\phi}$. Higher statistics are needed to provide a firm conclusion.

We briefly mention how the structure of the Wilson coefficients changes with the second ansatz $\widetilde{V}_0^{(\mathrm{III})}$. Bearing in mind that $\tilde{c}_{13} \ll 1$ in this ansatz, we list the structure of flavour mixing in RH sector in table 5.2. A comparison with table 5.1 shows that in the K system we only expect a change of a factor of two. In $B_{d,s}^0 - \bar{B}_{d,s}^0$ mixing the effects are automatically small. Therefore this ansatz is phenomenologically less appealing and we only pursue the ansatz $\widetilde{V}_0^{(\mathrm{II})}$ in the following.

Mixing term	K-mixing	B_d-mixing	B_s-mixing
	$s \to d$	$b \to d$	$b \to s$
$\widetilde{V}_{ti}^* \widetilde{V}_{tj}$	$\tilde{c}_{12}\tilde{s}_{12} e^{i(\phi_2^d - \phi_1^d)}$	$\tilde{c}_{12}\tilde{c}_{13} e^{i(\phi_3^d - \phi_1^d)}$	$\tilde{s}_{12}\tilde{c}_{13} e^{i(\phi_3^d - \phi_2^d)}$

Table 5.2.: Structures of flavour mixing in the RH sector contributing to particle anti-particle mixing for the parametrisation $\widetilde{V}_0^{(\mathrm{III})}$ as given in equation (2.78).

5.1.4. K^0–$\bar{K}^0$ mixing

We now take a closer look at $K_L - K_S$ mass difference, ΔM_K, and the CP-violating parameter ε_K. To this end we evaluate the off-diagonal element M_{12}^K of the neutral K-meson mass matrix according to equation (4.7) and make use of our effective Hamiltonian given in equations (5.2) and (5.3). We find

$$\left(M_{12}^K\right)_{\mathrm{NP}} = \frac{1}{3\Lambda^2} m_K F_K^2 \cdot \Big[\left(C_1^{VLL}(\mu_R, K) + C_1^{VRR}(\mu_R, K)\right) P_1^{VLL}(K)$$
$$+ C_1^{LR}(\mu_R, K) P_1^{LR}(K) \Big]^*, \qquad (5.13)$$

where

$$P_1^{VLL}(K) \approx 0.50, \qquad P_1^{LR}(K) \approx -52 \,. \qquad (5.14)$$

These values are derived from the analytic formulae of [133], setting the matching scale to $\mu_R = 1.5$ TeV, and taking the hadronic matrix elements from [171]. All necessary numerical values are collected in table 5.3.

Inserting the Wilson coefficients from equation (5.11) and using the formulae for ΔM_K and ε_K given in equations (4.8) and (4.9) respectively, we get

$$
\begin{aligned}
(\Delta M_K)_{\mathrm{RH}} &= (\Delta M_K)_{\mathrm{exp}} \times \Big[-2.5 \times 10^4 \times c_{RR}\tilde{c}_{12}^2 \cos(2\phi_{21}^d) \\
&\qquad -1.7 \times 10^3 \times c_{LR}\tilde{c}_{12} \cos(\phi_{21}^d - \beta + \beta_s) \Big] \frac{(3 \text{ TeV})^2}{\Lambda^2} \,, \quad (5.15) \\
(\varepsilon_K)_{\mathrm{RH}} &= |\varepsilon_K|_{\mathrm{exp}}\, e^{i\phi_\epsilon} \times \Big[3.7 \times 10^6 \times c_{RR}\tilde{c}_{12}^2 \sin(2\phi_{21}^d) \\
&\qquad +2.5 \times 10^5 \times c_{LR}\tilde{c}_{12} \sin(\phi_{21}^d - \beta + \beta_s) \Big] \frac{(3 \text{ TeV})^2}{\Lambda^2} \,, \quad (5.16)
\end{aligned}
$$

parameter	value		parameter	value
F_K	(155.8 ± 1.7) MeV [94]		ΔM_K	$(5.292 \pm 0.009) \times 10^{-3}\mathrm{ps}^{-1}$ [74]
F_{B_d}	(192.8 ± 9.9) MeV [94]		ΔM_d	(0.507 ± 0.005) ps^{-1} [79]
F_{B_s}	(238.8 ± 9.5) MeV [94]		ΔM_s	(17.77 ± 0.12) ps^{-1} [79]
$\hat{B}_K$	0.725 ± 0.026 [94]		$|V_{tb}|$	1 ± 0.06 [172]
$\hat{B}_{B_d}$	1.26 ± 0.11 [94]		$|V_{td}|$	$(8.3 \pm 0.5) \times 10^{-3}$ [172]
$\hat{B}_{B_s}$	1.33 ± 0.06 [94]		$|V_{ts}|$	0.040 ± 0.003 [172]
M_K	0.497614 GeV [74]		$\sin(2\beta_s)$	0.038 ± 0.003 [172]
M_{B_d}	5.2795 GeV [74]		γ	1.09 ± 0.12 [172]
M_{B_s}	5.3664 GeV [74]		$\varepsilon_K^{\mathrm{exp}}$	$(2.229 \pm 0.01) \times 10^{-3}$ [74]
$m_t(m_t)$	(163.5 ± 1.7) GeV [173]		$S_{\psi K_S}^{\mathrm{exp}}$	0.672 ± 0.023 [79]

Table 5.3.: Numerical input parameters for $\Delta F = 2$ observables.

while for numerical values we have again used table 5.3. We have used the usual convention for the phases β and β_s, in particular

$$V_{td} = |V_{td}|e^{-i\beta} \quad \text{and} \quad V_{ts} = -|V_{ts}|e^{-i\beta_s}\,. \tag{5.17}$$

It turns out that the RH contribution can be significant, independent of the size of the new CP-violating phase ϕ_{21}^d, and strongly constrains other parameters as shown below. Setting ϕ_{21}^d to zero we obtain

$$c_{RR}\,\tilde{c}_{12}^2 \quad < \quad 2.0 \times 10^{-5}\,, \qquad \text{from} \qquad (\Delta M_K)_{\mathrm{RH}} \quad < \quad 0.5(\Delta M_K)_{\mathrm{exp}}\,, \tag{5.18}$$
$$c_{LR}\,\tilde{c}_{12} \quad < \quad 1.0 \times 10^{-6}\,, \qquad \text{from} \qquad |\varepsilon_K|_{\mathrm{RH}} \quad < \quad 0.1|\varepsilon_K|_{\mathrm{SM}}\,. \tag{5.19}$$

When we turn on the phase ϕ_{21}^d the bound on $c_{RR}\tilde{c}_{12}^2$ becomes stronger while the bound on $c_{LR}\tilde{c}_{12}$ can be weakened down to 3×10^{-4}. However, this is fine-tuned scenario where new phase ϕ_{21}^d and the CKM phase of $V_{ts}^*V_{td}$ exactly cancel each other.

5.1.5. $B_{d,s}^0 - \bar{B}_{d,s}^0$ mixing

We now turn to $B_d^0 - \bar{B}_d^0$ and $B_s^0 - \bar{B}_s^0$ mixing. Since the derivation is completely analogous to the $K^0 - \bar{K}^0$ mixing, we just summarise the results here. The NP contribution of the off-diagonal element M_{12}^q with $q = d, s$ for the corresponding mass matrix is given by

$$(M_{12}^q)_{\mathrm{NP}} = \frac{1}{3\Lambda^2}m_{B_q}F_{B_q}^2\Big[\left(C_1^{VLL}(\mu_R, B) + C_1^{VRR}(\mu_R, B)\right)P_1^{VLL}(B)$$
$$+ C_1^{LR}(\mu_R, B)P_1^{LR}(B)\Big]^*\,, \tag{5.20}$$

with

$$P_1^{VLL}(B) \approx 0.70, \qquad P_1^{LR}(B) \approx -3.2\,, \tag{5.21}$$

where we have used the above stated procedure with a matching scale of $\mu_R = 1.5$ TeV. Adding the SM and NP part as shown in (4.10), we thus obtain

$$(M_{12}^d)_{\text{SM+RH}} = (M_{12}^d)_{\text{SM}} \times \Big[1 +$$

$$\Big(-6.1 \times 10^3 \times c_{RR}\tilde{c}_{12}^2 e^{-2i(\phi_{31}^d + \beta)} \pm 4.7 \times 10^2 \times c_{LR}\tilde{c}_{12} e^{-i(\phi_{31}^d + \beta)} \Big) \frac{(3 \text{ TeV})^2}{\Lambda^2} \Big] \quad (5.22)$$

$$(M_{12}^s)_{\text{SM+RH}} = (M_{12}^s)_{\text{SM}} \times \Big[1 +$$

$$\Big(-2.5 \times 10^2 \times c_{RR} e^{-2i(\phi_{32}^d + \beta_s)} \mp 0.9 \times 10^2 \times c_{LR} e^{-i(\phi_{32}^d + \beta_s)} \Big) \frac{(3 \text{ TeV})^2}{\Lambda^2} \Big] . \quad (5.23)$$

Taking into account the bounds on $c_{RR}\tilde{c}_{12}^2$ and $c_{LR}\tilde{c}_{12}$ from in (5.18) and (5.19), we realise that the kaon bounds imply, as already anticipated in our early analysis above, negligible effects in B_d mixing. In the B_s system larger effects are possible, especially when $c_{RR,LR}$ are in the 10^{-3}–10^{-2} range and $\tilde{c}_{12}$ is small enough to satisfy the kaon bounds. We obtained these results under the assumption of a large non-standard $S_{\psi\phi}$. This will be elaborated on in more detail in the following section. However, it should be briefly stated that new experimental input lowering the effects in the B_s system would imply bigger effects in B_d mixing within RHMFV.

5.1.6. Combined fit of ε_K and B_s mixing

For a more detailed analysis we now consider the constraints from ε_K and B_s mixing simultaneously. As before we want to assume a large $S_{\psi\phi}$, then

$$\frac{(\Delta M_s)_{\text{exp}}}{(\Delta M_s)_{\text{SM}}} \approx 0.96 \pm 0.15 \qquad \text{and} \qquad S_{\psi\phi} \approx 0.6 \pm 0.3 . \quad (5.24)$$

These two conditions for B_s mixing allow us to set up a system of two equations which can be solved. One obtains conditions for coupling coefficients and phases, which we will apply later in the analysis of rare decays.

For example, assuming the RR operator in (5.23) to be dominant ($c_{RR} \gg c_{LR}$), we obtain

$$\frac{(\Delta M_s)_{\text{exp}}}{(\Delta M_s)_{\text{SM}}} = \frac{(\Delta M_s)_{\text{SM+RH}}}{(\Delta M_s)_{\text{SM}}} = \Big| 1 - 2.6 \times 10^2 \times c_{RR} e^{-2i\phi_{32}^d} \Big| , \quad (5.25)$$

$$S_{\psi\phi} = -\frac{2.6 \times 10^2 \times c_{RR} \sin(2\phi_{32}^d)}{\Big| 1 - 2.6 \times 10^2 \times c_{RR} e^{-2i\phi_{32}^d} \Big|} . \quad (5.26)$$

The solutions for this case are given by

$$c_{RR} \approx \pm 7.3 \times 10^{-3} \quad \text{and} \quad \sin(2\phi_{32}^d) \approx \mp 0.30 ,$$
$$c_{RR} \approx \pm 2.3 \times 10^{-3} \quad \text{and} \quad \sin(2\phi_{32}^d) \approx \mp 0.95 . \quad (5.27)$$

operator	size of coefficient	suppression
RH charged current	$\mathcal{O}(1)$	tree-level
$\Delta F = 2$	$1/(16\pi^2) \approx 6 \times 10^{-3}$	loop

Table 5.4.: Size of coefficients and level of suppression for different observables.

We obtain coupling coefficients of $\mathcal{O}(10^{-3})$ which are substantially lower than the $\mathcal{O}(1)$ Wilson coefficients determined from charged-currents. Naïvely the small value of c_{RR} does not seem natural, however this can be understood from the fact that $\Delta F = 2$ operators are loop-suppressed with respect to charged current operators. This is summarised in table 5.4.

Now we want to investigate whether these solutions for the B_s mixing parameters also satisfy the kaon bounds. As we will show in detail in the following section, ε_K does not require contributions from new CP-violating phases within RHMFV in order to attain a better agreement with the experimental value than the SM. However, there is still room for an extra contribution for NP in equation (5.16) since theoretical errors allow for $\approx \pm 10\%$ variation of the SM amplitude. For this condition we find using equation (5.27),

$$|\tilde{c}_{12}||\sin(2\phi_{21}^d)|^{1/2} < 1.9 \times 10^{-3} , \qquad \text{for } |c_{RR}| \approx 7.3 \times 10^{-3} ,$$
$$|\tilde{c}_{12}||\sin(2\phi_{21}^d)|^{1/2} < 3.4 \times 10^{-3} , \qquad \text{for } |c_{RR}| \approx 2.3 \times 10^{-3} . \qquad (5.28)$$

Even though these values are small this does not imply that they are fine-tuned. One can see that a CP-violating phase of $\mathcal{O}(10^{-1})$ corresponds to a maximal mixing angle $\tilde{c}_{12}$ of $\mathcal{O}(10^{-2})$, which is still larger than $|V_{ub}|$ in the CKM matrix.

When the LR operator provides the dominant contribution ($c_{RR} \ll c_{LR}$) to B_s mixing, more fine-tuning is required due to the large chiral enhancement of the left-right operator in ε_K. This can be seen easily if we repeat the derivations from above for this case. The two conditions on B_s mixing then read

$$c_{LR} \approx \pm 2.0 \times 10^{-2} \quad \text{and} \quad \sin(2\phi_{32}^d) \approx \mp 0.30 ,$$
$$c_{LR} \approx \pm 0.6 \times 10^{-2} \quad \text{and} \quad \sin(2\phi_{32}^d) \approx \mp 0.95 , \qquad (5.29)$$

thus leading to

$$|\tilde{c}_{12}\sin(\phi_{21}^d - \beta + \beta_s)| < 0.2 \times 10^{-4} , \qquad \text{for } |c_{LR}| \approx 2.0 \times 10^{-2} ,$$
$$|\tilde{c}_{12}\sin(\phi_{21}^d - \beta + \beta_s)| < 0.6 \times 10^{-4} , \qquad \text{for } |c_{LR}| \approx 0.6 \times 10^{-2} . \qquad (5.30)$$

This clearly shows that a more stringent bound is obtained compared to equation (5.28).

5.1.7. Effects due to $\sin(2\beta)$ enhancement

Let us take a closer look at ε_K. As RH currents favour the inclusive determination giving the "true" $|V_{ub}|$, one can immediately see that the value for $\sin(2\beta)_{\text{tree}}^{\text{RH}}$ obtained is substantially higher than the corresponding result obtained in the SM, where the inclusive

and exclusive determinations of $|V_{ub}|$ are averaged. In particular, following [172] we obtain $\sin(2\beta)_{\text{tree}}^{\text{RH}} = 0.77 \pm 0.05$ while the SM value reads $\sin(2\beta)_{\text{tree}}^{\text{SM}} = 0.734 \pm 0.034$ [172]. It follows that due to the $\sin(2\beta)$ enhancement, the tension between the experimental value of ε_K and its prediction within the SM is automatically resolved within our framework.

However, as the NP contribution to B_d mixing is constrained to be negligible, we expect $S_{\psi K_S}^{\text{RH}}$ to be significantly larger than the experimental value $S_{\psi K_S}^{\text{exp}} = 0.672 \pm 0.023$ [79]. As a result the existing tension between these two values increases. Our result is about 2σ larger than the measured value. This means that $S_{\psi K_S}$ cannot be solved by RH currents alone in this framework. However, a significantly lower measured value of $S_{\psi\phi}$ might allow effects in B_d mixing. This could then lead to a large enough new phase φ_{B_d} in B_d mixing, contributing to $S_{\psi K_S}$ according to equation (4.17), to ease the tension.

5.2. $\Delta F = 1$ observables in RHMFV

5.2.1. The effective $\Delta F = 1$ Lagrangian of RHMFV

After having studied the details of RHMFV contributions to $\Delta F = 2$ processes, we now consider the extent to which RHMFV manifests itself within $\Delta F = 1$ processes. Once more we start with the effective Lagrangian containing the operators of equation (2.28), which we classified in section 2.3.5. The $\Delta F = 1$ effective Lagrangian then simply reads

$$\mathcal{L}^{\Delta F=1} = \frac{c_{R_{Z1}}}{\Lambda^2} O_{R_{Z1}}^{(6)} + \frac{c_{R_{Z2}}}{\Lambda^2} O_{R_{Z2}}^{(6)} \ . \tag{5.31}$$

The flavour blind coefficients $c_{R_{Z1}}$ and $c_{R_{Z2}}$ encode the high energy dynamics which can arise e.g. within a left-right symmetric framework via a heavy Z_R boson. Note that due to the insertion of Yukawa matrices $(Y_u^\dagger Y_u)_{ij}$ in the operators $O_{R_{Z1}}^{(6)}$ and $O_{R_{Z2}}^{(6)}$, a special flavour structure is selected.

The new dimension six operators generate an effective $\bar{d}_R^i \gamma^\mu d_R^j Z_\mu$ coupling, leading to the main contributions to $\Delta F = 1$ processes. This effective coupling arises after electroweak symmetry breaking and has the following form:

$$\mathcal{L}_{\text{eff}}^{(Z_R)} = -\frac{g}{c_W} \frac{v^2(c_{R_{Z1}} + 2c_{R_{Z2}})}{2\Lambda^2} y_t^2 (\widetilde{V}_{ti}^* \widetilde{V}_{tj}) \bar{d}_R^i \gamma^\mu d_R^j Z_\mu \ , \tag{5.32}$$

where we henceforth make use of the compact notation $c_W = \cos\Theta_W$ and $s_W = \sin\Theta_W$.

In order to clarify the notation convention, we provide the full effective couplings of the Z boson to down-type quarks

$$\mathcal{L}_{\text{eff}}^Z = \frac{g}{c_W} \left(g_L^{ij} \ \bar{d}_L^i \gamma^\mu d_L^j + g_R^{ij} \ \bar{d}_R^i \gamma^\mu d_R^j \right) Z_\mu \ . \tag{5.33}$$

63

The LH coupling g_L^{ij} is only determined by the SM, and is given by

$$(g_L^{ij})_{\text{SM}} = \left(-\frac{1}{2} + \frac{1}{3}s_W^2\right)\delta_{ij} + \frac{g^2}{8\pi^2}V_{ti}^*V_{tj}C_0(x_t) , \qquad x_t = \frac{m_t^2}{m_W^2} . \qquad (5.34)$$

where $C_0(x_t)$ describes the Z vertex function arising from the one loop penguin diagram in the 't Hooft-Feynman gauge and can be found in [132]. The RH coupling consists of both SM and new RH contribution

$$g_R^{ij} = (g_R^{ij})_{\text{SM}} + (\Delta g_R^{ij})_{RH} , \qquad (5.35)$$

where

$$(g_R^{ij})_{\text{SM}} = \frac{1}{3}s_W^2\delta_{ij} , \qquad (5.36)$$

$$(\Delta g_R^{ij})_{RH} = -\frac{v^2(c_{R_{Z1}} + 2c_{R_{Z2}})}{2\Lambda^2}y_t^2\widetilde{V}_{ti}^*\widetilde{V}_{tj} . \qquad (5.37)$$

As it turns out it will be useful to introduce an effective coupling written as

$$c_{Z_R}^{\text{eff}} = (c_{R_{Z1}} + 2c_{R_{Z2}})\frac{(3 \text{ TeV})^2}{\Lambda^2} . \qquad (5.38)$$

Since $c_{R_{Zi}} = \mathcal{O}(1)$, for $\Lambda = 3$ TeV this effective coupling is $\mathcal{O}(1)$, hence guaranteeing a transparent description.

5.2.2. Effective Hamiltonians of rare K and B decays

Now we are prepared to collect the effective Hamiltonians relevant for the decays to be considered. We concentrate on decays with a lepton pair in the final state, in particular $B_{s,d} \to \mu^+\mu^-$, $B \to \{X_s, K, K^*\}\nu\bar{\nu}$ and $K \to \pi\nu\bar{\nu}$.

The effective Hamiltonian for $B_{s,d} \to \mu^+\mu^-$ reads

$$\mathcal{H}_{\text{eff}} = -\frac{4G_F}{\sqrt{2}}\frac{\alpha}{2\pi s_W^2}V_{tb}^*V_{tq}\left[Y_{LL}(\bar{b}_L\gamma^\mu q_L)(\bar{\mu}_L\gamma_\mu\mu_L) + Y_{LR}(\bar{b}_L\gamma^\mu q_L)(\bar{\mu}_R\gamma_\mu\mu_R)\right.$$
$$\left. + Y_{RL}(\bar{b}_R\gamma^\mu q_R)(\bar{\mu}_L\gamma_\mu\mu_L) + Y_{RR}(\bar{b}_R\gamma^\mu q_R)(\bar{\mu}_R\gamma_\mu\mu_R)\right] , \quad (5.39)$$

where $q = d, s$. Note that the full basis of operators mentioned in equation (4.30) appears, while in the SM only the first two operators contribute. Hence, the SM limit is given by $Y_{LL} - Y_{LR} = Y_0(x_t)$ and $Y_{RR} = Y_{RL} = 0$. In case of RHMFV, the new RH contributions only affect Y_{RL} and Y_{RR}. These can be derived using the effective coupling from equation (5.32). We obtain

$$Y_{RL} - Y_{RR} = -T\frac{\widetilde{V}_{tb}^*\widetilde{V}_{tq}}{V_{tb}^*V_{tq}} , \qquad Y_{RL} + Y_{RR} = -(1 - 4s_W^2)\,T\,\frac{\widetilde{V}_{tb}^*\widetilde{V}_{tq}}{V_{tb}^*V_{tq}} , \qquad (5.40)$$

where we have introduced

$$T = (c_{R_{Z1}} + 2c_{R_{Z2}})\frac{4\pi^2 v^2 y_t^2}{g^2 \Lambda^2} = 0.55 \times \left(\frac{m_t(m_t)}{163.5 \text{ GeV}}\right)^2 c_{Z_R}^{\text{eff}} \,. \tag{5.41}$$

As the ν_R fields are assumed to be heavy enough to not contribute to the decay $B \to \{X_s, K, K^*\}\nu\bar{\nu}$, the construction of the effective Hamiltonian turns out to be simpler. We have

$$\mathcal{H}_{\text{eff}} = \frac{4G_F}{\sqrt{2}}\frac{\alpha}{2\pi s_W^2}V_{tb}^*V_{ts} \times \left[X_{LL}(B_s)(\bar{b}_L\gamma^\mu s_L) + X_{RL}(B_s)(\bar{b}_R\gamma^\mu s_R)\right] \times (\bar{\nu}_L\gamma_\nu\nu_L)\,, \tag{5.42}$$

where

$$X_{RL}(B_s) = -T\,\frac{\widetilde{V}_{tb}^*\widetilde{V}_{ts}}{V_{tb}^*V_{ts}} \,. \tag{5.43}$$

Again, let us compare to the SM, where $X_{RL} = 0$ and $X_{LL} \equiv X_{\text{SM}} = 1.464\pm0.041$ [169].

In case of $K \to \pi\nu\bar{\nu}$ we similarly obtain

$$\mathcal{H}_{\text{eff}} = \frac{4G_F}{\sqrt{2}}\frac{\alpha}{2\pi s_W^2}V_{ts}^*V_{td} \times \left[X_{LL}(K)(\bar{s}_L\gamma^\mu d_L) + X_{RL}(K)(\bar{s}_R\gamma^\mu d_R)\right] \times (\bar{\nu}_L\gamma_\nu\nu_L)\,, \tag{5.44}$$

with

$$X_{RL}(K) = -T\,\frac{\widetilde{V}_{ts}^*\widetilde{V}_{td}}{V_{ts}^*V_{td}} \,. \tag{5.45}$$

Note that we only show the leading top-quark contribution for simplicity. While in $K_L \to \pi^0\nu\bar{\nu}$ the charm contributions can be safely neglected, we include them in our phenomenological analysis of $K^+ \to \pi^+\nu\bar{\nu}$.

5.2.3. $B_{s,d} \to \mu^+\mu^-$

We now examine the decays $B_{s,d} \to \mu^+\mu^-$. To this end we evaluate the matrix elements as described in section 4.3.1. Separating the quark and leptonic parts according to equation (4.31) we note that the branching ratio, obtained from the effective Lagrangian (5.39), can be deduced from the SM one (see for example [154]) without repeating the full derivation. Only the following replacement has to be made:

$$Y_0(x_t) \to Y_{LL} + Y_{RR} - Y_{RL} - Y_{LR} \equiv Y_{tot}\,. \tag{5.46}$$

The final result can then be written as

$$\text{Br}(B_s \to \ell^+\ell^-) = \tau(B_s)\frac{G_F^2}{\pi}\left(\frac{\alpha}{4\pi s_W^2}\right)^2 F_{B_s}^2 m_l^2 m_{B_s}\sqrt{1 - 4\frac{m_l^2}{m_{B_s}^2}}|V_{tb}^*V_{ts}|^2|Y_{tot}|^2\,, \tag{5.47}$$

65

while for $\mathrm{Br}(B_d \to \ell^+\ell^-)$ one has to substitute $s \to d$.

We now turn to the derivation of further constraints on the flavour structure of the RH mixing matrix and the effective coupling $c_{Z_R}^{\mathrm{eff}}$ from the $B_{s,d} \to \mu^+\mu^-$ decays. Using the RH mixing matrix shown in equation (2.77) we can insert $\widetilde{V}_{tb}^* \widetilde{V}_{td} \approx \pm \tilde{c}_{12} e^{i\phi_{31}^d}/2$ and $\widetilde{V}_{tb}^* \widetilde{V}_{ts} \approx \pm \tilde{s}_{12} e^{i\phi_{32}^d}/2$ into equation (5.40) and then use the result to find the two branching ratios normalised to the SM ones:

$$\mathrm{Br}(B_s \to \ell^+\ell^-) = \mathrm{Br}(B_s \to \ell^+\ell^-)_{\mathrm{SM}} \left| 1 \mp 7.8 \times \tilde{s}_{12} e^{i\phi_{32}^d} \, c_{Z_R}^{\mathrm{eff}} \right|^2 ,$$

$$\mathrm{Br}(B_d \to \ell^+\ell^-) = \mathrm{Br}(B_d \to \ell^+\ell^-)_{\mathrm{SM}} \left| 1 \pm 37 \times \tilde{c}_{12} e^{i\phi_{31}^d} \, c_{Z_R}^{\mathrm{eff}} \right|^2 . \qquad (5.48)$$

These two branching ratios only depend on four parameters.

Using both SM values and experimental limits for the branching ratios, as given in table 4.2, it is easy to verify that under maximal interference with the SM the following bounds hold:

$$\left| \tilde{s}_{12} c_{Z_R}^{\mathrm{eff}} \right| < 0.54 , \qquad \left| \tilde{c}_{12} c_{Z_R}^{\mathrm{eff}} \right| < 0.30 . \qquad (5.49)$$

From this a very interesting conclusion can be drawn: combining the two bounds in equation (5.49), we obtain the following constraint

$$\left| c_{Z_R}^{\mathrm{eff}} \right| < 0.62 , \qquad (5.50)$$

independent of $\tilde{c}_{12}$. We will make use of this result below in the course of our further analysis.

Since a measurement of the branching ratio $\mathrm{Br}(B_s \to \mu^+\mu^-)$ in the upcoming years is likely, it is interesting to ask about its maximal enhancement. It is possible to further constrain the flavour structure by considering the bounds from $\mathrm{Br}(B_{s,d} \to X_s \ell^+\ell^-)$ [158, 174]. Using the results from [158] we can deduce

$$|T| \times \left| \frac{\widetilde{V}_{tb}^* \widetilde{V}_{ts}}{V_{tb}^* V_{ts}} \right| < 1.07 , \qquad (5.51)$$

at the 90% C.L. level and hence

$$\left| \tilde{s}_{12} c_{Z_R}^{\mathrm{eff}} \right| < 0.15 . \qquad (5.52)$$

This bound is stronger than the one obtained from equation (5.49) and therefore has impact on the maximal possible enhancement of $\mathrm{Br}(B_s \to \mu^+\mu^-)$. Together with equation (5.48) we find that the maximal enhancement in $\mathrm{Br}(B_s \to \mu^+\mu^-)$ over its SM value is not expected to exceed a factor of 5. It follows that the constraint from $\mathrm{Br}(B_s \to X_s \ell^+\ell^-)$ precludes $\mathrm{Br}(B_s \to \mu^+\mu^-)$ near the present experimental bound.

For $\text{Br}(B_s \to \mu^+\mu^-)$, the deviations can still be $\mathcal{O}(1)$, but do not reach the experimental bound. Additionally, they then push the effects in $\text{Br}(B_d \to \mu^+\mu^-)$ to be very small. Hence in case of an $\mathcal{O}(1)$ enhancement in $\text{Br}(B_s \to \mu^+\mu^-)$ compared to the SM, RHMFV clearly predicts no visible deviations compared to the SM in $\text{Br}(B_d \to \mu^+\mu^-)$. Under the assumption of a large $S_{\psi\phi}$, where $\tilde{s}_{12} \approx 1$ and $\tilde{c}_{12} < 10^{-2}$, effects in $\text{Br}(B_d \to \mu^+\mu^-)$ are completely negligible.

5.2.4. $B \to \{X_s, K, K^*\}\nu\bar{\nu}$

Right-handed currents in the decays $B \to \{X_s, K, K^*\}\nu\bar{\nu}$ have been studied extensively in the past. We can apply the results of the general studies of [158, 174] in our present approach. In particular, following [158], the branching ratios of the $B \to \{X_s, K, K^*\}\nu\bar{\nu}$ decays can be expressed in terms of two additional parameters:

$$
\begin{align}
\text{Br}(B \to K\nu\bar{\nu}) &= \text{Br}(B \to K\nu\bar{\nu})_{\text{SM}} \times [1 - 2\eta]\,\epsilon^2 \;, \tag{5.53}\\
\text{Br}(B \to K^*\nu\bar{\nu}) &= \text{Br}(B \to K^*\nu\bar{\nu})_{\text{SM}} \times [1 + 1.31\eta]\,\epsilon^2 \;, \tag{5.54}\\
\text{Br}(B \to X_s\nu\bar{\nu}) &= \text{Br}(B \to X_s\nu\bar{\nu})_{\text{SM}} \times [1 + 0.09\eta]\,\epsilon^2 \;, \tag{5.55}
\end{align}
$$

where the new variables encode the NP part [175, 176]. The SM branching ratios can be found in table (4.2). In our model, using the effective Hamiltonian (5.42), we obtain

$$
\epsilon^2 = \frac{|X_{LL}|^2 + |X_{RL}|^2}{|X_{LL}^{\text{SM}}|^2} \;, \qquad \eta = \frac{-\text{Re}\,(X_{LL}^* X_{RL})}{|X_{LL}|^2 + |X_{RL}|^2} \;. \tag{5.56}
$$

Note that we have suppressed the reference to the B_s system in our notation of the functions $X_{LL,LR}$. As RHMFV only considers the corrections in the RH sector, we restrict ourselves to the X_{RL} function. Inserting X_{RL} from equation (5.43), as a result we obtain

$$
\epsilon^2 = 1 + \frac{T^2}{X_0^2(x_t)}\left|\frac{\widetilde{V}_{tb}^* \widetilde{V}_{ts}}{V_{tb}^* V_{ts}}\right|^2 \approx 1 + 22.1 \times |\tilde{s}_{12} c_{Z_R}^{\text{eff}}|^2 \;, \tag{5.57}
$$

$$
\eta = \frac{T}{\epsilon^2 X_0(x_t)}\text{Re}\left(\frac{\widetilde{V}_{tb}^* \widetilde{V}_{ts}}{V_{tb}^* V_{ts}}\right) \approx \mp \frac{4.7 \times \tilde{s}_{12}\cos(\phi_{32}^d) c_{Z_R}^{\text{eff}}}{1 + 22.1 \times |\tilde{s}_{12} c_{Z_R}^{\text{eff}}|^2} \;. \tag{5.58}
$$

At this stage we want to stress that the expressions of the branching ratios in equations (5.53)–(5.55) describe only the short-distance contributions as already mentioned in section 4.3.2.

Now we are ready to draw various interesting conclusions. Firstly, we take a look at the maximal possible enhancement. Assuming the bound on $\tilde{s}_{12} c_Z^{\text{eff}}$ in equation (5.52), the branching ratios of the exclusive decays $B \to \{K, K^*\}\nu\bar{\nu}$ can be enhanced by more than a factor of two over the corresponding SM value. In the inclusive mode, $B \to X_s\nu\bar{\nu}$, the effects are smaller and maximally a 50% enhancement can be reached. Overall a similar pattern compared to that from the determination of $|V_{ub}|$ in section 2.4.2 describes all
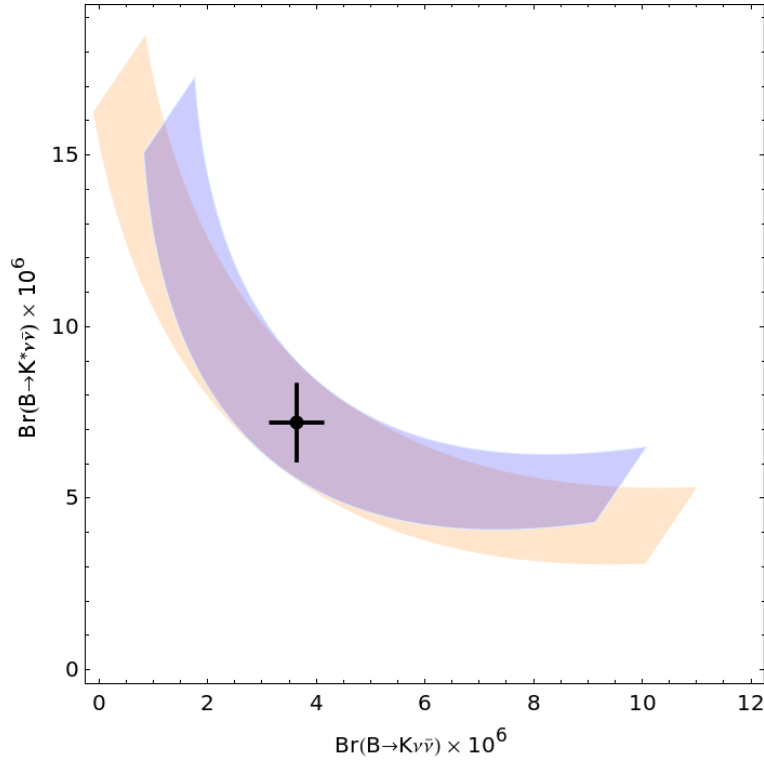
Figure 5.1.: Correlation between $\mathrm{Br}(B \to K\nu\bar\nu)$ and $\mathrm{Br}(B \to K^*\nu\bar\nu)$ in RHMFV. The blue and the orange band correspond to $|\sin(2\phi^d_{32})| = 0.95$ and $|\sin(2\phi^d_{32})| = 0.30$, respectively. The black dot represents the SM value.

three decays $B \to \{X_s, K, K^*\}\nu\bar\nu$.

Further, we can study the effect of a large $S_{\psi\phi}$. As we mentioned in section 5.1.6, $S_{\psi\phi}$ can help to reduce the uncertainty on the CP-violating phase ϕ^d_{32}. Now we will make use of this fact and consider in figure 5.1 the correlation between $\mathrm{Br}(B \to K\nu\bar\nu)$ and $\mathrm{Br}(B \to K^*\nu\bar\nu)$. We show two bands corresponding to the values of equation (5.27), a blue band for $|\sin(2\phi^d_{32})| = 0.95$ and an orange band for $|\sin(2\phi^d_{32})| = 0.30$. These two bands are almost indistinguishable. We observe a clear anti-correlation which can be seen as prediction of the RHMFV model. Both branching ratios can individually - but not together - be enhanced by more than a factor of two over the SM value, which is shown as a black dot with the corresponding error bars. It is worth mentioning that the two possible values of $|\sin(2\phi^d_{32})|$ are independent of the operator dominating $S_{\psi\phi}$.

It would also be interesting to study the correlation between $\mathrm{Br}(B \to K\ell^+\ell^-)$ and $\mathrm{Br}(B \to K^*\ell^+\ell^-)$. However, additional operators contribute in this case. Consequently, the correlation is expected to be less clean and our approximation of considering only the two $\Delta F = 1$ operators of equation (2.28) might also not be sufficient. This analysis is beyond the scope of this thesis.

5.2.5. $K \to \pi \nu \bar{\nu}$

Next we want to examine the $K \to \pi \nu \bar{\nu}$ decays. The branching ratios under inclusion of the RH effects can be written as [162, 168, 177–179]

$$\text{Br}(K^+ \to \pi^+ \nu \bar{\nu}) = \kappa_+ \left[\left(\frac{\text{Im} X_{\text{eff}}}{\lambda^5} \right)^2 + \left(\frac{\text{Re} X_{\text{eff}}}{\lambda^5} - P_c - \delta P_{c,u} \right)^2 \right], \tag{5.59}$$

$$\text{Br}(K_L \to \pi^0 \nu \bar{\nu}) = \kappa_L \left(\frac{\text{Im} X_{\text{eff}}}{\lambda^5} \right)^2, \tag{5.60}$$

where $\lambda = |V_{us}|$, $\kappa_+ = (5.173 \pm 0.025) \times 10^{-11} (\lambda/0.225)^8$ [179] and $\kappa_L = (2.29 \pm 0.03) \times 10^{-10} (\lambda/0.225)^8$ [168]. For the $K^+ \to \pi^+ \nu \bar{\nu}$ mode one needs additional dimension-six charm quark corrections and subleading long-distance effects are summarised in $P_c = 0.372 \pm 0.015$ [162, 169, 177] and $\delta P_{c,u} = 0.04 \pm 0.02$ [178], respectively. The function X_{eff}, given by

$$X_{\text{eff}} = V_{ts}^* V_{td} (X_{LL} + X_{RL}), \tag{5.61}$$

is connected to the effective Hamiltonian in (5.44) and X_{RL} explicitly is shown in equation (5.45). It turns out that it is useful to rewrite X_{eff} so that the SM part can be factorised. Then it has the following form

$$X_{\text{eff}} = V_{ts}^* V_{td} X_{\text{SM}} (1 + \xi e^{i\theta}) \tag{5.62}$$

where $X_{\text{SM}} = 1.464 \pm 0.041$ [169] and ξ and θ are real parameters which yield the SM amplitude in the zero limit. It is easy to verify that these parameters are given by

$$\xi e^{i\theta} = -\frac{T}{X_{\text{SM}}} \frac{\widetilde{V}_{ts}^* \widetilde{V}_{td}}{V_{ts}^* V_{td}} \approx 5.6 \times 10^2 \times \tilde{c}_{12} \tilde{s}_{12} e^{i(\phi_{21}^d + \beta - \beta_s)} c_{Z_R}^{\text{eff}}. \tag{5.63}$$

Considering these results it is clear that the RH contributions can cause large effects, and the bound from in equation (5.52) still leaves room for sizable new contributions. However, as flavour parameters are also correlated with $\Delta F = 2$ observables, we note that the situation is more constrained. This is mainly due to the restriction on $\tilde{c}_{12}$ and ϕ_{21}^d after imposing a large non-standard $S_{\psi\phi}$ taking the ε_K constraint into account, as demonstrated in section 5.1.6.

We now analyse in detail the pattern obtained for the correlations between $\text{Br}(K^+ \to \pi^+ \nu \bar{\nu})$ and $\text{Br}(K_L \to \pi^0 \nu \bar{\nu})$, imposing the constraints from ε_K and $S_{\psi\phi}$. This correlation is shown in figure 5.2. The dashed line gives the model-independent Grossman-Nir bound [180]. We also show the experimental range for $\text{Br}(K^+ \to \pi^+ \nu \bar{\nu})$ [163] in the vertical band, while for $\text{Br}(K_L \to \pi^0 \nu \bar{\nu})$ only an upper bound exists. The black cross represents the SM prediction with its 1σ error. We have listed all details about the data and SM prediction in table 4.2.

Depending on which operator dominates $S_{\psi\phi}$ we obtain a different correlation due to different conditions on the phases:
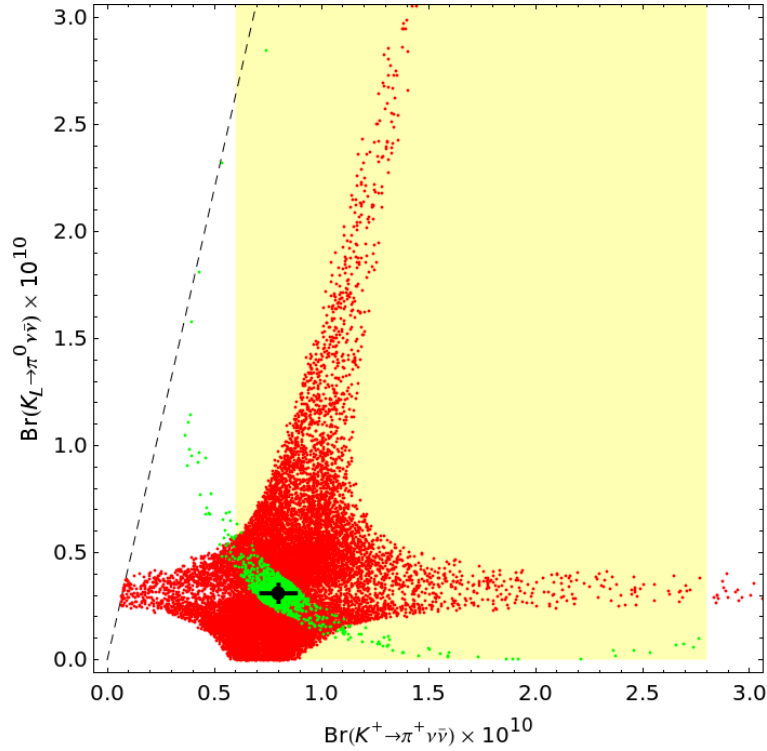
Figure 5.2.: Correlations between $\text{Br}(K^+ \to \pi^+ \nu\bar{\nu})$ and $\text{Br}(K_L \to \pi^0 \nu\bar{\nu})$ taking into account the ε_K constraint. The red and the green points correspond to a negligible or dominant contribution from the operator $\mathcal{Q}_1^{LR}$, respectively. The dashed line represents the Grossman-Nir bound [180]. The vertical band gives the 1σ experimental region and the SM prediction is given by a black cross.

1. First we consider the case with a dominant c_{RR}, shown in red points in figure 5.2. Here, the combined fit of ε_K and $S_{\psi\phi}$ yields condition (5.28), which we have taken into account. It turns out that $\mathcal{O}(1)$ deviations from the SM are still possible in both decays. With larger deviations in only one of the branching ratios shown in figure 5.2, we end up in a more fine-tuned scenario. The phase of ϕ_{12}^d has to be tuned in order to satisfy the ε_K constraint. As noted by [181], this structure is characteristic of all NP frameworks where the phase in $\Delta S = 2$ amplitudes is the square of the CP-violating phase in $\Delta S = 1$ FCNC amplitudes. For example, this is the case in the Littlest Higgs model with T parity [182].

2. Assuming now c_{LR} to be dominant, the bound on the combination of $\tilde{c}_{12}$ and ϕ_{21}^d in equation (5.30) is more stringent. Following from that it is not surprising that the correlation shown in figure 5.2 in green points, also turns out to be more constrained. Sizable deviations can only take place if the phase ϕ_{12}^d is tuned in the way such that $\sin(\phi_{12}^d - \beta + \beta_s) \approx 0$, which makes the bounds in equation (5.30) is less effective.

Finally, we want to stress that the driving force for the specific structure of the correlation in figure 5.2 is mainly determined from the ε_K constraint. So, even lowering the value for $S_{\psi\phi}$, the pattern of correlation remains intact.

5.2.6. Analysis of $Z \to b\bar{b}$

Finally, we take a look at $Z \to b\bar{b}$. The current experimental results are extracted from a global fit of electroweak data collected by the LEP and the SLD experiments [183], where

$$
\begin{aligned}
(g_L^{bb})_{\text{exp}} &= -0.4182 \pm 0.0015 \;, & (5.64) \\
(g_R^{bb})_{\text{exp}} &= +0.0962 \pm 0.0063 \;. & (5.65)
\end{aligned}
$$

It is well known that the LH coupling is in good agreement with the SM expectation. However, in the RH sector there is a large discrepancy between experimental data and SM prediction, which reads

$$
(\Delta g_R^{bb})_{\text{exp}} = (g_R^{bb})_{\text{exp}} - (g_R^{bb})_{\text{SM}} = (1.9 \pm 0.6) \times 10^{-2} \;. \tag{5.66}
$$

In principle RHMFV has room to explain this discrepancy. In RHMFV the numerical values derived from the coupling in equation (5.37) is

$$
(\Delta g_R^{bb})_{RH} \approx -0.15 \times 10^{-2} \times c_{Z_R}^{\text{eff}} \;, \tag{5.67}
$$

where we have taken $|\widetilde{V}_{tb}|^2 \approx 1/2$ from the results of the global fit of the RH mixing matrix of equation (2.77). Clearly for $c_{Z_R}^{\text{eff}} = \mathcal{O}(1)$ the value of equation (5.67) is one order of magnitude too small in order to explain the discrepancy from equation (5.66).

In principle, there is still room for RHMFV effects if we lower the scale of NP to $\Lambda = 1$ TeV and keep $c_{R_{Z1}}, c_{R_{Z2}} = \mathcal{O}(1)$, so that $c_{Z_R}^{\text{eff}}$ will increase. Taking into account the bound on $c_{Z_R}^{\text{eff}}$ from $B_{s,d} \to \mu^+\mu^-$ decays given in (5.50), we find that there is no room for raising the value of $c_{Z_R}^{\text{eff}}$. Hence, we conclude that the anomalous $Z \to b\bar{b}$ cannot be explained within our framework.

6. Flavour phenomenology and numerical analysis of the LRM

We have seen in the previous chapter that the effective theory approach of RHMFV allows us to establish specific correlations. However under the assumption of a large $S_{\psi\phi}$ some tension between the ε_K and $S_{\psi K_S}$ flavour observables remains. We now turn to a detailed analysis of the flavour phenomenology of the second model discussed within this thesis, the LRM. The study of flavour anomalies laid out in section 2.1.1, will be part of the discussion.

In chapter 3 we already got familiar with the most general setup of the LRM. Now, in this chapter we collect all formulae necessary for our analysis of $\Delta F = 2$ flavour observables and the decay $B \to X_s \gamma$, followed by a comprehensive numerical analysis. The goal of this analysis is to obtain a complete picture of the interplay of these observables, manifested in the structure of the RH mixing matrix V^R whose form we study in detail. Taking into account all relevant constraints simultaneously we investigate if the LRM is a realistic scenario for masses of the heavy gauge boson W_R in reach of the LHC. Further emphasis will be put on the study of the impact of the heavy Higgs fields on flavour observables.

6.1. $\Delta F = 2$ observables in the LRM

6.1.1. The effective Hamiltonian of the LRM

Before we start with a detailed description of $\Delta F = 2$ observables in the LRM, it should be stressed that these were the subject of various previous studies in this class of models [36, 38, 39, 96, 102, 104, 184–190]. We provide new insights such as the role of the heavy Higgs fields without making further restrictions on the electroweak parameter s, except those required by electroweak precision observables. Furthermore these observables will be part of a global and very general analysis instead of focusing on finding bounds on masses of the heavy particles as mainly done in the literature.

The starting point of our analysis is once again the effective Hamiltonian for $\Delta F = 2$ transitions, generally given by

$$\mathcal{H}_{\text{eff}}^{\Delta F=2} = \frac{G_F^2 M_{W_L}^2}{4\pi^2} \sum_i C_i(\mu) Q_i \,, \tag{6.1}$$

with Wilson coefficients and operators introduced in chapter 4. It is convenient to define the pre-factor with respect to the SM pre-factor as shown in equation (4.28). The list of relevant operators can be found in section 4.2.1, in particular in the K system operators from equations (4.2) and (4.3) have to be taken into account. Relevant operators for the B_q system can be obtained by changing appropriate flavour indices.

The Wilson coefficients obtain contributions from three classes of diagrams depending on the particles involved. In particular we distinguish between

- box diagrams with W_L and W_R exchanges: In principle these diagrams can involve $W_L W_L$, $W_L W_R$ and $W_R W_R$ in addition to internal quark lines, however the $W_R W_R$ contribution is highly suppressed by the heavy masses of gauge bosons.

- tree-level diagrams with neutral Higgses $H^0_{1,2}$: Higgs masses have to be very large (explicit values given below) if flavour bounds should be satisfied. Together with the $W_L W_R$ box, the neutral Higgs contributions constitute the main corrections in the LRM.

- box diagrams with charged Higgs $H^\pm$: As the charged Higgs $H^\pm$ have masses in the multiple TeV range only diagrams with $H^\pm$ and W_L are considered. Effects are generally expected to be small. Numerics shows that they are about two orders of magnitude smaller than the ones from neutral Higgses and the $W_L W_R$ box.

Hence we can summarise

$$C_i = \Delta_{\text{Box}} C_i + \Delta_{\text{H}^0} C_i + \Delta_{\text{H}^\pm} C_i. \tag{6.2}$$

6.1.2. Collection of relevant Wilson coefficients

We now turn to a detailed description of relevant Wilson coefficients.

As the mixing matrices V^L and V^R enter these coefficients in various combinations, we define, following [186],

$$\lambda_i^{AB}(K) = V_{is}^{A*} V_{id}^B, \qquad \lambda_i^{AB}(B_q) = V_{ib}^{A*} V_{iq}^B, \tag{6.3}$$

where $A, B = L, R$, $q = d, s$ and $i = u, c, t$.

Wilson coefficients from gauge boson box diagrams

Calculating the diagrams with internal gauge bosons $W_L W_L$, $W_L W_R$ and $W_R W_R$, respectively, as shown in figure 6.1, the following Wilson coefficients can be derived for the meson system $M = K, B_d, B_s$

$$\Delta_{\text{Box}} C_1^{VLL}(\mu_W, M) = \sum_{i,j=c,t} \lambda_i^{LL}(M) \lambda_j^{LL}(M) S_{LL}(x_i, x_j) \tag{6.4}$$
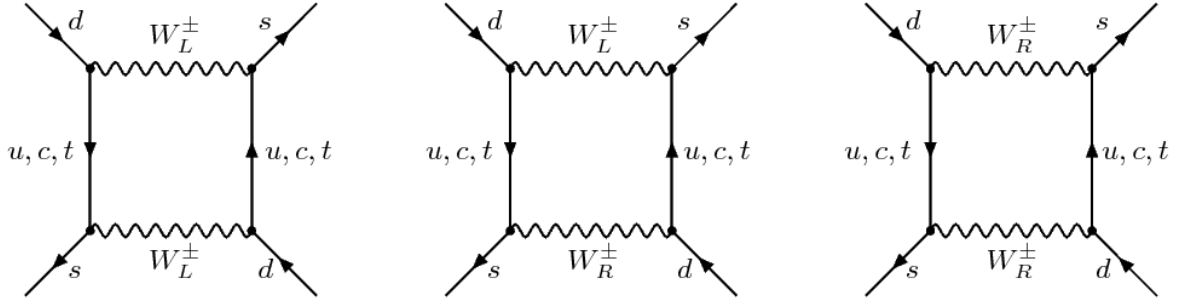
Figure 6.1.: Feynman diagrams for contributing gauge boson box diagrams

$$\Delta_{\text{Box}}C_2^{LR}(\mu_R, M) = \sum_{i,j=u,c,t} \lambda_i^{LR}(M)\lambda_j^{RL}(M)S_{LR}(x_i, x_j, \beta) \tag{6.5}$$

$$\Delta_{\text{Box}}C_1^{VRR}(\mu_R, M) = \sum_{i,j=c,t} \lambda_i^{RR}(M)\lambda_j^{RR}(M)S_{RR}(\tilde{x}_i, \tilde{x}_j), \tag{6.6}$$

where we have already chosen appropriate scales $\mu_W = \mathcal{O}(M_W, m_t)$ and $\mu_R = \mathcal{O}(M_{W_R})$ and made use of the following notation

$$x_i = \left(\frac{m_i}{M_{W_L}}\right)^2, \qquad \tilde{x}_i = \left(\frac{m_i}{M_{W_R}}\right)^2, \qquad \beta = \frac{M_{W_L}^2}{M_{W_R}^2}, \qquad r = \left(\frac{s_W}{c_W s_R}\right)^2. \tag{6.7}$$

We want to remark that in the limit of equal gauge couplings $g_L = g_R$ the factor r simplifies to $r = 1$. Using the definitions

$$I_1(x_i, x_j, \beta) = \frac{x_i \ln(x_i)}{(1-x_i)(1-x_i\beta)(x_i-x_j)} + (i \leftrightarrow j) - \frac{\beta \ln(\beta)}{(1-\beta)(1-x_i\beta)(1-x_j\beta)}, \tag{6.8}$$

$$I_2(x_i, x_j, \beta) = \frac{x_i^2 \ln(x_i)}{(1-x_i)(1-x_i\beta)(x_i-x_j)} + (i \leftrightarrow j) - \frac{\ln(\beta)}{(1-\beta)(1-x_i\beta)(1-x_j\beta)}, \tag{6.9}$$

$$F(x_i, x_j) = \frac{1}{4}\left[(4 + x_ix_j)I_2(x_i, x_j, 1) - 8x_ix_jI_1(x_i, x_j, 1)\right], \tag{6.10}$$

the loop functions are given by

$$S_{LL}(x_i, x_j) = F(x_i, x_j) + F(x_u, x_u) - F(x_i, x_u) - F(x_j, x_u) \tag{6.11}$$
$$S_{LR}(x_i, x_j, \beta) = 2\beta r\sqrt{x_ix_j}\left[(4 + x_ix_j\beta)I_1(x_i, x_j, \beta) - (1+\beta)I_2(x_i, x_j, \beta)\right] \tag{6.12}$$
$$S_{RR}(\tilde{x}_i, \tilde{x}_j) = \beta r^2 S_{LL}(\tilde{x}_i, \tilde{x}_j) \tag{6.13}$$

These results are in agreement with the literature [36, 186, 187, 191, 192].

There are a few comments in order:

- The S_{LL} form of the SM loop function agrees with equation (4.28) and no corrections of $\mathcal{O}(\epsilon^2)$ are present.

- For the LL and RR contributions in equations (6.4) and (6.6) respectively, we have used the unitarity of the matrices V^L and V^R in order to eliminate internal u quark contributions, in other words the GIM mechanism. However this does not apply to the LR contribution.

- The loop function S_{LR}, in contrast to the results for S_{LL} and S_{RR}, is not gauge independent [191]. Gauge independence can be restored by including vertex and self-energy corrections to the tree-level neutral Higgs exchange, in particular when the $H_i^0 G^+ G'^-$ vertex is involved [187, 192]. Since these corrections leave S_{LR} without relevant modifications from our result in the 't Hooft-Feynman gauge, we neglect them.

Wilson coefficients from tree-level neutral Higgs exchange

Tree-level Higgs diagrams, as shown on the right-hand side in figure 6.2, are induced by the two flavour changing neutral Higgses H_1^0 and H_2^0 (for more details about the Higgs sector see appendix A). Generally they generate the operators $C_{1,2}^{SLL}$, $C_{1,2}^{SRR}$ and C_2^{LR}, but as the Higgs masses are equal at leading order the $C_{1,2}^{SLL}$ and $C_{1,2}^{SRR}$ contributions cancel each other. Thus even for non-degenerate Higgs masses, these contributions are of $\mathcal{O}(\epsilon^4)$ and negligible. Hence, the only relevant contribution from neutral Higgses is given by

$$\Delta_{\mathrm{H}^0} C_2^{LR}(\mu_H, K) = -\frac{16\pi^2}{\sqrt{2}M_H^2 G_F} u(s) \sum_{i,j=u,c,t} \lambda_i^{LR}(K)\lambda_j^{RL}(K)\sqrt{x_i(\mu_H)x_j(\mu_H)}, \quad (6.14)$$

where $M = K, B_d, B_s$ and $\mu_H = \mathcal{O}(M_H)$ and we have defined the function

$$u(s) = \left(\frac{1}{1-2s^2}\right)^2. \tag{6.15}$$

The choice of the matching scale will be explained in detail below. Our result in equation (6.14) is in agreement with [36] provided one takes the limit $s \ll 1$ which was chosen in that paper. In terms of a more general analysis the additional factor $u(s)$ is necessary since already for $s = 0.5$ we obtain an enhancement by a factor of 4.

Wilson Coefficients from charged Higgs box diagrams

Charged Higgs effects are automatically expected to be small compared to the previous NP effects since these one loop processes involve particles much heavier than the W_R mass but equal to the masses of the neutral Higgses, H_1^0 and H_2^0. We still want to include the main contribution given by boxes of $H^\pm$ and $W_L^\pm$, as shown on the left-hand side in figure 6.2, or with the corresponding Goldstone boson. Box diagrams involving a Higgs particle with solely other heavy particles can be safely neglected. Thus we also do not consider box diagrams with heavy neutral Higgs particles. Calculating the diagram in
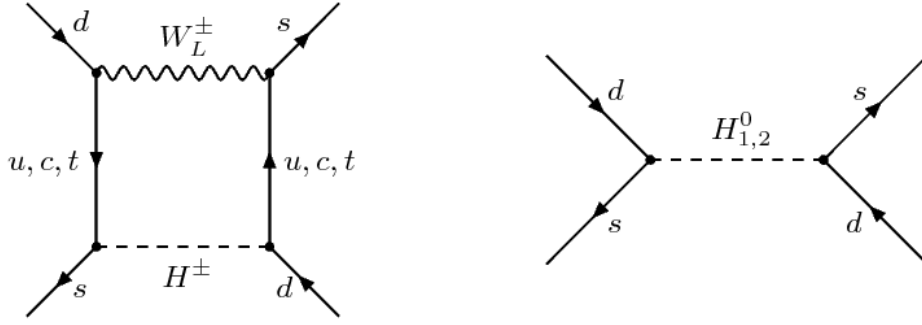
Figure 6.2.: Feynman diagrams for Higgs contributions

figure 6.2 we find

$$\Delta_{\mathrm{H}^\pm} C_2^{LR}(\mu_H, M) = \sum_{i,j=u,c,t} \lambda_i^{LR}(M)\lambda_j^{RL}(M) S_{LR}^H(x_i, x_j, \beta_H), \qquad (6.16)$$

where the loop function reads

$$S_{LR}^H(x_i, x_j, \beta_H) = 2\, u(s)\beta_H \sqrt{x_i(\mu_H)x_j(\mu_H)} \left[x_i x_j I_1(x_i, x_j, \beta_H) - I_2(x_i, x_j, \beta_H)\right], \quad (6.17)$$

and

$$\beta_H = \frac{M_{W_L}^2}{M_{H^\pm}^2}. \qquad (6.18)$$

Our result is consistent with the findings of [186] when taking the limit $s \ll 1$.

6.1.3. RG QCD corrections

In this section we address the issues of QCD renormalisation evolution of the effective Hamiltonian from high scales down to low energy scales at which the hadronic matrix elements are evaluated by lattice methods. In section 5.1.2 we have demonstrated the method in presence of a single high scale. In contrast to the procedure given there, now an intermediate high scale is involved. We briefly summarise the relevant scales:

- The SM box diagrams involve as usual dynamical W_L and the SM quarks. The appropriate scale is then $\mu_W = \mathcal{O}(M_W, m_t)$ [133].

- The intermediate high scale μ_R is fixed by the mass M_{W_R} of the heavy gauge boson W_R. Considering that $M_{W_R} \gg M_{W_L}$, the correct way to proceed would involve integrating out the heavy gauge boson and constructing an effective field theory where W_R does not act as a dynamical field. However our approximation is justified within the uncertainties of unknown parameters. Numerically we take $\mu_R = 2.5\,\mathrm{TeV}$.

- As we will demonstrate below Higgs masses of both charged and neutral Higgses must be even significantly larger than M_{W_R}. The high scale μ_H is then defined by their mass, hence $\mu_H = \mathcal{O}(M_H)$. Numerically we fix $\mu_H = 15\,\mathrm{TeV}$.

- Finally, as defined in section 5.1.2, there exists the low-energy scale of the decay in question, referred to as μ_L (or μ_b for B mesons).

Under these assumptions it is possible to encode perturbative and non-perturbative QCD effects in a known way into the effective parameters P_i. For our analysis only the values of the following coefficients are necessary:

- For box diagram contributions ($\mu_R = 2.5\,\text{TeV}$), we find

$$P_2^{LR}(K) = 73(4)(3), \quad P_2^{LR}(B_q) = 4.57(54)(25) \qquad (\text{Box}), \tag{6.19}$$

- For the Higgs contribution ($\mu_H = 15\,\text{TeV}$) the result reads

$$P_2^{LR}(K) = 88(5)(3), \quad P_2^{LR}(B_q) = 5.54(65)(30) \qquad (\text{Higgs}). \tag{6.20}$$

More details about the explicit calculation of the P_i factors can be found in [49].

Last but not the least, a small comment about the scales of quark masses is in order. Generally the scales of quark masses in our analysis are set to be $m_i(m_i)$ for $i = c,\ b,\ t$ and $2\,\text{GeV}$ for light quarks. Only in the Wilson coefficients involving heavy Higgs fields the quark masses are evaluated at μ_H.

6.1.4. Summary of $\Delta F = 2$ contributions

Now we are ready to give the final formulae for the off-diagonal elements of the mass mixing matrices of the various meson systems. We demonstrate the procedure for M_{12}^q.

It is convenient to make use of the following decomposition

$$M_{12}^q = (M_{12}^q)_{\text{SM}} + (M_{12}^q)_{\text{RR}} + (M_{12}^q)_{\text{LR}} \equiv \overline{(M_{12}^q)}_{\text{SM}} + (M_{12}^q)_{\text{LR}}. \tag{6.21}$$

This allows us to group contributions with the same RGE behaviour. We obtain

$$\overline{(M_{12}^q)}_{\text{SM}} = \frac{G_F^2}{12\pi^2} F_{B_q}^2 \hat{B}_{B_q} m_{B_q} M_W^2 \left[\lambda_t^{LL*}(B_q)\right]^2 \eta_B S_q^*(B_q), \tag{6.22}$$

where

$$S_q(B_q) = S_0(x_t) + \frac{\tilde{\eta}_B}{\eta_B} \frac{\Delta_{\text{Box}} C_1^{VRR}(\mu_R, B_q)}{\left[\lambda_t^{LL}(B_q)\right]^2}. \tag{6.23}$$

The first term gives the SM contribution as given in equation (4.29). As usual η_B defines the known SM QCD correction while $\tilde{\eta}_B/\eta_B \sim 0.95$ results from evolving the Wilson coefficients from μ_R down to μ_W and hence is independent of the particular meson system considered. The connection between SM loop functions and the one introduced in section 6.1.2 is explicitly given in this notation in appendix E.

As the Higgs effects enter at a higher scale than the boxes involving the gauge boson W_R, we combine them according to

$$\tilde{\Delta}_{\text{Higgs}} C_2^{LR}(\mu_R, B_q) = \Delta_{\text{H}^0} C_2^{LR}(\mu_H, B_q) + \Delta_{\text{H}^+} C_2^{LR}(\mu_H, B_q) \,, \tag{6.24}$$

such that all effects with the same RGE behaviour can be grouped together. Finally we obtain

$$(M_{12}^q)_{\text{LR}} = \frac{G_F^2 M_W^2}{12\pi^2} F_{B_q}^2 m_{B_q} \left[(\Delta_{\text{Box}} C_2^{LR}(\mu_R, B_q))^* P_2^{LR}(\mu_R) + \right. \tag{6.25}$$

$$\left. (\tilde{\Delta}_{\text{Higgs}} C_2^{LR}(\mu_H, B_q))^* P_2^{LR}(\mu_H) \right] \,. \tag{6.26}$$

For the $K^0 - \bar{K}^0$ system one simply has to replace the index B_q by K, and also η_B by η_2. Furthermore the SM part is modified by inclusion of the box diagrams involving an internal charm which could be neglected in case of the $B_q^0 - \bar{B}_q^0$ system. The corresponding loop functions are again collected in appendix E. The SM part of the mixing amplitude simplifies then to the formula as given in equation (4.28).

All further formulae for $\Delta F = 2$ observables necessary for our numerical studies have been presented in section 4.2.2. Together with the formulae of this section the observables ΔM_K, ΔM_q, ε_K, $S_{\psi K_S}$, $S_{\psi \phi}$, $\Delta \Gamma_q$ and A_{SL}^q can be straightforwardly obtained.

We briefly want to mention that in the LRM some observables, such as $S_{\psi K_S}$ and $S_{\psi \phi}$, can be modified by tree-level exchanges. This is due to the small right-handed couplings induced by W_L and W_R exchange, both being typically of $\epsilon^2 \sim \mathcal{O}(10^{-3})$. After evaluating matrix elements and QCD RG running effects we find that the weak phases of decay amplitudes can in principle be modified. However our numerical considerations show that these effects cause modifications in $S_{\psi K_S}$ and $S_{\psi \phi}$ in the 0.01% range. Thus we will not consider them here further and for details we refer to our publication [49].

6.1.5. The role of the neutral Higgs contributions

In this section we take a closer look at the role played by the neutral Higgs contributions. Since the main impact on the NP mixing amplitude comes from left-right operators, we concentrate on this contribution. We can decompose the amplitude in the following way

$$(M_{12}^q)_{\text{LR}} = \frac{G_F^2 M_W^2}{12\pi^2} F_{B_q}^2 m_{B_q} \sum_{i,j=u,c,t} [\lambda_i^{LR}(B_q) \lambda_j^{RL}(B_q)]^* R_{ij}(B_q) \,, \tag{6.27}$$

where we have defined

$$R_{ij}(B_q) = S_{LR}(x_i, x_j, \beta) P_2^{LR}(B_q, \mu_R) + S_{LR}^H(x_i, x_j, \beta_H) P_2^{LR}(B_q, \mu_H)$$
$$- \frac{16\pi^2}{\sqrt{2} M_H^2 G_F} u(s) \sqrt{x_i(\mu_H) x_j(\mu_H)} P_2^{LR}(B_q, \mu_H) \,.$$

We have separated the contributions of loop integrals and QCD running from contributions of left- and right-handed mixing matrices. These mixing matrices are contained in factors λ_i^{LR} and λ_i^{LR}. Analogously we can obtain the formulae for the $K^0 - \bar{K}^0$ system with B_q replaced by K.

We concentrate on the factor R_{ij}, which depends only on the electroweak parameter s apart from the heavy masses M_{W_R} and M_H. This setup is perfect to study the impact of the heavy masses for given values of s. In particular we choose $s = 0.1$ and $s = 0.5$, which are part of the best fit region shown in section 3.4.4 and summarised in equation (3.37).

In general we find that the neutral Higgs part represents the leading contributions, followed by gauge box contributions while charged Higgs contributions are negligible. Charged Higgs contributions are roughly two orders of magnitude smaller than the contributions from neutral Higgs and one order of magnitude smaller than the ones from charged gauge boson boxes. Thus when we are interested in the impact of the heavy Higgs contributions, it is sufficient to consider the neutral Higgs contribution denoted by $R_{tt}^H(K)$ with respect to the full factor $R_{tt}(K)$.

In figure 6.3 we display $R_{tt}^H(K)/R_{tt}(K)$ as a function of the neutral Higgs mass M_H for different values of M_{W_R}. First we consider the case $s = 0.1$. Even for a light W_R mass, $M_{W_R} = 400\,\text{GeV}$, which is already excluded by direct collider bounds, the neutral Higgs contributions for $M_H < 20\,\text{TeV}$ contribute at the 20% level to the total value. This example displays that the role of the neutral Higgs has been severely underestimated for many years, especially when the bounds on M_{W_R} were less stringent. With a more realistic mass $M_{W_R} > 2\,\text{TeV}$, the neutral Higgs contributions become only negligible if the Higgs masses are chosen to be very heavy, roughly $M_H > 100\,\text{TeV}$. However, we cannot simply decouple the Higgs contributions by choosing an arbitrarily high Higgs mass as in this case the Higgs sector would leave the perturbative range. This can be understood by considering the formula for the neutral Higgs mass as given in A.6 of appendix A. Since both M_{W_R} and M_H involve the parameter κ_R and hence cannot be fixed independently, the Higgs mass can only be increased while requiring a relatively low M_{W_R} by pushing the coupling α_3 into a non-perturbative regime. When assuming $s = 0.5$ the Higgs contributions become even more important.

In summary, in the LRM for a realistic choice of masses of $M_{W_R} = 2.6\,\text{TeV}$ and $M_H = 16\,\text{TeV}$ (corresponding to $s = 0.1$), the neutral Higgs contribution represents more than 80% of the total LR contribution. This result is surprising especially since these contributions have been neglected in most of the existing literature for LR models.

Finally we briefly want to mention that the hierarchical structure of the matrix R_{ij} has a profound impact on the resulting structure of the RH mixing matrix V^R. This is due to the fact that constraints from $\Delta F = 2$, in particular ϵ_K, set strong constraints on the LR operators. We will elaborate on these topics in our numerical analysis below.
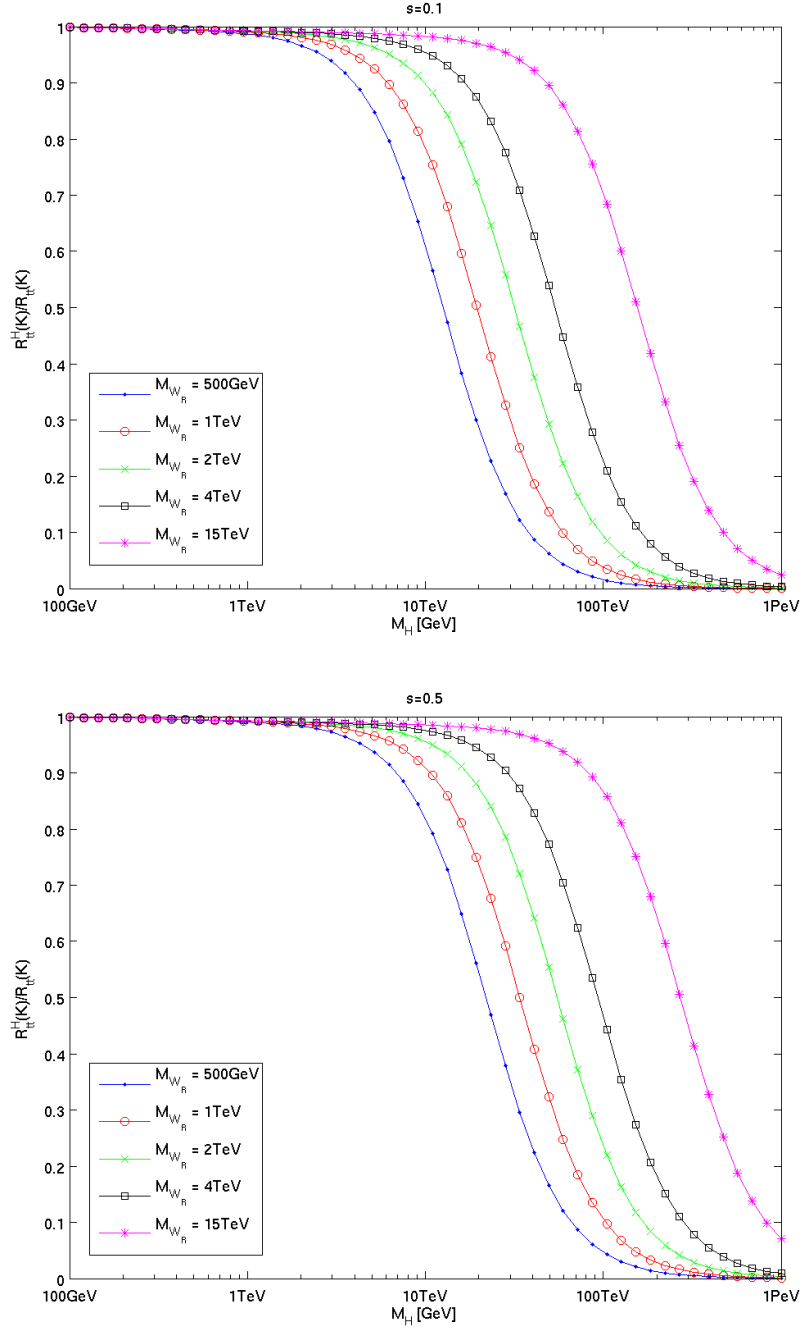
Figure 6.3.: The role of the neutral Higgs contribution quantified by $R_{tt}^H(K)/R_{tt}(K)$ as a function of M_H for different W_R masses for $s = 0.1$ and $s = 0.5$

6.2. The decay $B \to X_s\gamma$ in the LRM

6.2.1. The effective Hamiltonian

Due to its unique features of identifying deviations from the SM and acting generally as strong constraint for NP models, the decay $B \to X_s\gamma$ has attracted a lot of attention in various left-right models based on the $SU(2)_L \times SU(2)_R \times U(1)$ symmetry structure. Such studies can be found in [107, 151, 193–200]. In this section we make use of several results found by some of these authors, in order to study the relevant Wilson coefficients of dipole operators. Subsequently, corresponding RG QCD corrections will be elaborated and a formula for the branching ratio for the $B \to X_s\gamma$ decay presented.

The starting point of our considerations is as usual the effective Hamiltonian. At the low energy scale $\mu_b = \mathcal{O}(m_b)$ the effective Hamiltonian reads

$$\mathcal{H}_{\text{eff}}(b \to s\gamma) = -\frac{4G_{\text{F}}}{\sqrt{2}} V_{ts}^* V_{tb} \left[C_{7\gamma}(\mu_b)Q_{7\gamma} + C_{8G}(\mu_b)Q_{8G} \right] . \tag{6.28}$$

The pre-factor is chosen such that it matches with the normalisation from the SM calculations. We have already defined the operators above in equation (4.33). In principle the primed operators of equation (4.33) also have to be incorporated. However, we will give arguments below showing that they can be neglected. Note that primed operators already could be removed from the discussion in the SM as they appear suppressed by the ratio m_s/m_b relative to the unprimed ones.

6.2.2. The Wilson coefficients

Before we start considering relevant Wilson coefficients, we briefly want to recall the discussion of different scales in section 6.1.3. In the following we list the Wilson coefficients in terms of the corresponding high scale. The transformation to low energy Wilson coefficients $C_i(\mu_b)$ from high energy scales by means of renormalisation group methods is discussed in the following section.

SM Wilson coefficients from gauge bosons

The first group of Wilson coefficients consists of those already present in the SM, usually given at the scale $\mu_W = \mathcal{O}(M_W)$. The corresponding Feynman diagram for the $b \to s\gamma$ transition requires a chirality flip, which can only be achieved through a mass insertion in the initial or final state quark since the W_L couples in the SM only to LH quarks. Consequently the amplitude has to be either proportional to m_b in case of unprimed operators or to m_s for primed operators which then can be neglected due to the mass suppression. We summarise the results here

$$C_{7\gamma}^{\text{SM}}(\mu_W) = \frac{3x_t^3 - 2x_t^2}{4(x_t - 1)^4} \ln x_t + \frac{-8x_t^3 - 5x_t^2 + 7x_t}{24(x_t - 1)^3} \equiv C_{7\gamma}^{\text{SM}}(x_t) , \tag{6.29}$$

$$C_{8G}^{\mathrm{SM}}(\mu_W) = \frac{-3x_t^2}{4(x_t - 1)^4} \ln x_t + \frac{-x_t^3 + 5x_t^2 + 2x_t}{8(x_t - 1)^3} \,. \tag{6.30}$$

More information can be found in [129].

New Wilson coefficients from gauge bosons

In the LRM new contributions can appear since the gauge boson W_L can couple to the RH quarks. The leading NP contribution involving gauge bosons is then given by the diagram with a RH coupling in the vertex with the b-quark together with a chirality flip on the internal top quark line. This internal flip implies an enhancement factor of m_t/m_b with respect to the SM contribution and the reason for the importance of this contribution. The expressions for the corresponding Wilson coefficients have first been calculated by Cho and Misiak [151] at the scale μ_W. The choice of the scale μ_W was justified by their assumption of $M_{W_R} \sim \mathcal{O}(\mathrm{GeV})$. Since the bounds are now more stringent, we need coefficients at a scale of $\mu_R \gg \mu_W$. Using the results of Cho and Misiak [151] would in this case require that large logarithms $\log(\mu_R/\mu_W)$ have to be taken into account for a correct treatment of scales. However in view of the unknown mass M_{W_R} we decide that an approximate consideration is sufficient, assuming the result of [151] to be valid at μ_R. We then obtain

$$\Delta^{\mathrm{LR}}C_{7\gamma}(\mu_R) = A^{tb}\left[\frac{3x_t^2 - 2x_t}{2(1 - x_t)^3} \ln x_t + \frac{-5x_t^2 + 31x_t - 20}{12(1 - x_t)^2}\right], \tag{6.31}$$

$$\Delta^{\mathrm{LR}}C_{8G}(\mu_R) = A^{tb}\left[\frac{-3x_t}{2(1 - x_t)^3} \ln x_t + \frac{-x_t^2 - x_t - 4}{4(1 - x_t)^2}\right], \tag{6.32}$$

where

$$A^{tb} = \frac{m_t}{m_b} \, sc\epsilon^2 e^{i\alpha} \left(\frac{V_{tb}^R}{V_{tb}^L}\right) + \mathcal{O}(\epsilon^4) \,. \tag{6.33}$$

The m_t/m_b enhancement can be seen directly in A^{tb}. Furthermore we note the $\mathcal{O}(\epsilon^2)$ dependence. As we will see below, in order to build the branching ratio the sum of Wilson coefficients has to be squared so that finally at $\mathcal{O}(\epsilon^2)$ only the interference term with the SM contribution will enter.

Other contributions from gauge bosons

Now we briefly justify why the Wilson coefficients described above represent the only relevant NP contribution from gauge bosons at $\mathcal{O}(\epsilon^2)$. We first restrict our considerations to diagrams involving a W_L boson. In the next step we classify all possible contributions. In general each contribution is characterised by two properties: firstly the chirality of the gauge boson–quark couplings in the loop and secondly the type of operator, i.e. primed or unprimed. In the following we refer to different chiralities just as LL, RR and LR, where e.g. LL stands for the SM contribution. So far we have considered the LL contribution, primed and unprimed, and the unprimed LR contribution. Next to be considered is the primed LR contribution. This contribution originates from

the diagram with RH coupling in the vertex with the s-quark and chirality flip on the internal line. Similar to equation (6.33) the strength of the Wilson coefficient is given by

$$(A^{ts})^* = \frac{m_t}{m_b} \, sc\epsilon^2 e^{-i\alpha} \left(\frac{V_{ts}^R}{V_{ts}^L} \right)^* + \mathcal{O}(\epsilon^4) \,, \tag{6.34}$$

being also m_t/m_b enhanced and of $\mathcal{O}(\epsilon^2)$. However, when considering the branching ratio, primed operators do not interfere with the SM contribution, since we have omitted the small SM contributions to the primed operators. Thus at the level of the branching ratio this contribution appears at $\mathcal{O}(\epsilon^4)$ and can be neglected. Next, the unprimed and primed RR contributions lack the enhancement factor m_t/m_b both having the chirality flip on the external line and furthermore appear at $\mathcal{O}(\epsilon^4)$, so that we can neglect them.

Finally we take a look at diagrams involving the heavy W_R boson. The authors of [151] found all LR contributions negligible, similar arguments hold for the LL and RR case. This is mainly due to LL and RR contributions being then described by the SM loop functions, as given in equations in (6.29) and (6.30), but instead of $x_t = m_t^2/M_W^2$ they are mass suppressed with $\tilde{x}_t = m_t^2/M_{W_R}^2$.

New Wilson coefficients from charged Higgs bosons

The decay $B \to X_s\gamma$ receives important contributions through diagrams involving the charged Higgs boson. While often ignored in early works [102], currently it is established that these effects should not be neglected [193, 194, 196–198, 200]. Interestingly they are still important even when assuming the charged Higgs mass in the range of $\mathcal{O}(10\,\text{TeV})$. As found by these authors the corresponding amplitude also features the m_t/m_b enhancement. This property is unique in the framework of LR models, e.g. in the MSSM one finds a m_b or m_s dependence. Additionally the charged Higgs couplings are of $\mathcal{O}(1)$ so that the only suppression is induced by the heavy Higgs mass itself.

In order to obtain the contributing Wilson coefficients we use the results of [196, 200] while adapting their formulae to our notation. We obtain [196]

$$\Delta^{\text{H}^\pm} C_{7\gamma}(\mu_H) = -u(s) \left[sc\frac{m_t}{m_b} e^{i\alpha} \left(\frac{V_{tb}^R}{V_{tb}^L} \right) A_{H^+}^1(y) + 2s^2c^2 A_{H^+}^2(y) \right], \tag{6.35}$$

$$A_{H^+}^1(y) = \left[\frac{3y^2 - 2y}{3(1-y)^3} \ln y \; + \; \frac{5y^2 - 3y}{6(1-y)^2} \right], \tag{6.36}$$

$$A_{H^+}^2(y) = \frac{1}{3} A_{\text{SM}}(y) - A_{H^+}^1(y) \,, \tag{6.37}$$

$$A_{\text{SM}}(y) = -2C_{7\gamma}^{\text{SM}}(y) \,, \quad y = \frac{m_t^2}{M_{H^+}^2} \,. \tag{6.38}$$

Note that the SM loop function was given in equation (6.29) and following the arguments of appendix D we can again set $\alpha = 0$. The function $u(s)$ has been defined in

μ_R	1 TeV	2.5 TeV	10 TeV	15 TeV
κ_7	0.457	0.427	0.390	0.380
κ_8	0.125	0.128	0.130	0.130
κ_{LR}	0.665	0.778	0.953	1.005

Table 6.1.: *The relevant NP magic numbers at $\mu_b = 2.5\,\mathrm{GeV}$ and $\mu_t(m_t)$.*

equation (6.15). It is also remarkable that a large s, in particular close to the limit $s \to 1/\sqrt{2}$, is linked with a strong enhancement. However we should remember that this limit is not realistic since it implies $\kappa' = \kappa$, which leads to equal quark masses in up and down sectors (for more details see section 3.2.2).

6.2.3. QCD corrections

In the next step we want to include the RG QCD running. We include the SM QCD corrections up to the NNLO level following [165]. The NP contribution is only incorporated at the LO level, which was obtained on the basis of [151] and [201]. In principle matching conditions to the Wilson coefficients of LR operators at appropriate scales relevant for a NLO analysis are already available [199]. However such calculations are technically involved and would be redundant in view of the many free parameters present in this model.

We now turn to the explicit description of the QCD corrections. First, all Wilson coefficients have to be evolved down to the scale $\mu_b = 2.5$ GeV. We obtain

$$\Delta^{\mathrm{LR}} C_{7\gamma}(\mu_b) = \kappa_7(\mu_R)\, \Delta^{\mathrm{LR}} C_{7\gamma}(\mu_R) + \kappa_8(\mu_R)\, \Delta^{\mathrm{LR}} C_{8G}(\mu_R) + A^{cb} \kappa_{LR}(\mu_R)\,, \quad (6.39)$$

$$\Delta^{\mathrm{H}^\pm} C_{7\gamma}(\mu_b) = \kappa_7(\mu_H)\, \Delta^{\mathrm{H}^\pm} C_{7\gamma}(\mu_H)\,, \quad (6.40)$$

where the NP Wilson coefficients at high scale were given in (6.31), (6.32) and (6.35), respectively. The term proportional to

$$A^{cb} = \frac{m_c}{m_b}\, sc\epsilon^2 e^{i\alpha} \frac{V_{cb}^R}{V_{cb}^L}\,. \quad (6.41)$$

appears due to the mixing with new charged current operators. Since this mixing only occurs below the scale μ_R, it has to be included only once in equations (6.39) and (6.40). The κ's usually referred to as the NP magic numbers are collected in table 6.1 [201].[1]

The overall Wilson coefficient is finally given by

$$C_{7\gamma}(\mu_b) = C_{7\gamma}(\mu_b)^{\mathrm{SM}} + \Delta^{\mathrm{LR}} C_{7\gamma}(\mu_b) + \Delta^{\mathrm{H}^\pm} C_{7\gamma}(\mu_b)\,. \quad (6.42)$$

---

[1]This table is provided by Emmanuel Stamou.

6.2.4. The branching ratio

We are now ready to write down the branching ratio. Following the analysis of [201,202], we obtain

$$\text{Br}(B \to X_s\gamma) = \text{Br}(B \to X_s\gamma)_{\text{SM}} + \Delta\text{Br}\,, \tag{6.43}$$

where

$$\Delta\text{Br} = R \left[2\,\text{Re}\left\{ C_{7\gamma}(\mu_b)^{\text{SM}} \tilde{\Delta}^{\text{LR}} C_{7\gamma}(\mu_b) \right\} + \left| \tilde{\Delta}^{\text{LR}} C_{7\gamma}(\mu_b) \right|^2 \right]\,, \tag{6.44}$$

with

$$\tilde{\Delta}^{\text{LR}} C_{7\gamma}(\mu_b) = \Delta^{\text{LR}} C_{7\gamma}(\mu_b) + \Delta^{\text{H}^\pm} C_{7\gamma}(\mu_b)\,. \tag{6.45}$$

Furthermore we require

$$R = 0.00247\,, \qquad C_{7\gamma}(\mu_b)^{\text{SM}} = -0.353\,, \tag{6.46}$$

and [202]

$$\text{Br}(B \to X_s\gamma)_{\text{SM}} = (3.15 \pm 0.23) \times 10^{-4}\,. \tag{6.47}$$

In principle the last term in (6.44) can be dropped since it is of $\mathcal{O}(\epsilon^4)$. Finally we want to remark that the comparison of SM and experimental value (see section 4.3.2 for more details) favours $\Delta\text{Br} > 0$ leading to $\text{Re}\big(\tilde{\Delta}^{\text{LR}} C_{7\gamma}(\mu_b)\big) < 0$ and $\text{Re}\big(V_{tb}^R\big) > 0$.

6.2.5. The role of the charged Higgs contributions

Similar to our considerations in section 6.1.5, we now want to examine the $B \to X_s\gamma$ decay. We study the size of contributions from charged Higgs with respect to the full NP contribution, characterised by $\Delta^{\text{H}^\pm} C_{7\gamma}(\mu_b)/\tilde{\Delta}^{\text{LR}} C_{7\gamma}(\mu_b)$. Our results are presented in figure 6.4 where we show this ratio as a function of M_H for different values of M_{W_R} and two choices of s. Since both $\Delta^{\text{H}^\pm} C_{7\gamma}(\mu_b)$ and $\tilde{\Delta}^{\text{LR}} C_{7\gamma}(\mu_b)$ are dependent on the RH mixing matrix, we assume for V^R simply the identity matrix. This approximation is justified as the main contributions from both charged Higgs and gauge bosons are proportional to V_{tb}^R, hence the ratio of these two quantities gets barely modified. In this way we are able to extract the fact that the charged Higgs play an important role. In numbers, for $W_R > 2\,\text{TeV}$ and $M_H < 20\,\text{TeV}$ the charged Higgs contribution provides at least 20% and 50% of the NP contribution for $s = 0.1$ and $s = 0.5$, respectively. For high values of s the effects are much larger. This enhancement is in accordance with our previous expectations from the discussion of the behaviour of Higgs contributions close to the limit $s \to 1/\sqrt{2}$.

6.3. Strategy of the numerical analysis

6.3.1. Outline of the strategy

In the previous sections we have collected all relevant formulae for $\Delta F = 2$ processes and the decay $B \to X_s\gamma$ and constraints. We are now ready to perform a comprehen-
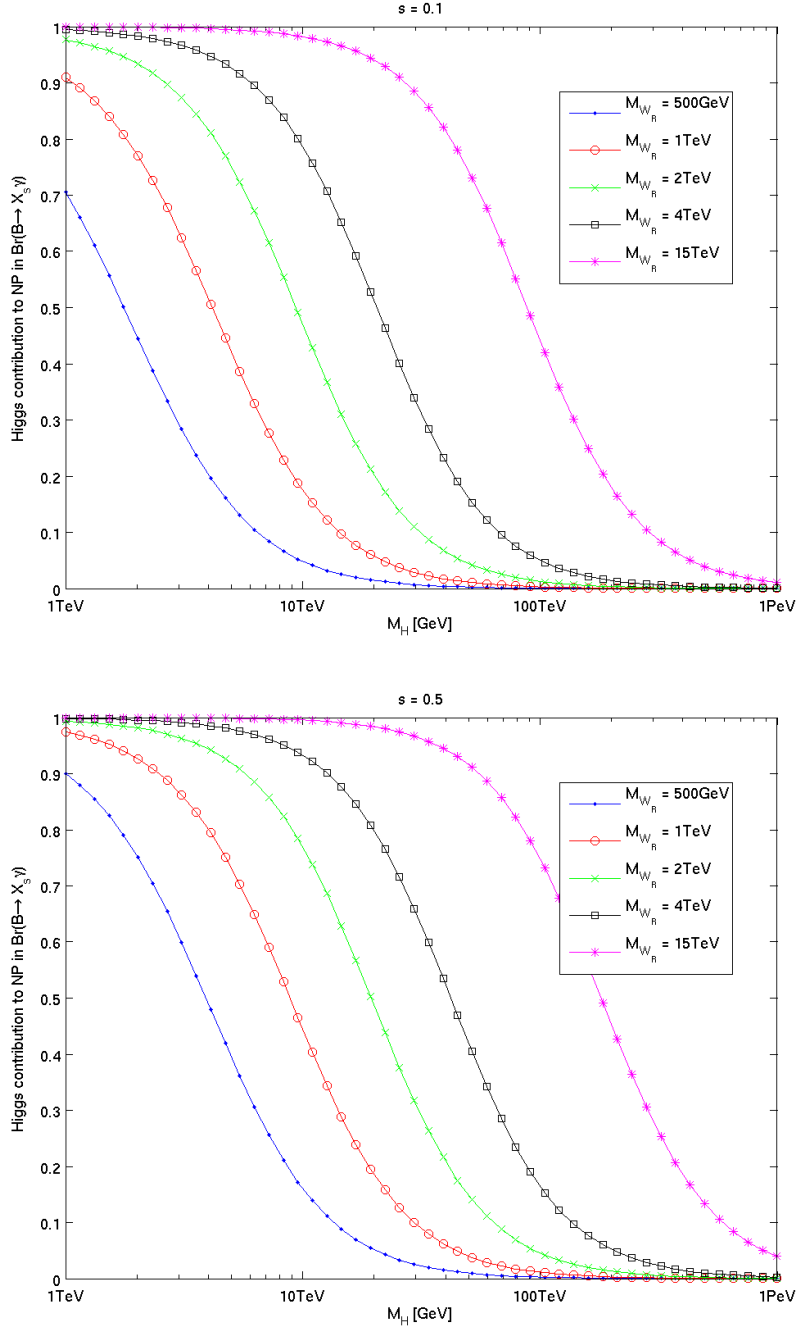
Figure 6.4.: The relative importance of the charged Higgs diagrams in the NP contributions to $\mathrm{Br}(B \to X_s\gamma)$ for $s = 0.1$ (top panel) and $s = 0.5$ (bottom panel) as a function of the Higgs mass for different W_R masses.

sive numerical analysis.

To this end we first have to discuss how to incorporate our results from our pre-analysis of EWP observables, as given in section 3.4.4 and summarised by our best fit region in equation (3.37). We realise that two parameters in equation (3.37) are very constrained and we are able to choose a benchmark point. In particular our choice reads

$$s_R = 0.80\,, \qquad\qquad \epsilon = 0.03\,. \qquad\qquad (6.48)$$

This choice affects the heavy masses M_{W_R} and M_H, where the latter additionally exhibits a strong dependence on the parameter s. The masses are then

$$M_{W_R} \approx 2.6\,\mathrm{TeV}\,, \qquad M_H \approx \frac{16}{\sqrt{1-2s^2}}\,\mathrm{TeV}\,, \qquad (6.49)$$

where have chosen $\alpha_3 = 8$ in the Higgs potential. This choice of α_3 ensures a high Higgs mass, together with suppressed effects in both $\Delta F = 2$ processes and the decay $B \to X_s\gamma$ as discussed in sections 6.1.5 and 6.2.5, respectively. It should be stressed that α_3 cannot be increased further without leaving the perturbative regime in the Higgs sector [36]. Concerning the mass of the heavy gauge boson W_R our benchmark point guarantees a value to be accessible at the LHC. Additionally, it is also useful to give a few characteristic parameters of flavour observables for our benchmark point

$$1.3 < \frac{\kappa}{\kappa'} < 9.9\,, \qquad r = \frac{g_R^2}{g_L^2} \approx 0.48\,, \qquad 8.9 \cdot 10^{-5} < sc\epsilon^2 < 4.3 \cdot 10^{-4}\,. \qquad (6.50)$$

The situation for s is less restricted. Since this parameter also has a profound impact on flavour observables, a general analysis can only be guaranteed when we study it for different values. Before we fix the considered region of s it is also useful to ask about the feedback from flavour observables on the electroweak parameters. The correlation between them enters mainly due to the function $u(s)$ present in the $B \to X_s\gamma$ decay but also in $\Delta F = 2$ processes. We have already mentioned that in the unphysical limit of $s \to 1/\sqrt{2}$ divergences would appear, hence it is obvious that flavour observables preclude s to be close to its maximal value. We find that the upper limit on s is mainly constrained by the charged Higgs contributions to $B \to X_s\gamma$ requiring $s < 0.64$. Consequently we find

$$0.1 < s < 0.6 \qquad\qquad (6.51)$$

to be phenomenologically viable. In summary, we want to emphasise that in view of many free parameters of the model the treatment of pre-constraining electroweak parameters is useful. Therefore in the following numerical analysis we use the EW benchmark point only varying the parameter s as discussed here.

Apart from EWP constraints, the constraints from tree-level decays (as summarised in section 3.3.3) and from the observables ΔM_K, ΔM_d, ΔM_s, ε_K, $S_{\psi K_S}$ and $\mathrm{Br}(B \to X_s\gamma)$ (as discussed above) are incorporated in our numerical analysis at the 2σ level. The

parameter scan is then performed by varying 13 parameters from the matrices V^L and V^R within in their allowed ranges. For V^R this implies that the mixing angles are varied within $0\ldots\pi/2$ while for phases we have $0\ldots2\pi$. On the other hand parameters of V^L are already quite constrained mainly due to the smallness of ε_K and the tree-level constraints, therefore we can pre-constrain ranges and improve the efficiency of the numerical analysis.

The goal of our analysis is to identify regions in parameter space consistent with all existing experimental constraints. This allows us to study the form of the matrix V^R, examine correlations of observables and make predictions for some them. Finally we can study the impact on the SM anomalies, which we have described in section 2.1.1.

6.3.2. Input data and error treatment

Before we describe our results we briefly want to discuss two basic ingredients of any numerical analysis, the input data and the treatment of uncertainties.

In table 6.2 we have collected all numerical values necessary for our analysis of the LRM. Running quark masses can be separately found in table 6.3. It should also be mentioned that values for P_i^a factors and magic numbers have already been given in section 6.1.3 and 6.2.3, respectively.

Uncertainties enter our analysis in two ways and would require a systematic treatment by error propagation. Input parameters and predictions for observables carry uncertainties from theoretical uncertainties and experimental input data. For example the input parameters $\sqrt{\hat{B}_{B_d}}F_{B_d}$ and $\sqrt{\hat{B}_{B_s}}F_{B_s}$ have uncertainties of about 5%. In the SM this would lead to an uncertainty of roughly 10% in the observables ΔM_d and ΔM_s [137]. In contrast, the observable ε_K suffers from much smaller uncertainties, which were mainly improved by more precise lattice calculations of [70, 204–207], estimate of long distance contributions [68, 71] and NNLO QCD perturbative corrections [72, 73]. Additionally, the values of all final observables are measured with respect to a certain precision, their errors lead to the fact that our constraints need to be fulfilled in specific ranges. Going back to our examples ΔM_d, ΔM_s and ε_K, this means that experimental values are so precise that their errors can be neglected for practical purposes. Further observables such as $S_{\psi K_S}$, $\mathrm{Br}(B \to X_s\gamma)$ and ΔM_K are known within 3%, 10% and 30% accuracy, respectively. Note that the latter value is much higher due to unknown long-distance contributions.

In view of the complexity of the formulae and many input parameters we decided not to perform a detailed error propagation, instead we require the final prediction for the observable to lie roughly within the two sigma range of experimental and theoretical uncertainties. This way allows a compact but approximate treatment of errors, which will be sufficient for our purposes.

$G_\mu = 1.16637(1) \cdot 10^{-5}\,\mathrm{GeV}^{-2}$	$\eta_1 = 1.87(76)$ [73]
$M_W = 80.399(23)\,\mathrm{GeV}$	$\eta_3 = 0.496(47)$ [72, 148]
$\alpha(M_Z) = 1/127.9$	$\eta_2 = 0.5765(65)$ [149]
$\alpha_s(M_Z) = 0.1184(7)$	$\eta_B = 0.55(1)$ [149, 150]
$\sin^2 \hat{\theta}_W = 0.23116(13)$	$F_K = 156.0(11)\,\mathrm{MeV}$
$m_K^0 = 497.614(24)\,\mathrm{MeV}$	$\hat{B}_K = 0.737(20)$
$\Delta M_K = 0.5292(9) \cdot 10^{-2}\,\mathrm{ps}^{-1}$	$F_{B_d} = 205(12)\,\mathrm{MeV}$
$|\varepsilon_K| = 2.228(11) \cdot 10^{-3}$	$F_{B_s} = 250(12)\,\mathrm{MeV}$
$m_{B_d} = 5279.5(3)\,\mathrm{MeV}$	$\hat{B}_{B_d} = 1.26(11)$
$m_{B_s} = 5366.3(6)\,\mathrm{MeV}$ [112]	$\hat{B}_{B_s} = 1.33(6)$
$\Delta M_d = 0.507(4)\,\mathrm{ps}^{-1}$	$F_{B_d}\sqrt{\hat{B}_{B_d}} = 233(14)\,\mathrm{MeV}$
$\Delta M_s = 17.77(12)\,\mathrm{ps}^{-1}$	$F_{B_s}\sqrt{\hat{B}_{B_s}} = 288(15)\,\mathrm{MeV}$
$\tau_{B_s} = 1.471(25)\,\mathrm{ps}$	$\hat{B}_{B_s}/\hat{B}_{B_d} = 1.05(7)$
$\tau_{B_d} = 1.519(7)\,\mathrm{ps}$	$\xi = 1.237(32)$ [94]
$\sin(2\beta)_{b \to c\bar{c}s} = 0.679(20)$ [114]	
$m_c(m_c) = 1.268(9)\,\mathrm{GeV}$ [94, 203]	
$m_t(m_t) = 163(1)\,\mathrm{GeV}$	
$m_b(2.5\,\mathrm{GeV}) = 4.60(3)\,\mathrm{GeV}$	

Table 6.2.: Collection of input parameters relevant for the numerical analysis of the LRM.

	2GeV	4.6GeV	172GeV	2.5TeV	15TeV
$m_u(\mu)(\mathrm{MeV})$	2.09(0)(9)	1.74(6)(7)	1.15(8)(5)	0.97(8)(4)	0.88(8)(4)
$m_d(\mu)(\mathrm{MeV})$	4.73(0)(11)	3.94(1)(9)	2.61(2)(6)	2.19(2)(5)	2.00(2)(5)
$m_s(\mu)(\mathrm{MeV})$	93.6(2)(11)	77.9(3)(9)	51.6(4)(6)	43.4(4)(5)	39.5(4)(5)
$m_c(\mu)(\mathrm{MeV})$	1089(7)(0)	907(6)(0)	601(5)(0)	505(4)(0)	460(4)(0)
$m_b(\mu)(\mathrm{GeV})$	–	4.074(19)(0)	2.702(14)(0)	2.268(12)(0)	2.068(12)(0)
$m_t(\mu)(\mathrm{GeV})$	–	–	162.3(10)(0)	136.3(9)(0)	124.2(8)(0)

Table 6.3.: The NLO running quark masses at different scales and corresponding statistical and systematic errors in the first and the second parenthesis, respectively.

6.4. Numerical results for observables

6.4.1. A general study of the matrix V^R

We now turn to the discussion of numerical results. We first want to focus on the structure of the RH mixing matrix V^R. Our scan allows us to find regions consistent with experimental constraints. Since V^R is a unitary matrix, the mixing angles of the RH mixing matrix are fixed by the knowledge of only three elements V_{us}^R, V_{ub}^R and V_{cb}^R. We will concentrate on them in the following.

First we examine the correlation of these elements, in particular we look at their dependence on the parameter s, which varies in its full range as defined in equation (6.51). In figure 6.5 we present the corresponding results, different values for s are described by its color. Since we have plotted points with large values for s in the foreground, one can deduce that allowed regions of parameter space grow with decreasing s. Actually, in spite of the fact that large regions show no points and hence are excluded by data, all three elements are able to reach values between zero and one individually. Yet, strong correlations only allow certain combinations.

The correlations of the absolute value of different elements V^R can be extracted better when we consider them in a three-dimensional plot as shown in figure 6.6 for $s = 0.1$.[2] The additional dimension clearly helps to distinguish the two branches which were already apparent in the two dimensional version. This time the colour encodes the measure of fine-tuning, defined by

$$\Delta_{\mathrm{BG}}^{\mathrm{mod}} = \frac{1}{N_{\mathrm{Obs}}} \sum_{i=1}^{N_{\mathrm{Obs}}} \Delta_{\mathrm{BG}}(O_i) = \frac{1}{N_{\mathrm{Obs}}} \sum_{i=1}^{N_{\mathrm{Obs}}} \max_{j} \left(\left| \frac{p_j}{O_i} \frac{\partial O_i}{\partial p_j} \right| \right) . \qquad (6.52)$$

Here we have modified the so-called Barbieri-Giudice Δ_{BG} measure [208], describing the sensitivity of an observable to a small variation of model parameters, by an additional summation over different observables. This sum guarantees that the fine-tuning of different observables is considered simultaneously. This measure is also useful since usually fine-tuning in several observables appears correlated. The measure of fine-tuning described by us is similar to the measure proposed by Athron and Miller [209], which however is less efficient to apply for numerical purposes. It should also be stressed that Δ_{BG} is only sensitive to fine-tuning in terms of cancellations between various contributions, but not to accidentally small parameters. In general it is useful to investigate the question of fine-tuning in such models like the LRM, since LR operators usually give sizable contributions to the NP contributions in $\Delta F = 2$ observables, which then can potentially induce large fine-tuning, especially for ε_K. An explicit example where this happens is the Randall Sundrum model with custodial protection where ε_K generally

---

[2]Due to the dependencies on many parameters we find it more transparent to study observables for specific values of s. For $\Delta F = 2$ we mainly consider $s = 0.1$, corresponding to a Higgs mass of $16\,\mathrm{TeV}$. In our study of $\mathrm{Br}(B \to X_s \gamma)$ we are explicitly interested in its s dependence.
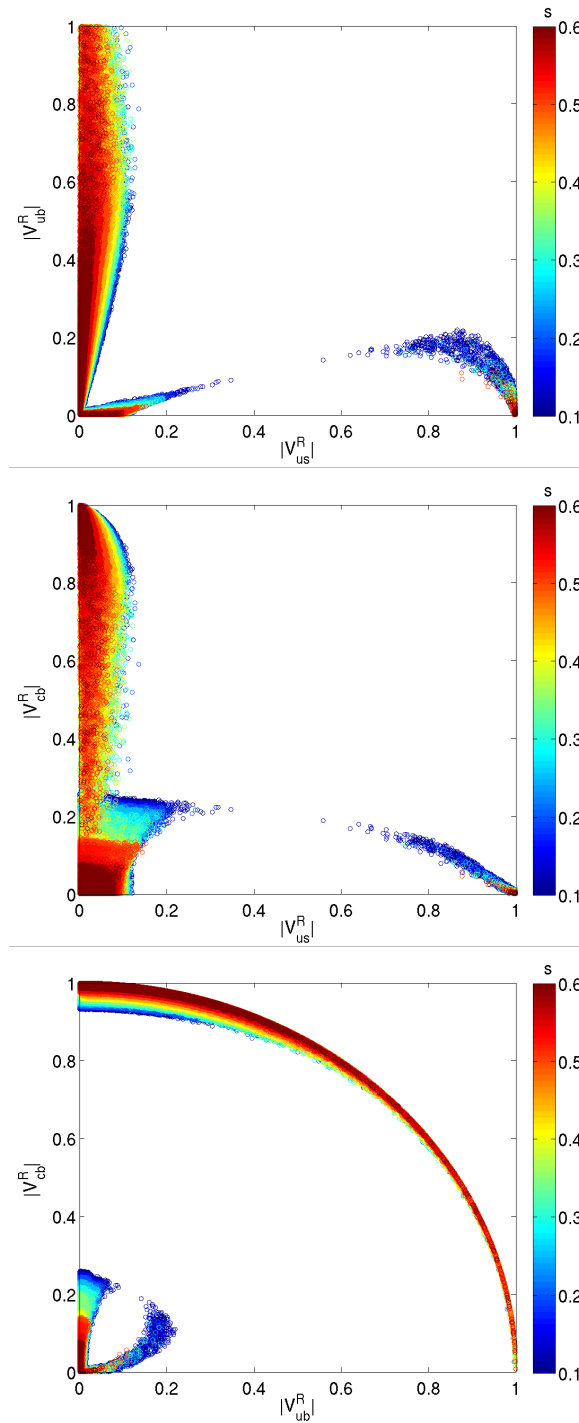
Figure 6.5.: The elements of the RH mixing matrix $|V_{us}^R|$, $|V_{ub}^R|$ and $|V_{cb}^R|$ as functions of each other. The colour encodes the parameter s.
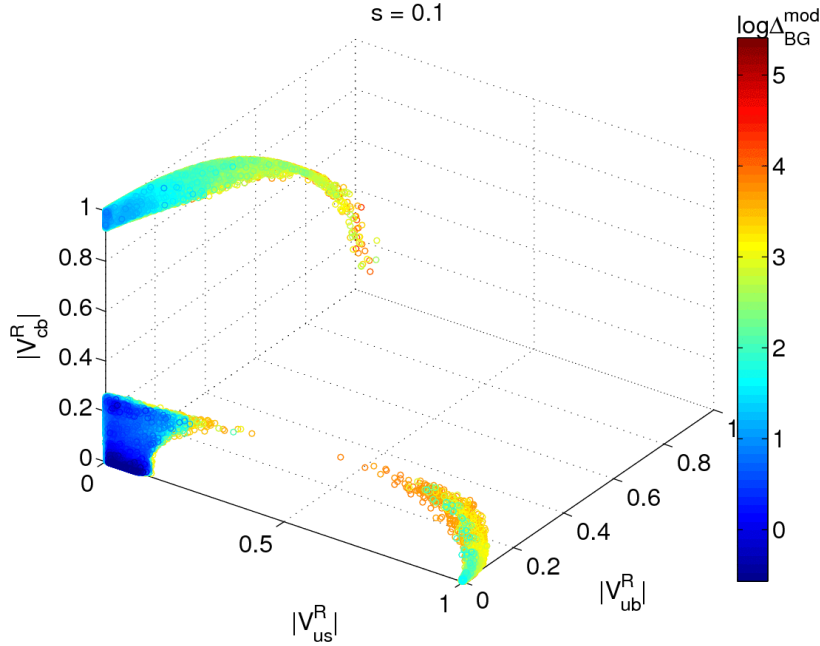
Figure 6.6.: The elements $|V_{us}^R|$, $|V_{ub}^R|$ and $|V_{cb}^R|$ in a three-dimensional plot, where the colour indicates $\log \Delta_{\mathrm{BG}}^{\mathrm{mod}}$.

suffers from a large fine-tuning [137, 210].

Let us go back to the description of figure 6.6 and see the situation in the LRM. In this plot the layers are chosen such that points with lower fine-tuning appear in front of points with higher fine-tuning. Thus in regions with low fine-tuning also highly fine-tuned points can exist. Figure 6.6 allows to distinguish between two regions with small fine-tuning, where we define "small" as $\Delta_{\mathrm{BG}}^{\mathrm{mod}} < 10$.

- In the so-called "normal hierarchy" scenario values for $|V_{us}^R|$, $|V_{ub}^R|$ and $|V_{cb}^R|$ are small. We are able to introduce a Wolfenstein-like parametrisation, which is the similar to the hierarchy in the CKM matrix, with largest entries on the diagonal.

- In the so-called "inverted hierarchy" scenario we have small values for $|V_{us}^R|$ and $|V_{ub}^R|$, but large $|V_{cb}^R|$. In contrast to the CKM matrix the size of entries of the $2, 3$ submatrix is inverted and leads to a very different pattern.

Numerically we find for both scenarios

$$|V_{td}^R| < 1.2 \cdot 10^{-2} \qquad \text{and} \qquad |V_{us}^R| < \left\{ \begin{array}{ll} 0.18 & (s = 0.1) \\ 0.13 & (s = 0.5) \end{array} \right. , \qquad (6.53)$$

where we have preferred to give the value for $|V_{td}^R|$, since here the bounds are more stringent than for $|V_{ub}^R|$. The "normal" and "inverted hierarchy" scenarios are then

characterised by the value of $|V_{cb}^R|$, in particular

$$
\begin{aligned}
|V_{cb}^R| &< 0.3\,, && \text{(normal hierarchy)} \\
|V_{cb}^R| &> 0.9\,. && \text{(inverted hierarchy)}
\end{aligned}
\tag{6.54}
$$

For both scenarios all constraints, including the constraint from ε_K, are satisfied while at the same time the fine-tuning in all observables is small.

For points outside these regions constraints are fulfilled, but they can exhibit a large fine-tuning. Therefore from phenomenological point of view these points are still viable although unnatural from the point of view of fine-tuning. An example of such a region is at small $|V_{cb}^R|$, large $|V_{us}^R|$ and $|V_{ub}^R| < 0.30$. The full branch for $|V_{ub}^R|$ is also allowed in the "inverted hierarchy" scenario. This branch is remarkable in view of the $|V_{ub}|$ problem, to which we will come back in a separate section below.

6.4.2. Estimating effects in different meson systems

We have already stated above that LR operators are known to renormalise strongly under RG evolution, especially in the K system as can be seen from the P_i^{LR} factors in both equation (6.19) and (6.20), leading to large NP effects in the K system. We have also discussed in section 6.1.5 that the dominant NP mixing amplitude is generated from LR operators. To go into more detail we have separated in equation (6.27) contributions from loop integrals and QCD running defined as $R_{ij}(M)$ with $M = K, B_d, B_s$, on which we focused in this section. We also found that $R_{tt}(M)$ yields the dominant contribution.

Now we take a look at the second contribution to the amplitude in equation (6.27), determined by the quark mixing matrices, in particular the factor $\lambda_i^{LR}(M)\lambda_j^{RL}(M)$. Having identified the valid regions of parameter space from our scan, our study of this factor will help us to estimate the contributions for different meson system. In order to investigate the particular impact of the matrix V^R on flavour processes, it is useful to consider this factor normalised to the SM contribution. Regrouping of left and right mixing matrices helps to simplify the relevant quantity according to

$$
\frac{\lambda_t^{LR}(M)\lambda_t^{RL}(M)}{\lambda_t^{LL}(M)\lambda_t^{LL}(M)} = \frac{\lambda_t^{RR}(M)}{\lambda_t^{LL}(M)}\,.
\tag{6.55}
$$

In figure 6.7 we present this factor in a three-dimensional plot for all three meson systems for $s = 0.1$. While in the K system in principle large effects are possible, the effects in the B_s system and the B_d system range from moderate to small. From these observations we can deduce a rough pattern for the hierarchy of NP effects, in particular $B_d < B_s \ll K$. Since the same factor enters rare K and $B_{d,s}$ decays, a similar pattern of effects is expected there. However we should stress that really large effects in the K system appear together with a large fine-tuning. This was expected since in this case the extraordinarily large tt contribution to $K^0 - \bar{K}^0$ mixing has to be canceled by some other contributions.
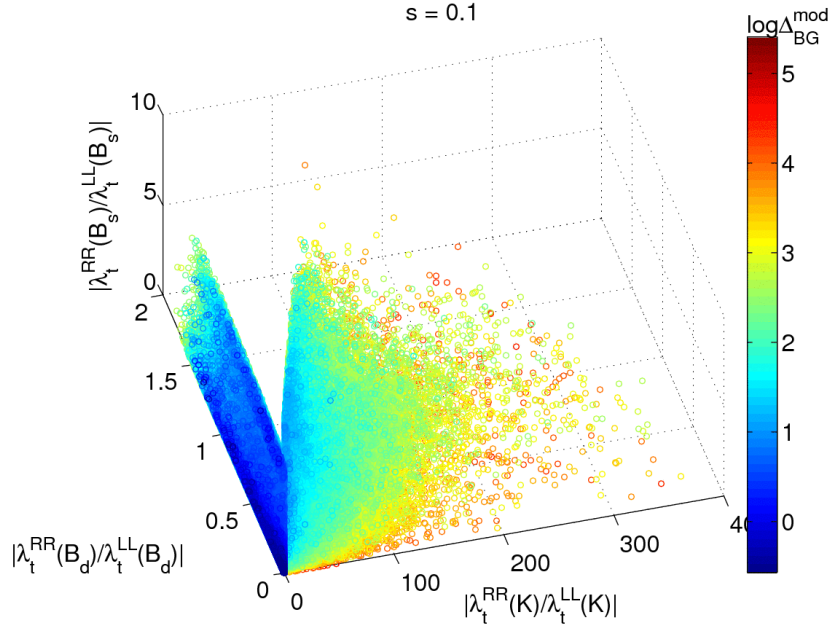
Figure 6.7.: The factor $|\lambda_t^{RR}(M)/\lambda_t^{LL}(M)|$ for $M = K, B_d, B_s$ in a three-dimensional plot. The colour coding corresponds to the logarithm of the fine-tuning $\Delta_{\mathrm{BG}}^{\mathrm{mod}}$.
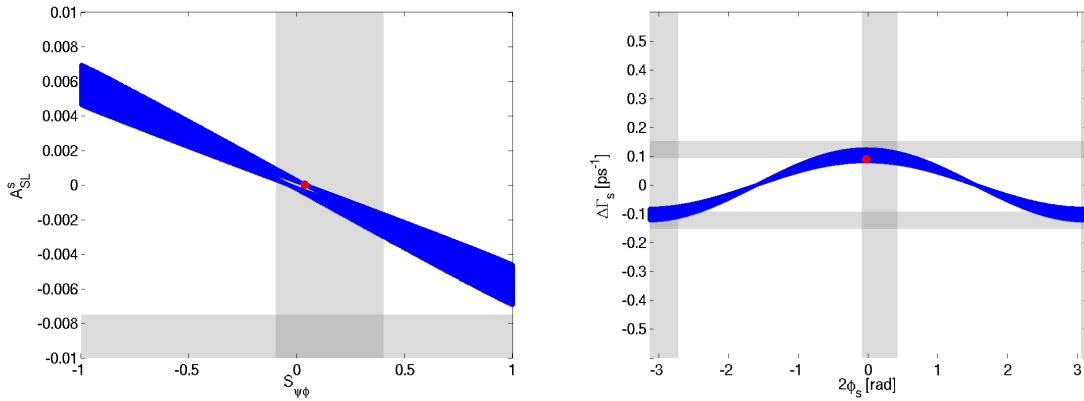
Figure 6.8.: Two model independent correlations: on the left panel A_{SL}^s and $S_{\psi\phi}$ and on the right panel $\Delta\Gamma_s$ and $2\phi_s$.

6.4.3. Model independent correlations

In view of the many free parameters involved in our analysis, our search for correlations offered limited results. The search for correlations can be improved by the study of rare decays, however this is beyond the scope of this thesis and will be addressed in future work. The only clear correlations which can be found so far are model independent such as the correlation of A_{SL}^s and $S_{\psi\phi}$ (mentioned in section 4.2.2) and the correlation of $\Delta\Gamma_s$ and ϕ_s. We show both correlations in figure 6.8, which are independent of the value of s.

6.4.4. Results for $B \to X_s\gamma$

In figure 6.9 we show the correlation between $\text{Br}(B \to X_s\gamma)$ and the CP-averaged branching ratio $\langle\text{Br}(B \to X_d\gamma)\rangle$. While we have discussed the decay $B \to X_s\gamma$ extensively within this thesis, more information about the calculation of $\langle\text{Br}(B \to X_d\gamma)\rangle$ can be found in our publication [49]. Here we restrict to the numerical discussion of $\text{Br}(B \to X_s\gamma)$. In the left panel of figure 6.9 we demonstrate the s dependence of $\text{Br}(B \to X_s\gamma)$. The qualitative enhancement of the branching ratio for increasing s could already be deduced from the structure of Wilson coefficients (for more details see section 6.2.2). The branching ratio depends linearly on $\text{Re}(V_{tb}^R)$, shown in the right panel of figure 6.9 for $s = 0.1$, also leading to a potential enhancement. Since the experimental value is still a bit above the value expected in the SM, in spite of relatively good agreement within corresponding errors, there is room for a moderate enhancement requiring a large s and a mainly real and positive contribution from V_{tb}^R.
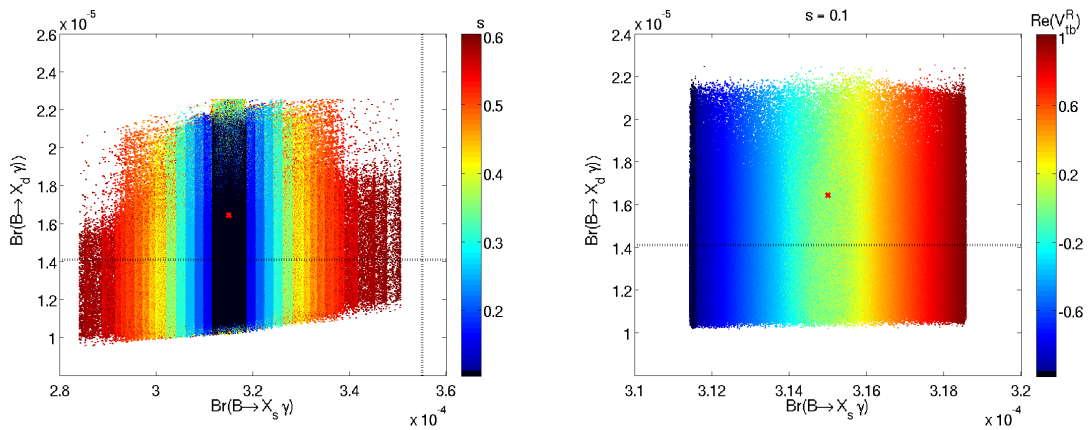
Figure 6.9.: The correlation of $\text{Br}(B \to X_s\gamma)$ and $\langle\text{Br}(B \to X_d\gamma)\rangle$. We display in colour the dependence on s and $\text{Re}(V_{tb}^R)$ in the left and right panel respectively. The red point in the center corresponds to the SM value and the dashed lines to experimental central value.
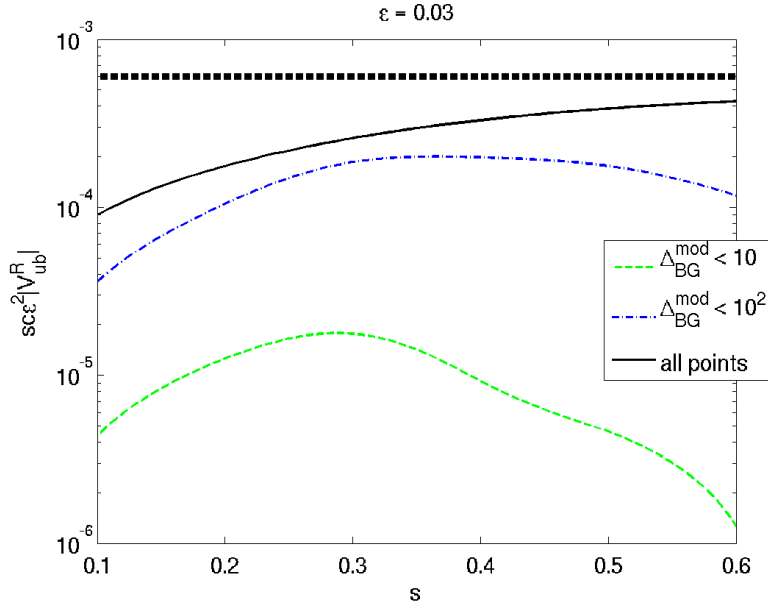
Figure 6.10.: Maximal value for $sc\epsilon^2|V_{ub}^R|$ as a function of s with respect to different amount of fine-tuning. The bold dashed and straight line represents the value $sc\epsilon^2|V_{ub}^R| \sim 0.6 \times 10^{-3}$, necessary for a solution of the $|V_{ub}|$ problem.

6.4.5. The $|V_{ub}|$ problem and other anomalies in the LRM

We now move on to the discussion of the flavour anomalies, which we have described in the SM context in section 2.1.1. In the LRM the situation is much less constrained due to the impact of many free parameters, hence tensions like the $\varepsilon_K - S_{\psi K_S}$ anomaly can be easily removed. Furthermore we have seen in figure 6.8 that the full range of values for $S_{\psi\phi}$ is possible in the LRM. Therefore, both an enhanced value of $S_{\psi\phi}$, but also the more recent value which even allows for a small negative $S_{\psi\phi}$, can be explained in the LRM.

Let us take a closer look at how the $|V_{ub}|$ problem manifests itself in the LRM. The $|V_{ub}|$ problem plays a very special role in this thesis since it was one of the main motivations for RHMFV. We have shown in figure 2.2 that for this model the $|V_{ub}|$ problem is solved by choosing the inclusive value as the true value for $|V_{ub}|$. The basic setup of the LRM is very similar and from our discussion of tree-level constraints in section 3.3.2 we would naively expect that in the LRM the $|V_{ub}|$ problem can be solved in a similar manner. The formulae in equation (3.23) and the values from table 3.2 allow us to estimate that we can obtain solution of the $|V_{ub}|$ problem if $sc\epsilon^2|V_{ub}^R| \sim 0.6 \times 10^{-3}$. In general EWP observables provide the bound $sc\epsilon^2 \leq 10^{-3}$, while we have seen from our study of $|V^R|$ that for arbitrary fine-tuning $|V_{ub}^R|$ is not constrained. This is a crude estimate and we have to study the s dependence of the full quantity (see figure 6.10) to resolve the question. Surprisingly, we find that a solution of the $|V_{ub}|$ problem cannot be provided within the LRM. In figure 6.10 this can be explicitly seen from the fact

that the maximal values of $sc\epsilon^2|V_{ub}^R|$ in the LRM do not cross the bold dashed line in that plot. The tension significantly increases if only points with small fine-tuning are considered. Finally we want to mention that a solution to the $|V_{ub}|$ problem is partially precluded by the increased lower bound on the mass of W_R suppressing the parameter ϵ.

6.4.6. A brief note on $Z \to b\bar{b}$

Similar to the considerations of section 5.2.6 for RHMFV, in the LRM we can examine whether RH currents in the framework of the LRM are able to resolve the $Z \to b\bar{b}$ anomaly. To this end one again has to analyse the effective diagonal couplings of the Z to down-type quarks as given in equation (5.33). The effective couplings can be derived explicitly in terms of the Feynman rules as given in appendix F. Since the new effects are of $\mathcal{O}(\epsilon^2) \sim 10^{-3}$ the discrepancy between experimental and SM value as given in equation (5.66) can also not be explained within the LRM. Another reason is also that the effective couplings in the LRM are not flavour dependent, hence even an enhanced value for the $Z \to b\bar{b}$ coupling would lead to inconsistent couplings for other flavours.

6.4.7. A soft lower bound on the heavy Higgs mass

In our previous considerations, we have worked with a heavy Higgs mass M_H at the edge of the perturbative regime by our choice of $\alpha_3 = 8$, only taking into account the dependence on the parameter s. This was favourable since in this case the new Higgs FCNCs are automatically suppressed. Now we want to turn the question around and ask how light the mass M_H actually can be taken while being in accordance with all experimental constraints. Obviously the constraints from the decay $B \to X_s\gamma$ provide a lower bound. We want to stress that our analysis has a few new features compared to the literature. Firstly we consider all constraints simultaneously and not separate as done in [36], for instance. Moreover we keep s as free parameter varying in the region allowed by EWP observables, which has a profound impact on the Higgs mass M_H. In many previous papers including [36], the authors usually use the limit $s \ll 1$. We proceed as follows: The heavy Higgs mass is varied between

$$\frac{2}{\sqrt{1-2s^2}}\,\mathrm{TeV} < M_H < \frac{16}{\sqrt{1-2s^2}}\,\mathrm{TeV}\,, \tag{6.56}$$

corresponding to $0.1 < \alpha_3 < 8$.

The result is very surprising and summarised compactly in figure 6.11. We can deduce from figure 6.11 the "soft lower" limit $M_H \gtrsim 2.4\,\mathrm{TeV}$ for the value $s = 0.1$. We carefully choose the word "soft", since we have made a crude parameter scan using points generated by our previous analyses. We cannot exclude that a more careful scan would reveal additional points being allowed for an even lower mass of M_H. We also want to remark that for such low Higgs masses the fine-tuning generally increases, although we also find points with $\Delta_{\mathrm{BG}}^{\mathrm{mod}} < 10$. Eventually a comment on the matrix
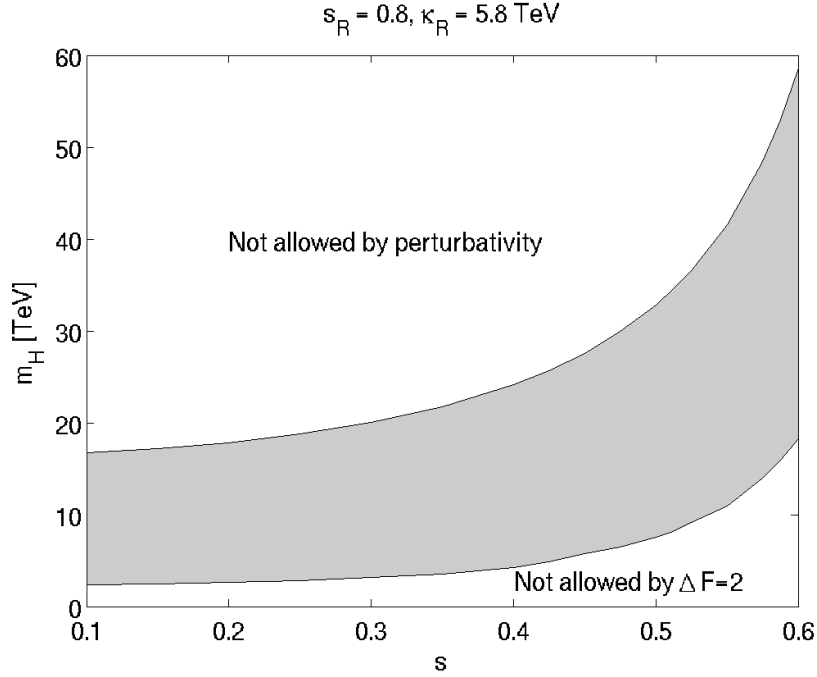
Figure 6.11.: The allowed range for the Higgs mass M_H as a function of s for EW benchmark point $\epsilon = 0.03$ and $s_R = 0.8$.

V^R is in order which is influenced by the change of the Higgs contributions. In order to compensate large Higgs effects for a low value of M_H this mixing matrix has to be very hierarchical. Approximately we find for the mixing angles

$$\tilde{s}_{12} \sim \mathcal{O}(10^{-2})\,, \qquad \tilde{s}_{13} \sim \mathcal{O}(10^{-4})\,, \qquad \tilde{s}_{23} \sim \mathcal{O}(10^{-3})\,. \tag{6.57}$$

Finally we want to comment on how these effects would affect the decay $B \to X_s\gamma$. Since $\mathrm{Br}(B \to X_{s,d}\gamma)$ depends on the diagonal element V_{tb}^R, the larger hierarchical structure of V^R has very little impact on it. Consequently a lower Higgs mass implies enhanced effects in this branching ratio.

6.5. Proposal for a simplified parametrisation of V^R

6.5.1. New ways of reduction of parameters

In the previous sections we have analysed the impact of the RH mixing matrix V^R in the most general way. To this end we have incorporated the most general parametrisation of V^R and imposed all existing constraints. Now we follow a very different strategy with the goal of finding a simplified parametrisation for V^R. This parametrisation should contain only a few free parameters while being in accordance with the experimental constraints. In the literature a few versions of V^R with reduced numbers of parameters already exist. However, some of them are already experimentally excluded like the

"pseudo-manifest" scenario [33–35]. Others are experimentally disfavoured such as the "manifest" scenario [32], the top-inspired approach [39] and some of the parametrisations of [38], mainly due to a very high bound on the W_R mass.

The motivation for a simplified RH mixing matrix from our side is very different from previous ideas. From our discussions above we know that the LRM has the potential to resolve SM anomalies, which were topic of section 2.1.1, except the $|V_{ub}|$ problem. The idea is now to find a simple matrix which still allows for a solution of these anomalies. Obviously $|V_{ub}|$ needs a different treatment here, which will be explained in the following section.

6.5.2. The treatment of $|V_{ub}|$

The LRM does not favour any particular measurement of $|V_{ub}|$, and hence allows for a wider range for its values within the experimental uncertainties. On the other hand SM tensions are closely correlated to the value chosen for $|V_{ub}|$ and can be shifted between several observables as we will demonstrate below. To this end it is useful to define different scenarios for $|V_{ub}|$:

1. **Small $|V_{ub}|$** - with the value $|V_{ub}| = 3.4 \times 10^{-3}$. In this scenario one obtains $S_{\psi K_S} \approx 0.675$ in the SM, in agreement with the data. The SM tension manifests in $|\varepsilon_K| \approx 1.8 \times 10^{-3}$ which is appreciably below the data.

2. **Large $|V_{ub}|$** - with the value $|V_{ub}| = 4.4 \times 10^{-3}$. In this scenario one obtains the SM value for ε_K in agreement with the data. The SM tension manifests in $S_{\psi K_S} \approx 0.82$ which is significantly above the data.

In the following we want to concentrate only on scenario 1. The reason for this is that the tensions within scenario 2 do not fully get resolved for the matrix which we propose below. In fact, a simultaneous suppression of both observables $S_{\psi K_S}$ and ΔM_s, which is required for this scenario, is not possible. Hence the tension of $S_{\psi K_S}$ can only be shifted to ΔM_s. It should be stressed that in view of parametric uncertainties the scenario 2 is not excluded.

6.5.3. The reduced parametrisation

Now we want to introduce the simplified mixing matrix, which only depends on two mixing angles $\tilde{s}_{13}$, $\tilde{s}_{23}$ and two phases ϕ_1 and ϕ_2 chosen from the first quadrant. The matrix can be deduced from our general parametrisation by setting $\tilde{s}_{12} = 0$ in V_0^R, which was given in equation (2.31). This choice automatically helps to soften the constraint from ΔM_K. In particular we obtain

$$V^R = \begin{pmatrix} -\tilde{c}_{13}e^{-i\phi_1} & 0 & \tilde{s}_{13} \\ -\tilde{s}_{23}\tilde{s}_{13}e^{i(\phi_2-2\phi_1)} & -\tilde{c}_{23}e^{-i\phi_1} & -\tilde{s}_{23}\tilde{c}_{13}e^{i(\phi_2-\phi_1)} \\ \tilde{c}_{23}\tilde{s}_{13}e^{-i\phi_1} & -\tilde{s}_{23}e^{-i\phi_2} & \tilde{c}_{23}\tilde{c}_{13} \end{pmatrix} . \tag{6.58}$$

This matrix is specially designed to give rise to simple expressions for the $\Delta F = 2$ observables and to resolve the SM tensions. We will demonstrate this in detail in the following sections.

6.5.4. Modifications to $\Delta F = 2$ observables

We now specify the formulae for $\Delta F = 2$ observables. The formulae can be kept very simple when we pre-constrain the ranges of the involved mixing angles by estimating the contributions to the different meson systems. We obtain

$$\tilde{s}_{13} \lesssim 0.02\,, \qquad \tilde{s}_{23} \lesssim 0.2 \qquad \text{and} \qquad \tilde{s}_{13}\tilde{s}_{23} \lesssim 10^{-5}\,, \tag{6.59}$$

coming from B_d system, B_s system and the most stringent from ε_K, respectively. For these ranges $\Delta M_{d,s}$, ε_K, $S_{\psi K_S}$ and $S_{\psi\phi}$ are fully dominated by top-top exchanges and are hence proportional to $\lambda_t^{LR}\lambda_t^{RL}$, whereas for ΔM_K $\lambda_t^{LR}\lambda_c^{RL}$ is also relevant. However, since the elements V_{td}^R and V_{cs}^R carry the same phase such top-charm contributions have no impact on ε_K. Only considering the dominant LR contributions and using the notation as introduced in equation (6.27), one can easily derive

$$(\text{Im } M_{12}^K)_{\text{LR}} = |R_{tt}(K)| \times \frac{G_F^2 M_W^2}{12\pi^2} F_K^2 m_K |V_{td}^L||V_{ts}^L|\tilde{c}_{23}\tilde{s}_{13}\tilde{s}_{23}\sin(\phi_2 - \phi_1 - \beta + \beta_s)\,, \tag{6.60}$$

for the $K^0 - \bar{K}^0$ system and

$$C_{B_q}e^{2i\varphi_{B_q}} = 1 - \frac{|R_{tt}(B_q)|}{S_0(x_t)\hat{B}_{B_q}\eta_B}\left[\frac{\lambda_t^{RR}(B_q)}{\lambda_t^{LL}(B_q)}\right]^*\,. \tag{6.61}$$

for the $B_q^0 - \bar{B}_q^0$. The simplified matrix in equation (6.58) yields

$$\left[\frac{\lambda_t^{RR}(B_d)}{\lambda_t^{LL}(B_d)}\right]^* = \frac{\tilde{c}_{23}\tilde{s}_{13}V_{tb}^R}{|V_{td}^L|}e^{i(\phi_1 - \beta)}\,, \qquad \left[\frac{\lambda_t^{RR}(B_s)}{\lambda_t^{LL}(B_s)}\right]^* = \frac{\tilde{s}_{23}V_{tb}^R}{|V_{ts}^L|}e^{i(\phi_2 - \beta_s)}\,, \tag{6.62}$$

and consequently

$$\sin 2\varphi_{B_d} = -\frac{|z_d|}{C_{B_d}}\frac{\tilde{c}_{23}\tilde{s}_{13}V_{tb}^R}{|V_{td}^L|}\sin(\phi_1 - \beta)\,, \quad \sin 2\varphi_{B_s} = -\frac{|z_s|}{C_{B_s}}\frac{\tilde{s}_{23}V_{tb}^R}{|V_{ts}^L|}\sin(\phi_2 - \beta_s)\,, \tag{6.63}$$

where we have defined

$$z_q = \frac{R_{tt}(B_q)}{S_0(x_t)\hat{B}_{B_q}\eta_B}\,. \tag{6.64}$$

For a reasonable choice of the parameters $M_{W_R} = 2.5\,\text{TeV}$, $M_H = 16\,\text{TeV}$ and $s = 0.1$, while additionally using only central values for remaining parameters, one finds

$$|R_{tt}(K)| = 9.1\,, \qquad |R_{tt}(B_q)| = 0.57\,, \qquad |z_d| = 0.36\,, \qquad |z_s| = 0.34\,. \tag{6.65}$$

Furthermore under the assumption of scenario 1, recalling that the SM value for $S_{\psi K_S}$ agrees already well with the experiment, we can approximately set $\phi_1 \approx \beta$ leading then to negligible NP effects in $S_{\psi K_S}$. Consequently, ε_K and $S_{\psi\phi}$ are governed by the phases $\phi_2 - 2\beta$ and ϕ_2, respectively. Reproducing the experimental value of ε_K requires then $\phi_2 > 2\beta - \beta_s$, which implies automatically an enhancement of $S_{\psi\phi}$. In the following we want to concentrate on correlations between ε_K, $S_{\psi K_S}$, $S_{\psi\phi}$, ΔM_d and ΔM_s.

6.5.5. Numerical results

We briefly want to illustrate our findings with the help of a simplified numerical analysis, neglecting the errors in the LH mixing matrix and other parameters. Instead, we fix all values to their central values according to section 3.3.3, except $|V_{ub}|$ which we have already defined in scenario 1 and $\gamma = 68°$. Mixing angles and phase of the simplified matrix for V^R were scattered under the following assumptions: we choose $\phi_1 = \beta$, $\tilde{s}_{13} = 3 \cdot 10^{-3}$ and the remaining parameters are varied according to $\tilde{s}_{23} < 0.2$ and $2\beta - \beta_s < \phi_2 < \pi + 2\beta - \beta_s$. This treatment allows a transparent demonstration of the behaviour of correlations. At the same time it displays how a more precise measurement of the CKM elements can help not only to find tensions between observables but also to deduce details of the underlying model.

In figure 6.12 we present the correlation between ε_K and $S_{\psi\phi}$. Here we have imposed the experimental constraints from ΔM_s and ΔM_d. We find that ε_K is in good agreement with the data for $\tilde{s}_{23} \gtrsim 0.05$ and $45° < \phi_2 < 50°$, in turn enhancing $S_{\psi\phi}$ with respect to its SM value. As one can easily deduce a larger value for ϕ_2 is linked to a smaller $\tilde{s}_{23}$ in order to satisfy the experimental data on ε_K. Thus the ε_K anomaly is solved and in case of a precise measurement of $S_{\psi\phi}$ the values for $\tilde{s}_{23}$ and ϕ_2 can be extracted.

Now we have to examine whether the tension in ε_K is resolved and not just shifted to a different set of observables. To this end we consider the correlation between ΔM_d and ΔM_s normalised to their SM values as illustrated in figure 6.13. Here we also have taken into account the constraint from ε_K. We realise that values for both mass differences lie somewhat below their SM predictions, which is favoured by experimental data. To go into more detail, ΔM_d is very close to its experimental central value. It is not surprising that the value of ΔM_d varies only in a very small range, since this observable is mainly influenced by ϕ_1 and $\tilde{s}_{13}$ which are fixed in our consideration. The observable ΔM_s can also be suppressed. Requiring that the values lie in the allowed experimental region (indicated by the grey band), we find that due to the correlation with $S_{\psi\phi}$ the following values are preferred: moderate enhancement with $S_{\psi\phi} \lesssim 0.4$ (light-blue points) or large enhancement with $S_{\psi\phi} \sim 1$ (red points). The latter value however is disfavoured by the latest data from LHCb.

Finally we want to mention that a nice "side effect" of our simplified matrix is that the V_{tb}^R value is close to one. The branching ratio $\text{Br}(B \to X_s \gamma)$ is then automatically enhanced with respect to its SM value, which is favoured by experimental data.

6.5.6. Outlook

In the previous sections we have introduced a new simplified parametrisation for V^R and demonstrated that SM flavour tensions can be resolved. Here we want to quote a reference point, in particular

$$\tilde{s}_{13} = 3 \cdot 10^{-3}\,, \qquad \tilde{s}_{23} = 0.03\,, \qquad \phi_1 = \beta = 21°\,, \qquad \phi_2 = 50°\,, \tag{6.66}$$
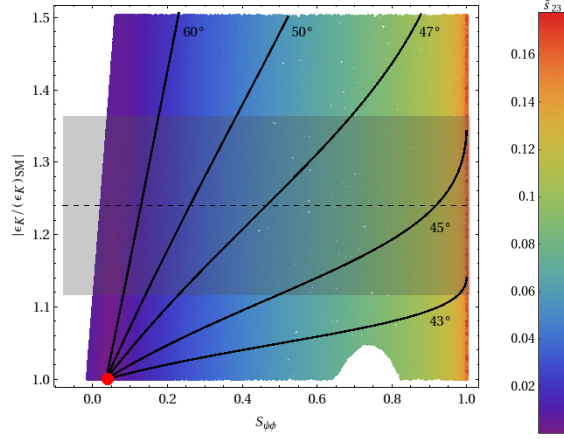
Figure 6.12.: Correlation between $S_{\psi\phi}$ and ε_K in scenario 1 for fixed values of $\phi_1 = \beta$ and $\tilde{s}_{13} = 3 \cdot 10^{-3}$. The red dot denotes the central SM value. The black curves illustrate the lines of a constant ϕ_2 while values for $\tilde{s}_{23}$ are encoded in colour. The grey band corresponds to the region of ε_K preferred by experimental data.
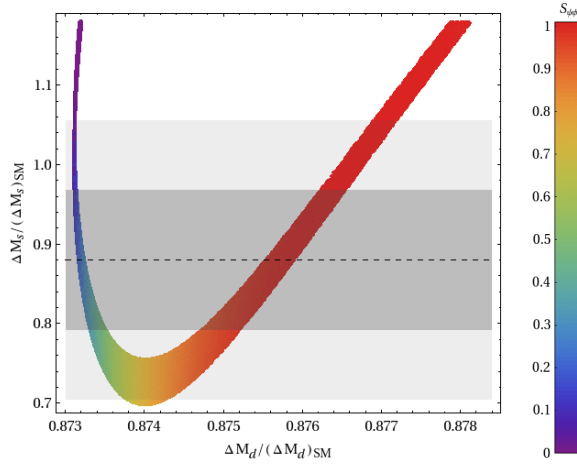
Figure 6.13.: Correlation between ΔM_d and ΔM_s in scenario 1 for fixed values of $\phi_1 = \beta$ and $\tilde{s}_{13} = 3 \cdot 10^{-3}$. Different values for $S_{\psi\phi}$ are encoded in colour. The grey band represents the preferred experimental region.

which represents a possible solution. The observables of our consideration are then given by

$$S_{\psi K_S} \approx 0.67\,, \qquad |\varepsilon_K| \approx 2.2 \cdot 10^{-3}\,, \qquad S_{\psi\phi} \approx 0.27\,, \qquad (6.67)$$

and

$$\Delta M_d \approx 0.51\,\mathrm{ps}^{-1}\,, \qquad \Delta M_s \approx 17.4,\mathrm{ps}^{-1}\,. \qquad (6.68)$$

It should be mentioned that our matrix V^R is chosen in the most simple way and a further reduction of parameters would not allow a resolution of the SM anomalies. However, there might exist other simplified parametrisations which are equally effective. We also want to remark again that in our discussion so far we have neglected both theoretical and parametric uncertainties in order to establish various correlations cleanly.

In summary, we are able to draw conclusion about a possible structure of V^R only using hints from existing flavour data. With improved measurements, especially of the observables $S_{\psi\phi}$, $S_{\psi K_S}$ and $|V_{ub}|$, such methods will gain in importance. It should also be stressed that direct collider searches for NP are not sensitive to the structure of V^R. Thus, even in case of a discovery of a heavy W_R directly, the study of flavour physics is indispensable in order to reveal details about a specific model. In this sense low energy flavour data can give us remarkable and complementary information about physics at high energy scales.

7. Comparison with other models

After having studied two different approaches towards RH currents in detail, it is now interesting to summarise both the common grounds and differences. Furthermore we want to compare the two models with other bottom-up and top-down approaches. The models in comparison are consciously chosen with properties similar to their counterpart, although we will demonstrate that in spite of these similar patterns different results in flavour observables can be obtained. We compare two effective approaches which incorporate the idea of MFV in two different ways. RHMFV makes use of an extended MFV principle, matched to the idea of RH currents. In the second effective approach in the 2HDM$_{\overline{\text{MFV}}}$ [54, 211], a two Higgs doublet model, the MFV hypothesis is implemented with additional flavour blind phases. We also compare the LRM with the Randall Sundrum model with custodial protection (RSc). The comparison of these models is attractive since both top-down approaches have the same gauge group and exhibit a similar symmetry breaking pattern.

7.1. Comparison of RHMFV and the LRM

7.1.1. Comparison of the theoretical setups

Let us start by comparing the two models which are the main topic of this thesis. First of all both approaches address right-handed currents in a quite different way. While in RHMFV we consider an effective theory, the LRM can be understood as a full renormalisable theory.

Comparing the symmetry structure of the two frameworks we realise that both are based on the $SU(2)_L \times SU(2)_R \times U(1)_{B-L}$ setup. Whereas in RHMFV the symmetry acts globally, in the LRM it is gauged and hence local. Consequently the particle content is different in each case. The LRM features the heavy gauge bosons W_R and Z' together with a bunch of heavy Higgs particles, where only the two flavour changing Higgses H_1^0 and H_2^0 and the H^+ as discussed above play a role in our analysis. On the other hand in RHMFV only SM particles contribute directly. The number of parameters is similar in both models, with the RH mixing matrix providing in each case 9 additional parameters. While the same general parametrisation can be chosen for this matrix, phenomenologically both scenarios turn out to be very different. We will discuss this in more detail in the following section.

We have a similar right-handed scale in both models. In particular the typical scales

are set by the parameters $\varepsilon_R = \mathcal{O}(10^{-3})$ and $cs\epsilon^2 < \mathcal{O}(10^{-3})$ for RHMFV and the LRM respectively. It should be stated that while in RHMFV the scale is fixed by data from tree-level decays, in the LRM we obtain it by the study of EWP observables and direct bounds on the M_{W_R} mass.

The FCNC protection mechanisms of both models are very different. While in RHMFV we imposed a generalised MFV principle, in the LRM the GIM mechanism linked to the unitarity of the mixing matrices provides a partial protection. In contrast to the SM, flavour violation is mainly introduced by the non-standard tree-level Higgs contributions. These dangerous contributions can be softened by a large Higgs mass. A mass as low as 3 TeV is allowed without violating experimental constraints. However, in this case the RH mixing matrix has to exhibit a very special structure in order to keep the NP effects under control. It should be noted that the GIM mechanism is violated in the left-right contributions to Wilson coefficients.

The LRM cannot be matched to RHMFV just by integrating out the heavy fields. We provide two arguments to justify this statement. The first is obvious, only a very specific and non-trivial pattern of symmetry breaking can be linked with the spurions responsible for breaking the custodial symmetry in RHMFV. The generalised MFV assumptions provide a specific flavour structure for the effective couplings, which are absent in the more general case of the LRM. Secondly, the operator structure of both models is qualitatively different. By construction, RHMFV involves only the operators $\mathcal{Q}_1^{VLL}$, $\mathcal{Q}_1^{VRR}$ and $\mathcal{Q}_1^{LR}$. The operator Q_2^{LR} is assumed to be generated only by QCD corrections. As we have previously shown, in the LRM we can classify the impact of operators into three main categories:

- The tree-level exchange of a colourless Higgs scalar generates the operators Q_1^{SLL}, Q_1^{SRR} and Q_2^{LR}, but in our case keeping contributions up to $\mathcal{O}(\epsilon^2)$ only the LR contribution matters.

- Charged Higgs box diagrams generate the same operator Q_2^{LR} as in the neutral tree-level case, at $\mathcal{O}(\epsilon^2)$.

- Box diagrams with internal charged gauge bosons carrying both LH and RH couplings generate the operators Q_1^{VLL}, Q_1^{VRR} and Q_2^{LR} at $\mathcal{O}(\epsilon^2)$. The operator Q_1^{LR} is also generated but emerges with its leading term at $\mathcal{O}(\epsilon^4)$ and is thus neglected in our analyses.

In the LRM the leading effect for Q_1^{LR} comes from QCD operator mixing. In spite of the fact that the inclusion of scalar currents provides a larger basis of operators, the main difference of both models effectively occurs only in the appearance of the operators Q_1^{LR} and Q_2^{LR}. In an explicit model the operator Q_1^{LR} (together with the operators Q_1^{VLL} and Q_1^{VRR}) usually appears in the presence of a tree-level exchange of a colourless gauge boson with LH and RH couplings, such as typical for Z' models or gauge flavour models [212]. Hence the effective $\Delta F = 2$ Hamiltonian of RHMFV should correspond

to a full theory where such exchanges are involved. This is clearly not the case in the LRM, where NP enters mainly through the impact of the operator Q_2^{LR}.

In summary, the two approaches considered in this thesis provide a complementary view of RH currents. We stress again that RHMFV cannot just be seen as an effective theory of the LRM with the heavy particles integrated out.

7.1.2. Comparison of the flavour phenomenology

The differences elaborated above can be seen in the phenomenology. First we want to compare the structure of the RH mixing matrices. In RHMFV the RH matrix was constructed with the motivation of a large $S_{\psi\phi}$. On the other hand, in the LRM possible structures are obtained as results of our numerical analysis, starting from the most general parametrisation. It turns out that their particular structure is very different. This can be explicitly deduced from the size of elements by comparing figure 6.6 and the entries of the matrix given in equation (5.10) corresponding to the LRM and RHMFV respectively. With more precise data a measurement of their corresponding entries could help to distinguish both scenarios. Furthermore we have already demonstrated in detail that unlike in RHMFV the $|V_{ub}|$ problem cannot be solved in the LRM. This is partly since the experimental bound on the mass of W_R has been increased.

Now we turn to $\Delta F = 2$ observables. RHMFV was originally designed to explain a large $S_{\psi\phi}$. In order to obtain a small or even negative $S_{\psi\phi}$ one would have to redo the analysis under this special requirement. Our LRM analysis is in this context much more flexible since we obtain $S_{\psi\phi}$ as a prediction, where values in the full range are possible. In the LRM, all SM tensions of flavour observables can be resolved, even with a reduced parametrisation. This is not the case in RHMFV where the $S_{\psi K_S}- \sin(2\beta)$ tension remains. Further, in RHMFV the ε_K constraint implies potentially large effects in B_s mixing together with negligible effects in B_d mixing. A similar pattern exists in rare $B_{d,s}$ decays. The B_q sector of the LRM follows a structure similar to RHMFV. In more detail we have identified a rough hierarchy pattern of NP effects $B_d < B_s \ll K$. A future study of rare decays within the LRM will help to distinguish both models by their correlations. Finally, neither model explains the anomalous $Zb\bar{b}$ coupling.

7.2. RHMFV versus 2HDM$_{\overline{\text{MFV}}}$

7.2.1. A very brief review of the 2HDM$_{\overline{\text{MFV}}}$ model

In this section we want to give a brief summary of the 2HDM$_{\overline{\text{MFV}}}$ framework. For a detailed model description we refer to the original papers [54, 211]. Subsequently, we compare their main findings to RHMFV and elaborate differences as well as prospects of both models.

As already mentioned above the 2HDM$_{\overline{\text{MFV}}}$ belongs to the class of two Higgs doublet models. The Yukawa interaction includes in this case separate terms for both Higgs doublets, which couple to up and down quarks. Consequently, the mass matrices for up and down quarks appear as linear combinations of up and down Yukawas couplings, respectively, and hence cannot be simultaneously diagonalised for generic Yukawa couplings. This is the origin of potentially dangerous Higgs mediated FCNCs at tree-level. A realistic model hence seeks for an appropriate suppression mechanism of such contributions, which is guaranteed in [54] by inclusion of the MFV principle.

The flavour symmetry, identical to the original MFV setup and given in equation (2.4), is only broken by two independent terms Y_d and Y_u similar to the original setup. Hence spurions will follow the known transformation properties as given in (2.5). Due to this property the Yukawa coupling matrices in the two Higgs doublet case can be expanded at lowest order in Y_d and Y_u, respectively. More generally speaking one obtains a polynomial containing the two left-handed flavour invariant combinations $Y_u Y_u^\dagger$ and $Y_d Y_d^\dagger$. The corresponding coupling coefficients are in general taken to be real, but it is consistent with the MFV principle if they additionally carry new flavour-blind CP-violating phases [80–82]. At this stage the role of electric dipole moments (EDMs) is often discussed, which are known to set strict bounds on such flavour blind phases (FBPs). However a detailed analysis of the authors in [211] shows that the upper bounds from EDMs still allows for sizable effects from FBPs.

For completeness it should be mentioned that additional phases in the Higgs sector, in particular the Higgs potential, can be present. These then enter into the mixing induced CP asymmetries $S_{\psi K_S}$ and $S_{\psi\phi}$, and can hence change their correlation. We will not follow this aspect here further. However, it should be noted that this possibility is interesting since the most recent data on $S_{\psi\phi}$ indicates that some FBPs in the Higgs potential might be necessary.

7.2.2. Comparison of theoretical aspects

At first sight the two setups of RHMFV and 2HDM$_{\overline{\text{MFV}}}$ seem to be very similar. Both are effective approaches implementing the idea of MFV. However, the flavour groups in each case are different. Our LR symmetric flavour group is less constraining than the full MFV group in (2.4). Here we should also mention the additional FBPs exist in the two Higgs doublet case which do not appear in RHMFV. Finally there is an extended Higgs sector in (2.4), opening the possibility for new scalar contributions, while in our approach we have a SM Higgs sector. Obviously, this leads to an extended particle content in the Higgs sector for the 2HDM$_{\overline{\text{MFV}}}$ model, including three neutral Higgs fields with flavour violating couplings and additionally charged Higgs fields. We want to remark that two spurions $P_{u,d}$ in RHMFV can also be interpreted as the remnant of two different VEVs stemming from a two Higgs doublet model. The Higgs can then be understood as an effective light Higgs appearing from a linear combination of two Higgs fields with similar VEVs and heavy masses.

Let us now take a closer look at the operator structure. As we have seen in equations (5.5) and (5.8), at the high scale RHMFV selects $\mathcal{Q}_1^{VRR}$ and $\mathcal{Q}_1^{LR}$, while Higgs exchanges in $2\text{HDM}_{\overline{\text{MFV}}}$ mainly take place through $\mathcal{Q}_2^{LR}$. It should be stressed that these high scales differ in the particular models. The masses of the new neutral scalars is expected to be smaller by one order of magnitude than the relevant scales for RH currents. Under consideration of QCD renormalisation group effects in RHMFV the operator basis is given by equation (4.2), while for $2\text{HDM}_{\overline{\text{MFV}}}$ the full set of operators as given by both equation (4.2) and (4.3) has to be considered. Interestingly the RG effects for P_1^{LR} and P_2^{LR} are roughly of the same size.

In spite of the fact that both models control FCNCs by the MFV mechanism or some extended version, practically the suppression turns out to be very different. Considering $\Delta F = 2$ observables in case of $2\text{HDM}_{\overline{\text{MFV}}}$ one realises that the Wilson coefficients of the NP contributions in $K^0 - \bar{K}^0$, $B_d^0 - \bar{B}_d^0$ and $B_s^0 - \bar{B}_s^0$ mixing come with a mass suppression proportional to the product of their external quark masses according to $m_s m_d$, $m_b m_d$ and $m_b m_s$, respectively. In RHMFV the breaking of flavour universality of non-standard contributions is entirely determined through the RH mixing matrix.

7.2.3. Comparison of the flavour phenomenology

Now we are ready to compare the phenomenology of $\Delta F = 2$ observables. Obviously in $2\text{HDM}_{\overline{\text{MFV}}}$, the NP contributions are mainly determined by the mass pattern described above, leading to negligible effects in $K^0 - \bar{K}^0$, followed by suppressed effects in $B_d^0 - \bar{B}_d^0$ while in $B_s^0 - \bar{B}_s^0$ mixing larger effects are possible. The particular size of contributions in B_d and B_s system appears in a correlated manner, approximately the following relation is valid [52]

$$\varphi_{B_d} \approx \frac{m_d}{m_s} \varphi_{B_s} \approx \frac{1}{17} \varphi_{B_s} \,. \tag{7.1}$$

Hence the FBPs only have impact on $\Delta B = 2$ transitions. This implies that the highly constrained ε_K is not directly affected. The modification of the relation between the CKM phase β and the NP phase φ_{B_d} according to equation (4.17) allows to extract a "true" value for β which is enhanced with respect to the SM result. Therefore it is in favour of relaxing the SM tension existing in ε_K and $\sin(2\beta)$. Furthermore the correlation of phases (7.1) allows for a large CP-violating phase in $B_s^0 - \bar{B}_s^0$ mixing, hence a large $S_{\psi\phi}$, while at the same time the tension between the SM prediction and experimental value within $S_{\psi K_S}$ becomes weakened. Finding a negative value for $S_{\psi\phi}$ experimentally would rule out the model.

We note that the $2\text{HDM}_{\overline{\text{MFV}}}$ solves the ε_K problem in a way similar to the mechanism in RHMFV. Instead of increasing the SM tension in $S_{\psi K_S}$ like in RHMFV, the situation in the two Higgs doublet is favourable. Here we want to stress that in $2\text{HDM}_{\overline{\text{MFV}}}$ only the impact of the FBPs can give rise to CP violating effects big enough to explain sizable effects in B_s mixing in particular $S_{\psi\phi}$. Consequently the question arises whether

FBPs can also help to cure the problem in the RHMFV model.

Let us allow for a moment such phases in RHMFV. Then the expansion of contributing bilinears contains terms each with a complex coefficient. However the operator $O_{RR}^{(6)}$ of equation (2.26) consists of a squared bilinear, consequently the complex phase would cancel. Therefore such phases could just contribute to $O_{LR}^{(6)}$, given in equation (2.27), and then appear in the subsequently derived formulas only in terms containing the coefficient c_{LR}. We find that in this case the same effect as in the 2HDM$_{\overline{\text{MFV}}}$ cannot be reproduced and such phases cannot cure the tension in $S_{\psi K_S}$.

On the other hand it should be noted that the 2HDM$_{\overline{\text{MFV}}}$ model favours large values of $|V_{ub}|$. Here no natural explanations for the different determinations of $|V_{ub}|$ can be found as it was the case in RHMFV.

Finally, we compare $\Delta F = 1$ observables. Here the role of the decays $B_{s,d} \to \mu^+\mu^-$ is important. Due to the scalar FCNC operators in 2HDM$_{\overline{\text{MFV}}}$, both branching ratios can be enhanced by one order of magnitude relative to the SM value so that both decays can come close to their present experimental limit. This takes place without coming into conflict with constraints from ε_K and large $S_{\psi\phi}$. Moreover the known MFV relation is approximately preserved and a strict linear correlation is obtained. Recall that in RHMFV effects in $B_s \to \mu^+\mu^-$ were smaller, while in $B_d \to \mu^+\mu^-$ negligible after imposing a large $S_{\psi\phi}$. Hence the relation for $B_{s,d} \to \mu^+\mu^-$ typically obtained in MFV models is strongly violated here.

7.3. Comparison of the LRM and the RSc

7.3.1. The Randall-Sundrum model with custodial protection

In this section we want to compare the LRM to the Randall Sundrum model with custodial protection (RSc), which we have extensively studied in [19] and wherein a detailed model description can be found. Here we just briefly review the basic ideas of this class of models. Models with a warped extra dimension and bulk fields have received a lot of attention in the last years [13–16]. They not only provide a geometrical solution to the hierarchy problem, but also naturally generate the hierarchies of fermion masses and mixings [20, 21] while keeping FCNCs efficiently under control [213, 214].

The central feature of such models is a warped metric [13], given by

$$ds^2 = e^{-2ky}\eta_{\mu\nu}dx^\mu dx^\nu - dy^2 \, , \tag{7.2}$$

where the extra dimension, characterised by the variable y, appears with an exponential warp factor depending on a curvature scale k. The five dimensional space-time is then described by a brane scenario: two four-dimensional branes, the so called Planck and TeV brane, and the five-dimensional (5D) bulk along the extra dimension. The

effective energy scale turns out to be suppressed by the warp factor along the extra dimension. Since gravity propagates in the bulk while the Higgs field remains confined on the TeV brane, the warping then can generate the huge hierarchy between the scale of gravity and the electroweak scale.

In order to guarantee a sufficient suppression of higher dimensional operators, being linked to FCNCs and electroweak precision tests, SM fields have to propagate in the bulk. Hence fields appear five-dimensional and have to be treated in terms of Kaluza-Klein (KK) decomposition. Consequently each fields consists of a light zero mode, being assigned to the corresponding SM field, and a tower of heavy KK modes. In general the KK modes have masses of $\mathcal{O}(1\,\text{TeV})$ and hence are light enough to be accessible at LHC. Higher modes have increasing masses, thus it is phenomenologically justified to truncate the KK tower and restrict to the first mode as done in this analysis. In addition each mode is characterised by a profile in the bulk. In this way different flavours can be described by different localisations in the bulk. The overlap with the Higgs field on the TeV brane then determines the fermion mass. Thus, when assuming anarchical $\mathcal{O}(1)$ Yukawas in the 5D theory, the effective 4D Yukawas exhibit a hierarchical structure so that typical quark mass patterns are generated automatically.

The appearance of sources of flavour non-universalities in this class of models is two-fold. Due to the different fermion localisation in the bulk non-universalities remain in the gauge couplings after rotation to mass eigenstates. Furthermore electroweak gauge bosons of the same charge mix due to EWSB and leading for example to non-universalities in the Z coupling. To this end FCNCs can appear at tree-level [210, 213–215]. However, these potentially dangerous effects are controlled by a powerful protection mechanism, compactly described as the RS-GIM mechanism [213, 214]. It keeps the effects in flavour-changing transitions for light quark generations to be small.

In order to construct a realistic model of EWSB in this framework, constraints from electroweak precision tests, as given by the T parameter and the $Zb_L\bar{b}_L$ coupling, have to be taken into account [216, 217]. Consistency can be achieved by an enlargement of the bulk symmetry according to [17, 18, 23, 27, 218, 219]

$$G_{\text{bulk}} = SU(3)_c \times SU(2)_L \times SU(2)_R \times U(1)_X \times P_{LR}\,, \qquad (7.3)$$

where P_{LR} is a discrete symmetry interchanging the two $SU(2)$ groups. The symmetry breaking is achieved by a combination of choosing appropriate boundary conditions and spontaneous symmetry breaking due to the Higgs field. The EWSB induces a mixing between SM zero modes and heavy KK fields, leading to a non-trivial structure for flavour-changing transitions.

7.3.2. Comparison of the theoretical framework

The LRM and the RSc feature a few common properties. Starting from the fact that both are top-down approaches, the gauge group and its breaking pattern are similar in

both cases. However, we want to point out that in the 4D dual description of the RSc the $SU(2)_R$ appears as global symmetry according to the AdS/CFT correspondence. Furthermore the additional P_{LR} symmetry in RSc gives rise to equal left and right gauge couplings. This has been deliberately avoided in the LRM in order to create a more general framework and allow for a small left-right asymmetry. Furthermore the realisation of a brane scenario makes use of a new form of symmetry breaking implemented by boundary conditions. In both models we obtain new particles due to the enlarged symmetry, set to be at a NP scale around $(2-3)$ TeV. The KK expansion leads to additional modes for each gauge boson with respect to the LRM, such as the KK gluon, the KK photon. In the electroweak sector in total the new gauge bosons $W_H^\pm$, $W'^\pm$, Z_H and Z' appear. In the fermion sector of the RSc exotic charged fermions can arise, expected to be much lighter than the gauge boson states.

A striking difference is the fact that the RSc explains hierarchies. This refers to both the hierarchy problem as well as hierarchies in masses and mixings. In the LRM, the RH mixing matrix appears without explanation.

The flavour pattern of both models is very different. We have outlined the mechanisms of protection from large FCNCs in each model previously. Here we just summarise the fact that both models violate GIM in different ways. FCNCs at tree-level appear in both models. While in the LRM these tree-level contributions arise solely from the neutral Higgs diagrams, in the RSc tree-level transitions are mediated by the electroweak gauge bosons and the KK gluon. The dominant tree-level exchanges of the KK gluon then generate the operators Q_1^{VLL}, Q_1^{VRR}, Q_1^{LR} and Q_2^{LR}. Recall that in the LRM the exchange of colourless gauge bosons with LH and RH couplings lead to Q_1^{VLL}, Q_1^{VRR} and Q_2^{LR}. The operator Q_2^{LR} provides the dominant effects in $K^0 - \bar{K}^0$ mixing in the RSc, due to RG effects and chiral enhancement. For $B_q^0 - \bar{B}_q^0$ mixing Q_1^{VLL} turns out to be dominant. In principle tree-level flavour changing Higgs couplings also exist in the RSc but they play a subleading role [220, 221].

7.3.3. Comparison of the flavour phenomenology

Finally, we want to summarise very briefly the main effects observed in phenomenology [137, 222].

The strongest constraints in $\Delta F = 2$ observables in both models arise from the ε_K constraint. In the context of this observable in the RSc often a "fine-tuning problem" is mentioned implying a large fine-tuning in order to keep an anarchic structure of the 5D Yukawa couplings while keeping the KK scale low [210]. On the other hand in [222] it was shown that regions of parameter space with low fine-tuning exist being in accordance with all constraints from $\Delta F = 2$ observables. It should be stressed that the density of points in the corresponding plot of the same paper has only numerical but no physical significance. Therefore, we have avoided such a presentation in our analysis of the LRM. Still in the RSc the fine-tuning problem is more severe since it

gets reintroduced at one loop level due to the large 5D Yukawa couplings close to their perturbativity bound. In addition one of the main motivations for the RSc was a solution to the flavour hierarchy problem with anarchic fundamental couplings, while the LRM does not claim to provide a theory for flavour hierarchies.

In the RSc the effects on mass differences in the $B_q^0 - \bar{B}_q^0$ system are suppressed by the RS-GIM mechanism. However NP effects still enter such that the $S_{\psi K_S} - \sin(2\beta)$ tension can be resolved. Similar results are obtained in both models for the CP asymmetry $S_{\psi\phi}$, in particular $-1 < S_{\psi\phi} < 1$ can be found in both cases.

Let us now consider the results for rare decays. Since in the LRM we did not explicitly consider rare decays (except $B \to X_s\gamma$), we can only use our estimates from section 6.4.2 indicating a rough pattern of NP effects for rare decays according to $B_d < B_s \ll K$. Interestingly this pattern matches with the pattern obtained in the RSc: effects in in rare K decays are generally bigger than effects in B physics. We hope to study the detailed phenomenology of rare decays for the LRM in a separate publication.

Finally let us take a look at the decay $B \to X_s\gamma$. Generally the contributions in both models are of very different nature. While in the LRM the m_b suppression can be overcome by a chirality flip inside the loop, in the RSc the primed operators, dominantly $C'_{7\gamma}$, play an important role [1,214,223]. In both cases however the value for the branching ratio can be enhanced with respect to the SM value and brought into better agreement with the experiment.

Since the well-measured $\Delta F = 2$ observables mainly act as model constraints, from the point of view of flavour physics, only a study of rare decays their correlations will help to distinguish these two models. In this respect, direct collider searches can provide valuable information.

8. Summary and conclusion

The true nature of physics beyond the SM is one of the fundamental questions of contemporary particle physics. In order to test the viability of a specific model, one has to carefully take into account all experimental data, among which flavour observables play an important role. On one hand anomalies and tensions in flavour observables of the SM give us hints where NP can enter. On the other hand the constrained pattern of flavour observables as well as the identification of specific correlations make them an important tool to probe NP at the intensity frontier, complementary to direct collider searches at the energy frontier. Further, exploring TeV scale physics through direct collider searches is experimentally a highly complex undertaking. Due to the large amount of data, one needs a clue from theory where to look for NP. In contrast, the measurement of flavour observables does not depend on certain model assumptions but its results can be interpreted in the context of a specific model.

In the present thesis, we have addressed the question whether RH currents can provide a realistic NP framework in terms of a comprehensive analysis of flavour observables. In this analysis emphasis was put on the well-measured FCNC observables of the $\Delta F = 2$ sector related to the particle-antiparticle mixings $K^0 - \bar{K}^0$ and $B_{d,s}^0 - \bar{B}_{d,s}^0$, but various rare decays were also considered.

We have analysed two complementary models for RH currents taking a bottom-up and a top-down approach. These two approaches also differ in their inherent operator structure and their specific flavour protection mechanism. This implies that these two models cannot be matched by integrating out heavy particles in the explicit approach. Yet, both models have an underlying $SU(2)_L \times SU(2)_R \times U(1)_{B-L}$ electroweak symmetry structure in common, global in the bottom-up approach and local in the top-down approach, leading to RH currents. In both cases the flavour mixing of the RH sector is controlled by a new RH mixing matrix. A further key feature of such models with RH currents is that new left-right operators appear having significant impact on $\Delta F = 2$ observables. In more detail, in the RHMFV and in the LRM the operators Q_1^{LR} and Q_2^{LR} dominate respectively. Both operators are known to be strongly enhanced due to renormalisation group evolution to low energy scales and in the $K^0 - \bar{K}^0$ system the additional chiral enhancement of the hadronic matrix element has to be taken into account. Thus models with RH currents are automatically highly constrained by FCNC observables, especially by the precisely measured CP-violating parameter ε_K.

We first introduced the effective field theory approach of Right-Handed Minimal Flavour Violation. A central ingredient in this model is a left-right symmetric flavour group bro-

ken only by the Yukawa couplings, leading to an extended MFV principle. This specific flavour protection mechanism distinguishes our analysis from previous considerations of RH currents within the effective field theory framework. We have shown that in this model the RH mixing matrix can be determined by charged current data, theoretical bounds such as the unitarity constraint and phenomenological bounds such as the pattern of $\Delta F = 2$ observables. The determination of the full RH mixing matrix is a novel feature in contrast to previous considerations [45, 46] which mainly concentrated on the elements $|V_{ub}|$ and $|V_{cb}|$. The explicit form of this matrix and responsible factors for $\Delta F = 2$ observables are summarised in the schematic formula of equation (5.10) and in table 5.1 respectively. The new RH interactions are encoded in the effective theory by means of dimension six operators in accordance with the symmetry principles. This allows us to determine NP effects without specifying the fundamental theory but only with information about global symmetry and the pattern of its breakdown.

Our findings for the most important phenomenological implications of this model are as follows:

1. In this model the $|V_{ub}|$ problem can be solved, providing an explanation of the different values of $|V_{ub}|$ from measurements of inclusive and exclusive semi-leptonic decays. The inclusive value is favoured in this case, giving the "true" value for $|V_{ub}|$.

2. The ε_K anomaly can be understood since the increased "true" value for $|V_{ub}|$ goes in hand with an enhancement of $\sin 2\beta$. Thus experimental and theoretical values for ε_K can be automatically brought into better agreement, as opposed to the SM where inclusive and exclusive determinations are averaged, leading to a lower value of $\sin 2\beta$. New CP violating phases can still be present, since theoretical errors allow an extra contribution of $\sim \pm 10\%$ to ε_K, however they are not necessary.

3. A non-standard CP-violating phase in B_s mixing allows for a large $S_{\psi\phi}$, driving in conjunction with the ε_K constraint the effects in the B_d sector to be negligible.

4. Thus, the indicated small NP phase in the B_d sector and the large $\sin 2\beta$ imply that the $S_{\psi K_S}^{\mathrm{exp}} - \sin 2\beta$ tension becomes strengthened, unless $S_{\psi\phi}$ is SM-like, as we discuss below.

5. The desire for a large $S_{\psi\phi}$ implies small effects in rare B_d decays while contributions to rare B_s decays still can be sizable. As an explicit example, we have considered the decays $B_{d,s} \to \mu^+\mu^-$. The decay $B_d \to \mu^+\mu^-$ only obtains negligible corrections compared to the SM, while the branching ratio of $B_s \to \mu^+\mu^-$ maximally is enhanced by an additional factor of 5. Consequently, the strict correlation from MFV is violated in this framework. In particular, the study of the decay $B_s \to \mu^+\mu^-$ is interesting since it can be potentially measured within this year at the LHC.

6. We have also shown that there exists a well-defined pattern of correlations in various other decays. We have explicitly shown the correlations for $\mathrm{Br}(B \to K\nu\bar{\nu})$ and $\mathrm{Br}(B \to K^*\nu\bar{\nu})$ and for $\mathrm{Br}(K^+ \to \pi^+\nu\bar{\nu})$ and $\mathrm{Br}(K_L \to \pi^0\nu\bar{\nu})$. Significant deviations from the SM branching ratios are possible.

7. Finally, the anomalous RH $Zb\bar{b}$ coupling cannot be explained in RHMFV, precluded by the constraints from $B_{d,s} \to \mu^+\mu^-$.

In summary, not all tensions could be resolved within RHMFV. However, these tensions are within the uncertainties in measured and theoretical quantities. In our analysis we have assumed a large $S_{\psi\phi}$, motivated by the Tevatron results. Recent experimental developments now point towards a smaller or even negative value, but the statistics have to be improved in order to obtain a reliable and final answer. Still a large value $S_{\psi\phi} \sim 0.4$ is not excluded. A SM-like $S_{\psi\phi}$ would allow for larger effects in B_d mixing and potentially cure the $\sin 2\beta$ and $S_{\psi K_S}^{\mathrm{exp}}$ tension. In our effective theory approach, the assumption of a large $S_{\psi\phi}$ was implemented by hand. This helps to make certain simplifying approximations, which have significant impact on the phenomenology. Therefore, relaxing the assumption of a large $S_{\psi\phi}$ would require a completely renewed analysis, which is beyond the scope of this thesis. In this sense, our effective theory is limited. However, the effective theory approach makes it possible to explore regions of NP and estimate the magnitude of the NP effects without specifying the fundamental theory. Furthermore the systematic expansion can help to identify easily the leading operators and lend a transparent view on how they are bounded by various processes. This is in particular useful in $\Delta F = 2$ processes due to a small number of operators. In $\Delta F = 1$ processes the set of contributing operators is much larger.

The second model considered in this thesis is the Left-Right Asymmetric Model. We have adopted a very general framework allowing for a splitting in the left and right gauge couplings. Furthermore, the RH mixing matrix is incorporated in its most general parametrisation without further simplifying assumptions. Due to the enlarged gauge symmetry new particles appear in the gauge and in the Higgs sector, contributing to FCNC processes. In the $\Delta F = 2$ sector we concentrate on the following observables: the mass differences ΔM_K, ΔM_s and ΔM_d, the CP-violating parameter ε_K, the mixing induced CP asymmetries $S_{\psi K_S}$ and $S_{\psi\phi}$, the semileptonic asymmetry A_{SL}^q and the width difference $\Delta\Gamma_q$. These observables obtain new contributions, which arise through box diagrams due to W_R gauge boson and charged Higgs exchanges but dominantly through tree-level exchanges from heavy neutral Higgs bosons. We have also considered the decay $B \to X_s\gamma$, where NP contributions appear due to the $W_L - W_R$ mixing and dominantly through charged Higgs exchanges.

In view of many existing studies of LR models it is important to summarise once more the novelties of the present analysis.

- We kept the theoretical framework as general as possible.

- We have explicitly elaborated the importance of the contributions of heavy Higgs fields to flavour observables. On the contrary, many studies neglect the Higgs effects, citing the large mass of the heavy Higgs fields. Figures 6.3 and 6.4 summarise the importance of the neutral and charged Higgs fields for $\Delta F = 2$ observables and the decay $B \to X_s \gamma$ respectively.

- Our analysis includes an improved treatment of QCD corrections.

- We present an extensive set of Feynman rules, collected in appendix F.

- The central aspect of our consideration is a simultaneous analysis of the most interesting $\Delta F = 2$ observables and $B \to X_s \gamma$, while taking into account all relevant constraints such as from tree-level decays, electroweak precision tests and direct experimental bounds. We also require the mass W_R boson to be of the order $2 - 3$ TeV and hence accessible at the LHC. Since many previous studies concentrate on lower bounds for the masses of heavy new fields, such a comprehensive analysis is new.

In the following we summarise the main results of our phenomenological study

1. We determined phenomenologically viable structures of the RH mixing matrix. Our result is explicitly given in figure 6.5, showing allowed regions in parameter space in terms of $|V_{us}^{\mathrm{R}}|$, $|V_{ub}^{\mathrm{R}}|$ and $|V_{cb}^{\mathrm{R}}|$. We could identify two scenarios which satisfy all constraints including the dangerous ε_K-constraint without imposing a large fine-tuning of parameters.

2. We have shown that NP effects are expected to be the largest in the K system followed by effects in the B_s system. Smaller effects can be found in the B_d system. This pattern of hierarchy is compactly summarised in figure 6.7. This plot also allows us to predict a similar hierarchical pattern for rare decays within the corresponding meson systems.

3. We have explicitly considered the decay $B \to X_s \gamma$, which has a special role due to its precise measurement providing a strong constraint for any NP model. The LRM allows an enhancement of its branching ratio bringing theoretical and experimental values in better agreement compared to the SM value.

4. We studied the possibility of correlations between observables. In view of many free parameters only model-independent correlations exist such as the correlation of A_{SL}^s and $S_{\psi\phi}$, shown in figure 6.8. As can be seen the observable $S_{\psi\phi}$ can vary in the full range.

5. The anomalous RH $Zb\bar{b}$ coupling cannot be explained in the LRM.

6. Surprisingly, the $|V_{ub}|$ problem, being one of the main motivations for our considerations of RH currents, cannot be solved. This is mainly due to the increased bound on the mass of the W_R boson as indicated by LHC in conjunction with constraints from FCNC and EWP observables.

7. We also have investigated the question of a soft lower limit for the heavy Higgs mass. Interestingly, as shown in figure 6.11, a value as low as $M_H \sim 2.4\,\text{TeV}$ is in accordance with all constraints imposed by us.

8. We have presented a simplified parametrisation of the RH mixing matrix depending on only four free parameters, given in equation (6.58). While in the general parametrisation flavour anomalies could be solved due to many parameters, the proposed parametrisation still allows to remove all SM tensions between flavour observables demonstrated in the scenario of a small $|V_{ub}|$. This specific choice of $|V_{ub}|$ is justified since without a solution of the $|V_{ub}|$ problem any measured value, both inclusive or exclusive, is equally likely.

We have then compared both models considered in this thesis directly. Experimentally both models can be distinguished by the structure of the RH mixing matrix once more precise flavour data is available. A detailed study of rare decays and related correlations within the LRM is expected to improve such a distinction. However such an analysis is beyond the scope of this thesis and is left for future work. We have further compared RHMFV to another effective field theory approach: the two Higgs doublet model with MFV and flavour blind phases. The two models can be explicitly distinguished via the correlation of the decays $B_{d,s} \to \mu^+\mu^-$. The situation is less obvious when comparing the flavour phenomenology of the LRM to the Randall Sundrum model with custodial protection. The consideration of $\Delta F = 2$ observables and the decay $B \to X_s\gamma$ is not sufficient for a unique distinction between the models and a study of rare decays would be needed.

We are now able to answer the questions formulated in the introduction of this thesis:

- *Do RH currents provide a realistic extension of the SM?*
  Yes, with respect to the current available data RH currents provide a realistic NP framework.

- *Do they solve the existing tensions between flavour observables in the SM while satisfying all the existing bounds? In particular, can the new CP-violating phases cure the existing SM anomalies in CP-violating observables? And, can the $|V_{ub}|$ problem be solved?*
  In RHMFV the $S_{\psi K_S}^{\text{exp}}$ – $\sin 2\beta$ tension remains due to a negligible non-standard CP-violating phase in the B_d sector. However, in view of experimental and theoretical errors one cannot exclude the model by this argument. Other tensions in the flavour sector can be resolved in this model. In particular, the ε_K problem and the $|V_{ub}|$ problem are solved automatically. Furthermore a large $S_{\psi\phi}$ can also be incorporated. On the other hand, a small $S_{\psi\phi}$ is expected to improve the $S_{\psi K_S}^{\text{exp}}$ – $\sin 2\beta$ tension. In the LRM all flavour anomalies can be solved even with a reduced parametrisation of the RH mixing matrix. The only exception is the V_{ub} problem, which cannot be solved within this framework.

- *Can the new RH effects reach present experimental bounds?*
  In order to confirm the models considered within this thesis, and distinguish them from other NP models, more precise flavour data or explicit collider signals for the corresponding new heavy particles are required. New insights for both possibilities are expected in the current generation of LHC experiments. In the flavour sector a more precise measurement of the observable $S_{\psi\phi}$ would be helpful to probe both models considered here. In RHMFV a precise measurement of the decay $B_{d,s} \to \mu^+\mu^-$ would be particularly helpful. In the LRM a study of rare decays is needed in order to obtain sufficient information to distinguish the model clearly from other NP frameworks. From the estimates of the flavour effects in different meson sectors we expect the decays $K \to \pi\nu\bar{\nu}$ to be promising.

- *How far do the two approaches we follow overlap? Does the same RH mixing structure appear in both models?*
  The two models considered in this thesis are complementary in their operator structure and differ in the flavour protection mechanism. This difference is displayed explicitly in the structure of the RH mixing matrices.

- *What is the structure of the RH mixing matrix?*
  The specific flavour structures of the RH mixing matrix is given in RHMFV by the schematic formula of equation (5.10) and in the LRM summarised in figure 6.5.

Our analysis of RH currents was motivated by current flavour data. Already existing data puts strong constraints on the two NP scenarios of RH currents considered here. Yet, more precise data and the study of rare decays is required in order to decide whether RH currents exist in nature. The LHC can shed light on this question by not only providing data for important CP violating observables such as $S_{\psi\phi}$ but also probing the existence of the heavy gauge bosons W' and Z'.

Acknowledgements

I would like to thank Prof. Andrzej Buras for the great opportunity to be part of this active and excellent research group. You provided valuable guidance throughout my entire PhD. We had a great collaboration, not to mention the countless interesting discussions about research and classical music over coffee. Thank you for always being supportive, both as a PhD advisor and also as a personal mentor. I am grateful for the chance to talk at many conferences and workshops all over the world. Special thanks for sending me to TASI and helping me to keep contacts in the US - without your support this would not have been possible.

I would like to express my sincere thanks to Prof. Gino Isidori for very fruitful collaboration. I have learnt a lot from you, especially about the effective field theory approach. I would also like to thank you for your support for my academic career in many ways.

I warmly want to thank Dr. Monika Blanke who has been a great collaborator in many successful projects and has accompanied me from my first steps in particle physics. I found a close friend in you when I came to Munich, and you have been very helpful to me in both professional and personal matters. Many thanks for reading this thesis and giving useful comments on it.

I also want to thank Tillmann Heidsieck for the collaboration in the LRM project. Your wide-ranging computer knowledge has been useful for the project. In particular I want to thank you for the time you took to help me when my laptop crashed.

I am grateful for the help and support which I received by all, current and former, members of T31 group at the TUM. Thanks to Dr. Michaela Albrecht, Dr. Björn Duling and Dr. Stefania Gori for the collaboration in the Randall Sundrum project. Many thanks to Dr. Stefan Recksiegel for his technical support, which saved me many days of worries throughout my PhD. Furthermore I want to acknowledge the useful discussions with all my colleagues, in particular, Dr. Wolfgang Altmannshofer, Maria Valentina Carlucci, Dr. Jennifer Girrbach, Dr. Paride Paradisi and Dr. Christoph Promberger. Thank you also to Emmanuel Stamou, who provided table 6.1 within this thesis. Thanks also to our secretary Elke Krüger for always being helpful.

Furthermore I want to thank the people from TASI for an outstanding summer school and a great time at the foot of the Rocky Mountains.

Thank you to Dr. Steffen Rath for filling the coffee breaks with discussions about arts.

Appendix

A. The Higgs sector of the LRM

In the LRM the full Higgs Lagrangian is given by

$$
\mathcal{L}_{\text{Higgs}} = \text{Tr}[(D_\mu \Delta_L)^\dagger (D^\mu \Delta_L)] + \text{Tr}[(D_\mu \Delta_R)^\dagger (D^\mu \Delta_R)] + \text{Tr}[(D_\mu \phi)^\dagger (D^\mu \phi)] \\
+ V(\phi, \Delta_L, \Delta_R) \,,
\tag{A.1}
$$

where the covariant derivatives are given by

$$
\begin{aligned}
D_\mu \phi &= \partial_\mu \phi + i g_L (\overrightarrow{W}_{L\mu} \cdot \vec{\tau}) \phi - i g_R \phi (\overrightarrow{W}_{R\mu} \cdot \vec{\tau}) \,, \\
D_\mu \Delta_{(L,R)} &= \partial_\mu \Delta_{(L,R)} + i g_{(L,R)} \left[\overrightarrow{W}_{(L,R)\mu} \cdot \vec{\tau}, \ \Delta_{(L,R)} \right] + i g' B_\mu \Delta_{(L,R)} \,.
\end{aligned}
\tag{A.2}
$$

The Higgs potential in its left-right symmetric form can be written as [36, 101, 224, 225]

$$
\begin{aligned}
V(\phi, \Delta_L, \Delta_R) = &-\mu_1^2 \text{Tr}(\phi^\dagger \phi) - \mu_2^2 \left[\text{Tr}(\tilde{\phi}\phi^\dagger) + \text{Tr}(\tilde{\phi}^\dagger \phi) \right] - \mu_3^2 \left[\text{Tr}(\Delta_L \Delta_L^\dagger) + \text{Tr}(\Delta_R \Delta_R^\dagger) \right] \\
&+ \lambda_1 \left[\text{Tr}(\phi^\dagger \phi) \right]^2 + \lambda_2 \left\{ \left[\text{Tr}(\tilde{\phi}\phi^\dagger) \right]^2 + \left[\text{Tr}(\tilde{\phi}^\dagger \phi) \right]^2 \right\} + \lambda_3 \text{Tr}(\tilde{\phi}\phi^\dagger) \text{Tr}(\tilde{\phi}^\dagger \phi) \\
&+ \lambda_4 \text{Tr}(\phi^\dagger \phi) \left[\text{Tr}(\tilde{\phi}\phi^\dagger) + \text{Tr}(\tilde{\phi}^\dagger \phi) \right] \\
&+ \rho_1 \left\{ \left[\text{Tr}(\Delta_L \Delta_L^\dagger) \right]^2 + \left[\text{Tr}(\Delta_R \Delta_R^\dagger) \right]^2 \right\} \\
&+ \rho_2 \left[\text{Tr}(\Delta_L \Delta_L) \text{Tr}(\Delta_L^\dagger \Delta_L^\dagger) + \text{Tr}(\Delta_R \Delta_R) \text{Tr}(\Delta_R^\dagger \Delta_R^\dagger) \right] \\
&+ \rho_3 \text{Tr}(\Delta_L \Delta_L^\dagger) \text{Tr}(\Delta_R \Delta_R^\dagger) \\
&+ \rho_4 \left[\text{Tr}(\Delta_L \Delta_L) \text{Tr}(\Delta_R^\dagger \Delta_R^\dagger) + \text{Tr}(\Delta_L^\dagger \Delta_L^\dagger) \text{Tr}(\Delta_R \Delta_R) \right] \\
&+ \alpha_1 \text{Tr}(\phi^\dagger \phi) \left[\text{Tr}(\Delta_L \Delta_L^\dagger) + \text{Tr}(\Delta_R \Delta_R^\dagger) \right] \\
&+ \left\{ \alpha_2 e^{i\delta_2} \left[\text{Tr}(\tilde{\phi}\phi^\dagger) \text{Tr}(\Delta_L \Delta_L^\dagger) + \text{Tr}(\tilde{\phi}^\dagger \phi) \text{Tr}(\Delta_R \Delta_R^\dagger) \right] + \text{h.c.} \right\} \\
&+ \alpha_3 \left[\text{Tr}(\phi \phi^\dagger \Delta_L \Delta_L^\dagger) + \text{Tr}(\phi^\dagger \phi \Delta_R \Delta_R^\dagger) \right] \\
&+ \beta_1 \left[\text{Tr}(\phi \Delta_R \phi^\dagger \Delta_L^\dagger) + \text{Tr}(\phi^\dagger \Delta_L \phi \Delta_R^\dagger) \right] \\
&+ \beta_2 \left[\text{Tr}(\tilde{\phi} \Delta_R \phi^\dagger \Delta_L^\dagger) + \text{Tr}(\tilde{\phi}^\dagger \Delta_L \phi \Delta_R^\dagger) \right] \\
&+ \beta_3 \left[\text{Tr}(\phi \Delta_R \tilde{\phi}^\dagger \Delta_L^\dagger) + \text{Tr}(\phi^\dagger \Delta_L \tilde{\phi} \Delta_R^\dagger) \right] \,.
\end{aligned}
\tag{A.3}
$$

A total of 18 parameters are involved, where we have only one phase δ_2 and real coupling parameters otherwise. It is sufficient to consider the left-right symmetric version of the potential without generalisation since flavour physics is independent of details of the Higgs sector, as we will demonstrate below.

We now show that only the parameter α_3 is important for our flavour analysis, entering in the mass of neutral and charged Higgses. To this end we have to diagonalise the Higgs potential (A.3). We start with the neutral Higgs states, which form an 8×8 mass matrix. This matrix can be systematically diagonalised by making use of perturbation theory. Instead of following the assumption $\kappa' \ll \kappa$ by the authors of [36], we keep our analysis more general and allow for an arbitrary parameter s. This is preferred from the phenomenological point of view, in particular by the analysis of EWP observables as indicated in section 3.4.4.

Out of six neutral Higgs fields we are only interested in the flavour-changing neutral Higgs fields H_1^0 and H_2^0. We obtain the following mass eigenstates

$$H_1^0 = \sqrt{2}\left(-s\,\mathrm{Re}\,\phi_1^0 + c\,\mathrm{Re}(e^{-i\alpha}\phi_2^0)\right), \tag{A.4}$$

$$H_2^0 = \sqrt{2}\left(s\,\mathrm{Im}\,\phi_1^0 + c\,\mathrm{Im}(e^{-i\alpha}\phi_2^0)\right), \tag{A.5}$$

with identical masses at leading order

$$M_{H_1^0} = M_{H_2^0} = \sqrt{\frac{\alpha_3}{1-2s^2}}\,\kappa_R = \left(\alpha_3\sqrt{u(s)}\right)^{\frac{1}{2}}\kappa_R \equiv M_H\,. \tag{A.6}$$

The lightest Higgs field h_0, given by

$$h^0 = \sqrt{2}\left(c\,\mathrm{Re}\,\phi_1^0 + s\,\mathrm{Re}(e^{-i\alpha}\phi_2^0)\right), \tag{A.7}$$

can be identified as the SM Higgs with a mass of $\mathcal{O}(v)$.

The knowledge of Higgs mass eigenstates allows us to deduce leading order couplings of the heavy flavour violating Higgses H_1^0 and H_2^0. We realise that flavour dynamics is not sensitive to the detailed structure of the potential, therefore leading order couplings do not depend on further parameters of the Higgs potential. Consequently, it is justified to assume the parity symmetric case for the potential with fewer parameters than the general potential. We want to also mention that the SM Higgs couplings are now flavour violating. However this occurs at higher order so the effects are expected to be negligible.

Similarly one can proceed with the charged Higgs fields, whose effects are subleading in $\Delta F = 2$ processes as they take place at the one loop order [102], but can still be important for $B \to X_q\gamma$ decays [193, 194, 196–198, 200]. Again only leading order terms in couplings and masses are important. Finding the eigenvalues of the 4×4 matrix mass matrix of single charged fields yields the relevant masses and mass eigenstates of

the two charged Higgs fields. Couplings to fermions can be deduced from the Yukawa interaction. Only one of these fields couples to quarks in leading order, which we denote by H^+, in particular given by

$$H^{\pm} = se^{\pm i\alpha}\phi_1^{\pm} + c\phi_2^{\pm}\,. \tag{A.8}$$

The leading order mass of this field is identical to the one of the flavour changing neutral Higgses, hence

$$M_{H^+} = M_H\,. \tag{A.9}$$

Thus this mass cannot be chosen be light as assumed in some literature.

All our findings agree with results of [36] in the limit of $s \ll 1$ as implied by their assumption of the hierarchy $\kappa' \ll \kappa$. Earlier studies can be found in [224, 225].

B. Goldstone bosons of the LRM

In this appendix we collect all Goldstone boson fields in the LRM, obtained by the method used by [226]. This procedure allows us to determine the physical Higgs states up to linear combinations. In order to obtain the full mass eigenstates one has to diagonalise the Higgs potential. In contrast, Goldstone bosons can be fully determined by this method.

The Goldstone bosons of $W^{\pm}$ and $W'^{\pm}$ are then given by

$$G^{\pm} = \pm i\left[c\left(1 - s^4\epsilon^2\right)\phi_1^{\pm} - se^{\mp i\alpha}\left(1 - c^4\epsilon^2\right)\phi_2^{\pm} - \sqrt{2}cse^{\mp i\alpha}\epsilon\delta_R^{\pm}\right]\,, \tag{B.10}$$

$$G'^{\pm} = \mp i\left[\left(1 - \frac{\epsilon^2}{4}\right)\delta_R^{\pm} + \frac{se^{\pm i\alpha}}{\sqrt{2}}\epsilon\phi_1^{\pm} - \frac{c}{\sqrt{2}}\epsilon\phi_2^{\pm}\right]\,. \tag{B.11}$$

For the neutral Goldstone boson of Z and Z' we obtain

$$G^0 = \sqrt{2}\left(1 - \frac{c_R^4}{8}\epsilon^2\right)\pi^0 - \frac{c_R^2}{\sqrt{2}}\epsilon\,\mathrm{Im}\,\delta_R^0\,, \tag{B.12}$$

$$G'^0 = -\sqrt{2}\left(1 - \frac{c_R^4}{8}\epsilon^2\right)\mathrm{Im}\,\delta_R^0 - \frac{c_R^2}{\sqrt{2}}\epsilon\pi^0\,, \tag{B.13}$$

where we have defined $\pi^0 = c\,\mathrm{Im}\,\phi_1^0 - s\,\mathrm{Im}(e^{-i\alpha}\phi_2^0)$.

C. Gauge bosons in the LRM

In this appendix we consider gauge boson mass matrices, which can be deduced from the relevant terms of the kinetic Higgs Lagrangian in equation (A.1) using the covariant derivatives in equation (A.2). The two step breaking goes in hand with a two step

rotation of neutral gauge boson fields analogous to our approach in [19], where it is useful to define the following mixing angles

$$s_R = \frac{g'}{\sqrt{g'^2 + g_R^2}}, \quad c_R = \sqrt{1 - s_R^2}, \quad s_W = \frac{s_R}{\sqrt{(g_L/g_R)^2 + s_R^2}}, \quad c_W = \sqrt{1 - s_W^2}. \tag{C.14}$$

Diagonalising in the next step both neutral and charged mass matrices yields the corresponding mass eigenstates and masses. For charged gauge bosons we obtain as mass eigenstates

$$W^{\pm} = W_L^{\pm} + sce^{\mp i\alpha}\frac{s_R c_W}{s_W}\epsilon^2 W_R^{\pm}, \tag{C.15}$$

$$W'^{\pm} = W_R^{\pm} - sce^{\pm i\alpha}\frac{s_R c_W}{s_W}\epsilon^2 W_L^{\pm}, \tag{C.16}$$

and masses

$$(M_W)^2 = \frac{e^2 v^2}{2s_W^2}\left(1 - 2s^2 c^2 \epsilon^2\right), \tag{C.17}$$

$$(M_{W_R})^2 = \frac{e^2 \kappa_R^2}{c_W^2 s_R^2}\left(1 + \frac{1}{2}\epsilon^2\right). \tag{C.18}$$

In the neutral sector, both mass eigenstates

$$A = s_W W_L^3 + s_R c_W W_R^3 + c_R c_W B, \tag{C.19}$$

$$Z = c_W W_L^3 - s_R s_W \left(1 - \frac{c_R^4}{4s_W^2}\epsilon^2\right) W_R^3$$

$$\quad - c_R s_W \left(1 + \frac{s_R^2 c_R^2}{4s_W^2}\epsilon^2\right) B \tag{C.20}$$

$$Z' = -\frac{s_R c_R^3 c_W}{4s_W}\epsilon^2 W_L^3 + c_R \left(1 + \frac{s_R^2 c_R^2}{4}\epsilon^2\right) W_R^3$$

$$\quad - s_R \left(1 - \frac{c_R^4}{4}\epsilon^2\right) B, \tag{C.21}$$

and masses

$$(M_A)^2 = 0, \tag{C.22}$$

$$(M_Z)^2 = \frac{e^2 v^2}{2s_W^2 c_W^2}\left(1 - \frac{c_R^4}{4}\epsilon^2\right), \tag{C.23}$$

$$(M_{Z'})^2 = \frac{2e^2 \kappa_R^2}{s_R^2 c_R^2 c_W^2}\left(1 + \frac{c_R^4}{4}\epsilon^2\right). \tag{C.24}$$

are easy to verify.

D. Parameter counting in the LRM

We want to proceed with a brief counting of the relevant parameters for our analysis in the LRM.

In the gauge sector, we have the parameters from the strong coupling g_s and the electroweak gauge couplings

$$g_L, \quad g_R, \quad g', \tag{D.25}$$

providing one additional parameter with respect to the SM.

At the first sight, many new parameters seem to emerge from the Higgs sector. However as we show in appendix A, of the 18 parameters of the potential, only one (to be more precise α_3) is relevant here, parametrising the masses of neutral flavour changing Higgses H_1^0 and H_2^0 and the charged Higgs H^+.

Furthermore we have to count the parameters from VEVs with corresponding phases. Also here it turns out that in practice none of the phases defined in section 3.2.2 have an impact on flavour physics. This is easy to verify: the phase factor $e^{i\alpha}$ always appears in combination with the RH mixing matrix V^R. Since V^R is unitary and every element of V^R carries phases, the phase α can be eliminated by a redefinition of phases in V^R. Additionally another argument holds for flavour observables: the phase α cancels out in all expressions for FCNC processes. We also set $\kappa_L = 0$ and hence neglect the corresponding phase. Finally the remaining parameters from VEVs read

$$v = \sqrt{\kappa^2 + \kappa'^2}, \quad s = \kappa'/v, \quad \kappa_R, \tag{D.26}$$

where apart from the SM VEV v two additional parameters can be counted.

Finally, most new parameters stem from the Yukawa couplings. In general the Yukawas y_{ij} and $\tilde{y}_{ij}$ are arbitrary complex matrices with 9 real parameters and 9 phases each. In complete analogy to the RH matrix in RHMFV we can adopt the $SU(3)_L \times SU(3)_R$ flavour symmetry and remove unphysical phases. The outcome in terms of remaining parameters are six quark masses, four parameters from the CKM matrix V^L (three angles and one phase) and the RH mixing matrix V^R adding 3 real mixing angles and 6 complex phases.

In total the LRM contains 13 more parameters relative to the SM, out of which 9 describe V^R. Finally in section 6.5 we introduce a simplified parametrisation with only four parameters.

E. SM loop functions

The $\Delta F = 2$ loop function for VLL operators, as given in section 6.1.2, simplifies to the known SM form as follows

$$S_0(x_t) \equiv S_{LL}(x_t, x_t) = \frac{4x_t - 11x_t^2 + x_t^3}{4(1 - x_t)^2} - \frac{3x_t^3 \ln x_t}{2(1 - x_t)^3} , \qquad \text{(E.27)}$$

$$S_0(x_c) \equiv S_{LL}(x_c, x_c) \approx x_c , \qquad \text{(E.28)}$$

$$S_0(x_c, x_t) \equiv S_{LL}(x_t, x_c) \approx x_c \left[\ln \frac{x_t}{x_c} - \frac{3x_t}{4(1 - x_t)} - \frac{3x_t^2 \ln x_t}{4(1 - x_t)^2} \right] . \qquad \text{(E.29)}$$

The last two formulae only contain linear terms in $x_c \ll 1$, since higher orders can be safely neglected.

F. Feynman rules of the LRM

Finally we want to present a collection of Feynman rules for the LRM. We give couplings up to $\mathcal{O}(\epsilon^2)$ corrections except in the Higgs sector where for our purposes $\mathcal{O}(1)$ couplings are sufficient. All couplings are given in mass eigenstates. Note that we stick to the "correct" notation of W and W', as introduced in appendix C.

Triple gauge couplings, as given in table F.6, exhibit a specific Dirac structure. In order keep the table concise, we have only collected coefficients $\mathcal{C}$ of the respective couplings, being defined by
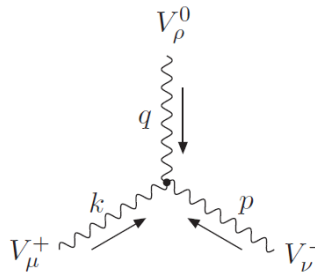
$$\mathcal{C} \left[\eta_{\mu\nu}(k - p)_\rho + \eta_{\nu\rho}(p - q)_\mu + \eta_{\rho\mu}(q - k)_\nu \right] ,$$

Note that $V_\mu^+ = W_\mu^+, W_\mu'^+$, $V_\nu^- = W_\nu^-, W_\nu'^-$, $V_\rho^0 = A_\rho, Z_\rho, , Z_\rho'$, and k, p, q are their incoming momenta.

	A_μ	G_μ^a
$\bar{u}_L^i u_L^i X_\mu$	$-i\frac{2}{3}e\gamma^\mu$	$-ig_s\gamma^\mu t^a$
$\bar{u}_R^i u_R^i X_\mu$	$-i\frac{2}{3}e\gamma^\mu$	$-ig_s\gamma^\mu t^a$
$\bar{d}_L^i d_L^i X_\mu$	$-i(-\frac{1}{3})e\gamma^\mu$	$-ig_s\gamma^\mu t^a$
$\bar{d}_R^i d_R^i X_\mu$	$-i(-\frac{1}{3})e\gamma^\mu$	$-ig_s\gamma^\mu t^a$

Table F.1.: Fermion couplings to the massless gauge bosons X_μ, i.e. the photon A_μ and the gluons G_μ^A.

	W^+	W'^+
$\bar{u}_L^i d_L^j X_\mu^+$	$-\frac{ie}{\sqrt{2}s_W}V_{ij}^L\gamma^\mu$	$+\frac{iecse^{-i\alpha}s_R c_W}{\sqrt{2}s_W^2}\epsilon^2 V_{ij}^L\gamma^\mu$
$\bar{u}_R^i d_R^j X_\mu^+$	$-\frac{iecse^{i\alpha}}{\sqrt{2}s_W}\epsilon^2 V_{ij}^R\gamma^\mu$	$-\frac{ie}{\sqrt{2}s_R c_W}V_{ij}^R\gamma^\mu$

Table F.2.: Fermion couplings to charged gauge bosons W^+ and W'^+.

	Z	Z'
$\bar{u}_L^i u_L^i X_\mu$	$-\frac{ie}{s_W c_W}(\frac{1}{2}-\frac{2}{3}s_W^2-\frac{1}{24}s_R^2 c_R^2\epsilon^2)\gamma^\mu$	$ie\,(\frac{1}{6}\frac{s_R}{c_R c_W}+\frac{1}{8}(\frac{c_W c_R^3 s_R}{s_W^2}-\frac{c_R^3 s_R}{3c_W})\epsilon^2)\gamma^\mu$
$\bar{d}_L^i d_L^i X_\mu$	$-\frac{ie}{s_W c_W}(-\frac{1}{2}+\frac{1}{3}s_W^2-\frac{1}{24}s_R^2 c_R^2\epsilon^2)\gamma^\mu$	$ie\,(\frac{1}{6}\frac{s_R}{c_R c_W}-\frac{1}{8}(\frac{c_W c_R^3 s_R}{s_W^2}+\frac{c_R^3 s_R}{3c_W})\epsilon^2)\gamma^\mu$
$\bar{u}_R^i u_R^i X_\mu$	$-\frac{ie}{s_W c_W}(-\frac{2}{3}s_W^2+\frac{c_R^2}{8}(c_R^2-\frac{1}{3}s_R^2)\epsilon^2)\gamma^\mu$	$-\frac{ie}{c_W s_R c_R}(\frac{1}{2}-\frac{2}{3}s_R^2+\frac{c_R^4 s_R^2}{6}\epsilon^2)\gamma^\mu$
$\bar{d}_R^i d_R^i X_\mu$	$-\frac{ie}{s_W c_W}(\frac{1}{3}s_W^2-\frac{c_R^2}{8}(c_R^2+\frac{1}{3}s_R^2)\epsilon^2)\gamma^\mu$	$-\frac{ie}{c_W s_R c_R}(-\frac{1}{2}+\frac{1}{3}s_R^2-\frac{c_R^4 s_R^2}{12}\epsilon^2)\gamma^\mu$

Table F.3.: Fermion couplings to neutral gauge bosons Z and Z'.

	G^+	G'^+
$\bar{u}_L^i d_R^j X^+$	$\frac{e}{\sqrt{2}M_W s_W}\left(m_d^j V_{ij}^L - cse^{i\alpha}m_u^i\epsilon^2 V_{ij}^R\right)$	$-\frac{em_u^i}{\sqrt{2}c_W s_R M_{W_R}}V_{ij}^R$
$\bar{u}_R^i d_L^j X^+$	$-\frac{e}{\sqrt{2}M_W s_W}\left(m_u^i V_{ij}^L - cse^{i\alpha}m_d^j\epsilon^2 V_{ij}^R\right)$	$\frac{em_d^j}{\sqrt{2}c_W s_R M_{W_R}}V_{ij}^R$

Table F.4.: Fermion couplings to charged Goldstone bosons.

	G^0	G'^0
$\bar{u}_L^i u_R^i X^0$	$\frac{em_u^i}{2c_W s_W M_Z}\left(1 - \frac{c_R^4}{4}\epsilon^2\right)$	$-\frac{ec_R m_u^i}{2s_R c_W M_{Z'}}$
$\bar{d}_L^i d_R^i X^0$	$-\frac{em_d^i}{2c_W s_W M_Z}\left(1 - \frac{c_R^4}{4}\epsilon^2\right)$	$\frac{ec_R m_d^i}{2s_R c_W M_{Z'}}$

Table F.5.: Fermion couplings to neutral Goldstone bosons G^0 and G'^0.

	Z	Z'	A
$W^+ W^- X$	$ie\frac{c_W}{s_W}$	$-ie\frac{c_R^3 s_R c_W}{4s_W^2}\epsilon^2$	ie
$W^+ W'^- X$	$-ie\frac{cse^{i\alpha}s_R}{s_W^2}\epsilon^2$	$ie\frac{cse^{i\alpha}c_R}{s_W}\epsilon^2$	0
$W'^+ W^- X$	$-ie\frac{cse^{-i\alpha}s_R}{s_W^2}\epsilon^2$	$ie\frac{cse^{-i\alpha}c_R}{s_W}\epsilon^2$	0
$W'^+ W'^- X$	$-ie\left(\frac{s_W}{c_W} - \frac{c_R^4}{4c_W s_W}\epsilon^2\right)$	$ie\frac{c_R}{c_W}\left(\frac{1}{s_R} + \frac{c_R^2 s_R}{4}\epsilon^2\right)$	ie

Table F.6.: Triple gauge couplings, involving either Z, Z' or the photon, respectively.

	Z	A
$G^+(p)G^-(q)X_\mu$	$-\frac{ie}{2c_W s_W}(p-q)_\mu\left[1 - 2s_W^2 + \left(\frac{c_R^4}{4} - 2s^2 c^2\right)\epsilon^2\right]$	$-ie(p-q)_\mu$
$G'^+(p)G^-(q)X_\mu$	$\frac{iecse^{-i\alpha}}{\sqrt{2}c_W s_W}\epsilon(p-q)_\mu$	0
$G'^+(p)G'^-(q)X_\mu$	$ie\frac{s_W}{c_W}(p-q)_\mu\left[1 - \frac{1-s_R^2 c_R^2}{4s_W^2}\epsilon^2\right]$	$-ie(p-q)_\mu$

Table F.7.: Charged Goldstone boson couplings to the photon and the Z boson.

$G^+(p)G^-(q)Z'_\mu$	$-\frac{iec_R}{2s_R c_W}(p-q)_\mu\left[1 - \frac{s_R^2 c_R^4(1-2s_W^2)+8s^2 c^2 s_W^2(1+s_R^2)}{4c_R^2 s_W^2}\epsilon^2\right]$
$G'^+(p)G^-(q)Z'_\mu$	$\frac{iecse^{-i\alpha}(1+s_R^2)}{\sqrt{2}c_R s_R c_W}\epsilon(p-q)_\mu$
$G'^+(p)G'^-(q)Z'_\mu$	$\frac{ies_R}{c_R c_W}(p-q)_\mu\left[1 - \frac{1+s_R^2(1+c_R^4)}{4s_R^2}\epsilon^2\right]$

Table F.8.: Charged Goldstone boson couplings to the Z' boson.

	W
$G^0(p)G^-(q)X^+_\mu$	$\frac{ie}{2s_W}(p-q)_\mu\left[1-\frac{1}{8}(c_R^4-8s^2c^2)\epsilon^2\right]$
$G'^0(p)G^-(q)X^+_\mu$	$-\frac{iec_R^2}{4s_W}\epsilon(p-q)_\mu$
$G^0(p)G'^-(q)X^+_\mu$	$-\frac{iecse^{i\alpha}}{\sqrt{2}s_W}\epsilon(p-q)_\mu$
$G'^0(p)G'^-(q)X^+_\mu$	$\frac{iecse^{i\alpha}(2+c_R^2)}{2\sqrt{2}s_W}\epsilon^2(p-q)_\mu$

Table F.9.: Couplings of charged and neutral Goldstone bosons to the W boson.

	W'
$G^0(p)G^-(q)X^+_\mu$	$\frac{iecse^{-i\alpha}}{c_Ws_R}(p-q)_\mu\left[1-\frac{1}{2}\left(\frac{c_R^4}{4}+\frac{s_R^2}{s_W^2}-2s^2c^2\right)\epsilon^2\right]$
$G'^0(p)G^-(q)X^+_\mu$	$\frac{iecse^{-i\alpha}(2-c_R^2)}{2c_Ws_R}\epsilon(p-q)_\mu$
$G^0(p)G'^-(q)X^+_\mu$	$-\frac{ies_R}{2\sqrt{2}c_W}\epsilon(p-q)_\mu$
$G'^0(p)G'^-(q)X^+_\mu$	$\frac{ie}{\sqrt{2}c_Ws_R}(p-q)_\mu\left[1-\frac{1}{8}(1+s_R^4)\epsilon^2\right]$

Table F.10.: Couplings of charged and neutral Goldstone bosons to the W' boson.

	G^0	G'^0
$W^+W^-X^0$	0	0
$W^+W'^-X^0$	$-\frac{2ecse^{i\alpha}M_Z}{s_R}g_{\mu\nu}$	$\frac{ec_R^3cse^{i\alpha}M_{Z'}}{2s_W}\epsilon^2 g_{\mu\nu}$
$W'^+W'^-X^0$	0	0

Table F.11.: Couplings of charged gauge bosons to the Goldstone bosons G^0 and G'^0, respectively.

	G^+	G'^+
$W_\mu^- A_\nu X^+$	$-eM_W g_{\mu\nu}$	0
$W_\mu'^- A_\nu X^+$	0	$-eM_{W_R} g_{\mu\nu}$
$W_\mu^- Z_\nu X^+$	$\frac{es_W M_W}{c_W} g_{\mu\nu} \left(1 - \frac{c_R^4 - 8s^2 c^2}{4s_W^2}\epsilon^2\right)$	0
$W_\mu'^- Z_\nu X^+$	$\frac{2ecse^{i\alpha} M_W}{c_W^2 s_R} g_{\mu\nu}$	$\frac{es_W M_{W_R}}{c_W}\left(1 - \frac{1+s_R^4}{4s_W^2}\epsilon^2\right) g_{\mu\nu}$
$W_\mu^- Z'_\nu X^+$	$-\frac{ec_R M_W}{c_W s_R} g_{\mu\nu}$	$\frac{2ecse^{-i\alpha} M_{W_R}}{c_R s_W}\epsilon^2 g_{\mu\nu}$
$W_\mu'^- Z'_\nu X^+$	$\frac{2ecse^{i\alpha}s_W(1+s_R^2)M_W}{c_W^2 s_R^2 c_R} g_{\mu\nu}$	$\frac{e(1+s_R^2)M_{W_R}}{c_R s_R c_W}\left(1 - \left(\frac{1}{2} + \frac{s_R^2 c_R^4}{4(1+s_R^2)}\right)\epsilon^2\right) g_{\mu\nu}$

Table F.12.: Couplings of charged and neutral gauge bosons to the Goldstone bosons G^+ and G'^+, respectively.

	H_1^0	H_2^0
$\bar{d}_L^i d_R^j X^0$	$-i\,\eta(s)\left(e^{i\alpha}m_u^a V_{ai}^{L*}V_{aj}^R - 2csm_d^i\delta_{ij}\right)$	$\eta(s)\left(e^{i\alpha}m_u^a V_{ai}^{L*}V_{aj}^R - 2csm_d^i\delta_{ij}\right)$
$\bar{d}_R^i d_L^j X^0$	$-i\,\eta(s)\left(e^{-i\alpha}m_u^a V_{ai}^{R*}V_{aj}^L - 2csm_d^i\delta_{ij}\right)$	$-\eta(s)\left(e^{-i\alpha}m_u^a V_{ai}^{R*}V_{aj}^L - 2csm_d^i\delta_{ij}\right)$
$\bar{u}_L^i u_R^j X^0$	$-i\,\eta(s)\left(e^{-i\alpha}m_d^a V_{ai}^L V_{aj}^{R*} - 2csm_u^i\delta_{ij}\right)$	$-\eta(s)\left(e^{-i\alpha}m_d^a V_{ai}^L V_{aj}^{R*} - 2csm_u^i\delta_{ij}\right)$
$\bar{u}_R^i u_L^j X^0$	$-i\,\eta(s)\left(e^{i\alpha}m_d^a V_{ai}^R V_{aj}^{L*} - 2csm_u^i\delta_{ij}\right)$	$\eta(s)\left(e^{i\alpha}m_d^a V_{ai}^R V_{aj}^{L*} - 2csm_u^i\delta_{ij}\right)$

Table F.13.: Leading order flavour-violating couplings of fermions to the neutral Higgses. The masses m_u^a and m_d^a denote the ath up and down quark mass, respectively. Summation over a is understood. The pre-factor $\eta(s)$ is defined by
$$\eta(s) = \frac{1}{\sqrt{2}(1-2s^2)v}\,.$$

$\bar{u}_L^i d_R^j H^+$	$-\frac{i}{(1-2s^2)v}\left(m_u^i V_{ij}^R - 2cse^{-i\alpha}V_{ij}^L m_d^j\right)$
$\bar{u}_R^i d_L^j H^+$	$\frac{i}{(1-2s^2)v}\left(V_{ij}^R m_d^j - 2cse^{-i\alpha}m_u^i V_{ij}^L\right)$

Table F.14.: Couplings of the heavy charged Higgs to fermions. Here m_u^a and m_d^a denote the ath up and down quark mass, respectively.

Bibliography

[1] G. Isidori, Y. Nir, and G. Perez, *Flavor Physics Constraints for Physics Beyond the Standard Model*, *Ann.Rev.Nucl.Part.Sci.* **60** (2010) 355, [`arXiv:1002.0900`].

[2] G. D'Ambrosio, G. F. Giudice, G. Isidori, and A. Strumia, *Minimal flavour violation: An effective field theory approach*, *Nucl. Phys.* **B645** (2002) 155–187, [`hep-ph/0207036`].

[3] R. S. Chivukula and H. Georgi, *Composite Technicolor Standard Model*, *Phys. Lett.* **B188** (1987) 99.

[4] L. J. Hall and L. Randall, *Weak scale effective supersymmetry*, *Phys. Rev. Lett.* **65** (1990) 2939–2942.

[5] A. J. Buras, P. Gambino, M. Gorbahn, S. Jager, and L. Silvestrini, *Universal unitarity triangle and physics beyond the standard model*, *Phys. Lett.* **B500** (2001) 161–167, [`hep-ph/0007085`].

[6] A. J. Buras, *Minimal flavor violation*, *Acta Phys. Polon.* **B34** (2003) 5615–5668, [`hep-ph/0310208`].

[7] C. D. Froggatt and H. B. Nielsen, *Hierarchy of Quark Masses, Cabibbo Angles and CP Violation*, *Nucl. Phys.* **B147** (1979) 277.

[8] N. Cabibbo, *Unitary Symmetry and Leptonic Decays*, *Phys. Rev. Lett.* **10** (1963) 531–532.

[9] M. Kobayashi and T. Maskawa, *CP Violation in the Renormalizable Theory of Weak Interaction*, *Prog. Theor. Phys.* **49** (1973) 652–657.

[10] S. L. Glashow, J. Iliopoulos, and L. Maiani, *Weak Interactions with Lepton-Hadron Symmetry*, *Phys. Rev.* **D2** (1970) 1285–1292.

[11] J. C. Montero and V. Pleitez, *Custodial symmetry and extensions of the standard model*, *Phys. Rev.* **D74** (2006) 115014, [`hep-ph/0607144`].

[12] S. Willenbrock, *Symmetries of the standard model*, `hep-ph/0410370`.

[13] L. Randall and R. Sundrum, *A large mass hierarchy from a small extra dimension*, *Phys. Rev. Lett.* **83** (1999) 3370–3373, [`hep-ph/9905221`].

[14] S. Chang, J. Hisano, H. Nakano, N. Okada, and M. Yamaguchi, *Bulk standard model in the Randall-Sundrum background*, Phys. Rev. **D62** (2000) 084025, [`hep-ph/9912498`].

[15] C. Csaki, J. Hubisz, and P. Meade, *TASI lectures on electroweak symmetry breaking from extra dimensions*, `hep-ph/0510275`.

[16] T. Gherghetta, *Les Houches lectures on warped models and holography*, `hep-ph/0601213`. 43 pages, 5 figures Report-no: UMN-TH-2429/06.

[17] K. Agashe, R. Contino, L. Da Rold, and A. Pomarol, *A custodial symmetry for Z b anti-b*, Phys. Lett. **B641** (2006) 62–66, [`hep-ph/0605341`].

[18] M. S. Carena, E. Ponton, J. Santiago, and C. E. M. Wagner, *Light Kaluza-Klein states in Randall-Sundrum models with custodial SU(2)*, Nucl. Phys. **B759** (2006) 202–227, [`hep-ph/0607106`].

[19] M. E. Albrecht, M. Blanke, A. J. Buras, B. Duling, and K. Gemmler, *Electroweak and Flavour Structure of a Warped Extra Dimension with Custodial Protection*, JHEP **09** (2009) 064, [`arXiv:0903.2415`].

[20] Y. Grossman and M. Neubert, *Neutrino masses and mixings in non-factorizable geometry*, Phys. Lett. **B474** (2000) 361–371, [`hep-ph/9912408`].

[21] T. Gherghetta and A. Pomarol, *Bulk fields and supersymmetry in a slice of AdS*, Nucl. Phys. **B586** (2000) 141–162, [`hep-ph/0003129`].

[22] C. Csaki, C. Grojean, H. Murayama, L. Pilo, and J. Terning, *Gauge theories on an interval: Unitarity without a Higgs*, Phys. Rev. **D69** (2004) 055006, [`hep-ph/0305237`].

[23] C. Csaki, C. Grojean, L. Pilo, and J. Terning, *Towards a realistic model of Higgsless electroweak symmetry breaking*, Phys. Rev. Lett. **92** (2004) 101802, [`hep-ph/0308038`].

[24] Y. Nomura, *Higgsless theory of electroweak symmetry breaking from warped space*, JHEP **11** (2003) 050, [`hep-ph/0309189`].

[25] R. Barbieri, A. Pomarol, and R. Rattazzi, *Weakly coupled Higgsless theories and precision electroweak tests*, Phys. Lett. **B591** (2004) 141–149, [`hep-ph/0310285`].

[26] H. Georgi, *Fun with Higgsless theories*, Phys. Rev. **D71** (2005) 015016, [`hep-ph/0408067`].

[27] G. Cacciapaglia, C. Csaki, G. Marandella, and J. Terning, *A new custodian for a realistic Higgsless model*, Phys. Rev. **D75** (2007) 015003, [`hep-ph/0607146`].

[28] J. C. Pati and A. Salam, *Are There Anomalous Lepton-Hadron Interactions?*, Phys. Rev. Lett. **32** (1974) 1083.

[29] R. N. Mohapatra and J. C. Pati, *A Natural Left-Right Symmetry*, *Phys. Rev.* **D11** (1975) 2558.

[30] R. N. Mohapatra and J. C. Pati, *Left-Right Gauge Symmetry and an Isoconjugate Model of CP Violation*, *Phys. Rev.* **D11** (1975) 566–571.

[31] G. Senjanovic and R. N. Mohapatra, *Exact Left-Right Symmetry and Spontaneous Violation of Parity*, *Phys. Rev.* **D12** (1975) 1502.

[32] G. Senjanovic, *Spontaneous Breakdown of Parity in a Class of Gauge Theories*, *Nucl. Phys.* **B153** (1979) 334.

[33] R. N. Mohapatra, F. E. Paige, and D. P. Sidhu, *Symmetry Breaking and Naturalness of Parity Conservation in Weak Neutral Currents in Left-Right Symmetric Gauge Theories*, *Phys. Rev.* **D17** (1978) 2462.

[34] D. Chang, *A Minimal Model of Spontaneous CP Violation with the Gauge Group $SU(2)_L \times SU(2)_R \times U(1)_{B-L}$*, *Nucl. Phys.* **B214** (1983) 435.

[35] H. Harari and M. Leurer, *Left-Right Symmetry and the Mass Scale of a Possible Right-Handed Weak Boson*, *Nucl. Phys.* **B233** (1984) 221.

[36] Y. Zhang, H. An, X. Ji, and R. N. Mohapatra, *General CP Violation in Minimal Left-Right Symmetric Model and Constraints on the Right-Handed Scale*, *Nucl. Phys.* **B802** (2008) 247–279, [`arXiv:0712.4218`].

[37] A. Maiezza, M. Nemevsek, F. Nesti, and G. Senjanovic, *Left-Right Symmetry at LHC*, *Phys. Rev.* **D82** (2010) 055022, [`arXiv:1005.5160`].

[38] P. Langacker and S. Uma Sankar, *Bounds on the Mass of W_R and the $W_L - W_R$ Mixing Angle ξ in General $SU(2)_L \times SU(2)_R \times U(1)$ Models*, *Phys. Rev.* **D40** (1989) 1569–1585.

[39] K. Kiers, J. Kolb, J. Lee, A. Soni, and G.-H. Wu, *Ubiquitous CP violation in a top inspired left-right model*, *Phys. Rev.* **D66** (2002) 095002, [`hep-ph/0205082`].

[40] M. Nemevsek, F. Nesti, G. Senjanovic, and Y. Zhang, *First Limits on Left-Right Symmetry Scale from LHC Data*, *Phys.Rev.* **D83** (2011) 115014, [`arXiv:1103.1627`].

[41] C. Grojean, E. Salvioni, and R. Torre, *A weakly constrained W' at the early LHC*, *JHEP* **1107** (2011) 002, [`arXiv:1103.2761`].

[42] R. N. Mohapatra and G. Senjanovic, *Neutrino mass and spontaneous parity nonconservation*, *Phys. Rev. Lett.* **44** (1980) 912.

[43] R. N. Mohapatra and G. Senjanovic, *Neutrino Masses and Mixings in Gauge Models with Spontaneous Parity Violation*, *Phys. Rev.* **D23** (1981) 165.

[44] C.-H. Chen and S.-h. Nam, *Left-right mixing on leptonic and semileptonic* $b \to u$ *decays*, *Phys. Lett.* **B666** (2008) 462–466, [arXiv:0807.0896].

[45] A. Crivellin, *Effects of right-handed charged currents on the determinations of* $|V_{ub}|$ *and* $|V_{cb}|$, *Phys. Rev.* **D81** (2010) 031301, [arXiv:0907.2461].

[46] R. Feger, T. Mannel, V. Klose, H. Lacker, and T. Luck, *Limit on a Right-Handed Admixture to the Weak* $b \to c$ *Current from Semileptonic Decays*, *Phys. Rev.* **D82** (2010) 073002, [arXiv:1003.4022].

[47] A. J. Buras, K. Gemmler, and G. Isidori, *Quark flavour mixing with right-handed currents: an effective theory approach*, *Nucl. Phys.* **B843** (2011) 107–142, [arXiv:1007.1993].

[48] K. Gemmler, *An effective look at right-handed currents and quark flavour mixing*, arXiv:1011.5368.

[49] M. Blanke, A. J. Buras, K. Gemmler, and T. Heidsieck, $\Delta F = 2$ *observables and* $B \to X_q \gamma$ *decays in the Left-Right Model: Higgs particles striking back*, *JHEP* **1203** (2012) 024, [arXiv:1111.5014].

[50] A. J. Buras, *Flavour Visions*, *PoS* **BEAUTY2011** (2011) 008, [arXiv:1106.0998].

[51] A. J. Buras, *Flavour Theory and the LHC Era*, arXiv:1009.1303.

[52] A. J. Buras, *Minimal flavour violation and beyond: Towards a flavour code for short distance dynamics*, *Acta Phys. Polon.* **B41** (2010) 2487–2561, [arXiv:1012.1447].

[53] G. Isidori, *The Challenges of Flavour Physics*, arXiv:1012.1981.

[54] A. J. Buras, M. V. Carlucci, S. Gori, and G. Isidori, *Higgs-mediated FCNCs: Natural Flavour Conservation vs. Minimal Flavour Violation*, *JHEP* **10** (2010) 009, [arXiv:1005.5310].

[55] A. J. Buras, *Flavour Theory: 2009*, *PoS* **EPS-HEP2009** (2009) 024, [arXiv:0910.1032].

[56] **CDF** Collaboration, T. Aaltonen *et. al.*, *First Flavor-Tagged Determination of Bounds on Mixing- Induced CP Violation in* $B_s^0 \to J/\psi\phi$ *Decays*, *Phys. Rev. Lett.* **100** (2008) 161802, [arXiv:0712.2397].

[57] **D0** Collaboration, V. M. Abazov *et. al.*, *Measurement of* B_s^0 *mixing parameters from the flavor- tagged decay* $B_s^0 \to J/\psi\phi$, *Phys. Rev. Lett.* **101** (2008) 241801, [arXiv:0802.2255].

[58] **Heavy Flavor Averaging Group (HFAG)** Collaboration, E. Barberio *et. al.*, *Averages of b-hadron properties at the end of 2006*, arXiv:0704.3575.

[59] **UTfit** Collaboration, M. Bona *et. al.*, *First Evidence of New Physics in b ↔ s Transitions*, `0803.0659`.

[60] **CDF and D0** Collaboration, G. Brooijmans, *Mixing and CP Violation at the Tevatron*, `arXiv:0808.0726`.

[61] A. Lenz and U. Nierste, *Numerical updates of lifetimes and mixing parameters of B mesons*, `arXiv:1102.4274`.

[62] J. Laiho, E. Lunghi, and R. Van De Water, *Lessons for new physics from CKM studies*, *PoS* **FPCP2010** (2010) 040, [`arXiv:1102.3917`].

[63] E. Lunghi and A. Soni, *Demise of CKM and its aftermath*, `arXiv:1104.2117`.

[64] **For the CDF** Collaboration, G. Giurgiu, *New Measurement of the B_s Mixing Phase at CDF*, *PoS* **ICHEP2010** (2010) 236, [`arXiv:1012.0962`].

[65] **D0** Collaboration, V. M. Abazov *et. al.*, *Measurement of the CP-violating phase $\phi_s^{J/\psi\phi}$ using the flavor-tagged decay $B_s^0 \rightarrow J/\psi\phi$ in 8 fb^{-1} of $p\overline{p}$ collisions*, `arXiv:1109.3166`.

[66] **LHCb** Collaboration, G. Raven, "B Physics Results from the LHC." Review talk, rather than LHCb specific, but featuring new LHCb results. `http://cdsweb.cern.ch/record/1378074?ln=en`, Aug, 2011.

[67] W. Altmannshofer and M. Carena, *B Meson Mixing in Effective Theories of Supersymmetric Higgs Bosons*, `arXiv:1110.0843`.

[68] A. J. Buras and D. Guadagnoli, *Correlations among new CP violating effects in $\Delta F = 2$ observables*, *Phys. Rev.* **D78** (2008) 033005, [`arXiv:0805.3887`].

[69] A. J. Buras and D. Guadagnoli, *On the consistency between the observed amount of CP violation in the K- and B_d-systems within minimal flavor violation*, *Phys. Rev.* **D79** (2009) 053010, [`arXiv:0901.2056`].

[70] **RBC** Collaboration, D. J. Antonio *et. al.*, *Neutral kaon mixing from 2+1 flavor domain wall QCD*, *Phys. Rev. Lett.* **100** (2008) 032001, [`hep-ph/0702042`].

[71] A. J. Buras, D. Guadagnoli, and G. Isidori, *On ε_K beyond lowest order in the Operator Product Expansion*, *Phys. Lett.* **B688** (2010) 309–313, [`arXiv:1002.3612`].

[72] J. Brod and M. Gorbahn, *ε_K at Next-to-Next-to-Leading Order: The Charm-Top-Quark Contribution*, *Phys. Rev.* **D82** (2010) 094026, [`arXiv:1007.0684`].

[73] J. Brod and M. Gorbahn, *The NNLO Charm-Quark Contribution to ϵ_K and ΔM_K*, `arXiv:1108.2036`.

[74] **Particle Data Group** Collaboration, C. Amsler *et. al.*, *Review of particle physics*, *Phys. Lett.* **B667** (2008) 1–1340.

[75] E. Lunghi and A. Soni, *Possible Indications of New Physics in B_d-mixing and in* $\sin(2\beta)$ *Determinations*, *Phys. Lett.* **B666** (2008) 162–165, [arXiv:0803.4340].

[76] E. Lunghi and A. Soni, *Possible evidence for the breakdown of the CKM-paradigm of CP-violation*, *Phys. Lett.* **B697** (2011) 323–328, [arXiv:1010.6069].

[77] **UTfit Collaboration** Collaboration, A. Bevan *et. al.*, *Update of the Unitarity Triangle Analysis*, *PoS* **ICHEP2010** (2010) 270, [arXiv:1010.5089].

[78] **CKMfitter** Collaboration, J. Charles *et. al.*, *CP violation and the CKM matrix: Assessing the impact of the asymmetric B factories*, *Eur. Phys. J.* **C41** (2005) 1–131, [hep-ph/0406184]. Updates available on http://ckmfitter.in2p3.fr/.

[79] **Heavy Flavor Averaging Group** Collaboration, E. Barberio *et. al.*, *Averages of b-hadron and c-hadron Properties at the End of 2007*, arXiv:0808.1297.

[80] A. L. Kagan, G. Perez, T. Volansky, and J. Zupan, *General Minimal Flavor Violation*, *Phys. Rev.* **D80** (2009) 076002, [arXiv:0903.1794].

[81] L. Mercolli and C. Smith, *EDM constraints on flavored CP-violating phases*, *Nucl. Phys.* **B817** (2009) 1–24, [arXiv:0902.1949].

[82] P. Paradisi and D. M. Straub, *The SUSY CP Problem and the MFV Principle*, *Phys. Lett.* **B684** (2010) 147–153, [arXiv:0906.4551].

[83] G. Isidori, *Effective theories of electroweak symmetry breaking*, *PoS* **CD09** (2009) 073, [arXiv:0911.3219].

[84] M. Antonelli, V. Cirigliano, G. Isidori, F. Mescia, M. Moulson, *et. al.*, *An Evaluation of $|V_{us}|$ and precise tests of the Standard Model from world data on leptonic and semileptonic kaon decays*, *Eur.Phys.J.* **C69** (2010) 399–424, [arXiv:1005.2323].

[85] V. Bernard, M. Oertel, E. Passemar, and J. Stern, *Tests of non-standard electroweak couplings of right-handed quarks*, *JHEP* **01** (2008) 015, [arXiv:0707.4194].

[86] M. Antonelli *et. al.*, *Flavor Physics in the Quark Sector*, *Phys. Rept.* **494** (2010) 197–414, [arXiv:0907.5386].

[87] M. Neubert, *B physics and CP violation*, *Int. J. Mod. Phys.* **A11** (1996) 4173–4240, [hep-ph/9604412].

[88] S. Faller, A. Khodjamirian, C. Klein, and T. Mannel, $B \to D^{(*)}$ *Form Factors from QCD Light-Cone Sum Rules*, *Eur. Phys. J.* **C60** (2009) 603–615, [arXiv:0809.0222].

[89] M. Okamoto, *Full determination of the CKM matrix using recent results from lattice QCD*, *PoS* **LAT2005** (2006) 013, [hep-lat/0510113].

[90] C. Bernard, C. E. DeTar, M. Di Pierro, A. El-Khadra, R. Evans, *et. al.*, *The $\bar{B} \to D^* \ell \bar{\nu}$ form factor at zero recoil from three-flavor lattice QCD: A Model independent determination of $|V_{cb}|$*, *Phys.Rev.* **D79** (2009) 014506, [arXiv:0808.2519].

[91] P. Gambino, T. Mannel, and N. Uraltsev, $B \to D^*$ *at zero recoil revisited*, *Phys. Rev.* **D81** (2010) 113002, [arXiv:1004.2859].

[92] A. G. Akeroyd and S. Recksiegel, *The effect of $H^\pm$ on $B^\pm \to \tau^\pm \nu_\tau$ and $B^\pm \to \mu^\pm \nu_\mu$*, *J. Phys.* **G29** (2003) 2311–2317, [hep-ph/0306037].

[93] **UTfit** Collaboration, M. Bona *et. al.*, *An Improved Standard Model Prediction Of $Br(B \to \tau\nu)$ And Its Implications For New Physics*, *Phys. Lett.* **B687** (2010) 61–69, [arXiv:0908.3470].

[94] J. Laiho, E. Lunghi, and R. S. Van de Water, *Lattice QCD inputs to the CKM unitarity triangle analysis*, *Phys. Rev.* **D81** (2010) 034503, [arXiv:0910.2928]. Updates available on http://latticeaverages.org/.

[95] J. C. Pati and A. Salam, *Lepton Number as the Fourth Color*, *Phys. Rev.* **D10** (1974) 275–289.

[96] G. Beall, M. Bander, and A. Soni, *Constraint on the Mass Scale of a Left-Right Symmetric Electroweak Theory from the $K_L - K_S$ Mass Difference*, *Phys. Rev. Lett.* **48** (1982) 848.

[97] G. Ecker and W. Grimus, ϵ, ϵ' *in a model with spontaneous P and CP violation*, *Phys. Lett.* **B153** (1985) 279–285.

[98] J. M. Frere *et. al.*, $K^0 - \bar{K}^0$ *in the $SU(2)_L \times SU(2)_R \times U(1)$ model of CP violation*, *Phys. Rev.* **D46** (1992) 337–353.

[99] G. Barenboim, J. Bernabeu, and M. Raidal, *Spontaneous CP-violation in the left-right model and the kaon system*, *Nucl. Phys.* **B478** (1996) 527–543, [hep-ph/9608450].

[100] P. Ball, J. M. Frere, and J. Matias, *Anatomy of Mixing-Induced CP Asymmetries in Left-Right-Symmetric Models with Spontaneous CP Violation*, *Nucl. Phys.* **B572** (2000) 3–35, [hep-ph/9910211].

[101] G. Barenboim, M. Gorbahn, U. Nierste, and M. Raidal, *Higgs sector of the minimal left-right symmetric model*, Phys. Rev. **D65** (2002) 095003, [hep-ph/0107121].

[102] R. N. Mohapatra, G. Senjanovic, and M. D. Tran, *Strangeness changing processes and the limit on the right-handed gauge boson mass*, Phys. Rev. **D28** (1983) 546.

[103] G. Barenboim, J. Bernabeu, J. Prades, and M. Raidal, *Constraints on the W_R mass and CP violation in left-right models*, Phys. Rev. **D55** (1997) 4213–4221, [hep-ph/9611347].

[104] Y. Zhang, H. An, X. Ji, and R. N. Mohapatra, *Right-handed quark mixings in minimal left-right symmetric model with general CP violation*, Phys. Rev. **D76** (2007) 091301, [arXiv:0704.1662].

[105] K. Hsieh, K. Schmitz, J.-H. Yu, and C. P. Yuan, *Global Analysis of General $SU(2) \times SU(2) \times U(1)$ Models with Precision Data*, Phys. Rev. **D82** (2010) 035011, [arXiv:1003.3482].

[106] D. Chang, R. Mohapatra, and M. Parida, *Decoupling Parity and $SU(2)_R$ Breaking Scales: A New Approach to Left-Right Symmetric Models*, Phys.Rev.Lett. **52** (1984) 1072.

[107] D. Guadagnoli, R. N. Mohapatra, and I. Sung, *Gauged Flavor Group with Left-Right Symmetry*, JHEP **04** (2011) 093, [arXiv:1103.4170].

[108] O. Khasanov and G. Perez, *On neutrino masses and a low breaking scale of left-right symmetry*, Phys. Rev. **D65** (2002) 053007, [hep-ph/0108176].

[109] P. Langacker, *Bounds on mixing between light and heavy gauge bosons*, Phys. Rev. **D30** (1984) 2008.

[110] M.-C. Chen and J. Huang, *TeV Scale Models of Neutrino Masses and Their Phenomenology*, arXiv:1105.3188.

[111] M. Czakon, J. Gluza, and J. Hejczyk, *Muon decay to one loop order in the left-right symmetric model*, Nucl. Phys. **B642** (2002) 157–172, [hep-ph/0205303].

[112] **Particle Data Group** Collaboration, K. Nakamura *et. al.*, *Review of particle physics*, J. Phys. **G37** (2010) 075021. Updates available on http://pdg.lbl.gov/.

[113] **Fermilab Lattice and MILC** Collaboration, J. A. Bailey *et. al.*, $B \to D^* l\nu$ at *zero recoil: an update*, PoS **LATTICE2010** (2010) 311, [arXiv:1011.2166].

[114] **Heavy Flavor Averaging Group** Collaboration, D. Asner *et. al.*, *Averages of b-hadron, c-hadron, and tau-lepton Properties*, `arXiv:1010.1589`. Updates available on `http://www.slac.stanford.edu/xorg/hfag/`.

[115] M. Okamoto, C. Aubin, C. Bernard, C. E. DeTar, M. Di Pierro, *et. al.*, *Semileptonic $D \to \pi/K$ and $B \to \pi/D$ decays in 2+1 flavor lattice QCD*, *Nucl.Phys.Proc.Suppl.* **140** (2005) 461–463, [`hep-lat/0409116`].

[116] M. Finkemeier, *Radiative corrections to π_{l2} and K_{l2} decays*, `hep-ph/9501286`.

[117] **D0** Collaboration, V. Abazov *et. al.*, *Precision measurement of the ratio* $\mathrm{B}(t \to Wb)/\mathrm{B}(t \to Wq)$ *and Extraction of V_{tb}*, *Phys.Rev.Lett.* **107** (2011) 121802, [`arXiv:1106.5436`].

[118] M. E. Peskin and T. Takeuchi, *Estimation of oblique electroweak corrections*, *Phys.Rev.* **D46** (1992) 381–409.

[119] C. P. Burgess, S. Godfrey, H. Konig, D. London, and I. Maksymyk, *Model independent global constraints on new physics*, *Phys. Rev.* **D49** (1994) 6115–6147, [`hep-ph/9312291`].

[120] H. Flacher, M. Goebel, J. Haller, A. Hocker, K. Monig, *et. al.*, *Revisiting the Global Electroweak Fit of the Standard Model and Beyond with Gfitter*, *Eur.Phys.J.* **C60** (2009) 543–583, [`arXiv:0811.0009`].

[121] A. Arbuzov, M. Awramik, M. Czakon, A. Freitas, M. Grunewald, *et. al.*, *ZFITTER: A Semi-analytical program for fermion pair production in e^+e^- annihilation, from version 6.21 to version 6.42*, *Comput.Phys.Commun.* **174** (2006) 728–758, [`hep-ph/0507146`]. Updates available on `http://zfitter.desy.de/`.

[122] **The ALEPH, DELPHI, L3, OPAL, SLD Collaborations, the LEP Electroweak Working Group, the SLD Electroweak and Heavy Flavour Groups**, *Precision Electroweak Measurements on the Z Resonance*, *Phys. Rept.* **427** (2006) 257, [`hep-ex/0509008`].

[123] M. Baak *et. al.*, *Updated Status of the Global Electroweak Fit and Constraints on New Physics*, `arXiv:1107.0975`.

[124] **ATLAS Collaboration** Collaboration, G. Aad *et. al.*, *Search for a heavy gauge boson decaying to a charged lepton and a neutrino in $1\,fb^{-1}$ of pp collisions at $\sqrt{s} = 7\,TeV$ using the ATLAS detector*, *Phys.Lett.* **B705** (2011) 28–46, [`arXiv:1108.1316`].

[125] **CMS** Collaboration, "Search for W' in the leptonic channels in pp Collisions at $\sqrt{s} = 7\,\mathrm{TeV}$." `http://cdsweb.cern.ch/record/1369201?ln=en`, 2011.

[126] **CMS** Collaboration, "Search for a heavy neutrino and right-handed W of the left-right symmetric model in pp collisions at $\sqrt{s} = 7\,\text{TeV}$." `http://cdsweb.cern.ch/record/1369255?ln=en`, 2011.

[127] E. Accomando, D. Becciolini, S. De Curtis, D. Dominici, L. Fedeli, *et. al.*, *Interference effects in heavy W'-boson searches at the LHC*, `arXiv:1110.0713`.

[128] **TWIST** Collaboration, R. Bayes *et. al.*, *Experimental Constraints on Left-Right Symmetric Models from Muon Decay*, *Phys. Rev. Lett.* **106** (2011) 041804.

[129] A. J. Buras, *Weak Hamiltonian, CP violation and rare decays*, `hep-ph/9806471`.

[130] K. G. Wilson, *Nonlagrangian models of current algebra*, *Phys. Rev.* **179** (1969) 1499–1512.

[131] K. G. Wilson and W. Zimmermann, *Operator product expansions and composite field operators in the general framework of quantum field theory*, *Commun. Math. Phys.* **24** (1972) 87–106.

[132] G. Buchalla, A. J. Buras, and M. E. Lautenbacher, *Weak decays beyond leading logarithms*, *Rev. Mod. Phys.* **68** (1996) 1125–1144, [`hep-ph/9512380`].

[133] A. J. Buras, S. Jager, and J. Urban, *Master formulae for $\Delta F = 2$ NLO-QCD factors in the standard model and beyond*, *Nucl. Phys.* **B605** (2001) 600–624, [`hep-ph/0102316`].

[134] A. J. Buras, M. Misiak, and J. Urban, *Two-loop QCD anomalous dimensions of flavour-changing four-quark operators within and beyond the standard model*, *Nucl. Phys.* **B586** (2000) 397–426, [`hep-ph/0005183`].

[135] **Particle Data Group** Collaboration, W. Yao *et. al.*, *Review of Particle Physics*, *J.Phys.G* **G33** (2006) 1–1232.

[136] M. Blanke *et. al.*, *Particle antiparticle mixing, ε_K, $\Delta\Gamma_q$, A^q_{SL}, $A_{CP}(B_d \to \psi K_S)$, $A_{CP}(B_s \to \psi\phi)$ and $B \to X_{s,d}\gamma$ in the Littlest Higgs model with T-parity*, *JHEP* **12** (2006) 003, [`hep-ph/0605214`].

[137] M. Blanke, A. J. Buras, B. Duling, S. Gori, and A. Weiler, *$\Delta F = 2$ Observables and Fine-Tuning in a Warped Extra Dimension with Custodial Protection*, *JHEP* **03** (2009) 001, [`arXiv:0809.1073`].

[138] A. J. Buras *et. al.*, *Patterns of Flavour Violation in the Presence of a Fourth Generation of Quarks and Leptons*, *JHEP* **09** (2010) 106, [`arXiv:1002.2126`].

[139] **UTfit** Collaboration, M. Bona *et. al.*, *The UTfit collaboration report on the status of the unitarity triangle beyond the standard model. I. Model-independent analysis and minimal flavor violation*, *JHEP* **0603** (2006) 080, [`hep-ph/0509219`].

[140] R. Fleischer, *B physics and CP violation, Lect. Notes Phys.* **647** (2004) 42–77, [`hep-ph/0210323`].

[141] A. J. Buras, *Flavor physics and CP violation*, `hep-ph/0505175`.

[142] Z. Ligeti, M. Papucci, and G. Perez, *Implications of the measurement of the $B_s^0 - \bar{B}_s^0$ mass difference, Phys. Rev. Lett* **97** (2006) 101801, [`hep-ph/0604112`].

[143] M. Blanke, A. J. Buras, D. Guadagnoli, and C. Tarantino, *Minimal Flavour Violation Waiting for Precise Measurements of ΔM_s, $S_{\psi\phi}$, A_{SL}^s, $|V_{ub}|$, γ and $B_{s,d}^0 \to \mu^+\mu^-$, JHEP* **10** (2006) 003, [`hep-ph/0604057`].

[144] A. Lenz, *A simple relation for B_s-mixing, Phys.Rev.* **D84** (2011) 031501, [`arXiv:1106.3200`].

[145] **D0** Collaboration, V. M. Abazov *et. al.*, *Measurement of the anomalous like-sign dimuon charge asymmetry with $9fb^{-1}$ of $p\bar{p}$ collisions*, `arXiv:1106.6308`.

[146] S. Herrlich and U. Nierste, *Enhancement of the $K_L - K_S$ mass difference by short distance QCD corrections beyond leading logarithms, Nucl. Phys.* **B419** (1994) 292–322, [`hep-ph/9310311`].

[147] S. Herrlich and U. Nierste, *Indirect CP violation in the neutral kaon system beyond leading logarithms, Phys. Rev.* **D52** (1995) 6505–6518, [`hep-ph/9507262`].

[148] S. Herrlich and U. Nierste, *The Complete $|\Delta S| = 2$ Hamiltonian in the Next-To-Leading Order, Nucl. Phys.* **B476** (1996) 27–88, [`hep-ph/9604330`].

[149] A. J. Buras, M. Jamin, and P. H. Weisz, *Leading and next-to-leading QCD corrections to ε parameter and $B^0 - \bar{B}^0$ mixing in the presence of a heavy top quark, Nucl. Phys.* **B347** (1990) 491–536.

[150] J. Urban, F. Krauss, U. Jentschura, and G. Soff, *Next-to-leading order QCD corrections for the $B^0 - \bar{B}^0$ mixing with an extended Higgs sector, Nucl. Phys.* **B523** (1998) 40–58, [`hep-ph/9710245`].

[151] P. L. Cho and M. Misiak, *$b \to s\gamma$ decay in $SU(2)_L \times SU(2)_R \times U(1)$ extensions of the Standard Model, Phys. Rev.* **D49** (1994) 5894–5903, [`hep-ph/9310332`].

[152] **CDF** Collaboration, T. Aaltonen *et. al.*, *Search for $B_s^0 \to \mu^+\mu^-$ and $B_d^0 \to \mu^+\mu^-$ decays with 2 fb^{-1} of p and $\bar{p}$ collisions, Phys. Rev. Lett.* **100** (2008) 101802, [`arXiv:0712.1708`].

[153] **D0** Collaboration, V. M. Abazov *et. al.*, *Search for $B_s^0 \to \mu^+\mu^-$ at D0, Phys. Rev.* **D76** (2007) 092001, [`arXiv:0707.3997`].

[154] A. J. Buras, *Relations between $\Delta M_{s,d}$ and $B_{s,d} \to \mu\bar{\mu}$ in models with minimal flavor violation, Phys. Lett.* **B566** (2003) 115–119, [`hep-ph/0303060`].

[155] **BELLE** Collaboration, K. F. Chen *et. al.*, *Search for $B \to h^{(*)}\nu\bar{\nu}$ Decays at Belle*, *Phys. Rev. Lett.* **99** (2007) 221802, [arXiv:0707.0138].

[156] M. Bartsch, M. Beylich, G. Buchalla, and D. N. Gao, *Precision Flavour Physics with $B \to K\nu\bar{\nu}$ and $B \to Kl^+l^-$*, *JHEP* **11** (2009) 011, [arXiv:0909.1512].

[157] J. F. Kamenik and C. Smith, *Tree-level contributions to the rare decays $B^+ \to \pi^+\nu\bar{\nu}$, $B^+ \to K^+\nu\bar{\nu}$, and $B^+ \to K^{*+}\nu\bar{\nu}$ in the Standard Model*, *Phys. Lett.* **B680** (2009) 471–475, [arXiv:0908.1174].

[158] W. Altmannshofer, A. J. Buras, D. M. Straub, and M. Wick, *New strategies for New Physics search in $B \to K^*\nu\bar{\nu}$, $B \to K\nu\bar{\nu}$ and $B \to X_s\nu\bar{\nu}$ decays*, *JHEP* **04** (2009) 022, [arXiv:0902.0160].

[159] **BABAR** Collaboration, B. Aubert *et. al.*, *Search for $B \to K^*\nu\bar{\nu}$ decays*, *Phys. Rev.* **D78** (2008) 072007, [arXiv:0808.1338].

[160] **ALEPH** Collaboration, R. Barate *et. al.*, *Measurements of $Br(b \to \tau^-\bar{\nu}_\tau X)$ and $Br(b \to \tau^-\bar{\nu}_\tau D^{*\pm}X)$ and upper limits on $Br(B^- \to \tau^-\bar{\nu}_\tau)$ and $Br(b \to s\nu\bar{\nu})$*, *Eur. Phys. J.* **C19** (2001) 213–227, [hep-ex/0010022].

[161] **E391a** Collaboration, J. K. Ahn *et. al.*, *Search for the Decay $K_L^0 \to \pi^0\nu\bar{\nu}$*, *Phys. Rev. Lett.* **100** (2008) 201802, [arXiv:0712.4164].

[162] J. Brod and M. Gorbahn, *Electroweak Corrections to the Charm Quark Contribution to $K^+ \to \pi^+\nu\bar{\nu}$*, *Phys. Rev.* **D78** (2008) 034006, [arXiv:0805.4119].

[163] **E949** Collaboration, A. V. Artamonov *et. al.*, *New measurement of the $K^+ \to \pi^+\nu\bar{\nu}$ branching ratio*, *Phys. Rev. Lett.* **101** (2008) 191802, [arXiv:0808.2459].

[164] **Heavy Flavor Averaging Group (HFAG)** Collaboration, E. Barberio *et. al.*, *Averages of b-hadron properties at the end of 2005*, hep-ex/0603003.

[165] M. Misiak *et. al.*, *The first estimate of $Br(\bar{B} \to X_s\gamma)$ at $O(\alpha^2)$*, *Phys. Rev. Lett.* **98** (2007) 022002, [hep-ph/0609232].

[166] **SuperB** Collaboration, M. Bona *et. al.*, *SuperB: A High-Luminosity Asymmetric e^+e^- Super Flavor Factory. Conceptual Design Report*, arXiv:0709.0451.

[167] **SuperB** Collaboration, B. O'Leary *et. al.*, *SuperB Progress Reports – Physics*, arXiv:1008.1541.

[168] A. J. Buras, F. Schwab, and S. Uhlig, *Waiting for precise measurements of $K^+ \to \pi^+\nu\bar{\nu}$ and $K_L \to \pi^0\nu\bar{\nu}$*, *Rev. Mod. Phys.* **80** (2008) 965–1007, [hep-ph/0405132].

[169] A. J. Buras, M. Gorbahn, U. Haisch, and U. Nierste, *Charm quark contribution to $K^+ \to \pi^+ \nu\bar{\nu}$ at next-to-next-to-leading order*, *JHEP* **11** (2006) 002, [`hep-ph/0603079`].

[170] A. J. Buras, *Searching for new physics with rare decays and CP violation*, *J. Phys. Conf. Ser.* **171** (2009) 012004.

[171] R. Babich *et. al.*, $K^0 - \bar{K}^0$ *mixing beyond the standard model and CP- violating electroweak penguins in quenched QCD with exact chiral symmetry*, *Phys. Rev.* **D74** (2006) 073009, [`hep-lat/0605016`].

[172] **UTfit** Collaboration, M. Bona *et. al.*, *Model-independent constraints on* $\Delta F = 2$ *operators and the scale of new physics*, *JHEP* **03** (2008) 049, [`arXiv:0707.0636`].

[173] **For the CDF and D0** Collaboration, T. E. W. Group, *Combination of CDF and D0 Results on the Mass of the Top Quark*, `arXiv:0903.2503`.

[174] G. Buchalla, G. Hiller, and G. Isidori, *Phenomenology of nonstandard Z couplings in exclusive semileptonic* $b \to s$ *transitions*, *Phys. Rev.* **D63** (2000) 014015, [`hep-ph/0006136`].

[175] D. Melikhov, N. Nikitin, and S. Simula, *Right-handed currents in rare exclusive* $B \to (K, K^*)\nu\bar{\nu}$ *decays*, *Phys. Lett.* **B428** (1998) 171–178, [`hep-ph/9803269`].

[176] Y. Grossman, Z. Ligeti, and E. Nardi, *New limit on inclusive* $B \to X_s \bar{\nu}\nu$ *decay and constraints on new physics*, *Nucl. Phys.* **B465** (1996) 369–398, [`hep-ph/9510378`].

[177] A. J. Buras, M. Gorbahn, U. Haisch, and U. Nierste, *The rare decay* $K^+ \to \pi^+ \nu\bar{\nu}$ *at the next-to-next- to-leading order in QCD*, *Phys. Rev. Lett.* **95** (2005) 261805, [`hep-ph/0508165`].

[178] G. Isidori, F. Mescia, and C. Smith, *Light-quark loops in* $K \to \pi\nu\nu$, *Nucl. Phys.* **B718** (2005) 319–338, [`hep-ph/0503107`].

[179] F. Mescia and C. Smith, *Improved estimates of rare K decay matrix-elements from* K_{l3} *decays*, *Phys. Rev.* **D76** (2007) 034017, [`arXiv:0705.2025`].

[180] Y. Grossman and Y. Nir, $K_L \to \pi^0 \nu\bar{\nu}$ *beyond the standard model*, *Phys. Lett.* **B398** (1997) 163–168, [`hep-ph/9701313`].

[181] M. Blanke, *Insights from the Interplay of* $K \to \pi\nu\bar{\nu}$ *and* ε_K *on the New Physics Flavour Structure*, *Acta Phys. Polon.* **B41** (2010) 127, [`arXiv:0904.2528`].

[182] M. Blanke *et. al.*, *Rare and CP-Violating K and B Decays in the Littlest Higgs Model with T-Parity*, *JHEP* **01** (2007) 066, [`hep-ph/0610298`].

[183] **ALEPH, DELPHI, L3, OPAL, SLD, LEP Electroweak Working Group, SLD Electroweak Group, SLD Heavy Flavour Group** Collaboration, *Precision electroweak measurements on the Z resonance*, Phys.Rept. **427** (2006) 257–454, [hep-ex/0509008].

[184] G. Ecker, W. Grimus, and H. Neufeld, *Higgs induced flavor changing neutral interactions in $SU(2)_L \times SU(2)_R \times U(1)$*, Phys. Lett. **B127** (1983) 365.

[185] F. J. Gilman and M. H. Reno, *Restrictions from the neutral K and B meson systems on left-right symmetric gauge theories*, Phys. Rev. **D29** (1984) 937.

[186] G. Ecker and W. Grimus, *CP Violation and Left-Right Symmetry*, Nucl. Phys. **B258** (1985) 328–360.

[187] W.-S. Hou and A. Soni, *Gauge invariance of the $K_L - \bar{K}_S$ mass difference in left-right symmetric model*, Phys. Rev. **D32** (1985) 163.

[188] D. London and D. Wyler, *Left-right symmetry and CP violation in the B system*, Phys. Lett. **B232** (1989) 503.

[189] P. Ball and R. Fleischer, *An Analysis of B_s decays in the left-right symmetric model with spontaneous CP violation*, Phys.Lett. **B475** (2000) 111–119, [hep-ph/9912319].

[190] S. Sahoo, L. Maharana, A. Roul, and S. Acharya, *The masses of W_R, triplet Higgs, and Z' bosons in the Left-Right Symmetric Model*, Int. J. Mod. Phys. **A20** (2005) 2625–2638.

[191] D. Chang, J. Basecq, L.-F. Li, and P. B. Pal, *Comment on the $K_L - K_S$ mass difference in left-right model*, Phys. Rev. **D30** (1984) 1601.

[192] J. Basecq, L.-F. Li, and P. B. Pal, *Gauge invariant calculation of the $K_L - K_S$ mass difference in the left-right model*, Phys. Rev. **D32** (1985) 175.

[193] G. M. Asatrian and A. N. Ionnisian, *Rare B meson decays in $SU(2)_L \times SU(2)_R \times U(1)$ model*, Mod. Phys. Lett. **A5** (1990) 1089–1096.

[194] G. M. Asatryan and A. N. Ioannisyan, *The decay $b \to s\gamma$ in the $SU(2)_L \times SU(2)_R \times U(1)$ model*, Sov. J. Nucl. Phys. **51** (1990) 858–860.

[195] D. Cocolicchio, G. Costa, G. L. Fogli, J. H. Kim, and A. Masiero, *Rare B decays in left-right symmetric models*, Phys. Rev. **D40** (1989) 1477.

[196] K. S. Babu, K. Fujikawa, and A. Yamada, *Constraints on left-right symmetric models from the process $b \to s\gamma$*, Phys. Lett. **B333** (1994) 196–201, [hep-ph/9312315].

[197] K. Fujikawa and A. Yamada, *Test of the chiral structure of the top - bottom charged current by the process $b \to s\gamma$*, Phys. Rev. **D49** (1994) 5890–5893.

[198] G. M. Asatrian and A. Ioannisian, *CP-Violation in the Decay $b \to s\gamma$ in the Left-Right Symmetric Model*, Phys. Rev. **D54** (1996) 5642–5646, [hep-ph/9603318].

[199] C. Bobeth, M. Misiak, and J. Urban, *Matching conditions for $b \to s\gamma$ and $b \to sgluon$ in extensions of the standard model*, Nucl. Phys. **B567** (2000) 153–185, [hep-ph/9904413].

[200] M. Frank, A. Hayreter, and I. Turan, *B Decays in an Asymmetric Left-Right Model*, Phys. Rev. **D82** (2010) 033012, [arXiv:1005.3074].

[201] A. J. Buras, L. Merlo, and E. Stamou, *The Impact of Flavour Changing Neutral Gauge Bosons on $\bar{B} \to X_s\gamma$*, JHEP **1108** (2011) 124, [arXiv:1105.5146].

[202] M. Misiak and M. Steinhauser, *NNLO QCD corrections to the $B \to X_s\gamma$ matrix elements using interpolation in m_c*, Nucl. Phys. **B764** (2007) 62–82, [hep-ph/0609241].

[203] **HPQCD** Collaboration, I. Allison *et. al.*, *High-Precision Charm-Quark Mass from Current-Current Correlators in Lattice and Continuum QCD*, Phys. Rev. **D78** (2008) 054513, [arXiv:0805.2999].

[204] C. Aubin, J. Laiho, and R. S. Van de Water, *The Neutral kaon mixing parameter B(K) from unquenched mixed-action lattice QCD*, Phys.Rev. **D81** (2010) 014507, [arXiv:0905.3947].

[205] T. Bae, Y.-C. Jang, C. Jung, H.-J. Kim, J. Kim, *et. al.*, *B_K using HYP-smeared staggered fermions in $N_f = 2 + 1$ unquenched QCD*, Phys.Rev. **D82** (2010) 114509, [arXiv:1008.5179].

[206] **ETM** Collaboration, M. Constantinou *et. al.*, *B_K-parameter from $N_f = 2$ twisted mass lattice QCD*, Phys.Rev. **D83** (2011) 014505, [arXiv:1009.5606].

[207] Y. Aoki, R. Arthur, T. Blum, P. Boyle, D. Brommel, *et. al.*, *Continuum Limit of B_K from 2+1 Flavor Domain Wall QCD*, Phys.Rev. **D84** (2011) 014503, [arXiv:1012.4178].

[208] R. Barbieri and G. F. Giudice, *Upper Bounds on Supersymmetric Particle Masses*, Nucl. Phys. **B306** (1988) 63.

[209] P. Athron and D. J. Miller, *A New Measure of Fine Tuning*, Phys. Rev. **D76** (2007) 075010, [arXiv:0705.2241].

[210] C. Csaki, A. Falkowski, and A. Weiler, *The Flavor of the Composite Pseudo-Goldstone Higgs*, JHEP **0809** (2008) 008, [arXiv:0804.1954].

[211] A. J. Buras, G. Isidori, and P. Paradisi, *EDMs vs. CPV in $B_{s,d}$ mixing in two Higgs doublet models with MFV*, Phys. Lett. **B694** (2011) 402–409, [arXiv:1007.5291].

[212] B. Grinstein, M. Redi, and G. Villadoro, *Low Scale Flavor Gauge Symmetries*, *JHEP* **11** (2010) 067, [arXiv:1009.2049].

[213] S. J. Huber, *Flavor violation and warped geometry*, *Nucl. Phys.* **B666** (2003) 269–288, [hep-ph/0303183].

[214] K. Agashe, G. Perez, and A. Soni, *Flavor structure of warped extra dimension models*, *Phys.Rev.* **D71** (2005) 016002, [hep-ph/0408134].

[215] G. Burdman, *Flavor violation in warped extra dimensions and CP asymmetries in B decays*, *Phys. Lett.* **B590** (2004) 86–94, [hep-ph/0310144].

[216] K. Agashe, A. Delgado, M. J. May, and R. Sundrum, *RS1, custodial isospin and precision tests*, *JHEP* **08** (2003) 050, [hep-ph/0308036].

[217] K. Agashe and R. Contino, *The minimal composite Higgs model and electroweak precision tests*, *Nucl. Phys.* **B742** (2006) 59–85, [hep-ph/0510164].

[218] K. Agashe, R. Contino, and A. Pomarol, *The minimal composite Higgs model*, *Nucl. Phys.* **B719** (2005) 165–187, [hep-ph/0412089].

[219] R. Contino, L. Da Rold, and A. Pomarol, *Light custodians in natural composite Higgs models*, *Phys. Rev.* **D75** (2007) 055014, [hep-ph/0612048].

[220] A. J. Buras, B. Duling, and S. Gori, *The Impact of Kaluza-Klein Fermions on Standard Model Fermion Couplings in a RS Model with Custodial Protection*, *JHEP* **0909** (2009) 076, [arXiv:0905.2318].

[221] B. Duling, *A Comparative Study of Contributions to ϵ_K in the RS Model*, *JHEP* **1005** (2010) 109, [arXiv:0912.4208].

[222] M. Blanke, A. J. Buras, B. Duling, K. Gemmler, and S. Gori, *Rare K and B Decays in a Warped Extra Dimension with Custodial Protection*, *JHEP* **03** (2009) 108, [arXiv:0812.3803].

[223] M. Blanke, B. Shakya, P. Tanedo, and Y. Tsai, *The Birds and the Bs in RS: The $b \to s\gamma$ penguin in a warped extra dimension*, arXiv:1203.6650. 42 pages, 13 figures.

[224] N. G. Deshpande, J. F. Gunion, B. Kayser, and F. I. Olness, *Left-right symmetric electroweak models with triplet Higgs*, *Phys. Rev.* **D44** (1991) 837–858.

[225] K. Kiers, M. Assis, and A. A. Petrov, *Higgs sector of the left-right model with explicit CP violation*, *Phys. Rev.* **D71** (2005) 115015, [hep-ph/0503115].

[226] J. Hubisz, P. Meade, A. Noble, and M. Perelstein, *Electroweak precision constraints on the littlest Higgs model with T parity*, *JHEP* **01** (2006) 135, [hep-ph/0506042].